Université d'Évry-Val-d'Essonne **École doctorale Sitevry**
Numéro d'ordre ...

Trajectory control in curves, towards the Perceptive-ESC, through a Piecewise Affine approach

THÈSE

présentée et soutenue publiquement le 15 Novembre 2011

pour l'obtention du

Doctorat de l'Université d'Évry-Val-d'Essonne

(spécialité Automatique, Systèmes Productiques et Robotique)

par

André Benine-Neto

Composition du jury

Président :	Carlos Canudas-de-Wit	Directeur de Recherche au CNRS-GIPSA-LAB
Rapporteurs :	Didier Dumur	Professeur à Supélec
	Dominique Meizel	Professeur à l'ENSIL
	Brigitte d'Andréa Novel	Professeur à l'Ecole de Mines ParisTech
	Dimitri Peaucelle	Chargé de Recherche au LAAS-CNRS
	Andreas Eidehall	Ingénieur Volvo Car Corporation
	Nicoleta Minoiu-Enache	Ingénieur chez Renault S.A.
Directeur :	Saïd Mammar	Professeur à l'Université d'Évry-Val-d'Essonne

Laboratoire sur les Interactions Véhicules-Infrastructure-Conducteurs
IFSTTAR. 14, route de la Minière 78000 Versailles-Satory

Acknowledgments

First of all, I would like to thank my advisor Saïd Mammar, professor at Université d'Evry, for his theoretical support, solve-problems ideas and promptness throughout the entire research. I am very grateful for this cooperation which has resulted in two submitted journals and several conference papers. It has been a great pleasure to work with him.

I thank Didier Dumur and Dominique Meizel for their interest in my work, for accepting being the main reporters of the thesis and for their constructive feedback about the work. Equally, I appreciate the efforts of Brigitte d'Andréa-Novel, Dimitri Peaucelle, Andreas Eidehall and Nicoleta Minoui-Enache for being part of the board of inspection.

Also with important cooperation, I would like to express my appreciation to Stefano Scalzi for his continuous collaboration during the PhD program. I am very grateful for our technical discussions.

Benoit Lusetti has made available his support in a number of ways which certainly enriched the content of this thesis, specially concerning the practical implementation of the driver assistance systems on the prototype vehicle, for which I extend the acknowledgements also to Jean-Marie Chevreau and Michaël Messias.

It is a pleasure to thank Neil Atinkson for his royal English reviews of the thesis and articles as well as our friendship over the years.

I would like to thank Mariana Netto, for the support during the first two years of the Phd program, for the indications of pertinent seminars for the development of my thesis and mainly, with Jacques Erlich, director of LIVIC, for trusting my capacity and giving me the opportunity to became part of the research group at LIVIC with the funding from LCPC in the framework of program K.

I'd like to show my gratitude to the discussions with Sorin Olaru, William Pasillas-Lepine and Nicoleta Minoiu Enache. Their suggestions and contributions have not only contributed for this work but also to broaden my knowledge on piecewise affine systems, vehicle dynamics and driver assistance systems.

Several contributions have been provided by the colleagues from LIVIC whom I thank for the good working environment and conviviality. Séverine Somma, Isnié Rusani, Jacques Erlich and Didier Aubert mainly for administrative issues. Benoit Vanholme, Romain Gallen, Guillaume Saint Pierre, Aurélien Cord, Dominique Gruyer, Steve Pechberti, Jerome Perignon, Evangeline Pollard, Lydie Nouvelière, Francis Dupin, Sébastien Glaser and Hong-Tu-Luu, for several discussions that helped me not only technically, but also personally, to make this thesis possible.

Several people encouraged me to take part in the Phd program. I would like to thank professor Maria Helena Robert from UNICAMP (Universidade Estadual de Campinas) for providing a reference letter. Breno Hulle da Silveira and Volker Heumann, my former supervisors for supporting the decision of leaving the industry to start a PhD. Gilberto Gouvêa, former colleague at industry, for transmitting his passion and knowledge about vehicle dynamics. Mariana Moretti not only for informing and encouraging me to apply for the phD position, but also for hosting me during a conference. Mohammed El Katter for his excellent teaching skills that provided good knowledge of French language which certainly helped to quickly adapt to the life in France. I also thank my family and friends for the support during this 3 years of PhD program.

À Francesca et Ozzy,

"Essentially, all models are wrong, but some are useful",
George E. P. Box

Contents

List of Figures

List of Tables

Nomenclature

1 Mathematical symbols

Symbol	Description.
$x \in \mathbb{R}^+$	$x \in \mathbb{R}$ and $x \geq 0$.
$v \in \mathbb{R}^n$	v is a vector containing real values with n rows.
$A \in \mathbb{R}^{n \times m}$	A is a matrix containing real values with n rows and m columns.
$A_{i,j}$	Element of row i and column j of matrix A.
$A, B \in \mathbb{R}^{n \times m}$, $A > B$	$A_{i,j} > B_{i,j}$ for $i = 1, ..., n$ and $j = 1, ..., m$ (element-wise).
$A \succ 0$, $A \prec 0$	Matrix A is positive definite, respectively negative.
$A \succeq 0$, $A \preceq 0$	Matrix A is positive semi-definite, respectively negative.
$\lambda(P)$	Eigenvalues of Matrix $P \in \mathbb{R}^{n \times n}$.
$A \in \mathbb{R}^{n \times n}$, A^T	Transpose of Matrix A.
$A_{i,j} = *$	represents the transposed element of row j and column i, $* = {A_{j,i}}^T$.

2 Nomenclature for piecewise affine systems

Symbol	Description.
R_i	Operating region i of piecewise affine system.
$\mathcal{I}$	Set of operating regions.
M	Number of operating regions $i \in \mathcal{I} = \{1, ..., M\}$.
p_i	finite number of half-spaces that define an operating region.

3 Vehicle nomenclature

Symbol	Description.
CG	Centre of gravity.
m	Vehicle mass.
J	Vehicle inertia moment with respect to the vertical axis through the centre of gravity.
l_f	Distance from centre of gravity to front axle.
l_r	Distance from centre of gravity to rear axle.
l_s	Look-ahead distance.
ρ_{pref}	Road curvature.
v	Longitudinal velocity.
δ_f	Front wheel steering angle.
δ_p	Steering wheel angle.
β	Vehicle sideslip angle.
r	Vehicle yaw rate.
y_L	Lateral offset at look-ahead distance.
ψ_L	Relative yaw angle.
μ	Adhesion coefficient.
α_f	Front wheel sideslip angle.
α_r	Rear wheel sideslip angle.
F_{yf}	Front wheel lateral tyre force.
F_{yr}	Rear wheel lateral tyre force.
c_f	Front wheel cornering stiffness coefficient.
c_r	Rear wheel cornering stiffness coefficient.
d_{fi}	Slope of piecewise affine approximation of front tyre lateral force.
d_{ri}	Slope of piecewise affine approximation of rear tyre lateral force.
e_{fi}	Constant of piecewise affine approximation of front tyre lateral force.
e_{ri}	Constant term of piecewise affine approximation of rear tyre lateral force.
τ_p	Torque on steering wheel.
τ_{alg}	Wheel auto alignment torque.
τ_{on}	Threshold on driver torque on steering wheel for assistance activation.
τ_{off}	Threshold on driver torque on steering wheel for assistance deactivation.
η	Length of contact between tyre and ground.
B_s	Steering column damping coefficient.
R_s	Steering column gear ratio.
I_s	Steering column inertial moment.

4 Acronyms

Acronyms	Description.
ABS	Anti-lock Brake System.
ESC	Electronic Stability Control.
$ADAS$	Advanced Driving Assist Systems.
$LDWS$	Lane Departure Warning Systems.
$LKAS$	Lane Keeping Assist Systems.
PWL	Piecewise Linear.
PWA	Piecewise Affine.
PWQ	Piecewise Quadratic.
LMI	Linear Matrix Inequalities.
BMI	Bilinear Matrix Inequalities.
$LIVIC$	Laboratoire sur les Interactions Véhicules-Infrastructure-Conducteurs

Resumé

Les statistiques de la sécurité routière indiquent qu'une large part des accidents est due aux sorties de voie involontaires [BK11], [Fra10]. Deux conditions sont aggravantes parmi les causes de ces accidents. Premièrement, en conditions d'adhérence dégradées, notamment causées par la pluie, la neige où le verglas, la perte de stabilité du véhicule résulte d'une erreur du conducteur ou d'une sur-réaction en essayant de corriger la trajectoire du véhicule. Ainsi, aux Etats-Unis, 28% des accidents sont causés par un erreur de braquage et en France, les collisions latérales contribuent pour 30% des accidents (16% mortels).

Le manque d'attention du conducteur est aussi présent dans une grand partie des accidents, dont les sorties de voie involontaires. La fatigue et la distraction ont été liées aux causes des accidents, et représentent 36% et 25% respectivement, [BK11]. Selon [Weg11], 17% de tous les accidents aux États-Unis en 2009 concernait des conducteurs distraits.

Dans ce contexte, les avancées dans les technologies de capteurs et actionneurs ont permis le développement de systèmes d'aide à la conduite pour prévenir les accidents. Plusieurs types de ces systèmes sont déjà disponibles sur le marché, comme l'ABS[1] (système anti-blocage de roues) et l'ESC[2] (contrôle électronique de la stabilité) et utilisent uniquement des capteurs proprioceptifs. Ces systèmes sont très efficaces pour éviter l'instabilité du véhicule, notamment dans les situations d'adhérence dégradée. D'autre part, l'usage de capteurs extéroceptifs est présent dans les systèmes plus récents, comme l'ACC[3] (gestion de vitesse et d'inter-distance), LKAS[4] (Maintien dans la voie) et LDWS[5] (Alerte en sortie de voie). Ces systèmes sont capables de percevoir l'environnement du véhicule et non seulement avertir le conducteur en cas de danger, mais aussi d'agir sur la dynamique du véhicule pour éviter des accidents typiquement causées par manque d'attention ou la fatigue. Cependant, l'ESC agit sur la dynamique du véhicule en situations d'urgence alors que les systèmes d'alerte et d'évitement de sortie de voie sont généralement conçus pour les situations de faible sollicitation latérale.

Cette thèse traite le développement d'un système d'aide à la conduite, nommé ESC-perceptif, qui intègre les informations des capteurs extéroceptifs (Une camera vidéo montée en vision frontale) avec le contrôle de la vitesse de lacet afin d'éviter les sorties de voie involontaires, y compris pour des conditions de fortes sollicitations latérales ou d'adhérence dégradée. La prise en compte du phénomène de saturation de forces de contact pneumatiques-chaussée est essentielle pour la conception de l'ESC-Perceptif. Le comportement non-linéaire des efforts pneumatiques est traité par l'approche des systèmes affines par morceaux (PWA[6]). Cela permet de mener l'analyse et la synthèse de lois de commande en combinant les fonctions de Lyapunov avec la

[1] Anti-block System
[2] Electronic Stability Control
[3] Automatic Cruise Control
[4] Lane Keeping Assistance System
[5] Lane Departure Warning System
[6] Piecewise affine systems

résolution de problèmes d'optimisations sous contraintes d'inégalités matricielles linéaires (LMI) et bilinéaires (BMI).

Tout au long de la thèse, plusieurs contrôleurs affines par morceaux pour le développement de systèmes d'aide à la conduite sont présentés. Leur complexité et fonctionnalité sont abordées de façon graduelle, à partir d'une simple amélioration de la manœuvrabilité de véhicule jusqu'à l'ESC-perceptif, basé uniquement sur les capteurs disponibles sur les véhicules commercialisés. À chaque étape, les avantages de l'utilisation des systèmes PWA sont évalués

Un modèle du véhicule type bicyclette [Ack02] a été utilisé pour l'analyse et la synthèse de lois de commande. Ce modèle permet la représentation des phénomènes essentiels de la dynamique latérale du véhicule. Seules la translation latéral et la rotation de lacet sont considérées alors que les mouvements de roulis et tangage sont négligés. Les deux roues avant et arrières sont rassemblées en une seule au milieu de chaque essieu. Les efforts pneumatique-chaussée, normalement représentés par le modèle de Pacejka [Pac04], sont approximés par des fonctions affines par morceaux. Plusieurs simulations dans différentes conditions de vitesse, d'adhérence et de braquage ont permis de valider l'approximation du modèle non-linéaire du véhicule par le modèle affine par morceaux (PWA). Ce modèle PWA a été étendu pour prendre en compte le positionnement du véhicule sur la voie lors du développement d'assistances au maintien de voie.

Pour contourner les simplifications du modèle utilisé dans la synthèse, les systèmes d'aide à la conduite, conçus tout au long de la thèse, ont été validés avec l'aide du simulateur CarSim [Mac81], ou sur véhicule prototype pour la validation expérimentale.

Premièrement, seule la dynamique du véhicule à été évaluée dans la conception d'un ESC fondé sur le braquage actif du véhicule. Une structure PI (proportionnel-intégrateur), similaire à [B$^+$03], à été utilisée pour suivre une vitesse de lacet de référence. Afin de prendre en compte la non-linéarité des efforts pneumatiques-chaussée, cette structure a été étendue avec une loi de commande linéaire par morceaux, où la commutation est basée sur la vitesse de lacet. Les seuils de commutation ont été obtenus par une paramétrisation de la dynamique du véhicule par le régime permanent de la vitesse de lacet, la seule variable supposée mesurable. La commande linéaire par morceaux s'est avérée plus performante que la commande uniquement linéaire lors de simulations des situations d'urgence. Néanmoins, cette commande a été améliorée par l'inclusion d'une boucle de retour d'état et des conditions de commutation utilisant l'angle de dérive de roues avant. Cette assistance constitue une nette amélioration et présente moins d'oscillations en régime permanent. Elle a permis de valider les avantages de l'approche affine par morceaux. La stabilité de ces deux assistances a été prouvée par des fonctions de Lyapunov quadratiques par morceaux.

Pour le développement de l'assistance au maintien de voie, la courbure de la route peut être considérée comme un perturbation à rejeter. En connaissant les fonctions qui décrivent cette perturbation, le principe du modèle interne peut être appliqué afin de synthétiser des lois de commande. Cette méthode a été appliquée, dans un premier temps, au modèle linéaire du véhicule pour la synthèse d'un contrôleur par retour d'état qui a été validé expérimentalement. Le même système a été évalué aussi pour des manœuvres de type double changement de voie selon le standard ISO-3888-1, ce qui indique une application potentielle comme assistance pour l'évitement d'obstacle. L'extension pour prendre en compte la non-linéarité considère aussi le modèle interne dans une structure PIID linéaire par morceaux, pour la régulation de l'écart latéral, laquelle à été validée en simulation. Cette étape a permis de confirmer les performances plus satisfaisantes des contrôleurs linéaires par morceaux par rapport aux contrôleurs uniquement linéaires non seulement pour la dynamique du véhicule mais aussi pour l'assistance au maintien de voie. Cependant, la preuve de stabilité par des fonctions de Lyapunov quadratiques par morceaux est indépendant de la synthèse et effectuée après la choix de gains.

Afin de contourner cet inconvénient, les synthèses développées dans [RH03] ont été appliquées. Par le choix, à priori, des points d'équilibre de chaque région de l'espace d'état, les gains du contrôleur affine par morceaux peuvent être obtenus par la résolution d'un problème d'optimisation sous contraintes de type BMI. Une solution sous-optimale a été calculée par la méthode itérative V-K. Cette assistance d'évitement de sortie de voie involontaire a été validée expérimentalemente à l'aide des anneaux de composite montés sur les pneumatiques avant du véhicule prototype [Bou11]. Ce dispositif a permis de reproduire des conditions de faible adhérence à des vitesses relativement basses. Les véhicules actuellement commercialisés ne possèdent pas de capteur capable de mesurer l'angle de dérive du véhicule. Donc, une extension de cette assistance, fondée sur un contrôleur du type retour de sortie affine par morceaux, a été développée avec une structure composée d'observateur et régulateur, afin d'assurer la viabilité industrielle de cette application. L'assistance a été également validée sur le véhicule prototype sans perte de performances qui pouvait être causée par l'introduction de l'observateur. Ce dernier point répond à l'objectif principal de la thèse.

Les principales contributions de cette thèse peuvent être listées comme la proposition et analyse de la dynamique latérale du véhicule par les systèmes affines par morceaux; la proposition de systèmes de braquage actif et de maintien de voie qui prennent en compte le comportement non-linéaire des efforts pneumatiques-chaussé; le développement d'une assistance à la conduite pour l'évitement de sorties de voie basée sur les capteurs déjà disponibles sur le marché et capable d'intervenir en situation d'urgence.

Part I

Introduction

Chapter 1

Motivations and Methodology

Contents

1.1 Context

According to road safety statistics, unintended road departures caused either by a mistake or inattention of the driver or degraded road adhesion (rain, snow, ice) accounts for a great parcel of the accidents.

As reported by the ERSO[7] in [BK11], more than 106000 people were killed in single vehicle accidents[8] in the 16 European Union countries between 1999 and 2008. It represents one third of all traffic accident fatalities. Data from 2005 to 2008, reports that 40% of these accidents are due to incorrect direction (including lane departure) for European Union 23 (EU-23) countries. The same reason accounts for 8% of multiple vehicle accidents.

Concerning the weather conditions, in the EU-23 countries, more than one third of the total fatalities recorded when it snows are due to single vehicle accidents, whereas the respective percentage for rainy weather is less than 30% [BK11]. Statistics from ONISR[9] reveal that 21.1% of fatal accidents in France happened in 2009 in degraded meteorological conditions (rain, snow, haze, wind and fog) [Fra10].

Accidents due to the drivers' lack of attention also represent a significant proportion. In [BK11], reporting the accidents in EU-23, the critical events such as no action or late action are related, respectively, to 25% and 16% of multiple vehicle accidents. Regarding single vehicle accidents, 36% of the causes are linked to fatigue while 25% are linked to distraction, these two causes of accidents being among the 10 most frequent. According to [Weg11] the NHTSA[10]

[7] European Road Safety Observatory

[8] Type of road traffic accident in which only one vehicle and no other road user is involved. Run-off-road collisions, collisions with fallen rocks or debris in the road, rollover crashes within the roadway and collisions with animals are included in this category.

[9] Observatoire National interministériel de sécurité routière

[10] National Highway Traffic Safety Administration.

estimates that in 2009, 17% of all crashes in the United States involved distracted driving, representing nearly 5500 fatalities.

The ONISR estimates that, in 2009 in France the costs directly and indirectly involved in 4273 fatal road accidents amounts to 5.36 billion € [Fra10]. For the accidents involving hospitalised injured people (33323), the costs sum up to 4.52 billion €, and accidents with minor injuries or only material damage account for 0.78 billion €.

Efforts have been made to reduce the number of accidents and their severity. Advances in the technology of sensors and actuators have enabled the development of driver assistance systems to prevent accidents.

Concerning active safety, systems such as the ABS[11] and ESC[12] (also known by ESP[13] and other numerous manufacturer-specific names) are capable of recovering the vehicle stability and therefore avoid skidding, in emergency situations. Enhancing the vehicle manoeuvrability is also possible with active steering in vehicles equipped with steer-by-wire systems, in which the conventional mechanical steering elements are replaced by electrical actuators at the front (or rear) corners to turn the wheels. Such systems are based on proprioceptive sensors, in consequence they depend on the driver attentiveness to avoid an accident by acting on the vehicle dynamics.

Some development of active safety systems based on exteroceptive sensors have also been carried out in recent years, and systems such as assisted parking and ACC[14] are currently common in passenger vehicles, while automatic emergency braking systems are becoming more common. Regarding the lateral mode, examples of systems in development or recently available in the market are Lane Departure Warning Systems (LDWS), Lane Keeping Assistance Systems (LKAS) and Motor Primming Assistance. When vehicles are about to leave the lane, these systems warn the driver or aid him/her to correct the trajectory through steering actuators. The positioning of the vehicle with respect to the lane is in most of the cases obtained by a video system. On the contrary to ESC, the systems to avoid lane departure are usually designed to work only in situations with weak lateral solicitation.

The development of vehicle control to avoid lane departure considering strong lateral solicitations is still an open problem. The integration of information from vision systems with action on the vehicle steering dynamics, may enable the development of Advanced Driver Assistance System (ADAS) to prevent accidents in situations of strong lateral instability due to degraded adhesion conditions or driver's lack of attention. Moreover, in situations of vehicle lateral instability, acting only on the steering angle of the wheels may not be enough to recover the stability, therefore it is needed to add a control input on the yaw moment (differential torque or independent wheel braking).

Although linear modelling for analysis and control of engineering systems has been extensively studied and many tools for control design are available, they may not be adequate for the design of ADAS involving strong lateral solicitations, since the vehicle nonlinear behaviour plays an important role. Therefore the conception of the ADAS implies two challenges: firstly, to take into account the nonlinear behaviour of the vehicle and secondly to treat this properly in the control synthesis.

[11] Anti-Block System
[12] Electronic Stability Control
[13] Electronic Stability Program
[14] Automatic Cruise Control

1.2 Goals and contributions

The main objective of this thesis is the development of an ADAS to avoid lane departure caused by driver inattention. Moreover, it comprises an integrated control system which is able to anticipate the steering action by taking into account the environment of the vehicle (exteroceptive signals) such as LKAS and simultaneously cope with strong lateral instability (proprioceptive signals), if needed, as ESC. The combination of the characteristics of both systems in one leads to the vehicle safety oriented ADAS, which is named *Perceptive-ESC*.

It is implied from this main objective that the system must:

- improve the vehicle manoeuvrability taking into account the vehicle environment,
- perform well in straight or curved roads, as well as under variable road adhesion and load conditions.
- intervene when driver is not attentive, sharing the control of the vehicle with the driver,
- consider already available hardware in currently commercialised vehicles to avoid additional costs of implementation which could render the system commercially impracticable.

It can be seen, throughout this document, that several steps have been taken to achieve these objectives. Therefore, the topics listed above have been gradually considered in the development of the *Perceptive-ESC* . As a result, the main contributions of this thesis are:

- Use of hybrid models to capture the nonlinear lateral vehicle behaviour.
- Design of controllers for active steering, in which only the vehicle dynamics are taken into account, to improve the vehicle manoeuvrability in emergency situations.
- Design of the controllers for lane keeping in curved roads.
- Design of controllers for lane departure avoidance in emergency situations.
- Exploration of performance and limitations of hybrid system in the design of driving assistance systems for lateral mode.
- Proposals to reduce the number of sensors for the active steering and lane keeping assistance systems.
- Practical validation of the proposed assistances.

The methodology employed to achieve these contributions is described in the next section.

1.3 Methodology

The methodology used to achieve develop the *Perceptive-ESC* and achieve the goals listed above consisted on the development of several intermediate assistance systems with gradually increasing complexity. The main steps of the methodology can be listed in the following points:

1. **Research of adequate model to treat nonlinearity**. Through the literature review, the possibilities to represent the nonlinear behaviour of the lateral tyre forces have been searched. The piecewise affine systems (PWA) have been considered adequate for this kind of problem as well as the existing theoretical tools for analysis and control synthesis of this class of systems.

2. **Investigation of vehicle lateral dynamics modelled with piecewise affine system**. At this stage, the PWA vehicle models have been simulated and analysed in order to comprehend their behaviour in comparison with the nonlinear vehicle model.

3. **Yaw control by active steering**. In order to explore the potential of the PWA modelling for the control of vehicle dynamics, only the active steering has been used as a control input for the yaw dynamics. Besides being the natural choice to steer a vehicle, it keeps the control systems with a simple structure involving a single input, so that the advantages from the modelling can be evaluated.

4. **Piecewise linear control of vehicle dynamics**. A simple piecewise linear (PWL) control structure has been implemented for the development of active steering assistance, in order to evaluate the advantages of the PWL controller in stabilising the vehicle dynamics. A steer-by-wire configuration has been considered.

5. **PWA control of vehicle dynamics and positioning** The variables representing the positioning of the vehicle have been included in the model in order to design a lane departure avoidance system. Starting from a simple PWL controller designed to evaluate the vehicle response, the control structure and synthesis is gradually sophisticated in order to develop the *Perceptive-ESC* .

This methodology has provided the possibility to evaluate the feasibility, advantages and limitations of PWA controllers for vehicle lateral dynamics. These aspects are described in this document which is organised as presented in the next section.

1.4 Document organisation

This thesis is divided in four parts. The first part consists of this chapter describing the motivation goals and contributions of the thesis. The following chapter consists of a presentation of intelligent transportation systems and the state-of-the art of the driver assistance systems for lateral motion, with focus on the theoretical and practical aspects of yaw rate controllers, lane-departure-warning and lane-departure-avoidance systems. The currently commercialised driving assistance systems for the lateral mode are also presented in Chapter 2.

Part II is composed of two chapters. Chapter 3 introduces the main theoretical tools used in the design of the lateral driving assistance systems. It includes a review of the dynamical systems, Lyapunov stability and optimisation problems involving Linear and Bilinear Matrix Inequalities. Piecewise Affine Systems and the tools for analysis and control design of this specific class of Hybrid systems are also presented in this chapter. Chapter 4 presents the vehicle models used in the design of the assistances. Moreover, it introduces the simulation environment used for the evaluation of the controllers, as well as the prototype vehicle used in the practical implementation.

Part III comprises of Chapters 5 to 7. In each chapter, the control strategies and the evaluation of assistance systems are presented. Two active steering assistances, described in Chapter 5, are designed to track a yaw rate reference signal based on the yaw rate error. The first assistance is based only on the yaw rate while the second includes a state feedback loop in order to enhance the closed loop response.

Chapter 6 covers two controllers designed for lane keeping assistances. Both make use of the internal model concept to reject disturbances such as the road curvature. The first one is an extension of the work already developed in LIVIC based on a linear model. For the second

assistance a simple controller structure is deployed in order to evaluate the use of piecewise affine control applied to the lane departure avoidance problems.

In Chapter 7, the use of Lyapunov based control syntheses are explored in the design of three assistance systems for lane departure avoidance. The practical implementation of the assistances is also presented. The first two assistances are designed on the basis of a piecewise linear and piecewise affine state feedback controllers. The third assistance is based on a piecewise affine output feedback controller, which uses only sensors that are available in currently commercialised vehicles. Consequently it avoids the use of costly optical sensors.

The last part concludes the work, by recalling the main contributions and limits of the investigated methods. Perspectives for future research are also provided in Chapter 8.

Chapter 2

State of the art

Contents

In this chapter an overview of Intelligent Transportation Systems (ITS) is provided as well as a description of the main projects related to passenger vehicles.

The state of the art regarding driver assistance systems focusing on the vehicle lateral stability is also discussed. It includes an overview of the existing systems for lateral vehicle dynamics control and lane departure avoidance with the corresponding control strategies.

2.1 Intelligent transportation systems

Intelligent transportation systems is, despite lacking an unified definition, the term used to refer to the research and technologies employed not only to improve the traffic safety and comfort but also to reduce the travelling time, traffic congestion, fuel consumption and pollutant emissions.

The possibilities of use and development of road ITS can be focused mainly on the driver, vehicle, infrastructure and public power, as well as interactions of these. The next sections introduce the safety aspects involving each of these agents on road ITS.

Driver

Nowadays, the basic traffic rules are defined by an international treaty under the authority of the United Nations, the 1968 Vienna Convention on Road Traffic [Uni68]. Despite not being signed by all countries and some local variation in practise, these general rules are largely employed in the majority of countries.

According to the Vienna Convention on Road Traffic, (see [Uni68], Article 8), every moving vehicle must have a driver who must possess physical and mental ability to drive. Moreover, it is required that the driver is able to control his vehicle at all times.

The main function of ITS is then to keep the driver informed about his/her environment and potential dangerous situations, as well as to help him in the driving task enhancing the vehicle manoeuvrability, and reducing the risks of accidents.

Vehicle

Regarding the safety of vehicles, two main classes of systems exist, passive and active systems.

Passive systems consist of those designed to reduce the passenger injuries and vehicle damage when a collision occurs. Such devices include the vehicle body structure designed to absorb the impact of the collision and restraint devices such as seat belts, air-bags and seats with whiplash protection (prevent neck injury caused from rear end collision).

Active safety systems have as purpose to avoid and prevent the accidents, which may occur due to lack of maintenance, unexpected behaviour of the vehicle or drivers mistake caused either by misjudgement or lack of attention. Each of these accident causes are addressed by active safety systems.

Among the proprioceptive active safety systems, tyre pressure monitoring systems can help the driver cope with lack of maintenance while the manoeuvrability of the vehicles can be enhanced by the systems like ABS, ESC, Active steering and traction control systems which depend on the driver awareness.

Using exteroceptive sensors, active safety systems can perceive the environment around the vehicle and help the driver to avoid accidents caused by inattentiveness or misjudgement. Examples of such systems include ACC[15], Lane Keeping Assist (LKAS), Lane Change Assist (LCA), Intelligent Speed Adaptation (ISA) and emergency braking systems. These systems are based on cameras, with algorithms for the detection of lanes, signs and obstacles (pedestrians, other vehicles, etc) and sensors to monitor the vehicle's environment, helping the driver in case of degraded visibility (luminosity, blind-spot and hard-to-view areas) or inattention (unintended lane departure and frontal collision).

Infrastructure

The infrastructure in ITS can be equipped with communication systems in order to inform the drivers about the road conditions and potentially dangerous situations. Vehicles capable of emitting, receiving and interpreting information can also work as a transceiver to communicate with either the infrastructure or other vehicles. In case an accident occurs, it can be noticed by the infrastructure or informed by the vehicle using a communication system. Such information can be broadcast to warn other vehicles about the accident, and instruct them on how to proceed in order to enable a rescue unit to arrive faster at the accident scene. Dangerous situations, such as degraded road adhesion, can also be transmitted when experienced by vehicles in a given location, alerting other drivers. Such information exchange can also provide drivers with suggestion of alternative itineraries in case of congestion.

[15] Active Cruise Control

Governmental actions

The role of the governmental authorities is to regulate the use of safety equipment. For example, ABS is mandatory for all new vehicles produced for the European market. The authorities are also responsible for making propositions such as to equip all light new vehicles with ESC for the American market by August 2011 [Hig07] and for the European market by 2014 [Cou08].

Besides, governmental institutions have often also been a source of funding for research projects, which have provided significant advances in ITS. The development of the road ITS achieved through research projects is discussed in the next section.

2.1.1 Research projects on ITS

The research on ITS can be historically classified in four relatively distinct phases [YdB99]. The early research on ITS dates from the 60's and 70's and aimed to show the capacity of systems to increase the security and performance of road transportation. The need of complementary equipments and the size of computers at that time were the main bottleneck for the introduction of new systems, therefore most of the projects remained in the concept status, as for example the driver guidance information system [Kuh05].

From 1980 to 1995 major investments were made on the research for ITS, marked by ambitious projects like PROMETHEUS[16] in Europe, PATH[17] in the USA, and RACS[18] and ASV[19] in Japan. These projects were aimed mainly at the development of traffic management and information for drivers. Major changes to the infrastructure were required for the implementation of these projects, as for example, the embedment of permanent magnets along the road borders for vehicle guidance [PTH97, Shl07]. In consequence, most of the achievements from these projects have not been implemented on a larger scale. Nevertheless, they served as a basis for the next phase of research in ITS.

From 1995 to 2000, the automated road caught a lot of researchers attention. With the advances of video cameras, on board sensors and computers, the focus became fully automatic vehicles. Demonstrations from the project ARGO were performed in Europe, and the AHS[20] in USA showed the successful results of the projects. Still, the technologies developed could not be easily spread as real solutions for safety and congestion problems. Therefore the main public powers decided to prioritise research that could become commercialisable in the short term.

From 2000, concerns about sustainable development, multimodal transportation and safety became stronger, and research projects regarding the latter begun to integrate the driver for the development of Advanced Driving Assistance Systems (ADAS), as for example the project PReVENT-IP[21]. The same trend can be noticed with the current ITS projects such as HAVEit[22], which reinforces further the interaction between the driver and highly automated systems.

In this section, more details from some of the main projects on road ITS are provided, with an emphasis on the safety aspects. Some trends for the future research are also presented.

[16] PROgraMme for a European Traffic of Highest Efficiency and Unprecedented Safety
[17] Partners for Advanced Transportation TecHnology
[18] Road Automobile Communication Systems
[19] Advanced Safety Vehicle
[20] Automated Highway Systems
[21] Preventive and Active Safety Applications Integrated Project
[22] Highly Automated Vehicles for Intelligent Transport

PROMETHEUS

The project PROMETHEUS (1987-1995) was funded by EUREKA, an intergovernmental network for the support of market-oriented research and development and innovative projects. Being the first ITS project on a global scale, it counted on a budget of 749M€, for the creation of concepts and solutions for road traffic systems which are more efficient and less detrimental to the environment and guarantee an unprecedented degree of safety [Eur11].

Several car manufactures, electronic and automotive suppliers, research institutes, universities, traffic engineers and authorities took part in the project and some prototype vehicles were built during the project, being able to perform vision based environmental analysis such as road tracking, obstacle detection, lane traffic analysis and traffic sign recognition [PKL+94]. Moreover the prototype vehicles were able to operate autonomously on highways [PKL+94, HL95] and avoid collisions [Mat94, FHL92].

Even though the research activities and developments from the PROMETHEUS project did not directly become products, the achievements of the project were the basis for other projects on ITS, such as ARGO, and PReVENT, described in the sequel.

PATH

The California PATH was established in 1986 and it is administrated by the Institute of Transportation Studies from the University of California, Berkeley in collaboration with the California Department of Transportation (Caltrans). PATH is a multi-disciplinary program with the mission of developing solutions to the problems of California's surface transportation systems through cutting edge research in three main areas: Transportation Safety Research, Traffic Operations Research and Modal Applications Research [PAT11].

The research activities of the first 20 years of PATH is summarised in [Shl07], regarding the research devoted to safety, the project groupings include:

- Intersections and Cooperative Systems - crossing path vehicle crashes, safety aspects of cooperative driver-assist systems, Vehicle Infrastructure Integration.
- Driver behaviour - modelling and applications for safety and countermeasure studies of car following and lane changes, at roadway intersections, at-grade crossings
- Employee Safety - work zone warning signals, snow removal equipment. Emerging areas include speed enforcement, heavy truck safety, pedestrian safety and research with older driver safety.

Research devoted to road safety and reduction of accidents in the framework of PATH includes: the modelling of passenger and heavy-duty vehicles [PT90, TWWT01]; modelling of the driver [DS01, Pro01]; vehicle equipment for longitudinal and lateral control [PD98, FB01, CT03]; the longitudinal and lateral control of autonomous vehicles and vehicle platoons [GTP97, PTH97, SY99, HT91]; and situations of failure in sensors and control [TPZS97, TPT04].

ARGO

Based on the achievements of the PROMETHEUS project, the Department of Information Technology from the University of Parma, Italy, continued the research on autonomous vehicles by setting up in 1994 the ARGO project, funded by the Italian National Research Council.

The vehicle, equipped for autonomous driving, is able to follow lanes, recognise objects in the path and perform lane change manoeuvres. Moreover, it provides the functionality of warning of

dangerous situations in manual drive mode, and is able to take control in dangerous situations in supervised driving mode.

The environment recognition was based on video cameras only, so that information was acquired without altering the infrastructure of the roads.

In 1998 the system was tested in different road conditions, including rural roads. It accomplished tours of more than $175km$ in which the automatic driving mode was active for more than 85% of the travelled distance. Fig. 2.1 shown the autonomous vehicle from the project.

Figure 2.1: The ARGO autonomous vehicle [BBFC99].

The vehicle lateral control is based on a gain scheduling based proportional feedback from the lateral offset [BBF+99]. More detailed information about the project can be found in [BBFC99].

PReVENT-IP

The project PreVENT-IP was part of the 6^{th} Framework Programme and took place from 2004 to 2007, having a budget of 55M€. Similarly to PROMETHEUS, it was set up in a consortium, grouping 55 partners from 10 European countries including automotive manufactures and suppliers, research laboratories and institutes, universities, public and road authorities and associations.

The vision of the project consisted of creating an electronic security region around the vehicle through the development, integration and demonstration of a series of safety functions to provide information and assistance to the driver. These concepts are illustrated in Fig. 2.2. Contrary to other projects considering fully autonomous vehicles, PReVENT focused on the interaction between vehicle, environment and driver, such that the last is integrated in the intelligent vehicle system.

The final report of the project [SMI+08] provides a summary of the functions developed. They were structured in five complementary fields, named vertical activities:

- *Safe Speed and Safe Following.* These functions help drivers keep or choose a speed or inter-vehicle distance, allowing them to safely cope with the road situation they will meet in the following seconds. The approach is mostly autonomous.

- *Lateral Support.* This field deals with autonomous applications focusing on the lateral areas of a vehicle to help drivers keep their vehicle at the safest position in the lane, as well as warn them if the vehicle is about to run off the road.

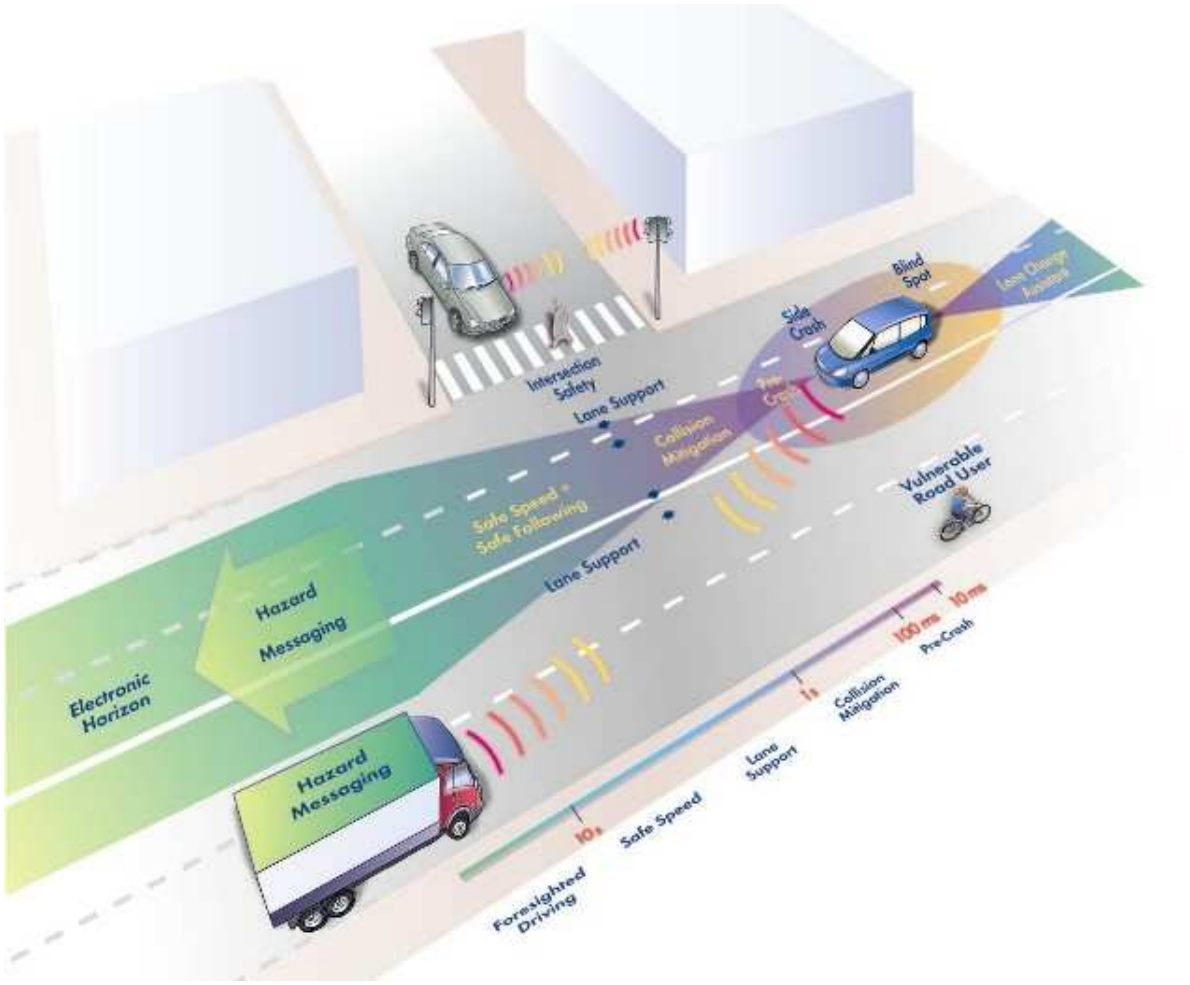

Figure 2.2: Illustration of the concepts vision of the European Project PReVENT-IP and a safety zone around the vehicle [SMI+08]

- *Intersection Safety.* This function field covers the investigation of autonomous and cooperative approaches to safety applications dedicated to approaching or passing intersections.
- *Vulnerable Road Users and collision Mitigation.* Collision mitigation and pre-crash protection systems focus on reduction of injuries and fatalities in case of unavoidable crashes (in particular during the last 2-3 seconds before the impact). Collision mitigation by braking significantly reduces kinetic energy of impact, thereby greatly reducing crash severity.
- *Cross-functional Activities.* An additional cross-functional field covering methodologies, common architectures, liability issues, and technology or standardisation oriented activities safeguards a common approach

The structure of the project also counted on horizontal activities to ensure the integration of the vertical functions. For that, common sets of sensors for different safety applications and sensor data fusion were specified and used in the evaluation of the performance enhancement and robustness of functions. Moreover a "code of practise" was created in order to develop, validate and introduce the ADAS to the market [SMI+08].

Often compared to PROMETHEUS for its amplitude and similar set up, the PReVENT project differs not only because it integrates the driver in the systems, but also for focusing on the use of already available technology and components, so that the project achievements could be easily commercialised.

DARPA Grand Challenge

The DARPA[23] (USA) has organised competitions of autonomous vehicles, named Darpa Grand Challenge, and funded cash awards of 1M $US\$$ for the winners having as main purpose the employment of autonomous vehicle technologies for military applications.

The first competition took place in 2004, and the teams were supposed to cover a 140-mile on- and off-road course from Barstow-CA to Primm-NV, in USA [DAR04]. None of the 15 finalist vehicles managed to finish the course. Nevertheless, the award was doubled and the competition took place in the following years. In 2005, five vehicles managed to complete the course [DAR05, IB06, TMD$^+$06]. In 2007, the competition took place in a 96-km urban environment including traffic situations such as such as merging, passing, parking and negotiating intersections [DAR08, BIS08a, BIS08b].

Despite the military purpose of this competition, most of the aspects regarding the safety of the vehicles were taken into account and advances were noticed in perception, control, and motion planning for intelligent autonomous vehicles operating in urban scenarios, therefore it can be considered as a contribution to the research for autonomous vehicles as means of transportation.

AKTIV

AKTIV[24] (2006-2010) was a project launched by a consortium supported by the German Federal Ministry for Economy and Technology involving 28 German partners from automotive industry (manufacturers and suppliers), electronic, telecommunication and software companies and research institutions.

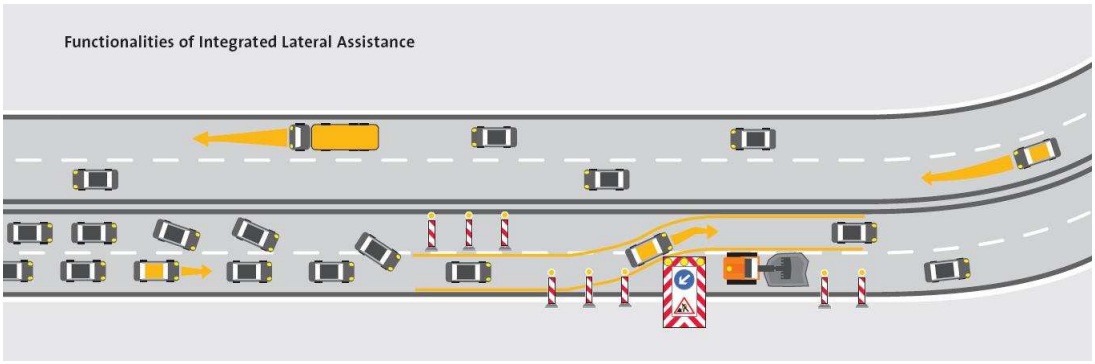

Figure 2.3: The functionalities of the integrate lateral assistance from project AKTIV [Sch10b].

Provided with an overall budget of 60M€ , the project objectives consisted of driver assistance- and traffic management systems, which: improve traffic safety for all participants; decrease the driver load and efficiently guide him to his destination; avoid traffic jams and better utilise the existing road capacity; make economic and ecological sense and have a sound legal basis; and are accepted by the society and the user. For that, 3 main groups were set-up, dealing with

[23] Defense Advanced Research Projects Agency
[24] Adaptive und Kooperative Technologien für den Intelligenten Verkehr

traffic management, cooperative cars and active safety [Sch10a]. Regarding the last group, the research activity was performed in 5 sub-projects [Sch10b]:

- *Active Hazard Braking* to avoid collisions and to mitigate consequences of accidents, but adapted to the traffic situation and equipped with a sophisticated detection of the driving environment, accurate interpretation of the situation and plausible system decision adapted to the driving scenario. The concept of intervention integrates the driver and is based on a graduated warning followed by braking and full braking, taking into account the driver alertness in the decision loop.

- *Integrated Lateral Assistance* is a continuous, integrated lateral guidance in the full speed range from 0 to 180 km/h for lane-keeping and lane-change. As shown in Fig. 2.3 this assistance is also able to handle scenarios such as construction on the road.

- *Intersection Assistance* was a sub-project that aimed the reduction of accidents at intersections by supporting the driver while entering, crossing or turning into an intersection with adequate warnings and intervention strategies triggered by the analysis of a selection of information gathered from onboard sensors, cooperative communication, integration of positioning and digital maps.

- *Pedestrian and Cyclist Safety* was a subprojet aimed at the improvement of the safety of vulnerable road-users. In case of imminent collision (in $2s$) the driver is warned by audible, visual or haptic signals, the pedestrian or cyclist is warned by front light blinks and horn honks. At $1s$ to the collision the brakes are fully engaged and at $0.5s$ a swerve manoeuvre in initiated, followed by activation of protection mechanisms on the hood and bumper, as well as exterior air-bag.

- *Driver Awareness and Safety* deals with the detection of driver alertness using surround sensor information and/or in-vehicle video cameras. The actual alertness level serves to adapt the strategies for warning and intervention in the application projects.

Demonstration of the developed systems took place at the end of the project, in order to provide an exchange of the acquired know-how.

VIAC

The VIAC[25] is a challenge consisting of driving autonomously four electric vehicles (shown in Fig. 2.4) from Parma, Italy to Shanghai, China organised by Vislab [Visa]. Partially funded by the European Research Council, the trip took place from July to October 2010. The first vehicle drove autonomously in parts of the 13000Km, but human intervention was required in some section and in critical situations. The other vehicles followed the first using vision system of GPS waypoints left by the leader vehicle. The vehicle sensors were constantly monitored resulting in 50terabytes of data that can be used in future research.

HAVEit

HAVEit project (2008-2011) is formed by a consortium of European automotive manufacturers and suppliers, universities and research laboratories and institutes with a budget of 30M€.

[25] Vislab Intercontinental Autonomous Challenge

Figure 2.4: Electric vehicles used in the challenge, obtained from [Visb]

It addresses the development of advanced driving assistance systems in highly automated vehicle applications with the purpose of enhancing comfort, safety and the efficient usage of energy.

Considering the varying performance of the driver, and therefore a variable requirement for level of assistance, the improvement of overall safety is handled by a variable task partition between the driver and automation, which supports the driver in monotonous driving tasks (e.g. queueing on crowded motorways) as well as in highly demanding tasks (e.g. automated merging into the traffic flow). The task repartition in the driver-copilot composed system is considered a key objective in the HAVEit project, since the driver must be given enough time to react properly and retake the control of vehicle in a situation which cannot be handled automatically by the highly automated system, as illustrated in Fig. 2.5. For this reason a step-wise strategy to handle back the vehicle control to the driver is chosen.

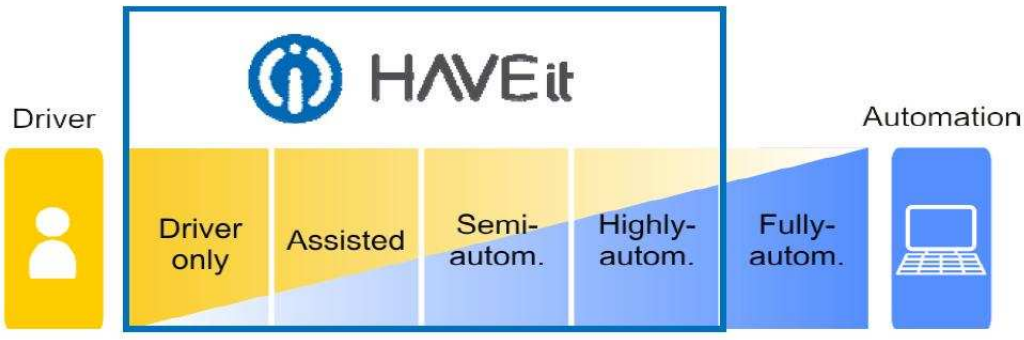

Figure 2.5: Level of automation and repartition of driving tasks in HAVEit project [HAV11].

Another measure to ensure safety among the project basis is the failure tolerant safe vehicle

architecture including advanced redundancy management.

The functionalities of the highly automated vehicles, which have been validated in 6 vehicles, includes: queue assistance, construction site assistance, temporary autopilot and active green driving. The deliverables and publications associated to HAVEit can be found in [HAV11].

2.1.2 Trends for research on safety related issues of ITS

The research on ITS has seen several main orientations in the last two decades. The first projects (PATH and PROMETHEUS) which proposed major investments on equipments for the infrastructure, have changed into the fully automatisation of the vehicles (ARGO) in a second step. The tendency in the end of the 90's changed, focusing on the assistance systems having the automation centred on the driver. Such strategy has been reinforced in recent projects such as HAVEit and AKTIV, where the interaction of the driver and the autonomous systems make up a great deal of the research activity.

According to the European Commission, the research applied to Intelligent Transportation Systems is one of the central planks for reducing road accidents. Further research on cooperative systems and intelligent infrastructure is expected, as well as on ADAS, which has already contributed to significant improvements on road safety, enabling several ADAS to be commercialised, such as ABS, ESP and LKA (more detailed in Section 2.2.2) [Eur10]. The human-machine interfaces has increasingly driven the attention of researchers, and it tends to continue as a key objective in future research. Moreover, driven by the demand for solution to the current safety and transportation issues, the research is prioritised for systems that can be employed in the market in a short time. Therefore, virtual testing methods can play an important role on the development of new applications.

Such trends noticed in the research of safety related issues on ITS are considered in the definition of the thesis objectives (see Section 1.2). The *Perceptive-ESC* is designed to be a highly automated assistance which shares the control of the vehicle with the driver, so that he/she is responsible for driving but is replaced by the assistance when he/she is considered unable to follow the lane. Moreover the use of only equipment that already exists in the commercialised vehicles, enables this proposal to be implemented in production without major additional investments. Such characteristics can also be found on the development of ADAS for the vehicle lateral stability, as described in detail in the next section.

2.2 ADAS for vehicle lateral stability

In this section the possibilities of enhancing the vehicle lateral stability are presented. Firstly, a description of the proprioceptive systems to enhance vehicle handling such as yaw rate controllers is provided. It is followed by a review on the exteroceptive ADAS for lane departure warning and lane departure avoidance, providing information on the control techniques explored in the research and commercialised solutions.

2.2.1 Yaw stability control

Safety critical situations may occur on the roads, causing vehicle skidding when the response of the car changes suddenly, for example under a reduction in the road adhesion (icy or wet pavement), or under disturbance torques like wind gusts, asymmetric road surface, tyre burst, a collision avoidance manoeuvre or other that forces the tyre to the limits. Usually drivers take from $0.5s$ to $1s$ to react in such critical safety situations, and inexperienced drivers may oversteer

the vehicle which clearly makes things even worse [Ack02]. Yaw stability control systems, also known as electronic stability systems (ESC) are automatic systems that continuously monitor the vehicle conditions to detect and minimise skids, helping the driver overcome dangerous situations, as illustrated in Fig. 2.6.

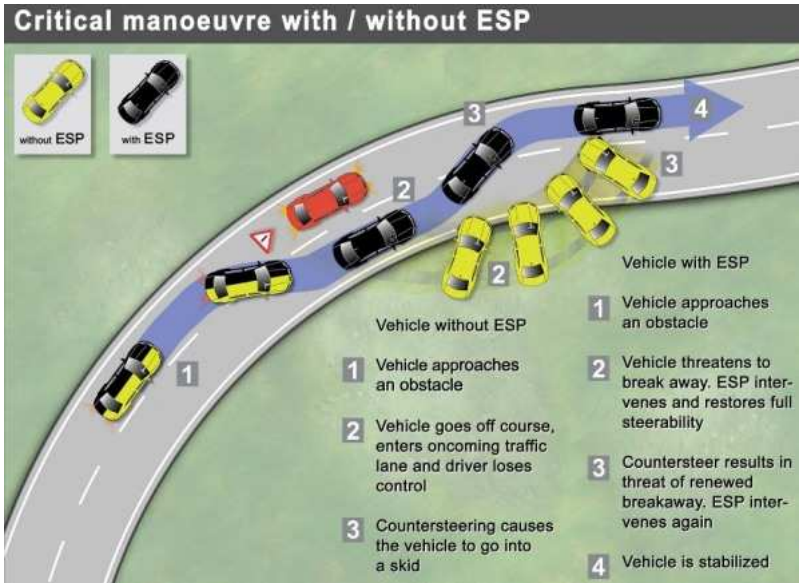

Figure 2.6: Functioning of ESC in critical situation (image from Bosch GmbH).

The acceptability and efficiency of yaw stability controllers have been assessed in studies carried out by the NHTSA[26]. Different data sets and methodologies were used in the studies, which considered accidentology statistics in the USA [Dan04]. Other studies regarding different countries are summarised in [GF05], which includes data from Statistischen Bundesamtes[27], EACS[28], Swedish Road Administration, and Japanese crash data compiled from ITARDA[29]. They have all found typically about 30% reduction in single vehicle crashes due to ESC.

There are mainly three types of actuators for yaw stability control [Raj06a]: The differential braking system applies differential braking between the left and right wheels; The active steering modifies the driver steering angle input adding correction to the wheel steering angles; and the active torque distribution, which uses active differentials and all-wheel-drive technology to independently control the drive torque on each wheel enabling the traction and yaw control.

Each of these types of actuation and some of the important research activities on their development and deployment are presented in the following.

Differential braking

Using differential braking is the most employed technique for yaw stability control under the commercial abbreviated names: ESP (Electronic Stability Program), VDC (Vehicle Dynamics Control), VSA (Vehicle Stability Assist), DSC (Dynamic Stability Control) among others. Such systems typically consist of four wheel speed sensors, yaw rate sensor, steering angle sensor,

[26] National Highway Traffic Safety Administration.
[27] German Government Statistics Office
[28] European Accident Causation Survey
[29] Institute for Traffic Accident Research and Data Analysis

lateral accelerometer, brake pressure sensors. Moreover an electronic control unit is required to compute the control input based on a comparison between the driver input and the response of the vehicle. The actuators are typically solenoid based hydraulic modulators which are available from anti-lock brake (ABS) system [Raj06a].

A more detailed description of the functioning of differential braking for yaw rate stability control is provided in [VZEP95, PUH95], in which a PID controller is used to track a desired yaw rate.

Control techniques for electronic stability systems using differential braking have been a subject of intense research in the last decades.

Gain Scheduled H_∞ control is designed in [OHA+99] to take into account variation of forward velocity and to ensure that the closed loop system satisfies a H_∞ norm condition which guarantees the stability of the vehicle, during the application of distributed brake force on the right and left wheels.

In [TJ05], a vehicle model considering nonlinear lateral and longitudinal tyre forces (Pacejka model) is used. The desired yaw moment is supposed to be given by a higher level controller, and the driver gives the steering input. The control objectives are: primarily to obtain the desired yaw moment; secondly to find the smallest vector of slip angles in order to minimise the use of brakes and avoid reduction of the lateral force. The activation of this controller is based on bounds for the vehicle sideslip angle and yaw rate, considered to be within the vehicle steerability. The controller is computed on the basis of a mp-NLP (multi-parametric Nonlinear Problem). Some simplifications are done in order to reduce complexity. An explicit piecewise linear approximation of the solution was generated using the algorithm in [Joh02a]. Results are shown by simulation.

A Linear Quadratic Regulator (LQR) is used in [ZTHZ06] for the yaw moment controller and sliding mode theory is applied to design the wheel slip controller. The results are presented in simulations for J-turn and lane change as well as practical experiments with degraded road adhesion step inputs on the steering wheel.

Sliding mode theory is also explored in [JYJ+08] for the yaw rate controller which takes into account the vehicle roll stability.

Active steering

Ackermann and co-authors have documented some significant work on active steering systems for yaw control of passenger cars [Ack02]. In such systems the driver is responsible for providing the necessary steering angle to follow a desired path, while the active steering control should be in charge of disturbance attenuation. The additional steering angle from the active steering control may be generated mechanically using a linear actuator or electrically on a steer-by-wire configuration.

Among the advantages of active steering control with respect to the differential braking for yaw stability it can be mentioned that:

- In torque generation from braking, the lever arm corresponds to half of the vehicle track-width while for steering it is approximately half of the wheel base, at approximately two times bigger. As a consequence, the force required to generate torque from steering is approximately half of that required from braking.

- When braking over surfaces with different adhesion condition on the left and right wheels (μ-split), the disturbance torque can be compensated only by reducing the braking force in vehicles equipped with differential braking. However if an active steering controller is

available, the braking effort does not need to be reduced and a counter steering action can be performed to achieve a straight and shorter braking path.

- Braking intervention usually takes place in emergency situations when the vehicle is close to skidding, therefore there is more wear of tyres and brake components and energy dissipated in this action than in steering control which can be performed continuously, attenuating small disturbances and providing more comfort to the passengers.

In the work [Ack97], the controller is obtained by decoupling the driver task from the disturbance attenuation. In other words, the influence of the yaw rate on the lateral acceleration is removed. Since a robust controller with respect to the road adhesion is intended, the lateral tyre forces are considered as a disturbance, and the decoupling is obtained by choosing the position of a point at a distance in front of the centre of gravity, such that the lateral acceleration at this point does not depend on the lateral rear force. The small angle approximations are considered, rendering the yaw rate unobservable from the front tyre slip angle. The stability of the decoupled system is proven by Lyapunov conditions.

Many patents exist for active steering systems, for example [PB02, B$^+$03], based on PI controllers. Research on active steering is also very extensive. Fig. 2.7 shows the architecture of an active steering system.

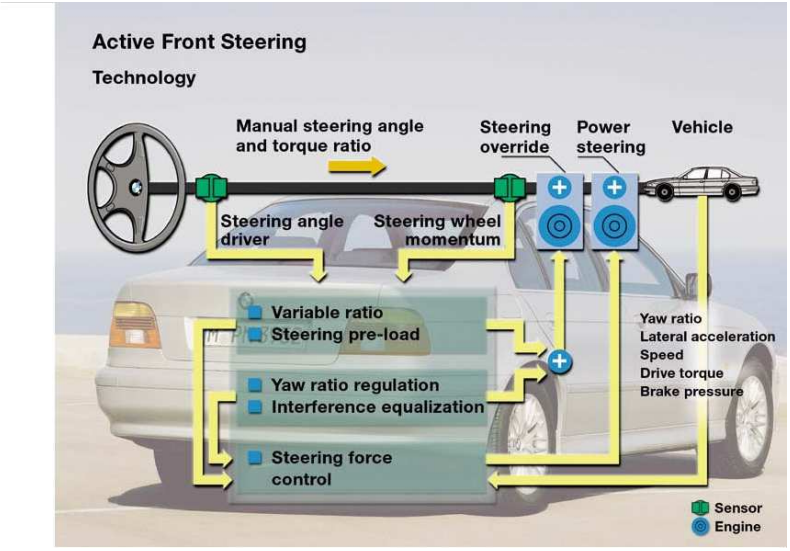

Figure 2.7: BMW active steering system.

The stability analysis of the vehicle lateral dynamics is presented in [OHTD98] showing that the model has a limited stability region which also depends on the driver steering wheel angle, two unstable equilibrium points and a stable one (bifurcation analysis). The authors propose a controller based on linear H_∞ control theory for the design of the front wheel controller.

A feedfoward on the steering action is used in [PHB01]. The proposed active steering system also uses a state feedback controller, based on a linear quadratic regulator, to ensure vehicle stability.

A comparison of two steering assistance systems using Model Predictive Control is described in [KC06]. The first consists of a linear driver steering controller while the second is a nonlinear steering control law based on multiple linearised vehicle and neuromuscular system models. The models are obtained from the linearisation of the nonlinear vehicle dynamics about set values

of front and rear wheel lateral slip. A controller is defined for each of the linearised models, and the control input is computed for all the linear subsystems and a switching function selects the steering controller with the least amount of error between the controller set points and the present vehicle slip angles.

A nonlinear Model predictive control is also applied in [FBA+07] for the front wheel steering assistance, supposing that the computational time could be reduced in order to develop a real-time application. In order to overcome the calculation time of the nonlinear MPC[30], a suboptimal model predictive controller is derived from the successive online linearisation of the vehicle model and computation of a linear MPC for the resulting linear time-varying system is applied. Both controllers are compared in experimental tests.

In [BPK07] a simple rational tyre model is used to preserve vehicle stability in extreme handling situations. A gain scheduled active steering control is designed solving linear matrix inequality (LMI).

Active torque distribution

All-wheel-drive systems, also known as full-time-4-wheel drive systems enable vehicles to operate in 2-wheel drive (either front or rear), and when needed, it automatically shifts to 4-wheel drive and distributes torque to all four wheels independently. This kind of technology enables vehicle handling without necessarily braking, as in the case of differential braking.

Mechanisms like a twin clutch torque biasing differential allow torque to be transferred to the inner and outer wheels at different ratios [SS99], they can be applied with a central differential to transfer torque to the front and rear wheels. Fig. 2.8 shows the torque distribution for oversteering and understeering vehicles negotiating a curve.

The advantages of the all wheel drive using differential torque distribution are also explored in [HWGB05]. An optimal control based on LQR is employed in the design of two feedback loops. The primary feedback loop is used to control the reference model while the second feedback loop compensates for the errors between the reference model and the vehicle.

Another comparison is provided in [OS06] between vehicles equipped with front-wheel-drive with a single open differential, rear-wheel-drive with a single open differential and all-wheel-drive with three open differentials each dividing torque in a 50:50 torque split. The control strategy is based on two parallel PIs, one for the control of the front-rear torque ratio and the other for the left-right torque ratio.

The increase in price and weight are the main drawbacks for larger commercialisation of such systems. On the other hand, with the development of electric driven cars and associated components, research has been dedicated to employment of one electric motor for each wheel [HR03, WWJS11], showing that such a configuration has good potential to enhance vehicle stability.

Combined active steering and differential braking

Work proposing the coordination of combined control actions on differential braking and active steering can also be found in literature.

In [HON99] a 7 DOF model, taking into account pitch and roll motion effects in the normal tyre forces, is used for the yaw rate controller design and coordination of the torque distribution and four-wheel steering. The synthesised controller is based on the nonlinear predictive control

[30] Model Predictive Control

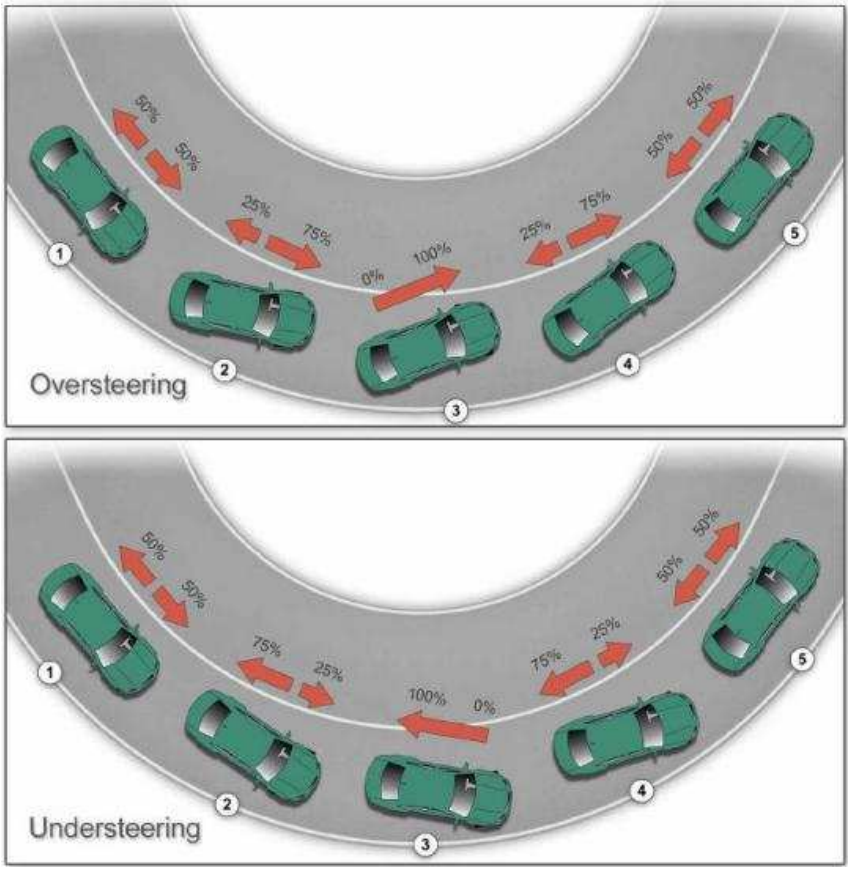

Figure 2.8: Active torque distribution between front and rear wheels for overteering (top) and understeering (bottom) vehicles negotiating a curve (image from [LMSN04]).

for continuous time systems [Lu95], considering a quadratic performance index used to minimise the error between the controlled and predefined trajectory.

Four-wheel steering and four-wheel torque (traction and braking) distribution are also explored by [OHMK06], in which a hierarchical control structure is adopted. The target forces and moments are computed by the first layer, based on the driver inputs from the pedals and steering wheel. A Second layer performs the distribution of the vehicle target motion to each of the wheels, using an algorithm based on Sequential Quadratic Programming to compute the magnitude and direction of each tyre force, considering the radius of friction circle of each tyre in order to maximise each tyre grip margin. The last layer controls each wheel motion.

In [Mam04] linear tyre forces are considered in the vehicle model, and the use of independent wheel braking is used for lane keeping purposes. The controller consists of an internal loop for handling improvement and an external loop for lane keeping assistance. The inner loop has a dynamic feedback controller on yaw rate and a dynamic feedforward controller of the steering angle to both, the tyre steering angle and yaw moment. The outer loop uses a feedback controller of the lateral displacement at look-ahead distance and relative yaw angle. The H_∞ coprime factors based method is used for the synthesis of inner loop feedback. A new vehicle model including this controller is computed and a new H_∞ optimisation is performed for the feedforward term. The outer loop is processed analogously to the inner one. A feedforward term is also used to compensate the road curvature. The results are presented from simulations

including real track data.

In [Aca09] a nonlinear vehicle model is used in which the tyre forces are according to Duggof's tyre model and the effects of roll and pitch motions are taken into account in the normal tyre forces. For the control synthesis, the vehicle model is transformed into a linear structure in the State Dependent Coefficient form. The control inputs are derived by solving the State Dependent Ricatti Equations at each point of vehicle states. Simulations show the performance of the controller on a 14 DOF nonlinear 3D vehicle model.

The lateral tyre forces have been modelled as piecewise affine systems in [BCBT09] for a steer-by-wire active steering controller. The discrete-time piecewise affine model is also converted into an equivalent mixed-logical-dynamics system [HSB01], which is used as a prediction model for the design of a hybrid model predictive controller [BM99] using a mixed integer quadratic program to compute online the coordinated control inputs, the steering angle and vehicle yaw moment (from differential braking).

The work of [PMB10] addresses the same application with a discrete-time piecewise affine model but the controller design takes into account disturbance realisations using set theoretical methods for control synthesis [BM08].

The nonlinear behaviour of the lateral tyre forces is also taken into account in [MBNGO11]. A Takagi-Sugeno model is obtained from the sector approximation of the Pacejka's model for tyre forces. Quadratic boundedness and Lyapunov stability are used to build invariant sets for the trajectories of the controlled system. These constraints are considered in the computation of the output feedback controller casted as a Linear and Bilinear Matrix Inequalities optimisation problem.

2.2.2 Lane departure warning systems

Lane departure warning systems consist of optic sensors (video cameras or infra-red sensor) and an algorithm for the lane detection. When the vehicle is about to leave the lane, without engaging the turning signals (indication of unintended lane departure), a warning is provided to the driver. Some commercialised passenger cars are already equipped with such systems, and the technology involved and warning provided may differ according to the car manufactures. Some detailed information about the existing systems are described in the next sections.

Commercialised lane departure warning systems

Citroën was the first European car manufacturer to introduce a lane departure warning system in the "C4" and "C5" models in 2005. The lanes are monitored by down-looking infra-red sensors and vibrations on the seat are used to warn of the lane departure. This feature is also available in the "C6" and "Peugeot-308" models [Cit]. Audi's lane departure warning systems, introduced in 2007 in the "Q7" model [Aud07], includes a forward-looking camera and the warnings consist of vibrations on the steering wheel.

BMW, GM and Volvo launched their LDWS in 2007 and 2008 on the core technology of "mobileye" [Mob]. It consists of vision based sensors and an algorithm to estimate vehicle position with respect to the lane and the time to lane crossing. The warnings provided to the driver in case of unintended lane departure may consist of sound, indication in the dashboard or vibration on the steering wheel, depending on the car manufacturer. Nowadays the system is available in several models.

2.2.3 Lane keeping assistance

Most of the LKAS present also the feature of warning of the lane departure by audible, visual or haptic means. Moreover, there is an electric powered steering system that provides part of the steering torque in order to keep the vehicle in the lane or delay its departure. The steering task is usually shared with the driver and his/her actions are prioritised over the automatic steering torque. For this reason, the assistance is gradually reduced or cut-off after a few seconds if the driver does not react. The following section presents an overview of the commercialised LKAS, which are in general conceived for situations of low lateral accelerations.

Commercialised lane keeping assist system

Nissan introduced the first lane keeping assistance system in commercialised vehicles in 2001 for the model "Cima" sold in Japan [IVs01]. The system is designed for roads with small curvature and it acts simultaneously with the driver, gradually reducing its contribution if the driver is not active. Such strategy enables the driver to be assisted but does not take over his/her responsibility from the steering task. The system architecture consists of a CCD video camera, steering actuator and an electronic control unit. The vehicle position on the lane and road geometry are estimated by the camera, and this information is used by the electronic control unit along with vehicle velocity and steering angle to compute the steering torque needed to keep the vehicle in the lane. Tone warning and vibrations on the steering wheel are triggered when the vehicle is about to depart from the lane. The steering control assistance delays the departure while the driver is expected to retake the control of the vehicle. The control is automatically suspended if the driver steers in the opposite direction. The same concept was introduced for the "Infinity FX" model in 2004 in the American market [Val04].

A similar strategy was implemented by Toyota in the "Crown Majesta" model in 2004 in Japan, which evolved in 2006 with the Lexus model "LS 460" using stereo cameras and more sophisticated object and pattern recognition [ABL07], which is also available in the European market.

A lane keeping assist system was launched by Honda in 2004 for the "Inspire" model. The system [Iih04] works together with an ACC and uses a C-MOS camera mounted above the interior rear view mirror for lane detection and trajectory planning. The assistance provides 80% of the steering torque, reducing the driver's burden on roads with a curvature radius above 230 $[m]$, vehicle speed between 65 $[km/h]$ and 100 $[km/h]$ and lateral acceleration below $0.2g$ (g is the gravitational acceleration 9.8 $[m/s^2]$), typically a motorway environment. The driver must remain attentive and he/she is responsible for providing the remaining torque for correct steering.

It can be noticed that the currently commercialised assistance systems to avoid lane departure are not adequate for situations of strong lateral solicitation. Fig. 2.9 provides a classification of the described driving assistance systems for lateral control in terms of usage scenarios concerning safety and comfort aspects, as well as the use of proprio- and exteroceptive signals. It can be noticed that the ESC are very efficient in demanding manoeuvres in term of lateral solicitation, however it is not capable of perceiving the vehicle environment. On the other hand, systems such as LKAS, LDW and LCA, which are also characterised as active safety, are more oriented to the passengers comfort and may not be so efficient when harsh direction changes are required. The proposal of integrating the proprio- and exteroceptive signals into the same ADAS, named *Perceptive-ESC* , may enlarge the usage scenarios as illustrated in the this figure.

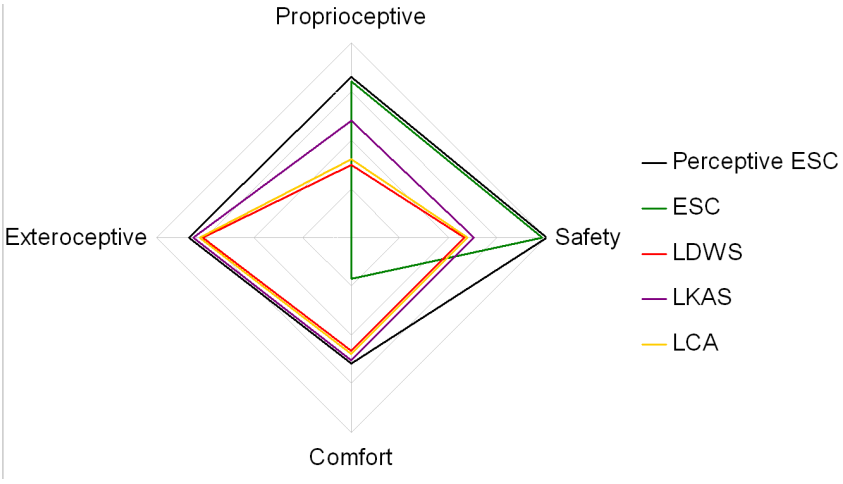

Figure 2.9: Classification of ADAS for lateral guidance.

2.2.4 Control strategies for lane keeping

Some strategies for controlling the vehicle dynamics and positioning are based on yaw rate controllers. The desired yaw rate is not computed based on the driver input but on the information acquired from the environment using the video sensor. It is the case of [MSON09] in which a nested control scheme is used. An outer loop consisting of a PIID (Proportional, double Integrator and Derivative) on the lateral offset and the reference model generates the desired yaw rate, which is tracked by a PI controller based on the yaw rate tracking error.

Similarly, in [Mam04] an outer loop uses the feedback controller of the lateral displacement at look-ahead distance and the relative yaw angle. The feedback controller is synthesised using H_∞ coprime factors. The resulting steering angle is added to the driver input, which feeds the internal loops for controlling the vehicle dynamics.

These two works are based on linear models of the tyre lateral forces therefore their performance in situations of strong lateral acceleration could not be shown.

The active steering controller from [FBA+07] is applied in an autonomous vehicle system, under the assumption that a trajectory planning system is available to provide the reference yaw rate, so that the desired trajectory is known over a finite horizon enabling the employment of MPC theory. Although a nonlinear model of the lateral tyre force is used in this case, the experimental tests could only be performed at low speed, due to the computational burden of the nonlinear MPC. The authors propose an approximation by using a linear parameter variant (LPV) model, which is able to overcome the computational burden, having the performance slightly degraded. Nevertheless, there is still the limitation that the trajectory planning system depends on measurements of the vehicle coordinates obtained from a differential GPS and on the cartography of the road.

Other control strategies for controlling the vehicle positioning which does not directly involve the tracking of a reference yaw rate, can be found in the literature.

In [WCP+08], the implementation of a lateral controller aided by vision system to avoid lane departure is described. In order to support human like driving behaviour, a Fuzzy Gain Scheduling (FGS) strategy is proposed for the steering control. It compensates for static feedback control and adjusts the steering effort by considering the lateral offset and instantaneous speed of the vehicle. Crossover model principle is applied to examine the utility of the designed controller.

Practical experiments were used to confirm results. Bicycle model was used to describe vehicle lateral dynamic. Road curvature is considered as noise to the system.

A combined automated lane keeping and drivers steering through a two degree-of-freedom closed-loop control strategy is presented in [CMR09] . In this implementation there is no on/off switching and the automated lane keeping control-loop is never opened. The driver has control over the manoeuvres, but the automated lane keeping brings the vehicle back to the centre of the lane when there is no driver steering action. The details of the lane keeping controller are described in [CR03]. The design of a lane keeping (lateral displacement tolerance of 0.2m from centreline) controller for typical highway conditions is addressed in this paper. The single input is the steering angle and a vision system provides the measurements of lateral displacement and angular orientation of the vehicle with respect to the centreline. The SITO control problem is implemented by solving a SISO disturbance attenuation problem, formulated in the $H_{\infty/\mu}$ framework in the presence of uncertain parameters. Tests conducted showed that the SISO controller was able to fulfil the specifications.

A comparison of four controllers implemented at LIVIC[31] is presented in [CSNM04]. The controllers are based on output feedback self-tuning, H_∞, Fuzzy logic and Proportional. They are applied on a vehicle linearised single track model, with the purpose of having zero error on lateral displacement at look-ahead distance using steering angle as input. Each controller was simulated on the testing track with curvature varying from zero to 0.025 $[m^{-1}]$, under the circumstances: variation of adherence coefficients, variation of longitudinal speed and wind introduction. Results show that the proportional controller presented systematically the largest errors. The self-tuning regulator has the best results, although it is the most difficult to implement in real life. Fuzzy and H_∞ have similar performances.

It can be noticed that the proposals from these three last references [WCP+08, CMR09, CSNM04] are also based on a linear vehicle model, and designed for typical motorway scenarios in which strong lateral accelerations are not required to negotiate the curves.

The control synthesis for lane keeping system based on Lyapunov techniques are discussed in the sequel.

Lyapunov based control synthesis

The lateral control approach based on potential field from the robots displacement theory has been explored by the authors in [GR01]. They proposed an artificial potential field linked to the lane, such that the corresponding energy is zero at the centre of the lane and it increases as the position moves to the lane edges. The authors extend the same concept in [RG06], introducing a degree of look-ahead along the roadway into the controller, which enables the decoupling of the lateral and longitudinal dynamics such that the last is removed from the bounding process. The controller is synthesised following a Lyapunov based bounding technique, which ensures maximal lateral displacements even in the presence of time varying disturbances. The need of measurements from a differential GPS with 2 antennas and a cartography of the desired path is one of the main limitations of this system.

Control synthesis for lane keeping assist systems based on Lyapunov quadratic functions and formulated as LMI or BMI optimisation problems are explored in the thesis [ME08]. The quadratic Lyapunov function is used to construct minimal ellipsoidal invariant sets that approximate externally the reachable set of the closed loop system. Additional constraints are used to limit the control input from the state feedback structure, and to ensure that a "normal driving

[31] Laboratoire sur les Interactions Véhicules-Infrastructure-Conducteurs

zone" is included in the invariant set. Different activation strategies are proposed, considering the driver awareness.

A lane keeping assistance designed in [MENML09] for roads with relatively small curvature uses LMI optimisation to create the invariant set. In [MELMN09] road curvatures are taken into account in the control synthesis casted as a BMI optimisation problem. Moreover a control strategy with feed-forward on the road curvature is also proposed. Composite Lyapunov functions are used in [MEMNL10] in order to obtain an invariant set that is closer to the polytopic normal driving zone.

In these works, only the linear domains of the tyre lateral forces are taken into account, and the tests are performed at situations of relatively small lateral acceleration.

In [MEMGL10] the authors proposed a control strategy to use simultaneously front wheel steering and differential braking as control inputs. These are computed by full state feedback with feedforward terms, designed to track a H_∞ performance index of a yaw rate reference model. The control synthesis is casted as a BMI optimisation problem to minimise a Lyapunov based invariant set in order to ensure boundedness of the state trajectories during the assistance intervention. Simulation results shown that the integrated control active steering and differential torque can handle the tyre force saturation, enhancing the vehicle stability. However the nonlinear behaviour of the tyre forces are not treated explicitly in the control synthesis, since it is based on a linear single track model.

A possibility to take into account the nonlinear behaviour of the lateral tire forces is proposed in [MMEG$^+$10] using a Takagi-Sugeno model. A parallel distributed controller is designed for the lane keeping. The simulation results show that this control structure can handle well the tyre force nonlinearities, however it requires estimation algorithms to obtain the wheel sideslip angles.

As it can be noticed the development of assistance systems for lane departure avoidance which take into account the lateral tyre force saturation is still an open topic for research.

2.3 Conclusion

In this chapter the main agents of road intelligent transportation systems have been presented as well as the major projects carried out in this field. The vision and objectives of the projects over the years have changed. It has been shown that the first ITS projects, as PROMETHEUS and PATH, required major investments in the infrastructure therefore the developed concepts have not been implemented in production series. In the late 90's, some research was devoted to develop a fully automated cars, as in the ARGOS project. However, more recent projects, such as PReVENT-IP and AKTIV, consider the interaction of the driver, vehicle and environment and effort has been concentrated on developing solutions that could be implemented in short-term. The latest projects, such as HAVEit, present solutions consisting of highly automated systems to intervene in dangerous situations or in tedious tasks during which the driver may loose attention. Moreover the most recent projects envisage contributions which can be deployed in short-term, therefore they are based on technologies which are already commercially available so that the public can benefit from them.

The technological advances have allowed significant increase in the electronics of the vehicles, with more sensors and computing units, such that active safety system like ABS in the end of the 80's and ESC in 1997 became regular in production series. Due to their effectiveness ABS became mandatory in all production vehicles in some markets and discussions are on-going to do the same with ESP.

More recently, in 2001 lateral control assistance was introduced in the Japanese market and later in 2005 in the European market as a lane departure warning system. It has been shown that these systems have been evolving, and car manufacturers are increasingly offering such driving assistance systems in their models.

It can also be noticed that these systems are designed such that the driver is always responsible for the control of the vehicle. The lane keeping systems are conceived to temporarily correct the vehicle trajectory, or provide part of the steering torque, but these input signals fade away if the driver does not react. Moreover, the current research developed in this field and commercialised lane keeping systems operate only in relatively gentle lane departures, being inefficient or even inactive when demanding direction changes are required.

The same limitation has been encountered in the bibliography review on vehicle lateral control. Since most of the proposals are based on linear models for the lateral tyre forces and designed for typically motorway scenarios, the assistance systems are not able to handle strong lateral solicitations. Although some proposals exist using models that cover the whole domain of lateral tyre force, their application is still limited either by the computational burden or dependency on high cost equipment.

Driver steering assistance systems, that are capable of avoiding lane departure even in strong lateral solicitation can be developed by the integration of the efficient safety aspects from ESC for demanding manoeuvres, with the monitoring of the environment and driver awareness, existing in the currently commercialised lateral assistance systems. For that, adequate models are required to take into account the nonlinear behaviour of the lateral tyre forces. One possibility to take into account the nonlinearities is through the use of piecewise affine systems, which is introduced in the next chapter with the main theoretical tools used in the development of lateral assistance systems.

Part II

Lyapunov based system control theory and vehicle model

Chapter 3

Theoretical background for system control

Contents

This chapter summarises the theoretical tools used in the design of the proposed driving assistance systems. Firstly, dynamic systems of differential equations are defined, followed by the concept of stability analysis based on Lyapunov functions. Such analysis and control synthesis are usually casted as optimisation problems involving Linear or Bilinear Matrix inequalities (LMI and BMI), therefore some important definitions involving convex optimisation as well as the definitions of LMI and BMI are presented in the third section.

An overview of Hybrid systems, and its class called Piecewise Affine (PWA) systems is detailed in the fourth section, while the last one presents the theoretical tool for Lyapunov based analysis and control synthesis for this class of systems.

3.1 Continuous dynamic systems

Definition 3.1.1 (Continuous dynamic system) *A continuous dynamic system is characterised by the differential equation*

$$\begin{cases} \dot{x}(t) = f(x(t), u(t), w(t)) \\ y(t) = h(x(t), u(t), w(t)), \quad t \in T \subset \mathbb{R}^+, \end{cases} \tag{3.1}$$

where $x \in \mathbb{R}^n$ represents the state vector. The system input consists of the control input $u \in \mathbb{R}^{n_u}$ and the exogenous input $w \in \mathbb{R}^{n_w}$. The exogenous input may represent a disturbance, a reference input or a noise that affects the system. The system output is described by the vector $y \in \mathbb{R}^{n_y}$, and $f : \mathbb{R}^{n+n_u+n_w} \to \mathbb{R}^n$ and $h : \mathbb{R}^{n+n_u+n_w} \to \mathbb{R}^{n_y}$ are continuous vector fields.

Definition 3.1.2 (Continuous dynamic system trajectory) *The trajectory of the continuous dynamic system* (3.1)*, is a continuous function, $\xi_x : T \to \mathbb{R}^n$, such that ξ_x is a solution of equation* (3.1) *for the initial condition $x(t_0) = x_0$, and known $u(t)$ and $w(t)$.*

Definition 3.1.3 (Linear continuous dynamic system) *A linear continuous dynamic system is described by:*

$$\begin{cases} \dot{x}(t) = A(t)x(t) + B_u(t)u(t) + B_w(t)w(t) \\ y(t) = C(t)x(t) + D_u(t)u(t) + D_w(t)w(t), \quad t \in T \subset \mathbb{R}^+, \end{cases} \tag{3.2}$$

where $A(t) \in \mathbb{R}^n$ is the system dynamics matrix, $B_u(t) \in \mathbb{R}^{n \times n_u}$ is the control input matrix, $B_w(t) \in \mathbb{R}^{n \times n_w}$ is the perturbation or reference matrix, $C(t) \in \mathbb{R}^{n_y \times n}$ is the observation matrix, and $D_u(t) \in \mathbb{R}^{n_y \times n_u}$ and $D_w(t) \in \mathbb{R}^{n_y \times n_w}$ are the transfer matrices from the input and perturbation to the outputs.

If the matrices describing the linear continuous dynamic system (3.2) are constant, then the system is called linear-time-invariant and it is represented by:

$$\begin{cases} \dot{x}(t) = Ax(t) + B_u u(t) + B_w w(t) \\ y(t) = Cx(t) + D_u u(t) + D_w w(t), \quad t \in T \subset \mathbb{R}^+. \end{cases} \tag{3.3}$$

Having defined the dynamic systems, some theoretical tools for the stability analysis are described in the subsequent section.

3.2 Lyapunov Stability

Lyapunov introduced in the late years of the 19th century a significant contribution to the stability analysis of dynamic systems.

Considering an autonomous system:

$$\dot{x}(t) = f(x(t)),\ t \in \mathbb{R}^+, \tag{3.4}$$

its equilibrium points can be defined as:

Definition 3.2.1 (Equilibrium points) *A state x_{eq} is an equilibrium point of the system, if once $x(t_0) = x_{eq}$, the system trajectory remains constant for all $t \in [t_0, \infty)$. For autonomous systems as in* (3.4)*, the equilibrium points are the solutions of $f(x(t)) = 0$.*

The definition of Lyapunov stability of the equilibrium point follows:

Definition 3.2.2 (Lyapunov stability) *An equilibrium point x_{eq} is said to be:*

- *Lyapunov stable if for every $\epsilon > 0$, there exists $\delta(\epsilon) > 0$, such that*

$$||x(0) - x_{eq}|| < \delta \Rightarrow ||x(t) - x_{eq}|| < \epsilon, \ \forall t \geq 0 \tag{3.5}$$

- *Unstable, if it is not stable,*
- *Asymptotically stable, if it is stable and δ can be chosen such that*

$$||x(0) - x_{eq}|| < \delta \Rightarrow \lim_{t \to +\infty} x(t) = x_{eq}, \tag{3.6}$$

if the system convergence is bounded by an exponential decay, the equilibrium point is said to be exponentially stable.

Remark 3.2.1 (Exponential stability for linear time-invariant systems)

Based on this stability concept, the following theorem has been developed:

Theorem 3.2.1 (Lyapunov stability theorem) *Considering $x_{eq} = 0$ an equilibrium point of system (3.4) and $\mathcal{D} \in \mathbb{R}^n$ a set containing the origin. Considering $V(x) : \mathcal{D} \to \mathbb{R}$ with continuous first order derivative, such that:*

$$\begin{gathered} V(0) = 0 \text{ and } V > 0, \forall x \in \mathcal{D} - \{0\} \text{ (V is positive definite)} \\ \dot{V}(x) \leq 0, \forall x \in \mathcal{D} \end{gathered} \tag{3.7}$$

Then, the equilibrium point $x_{eq} = 0$ is locally stable. Moreover, if,

$$\dot{V}(x) < 0, \forall x \in \mathcal{D} - \{0\} \tag{3.8}$$

then, the equilibrium point $x_{eq} = 0$ is asymptotic stable.

If the set $\mathcal{D}$ corresponds the whole state space $\mathbb{R}^n$ then, the stability is said to be global.

The function V that satisfies the conditions (3.7) is called Lyapunov function.

Remark 3.2.2 (Coordinate change to place equilibrium point) *Theorem 3.2.1 is stated for an equilibrium point located at the origin, nevertheless if $x_{eq} \neq 0$ for system (3.4), it is always possible to perform a coordinate change $z = x - x_{eq}$, to obtain an equivalent system:*

$$\dot{z} = f(x) = f(z + x_{eq}) \stackrel{\Delta}{=} g(z) \tag{3.9}$$

in which the solution of $g(z) = 0$ is $z_{eq} = 0$.

It is important to note that satisfying conditions (3.7), and therefore the existence of a Lyapunov function, is a sufficient condition to prove the stability of a dynamical system. On the other hand, being unable to find a Lyapunov function does not necessarily imply that the system is unstable.

Even though a Lyapunov function can often be constructed from conservation laws for many dynamic systems, a general method for constructing a Lyapunov function for nonlinear autonomous systems is still an open field of research. Often, quadratic forms for Lyapunov function candidates are used in the control discipline [BGFB94].

3.2.1 Quadratic Lyapunov function

Before defining the quadratic function, the definition of an important property of matrices is presented:

Definition 3.2.3 (Positive definite matrix) *A symmetric matrix $A \in \mathbb{R}^{n\times n}$ is said to be positive definite, represented by $A \succ 0$, if $v^T Av > 0$ for all $v \in \mathbb{R}^n - \{0\}$. A is said to be positive semi-definite, denoted by $A \succeq 0$ if the inequality is not strict ($v^T Av \geq 0$)*

A matrix $A \in \mathbb{R}^{n\times n}$ is negative definite if $-A \succ 0$. Analogously, it is negative semi-definite if $-A \succeq 0$

A positive definite quadratic function can be now defined as follows:

Definition 3.2.4 (Positive definite quadratic function) *The function $V : \mathbb{R}^n \to \mathbb{R}$ is a positive definite quadratic function if:*

$$V(x) = x^T Px, \text{ with } P \in \mathbb{R}^{n\times n},\ P = P^T, \text{ and } P \succ 0. \tag{3.10}$$

Since P is positive definite, the function $V(x)$ is positive and radially unbounded, therefore it can be used as a Lyapunov function candidate. If the second condition in (3.7) (*i.e.* $\dot{V}(x) < 0$) holds, then V(x) is a quadratic Lyapunov function.

For the linear time-invariant systems ($\dot{x} = Ax$), the existence of a quadratic Lyapunov function is not only a sufficient condition to prove the stability, it is a necessary condition.

Lemma 3.2.1 (Existence of a quadratic Lyapunov function) *Considering a linear autonomous time invariant system $\dot{x} = Ax$, $x \in \mathbb{R}^n$, $A \in \mathbb{R}^{n\times n}$. If A is Hurwitz, there exists a unique solution to the Lyapunov equation:*

$$A^T P + PA = -Q \tag{3.11}$$

for any Q definite positive, and the solution is:

$$P = \int_0^\infty e^{A^T t} Q e^{At} dt \tag{3.12}$$

Moreover, as Q is positive definite ($Q \succ 0$), so is P ($P \succ 0$).

3.2.2 Invariant sets

Invariant sets correspond to important properties, frequently used in the control discipline to draw conclusions on the asymptotic stability of dynamical systems. The definition of an invariant set can be expressed as:

Definition 3.2.5 (Invariant set [SL$^+$91]) *A set $\mathcal{S}$ is said to be invariant for a dynamical system if every system trajectory that starts from a point in $\mathcal{S}$ remains in $\mathcal{S}$ for all future time.*

It can be inferred that the equilibrium point of a dynamic system is an invariant set, as well as its domain of attraction. The following theorem allows the study of convergence of dynamical systems to cases more general than the equilibrium point.

Theorem 3.2.2 (Invariant set theorem [SL$^+$91]) *Consider an autonomous system of the form (3.4), with f continuous, and let $V(x) : \mathcal{D} \to \mathbb{R}$ with continuous first order derivative. Assume that:*

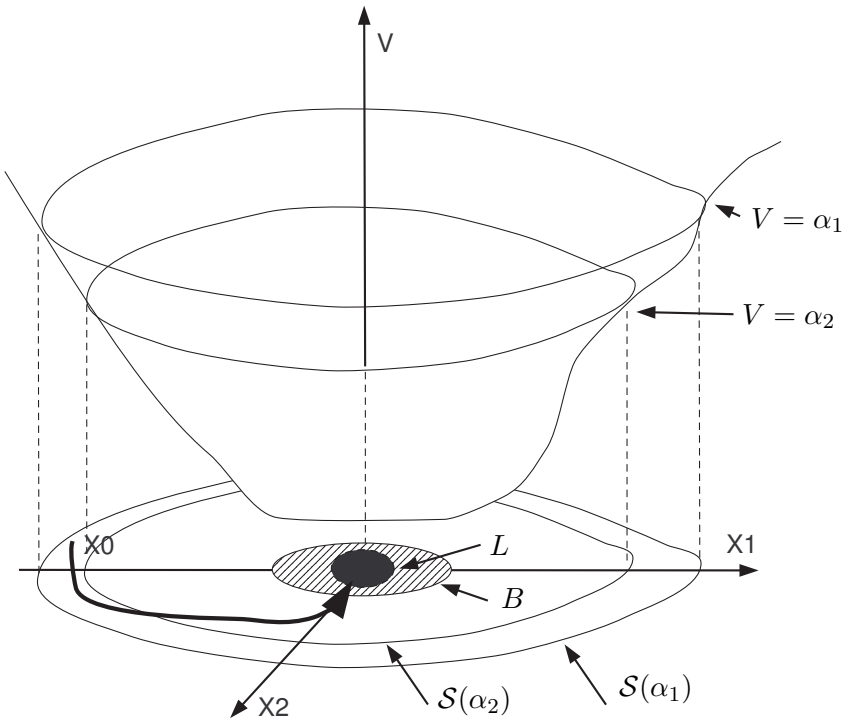

Figure 3.1: Convergence of the system trajectory to the invariant set L from the level curves of a Lyapunov function.

- *for some* $\alpha > 0$*, the region* $\mathcal{S}(\alpha) = \{x \in \mathcal{D} : V(x) < \alpha\}$ *is bounded.*

- $\dot{V}(x) \leq 0$ *for all* $x \in \mathcal{S}(\alpha)$

Let B *be the set of all points within* $\mathcal{S}(\alpha)$ *where* $\dot{V}(x) = 0$*, and* L *be the largest invariant set in* B*. Then every solution* $x(t)$ *originating in* $\mathcal{S}(\alpha)$ *tends to* L *as* $t \to \infty$*.*

The level curves of a Lyapunov function are invariant sets, described as $\mathcal{S}(\alpha) = \{x \in \mathcal{D} : V(x) \leq \alpha\}$, for $\alpha \in \mathbb{R},$. Considering the invariant set $\mathcal{S}(\alpha_1)$ obtained from the level curve of a Lyapunov function at $t = t_1$. From the definition of an invariant set (3.2.5) every trajectory starting in $\mathcal{S}(\alpha_1)$ does not leave this set. Since the Lyapunov function $V(x)$ decreases along time (*i.e.* $\dot{V}(x) < 0, \forall x \in \mathcal{D} - \{M\}$), the trajectories starting from $\mathcal{S}(\alpha_1)$ converge to a set $\mathcal{S}(\alpha_2)$ at $t = t_2$ for $t_2 \geq t_1$ and $\mathcal{S}(\alpha_1) \subset \mathcal{S}(\alpha_2)$.

Fig. 3.1 illustrates the geometrical interpretation of theorem 3.2.2 for a second order system. It also shows the convergence of the system trajectory to the concentric invariant sets obtained from the Lyapunov level curves.

If the set L corresponds to the equilibrium point, the system is asymptotically stable.

The computation of invariant sets and Lyapunov functions is often casted as LMI and BMI optimisation problems. The main definitions and concepts involving these optimisations are detailed in the next section.

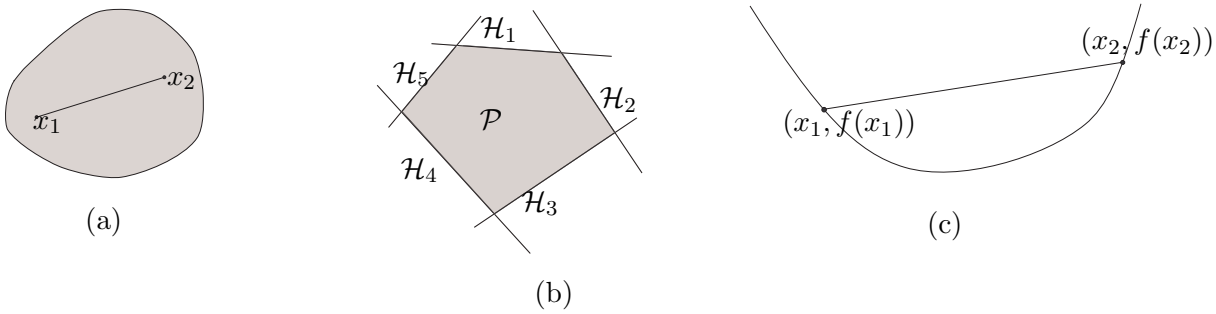

Figure 3.2: (a) Convex set, (b) Polytope and (c) Convex function

3.3 Linear and Bilinear matrix inequalities

As in a great variety of control problems, the algorithms used in the design of the proposed driving assistance systems are based on convex optimisation problems.

The optimisation problems often involve various constraints, which can be expressed as linear matrix inequalities (LMI). This concept was first introduced in the analysis of dynamical systems by the work of Lyapunov from the 1890's, discussing the stability of linear continuous dynamical systems. These LMIs can be solved analytically by solving a set of linear equations.

Historically, other important advances of the use of LMI in control engineering appear in the work of Luré (1940's) applying Lyapunov's method to a practical control problem of small order that could still be solved "by-hand", and later in the 1960's with the contributions of Yakubovich, Popov and Kalman that proposed graphical criteria (which is nowadays called positive-real lemma) for the solution of the LMI from Luré's problem.

By the 1970's an alternative solution for the LMIs in the positive-real lemma without the graphic methods for the LMIs could be employed solving a certain Riccati equation. In the next decade, it was observed that optimisation problems involving LMI constraints could be formulated as convex optimisation problems and solved by an algorithm that guaranteed to solve the problem [PS82]. Later on, interior-point algorithms were developed, solving linear (convex) programs in polynomial-time [NN94].

Although there is in general no analytical solution for convex optimisation problems, very efficient methods have been developed to solve them. Another advantage of convex optimisation is the property that if a local optimal solution, subjected to convex constraints, is found, then in fact it is the global optimal. Therefore it is largely employed in many fields, and frequently used in control synthesis.

The main notions of convexity are introduced in this section, followed by definitions of the convex optimisation problems involving LMIs and BMIs.

3.3.1 Convexity notions

Definition 3.3.1 (Convex set) *A set $\mathcal{C}$ is convex if the line segment between any two points in $\mathcal{C}$ lies in $\mathcal{C}$, i.e., if for any x_1, $x_2 \in \mathcal{C}$ and any γ with $0 \leq \gamma \leq 1$, the point $\gamma x_1 + (1-\gamma)x_2 \in \mathcal{C}$.*

Fig. 3.2 (a) illustrates a convex set for $\mathbb{R}^2$.

Property 3.3.1 (Intersection of convex sets) *The intersection of convex sets is also convex, i.e, if $\mathcal{C}_1$ and $\mathcal{C}_2$ are convex set, then $\mathcal{C} = \mathcal{C}_1 \cap \mathcal{C}_2$ is convex.*

Definition 3.3.2 (Hyperplane) *A hyperplane is a set of the form:*

$$\mathcal{H} \triangleq \{x \in \mathbb{R}^n : h^T x = g\} \tag{3.13}$$

with $h \in \mathbb{R}^n$, $h \neq 0$ and $g \in \mathbb{R}$.

A hyperplane divides $\mathbb{R}^n$ into two halfspaces. The halfspace is defined as follows:

Definition 3.3.3 (Halfspace) *A halfspace is a set of the form:*

$$\mathcal{H}_s \triangleq \{x \in \mathbb{R}^n : h^T x \leq g\}. \tag{3.14}$$

Having defined the hyperplanes and halfspaces, the polyhedron can be defined.

Definition 3.3.4 (Polyhedron) *A polyhedron is defined as solution of a finite number of linear equalities and inequalities:*

$$\mathcal{P} \triangleq \{x \in \mathbb{R}^n : h_i^T x \leq g_i,\ i = 1, ..., p\ \ h_j^T x = g_j,\ j = 1, ..., q\} \tag{3.15}$$

A polyhedron is the intersection of a finite number of halfspaces and hyperplanes, therefore polyhedra are convex sets (see Property 3.3.1). When a polyhedron is bounded it is called polytope.

Fig. 3.2 (b) shows a polytope in 2-D constructed by the intersection of 5 halfspaces.

Definition 3.3.5 (Ellipsoid) *An ellipsoid is a convex set of the form:*

$$\epsilon(P, x_c) \triangleq \{x \in \mathbb{R}^n : (x - x_c)^T P (x - x_c) \leq 1\} \tag{3.16}$$

where $P \in \mathbb{R}^{n \times n}$, $P = P^T$ (symmetric matrix), and $x_c \in \mathbb{R}^n$

The vector x_c determines the centre of the ellipsoid and the matrix $Q = P^{-1}$ determines its shape. The length of the semi-axes are given by the square-root of the eigenvalues of Q, and the direction of the semi-axes are given by the eigenvectors of Q.

This description of an ellipsoid corresponds to the image of a unit ball under affine mapping. Similarly, an ellipsoidal set can be described by

$$\epsilon = \{x \in \mathbb{R}^n : ||Ex + f|| < 1\} \tag{3.17}$$

The conversion of description (3.16) to (3.17) is obtained by:

$$E = P^{-1/2}, \qquad f = -Ex_c \tag{3.18}$$

When E is singular, the set in (3.17) is called degenerated ellipsoid, and the dimension of f corresponds to the rank of E. Degenerated ellipsoids are also convex.

Remark 3.3.1 (Quadratic Lyapunov function and ellipsoidal invariant set) *If $V(x) = x^T P x$ is a quadratic Lyapunov function for an autonomous system of the form* (3.4)*, then the corresponding level curves are ellipsoidal invariant sets, as follows:*

$$\mathcal{S}(\alpha) = \epsilon\left(\frac{1}{\alpha}P, 0\right) = \{x \in \mathbb{R}^n : V(x) = x^T \left(\frac{1}{\alpha}P\right) x \leq 1\} \tag{3.19}$$

Definition 3.3.6 (Convex function) *A function $f : \mathbb{R}^n \to \mathbb{R}$ is convex if its domain (denominated $\mathcal{D}_f$) is convex and if for all $x, y \in \mathcal{D}_f$ and γ with $0 \leq \gamma \leq 1$ the inequality*

$$f(\gamma x + (1-\gamma)y) \leq \gamma f(x) + (1-\gamma)f(y) \tag{3.20}$$

holds.

Geometrically, this inequality means that the line segment between $(x, f(x))$ and $(y, f(y))$, which is the chord from x to y, lies above the graph of f (fig. 3.2-(c)).

Definition 3.3.7 (Affine function) *A function $f : \mathbb{R}^n \to \mathbb{R}^m$ is affine if it is a sum of a linear function and a constant, i.e., it has the form $f(x) = Ax + b$, $A \in \mathbb{R}^{m \times n}$ and $b \in \mathbb{R}^m$.*

For an affine function, the equality (3.20) always holds, so all affine functions are convex.

3.3.2 Convex optimisation problem

Definition 3.3.8 (Convex optimisation problem) *A convex optimisation problem is described as*

$$\begin{array}{lll} \textit{minimise} & f_0(x) & \\ \textit{subject to} & f_i \leq 0 & i = 1, ..., p \\ & g_j(x) = 0 & j = 1, ..., q, \end{array} \tag{3.21}$$

where $f_0, ..., f_p$ and $g_j(x)$ for $j = 1, ..., q$ are convex functions.

Equivalently, the problem consists of finding an x that minimises $f_0(x)$ among all x that satisfy the inequality conditions (constraints) $f_i(x) \leq 0$, with $i = 1, ..., p$, and the equality conditions (constraints) $g_j(x) = 0$, for $j = 1, ..., q$. $x \in \mathbb{R}^n$ is the optimisation variable and the function $f_0 \in \mathbb{R}^n$ is the objective function or cost function. If there are no constraints the problem (3.21) is said to be unconstrained.

Remark 3.3.2 (Feasibility problem) *A feasibility problem consists of finding at least one solution of the optimisation variable (not necessarily an optimal solution) that satisfies the constraints.*

A fundamental property of convex optimisation problems is that:

Property 3.3.2 (Solution of convex optimisation problem) *Any locally optimal point is also globally optimal.*

Having defined the convex optimisation problems, the class of constraints involving linear matrix inequalities can be described.

3.3.3 Convex optimisation problem involving LMI

Definition 3.3.9 (Linear matrix inequalities (LMI)) *A linear matrix inequality (LMI) has the form:*

$$F(x) \triangleq F_0 + \sum_{i=1}^{p} x_i F_i \succ 0, \tag{3.22}$$

where $x_i \in \mathbb{R}^m$ are called decision variables, and the matrices $F_i \in \mathbb{R}^{n \times n}$ are symmetric (i.e., $F_i = F_i^T$).

Example 3.3.1 (Search of Lyapunov function for Linear time-invariant system)
Considering a linear time invariant system $\dot{x} = Ax$, a Lyapunov function candidate can be $V(x) = x^T Px$. Writing the Lyapunov conditions, the problem becomes:

$$\begin{array}{ll} \textit{find:} & P = P^T \\ \textit{subject to:} & P \succ 0 \\ & A^T P + PA \preceq 0 \end{array} \tag{3.23}$$

According to Lemma 3.2.1, when A is Hurwitz, there always exists a quadratic Lyapunov function for a linear time invariant system $\dot{x} = Ax$. This lemma ensures the feasibility of the LMI problem (3.23) *for a Hurwitz matrix A.*

Several solvers are available for solving LMIs on Matlab, such as *LMIlab* [Mat11] contained in the robust control toolbox, or the freely distributed *SeDuMi* [Pol]. Modelling languages such as *Yalmip* [Löf04] and CVX [GB11] (both freely distributed) are also available and are very useful to convert the optimisation problems into a computing language.

Often the constraints describing an optimisation problem are nonlinear. Schur's lemma can be used to convert some nonlinear convex constraints into LMIs. When the constraints are strict inequalities, the Schur's lemma can be described as:

Lemma 3.3.1 (Schur's Lemma) *Considering the symmetric matrices $Q(x)$ and $R(x)$, the matrix $S(x)$ that depend affinely in x. The constraints*

$$R(x) \succ 0, \qquad Q(x) - S(x)R(x)^{-1}S(x)^T \succ 0, \tag{3.24}$$

is equivalent to the LMI:

$$\begin{bmatrix} Q(x) & S(x) \\ S(x)^T & R(x) \end{bmatrix} \succ 0 \tag{3.25}$$

Testing the feasibility of convex quadratic constraints can also be expressed as LMIs, using the S-procedure:

Lemma 3.3.2 (S-Procedure) *Considering quadratic functions $\zeta_i(x) : \mathbb{R}^n \to \mathbb{R}$ for $i = 0, ...g$, such that:*

$$\zeta_i(x) = x^T P_i x + 2v_i^T x + c_i,\ P_i \in \mathbb{R}^{n\times n},\ P_i = P_i^T, v_i \in \mathbb{R}^n,\ c_i \in \mathbb{R}. \tag{3.26}$$

If there exist $\tau_j > 0$ for $j = 1, ...g$ such that:

$$\begin{gathered} \zeta_0(x) - \sum_{j=1}^{g} \tau_j \zeta_j(x) \geq 0,\ \forall x \in \mathbb{R}^n, \textit{then}, \\ \zeta_0(x) \geq 0\ \forall x \textit{ such that } \zeta_j(x) \geq 0. \end{gathered} \tag{3.27}$$

Applying the S-procedure may render the constraints conservative, but it is often useful to express them as LMIs.

Nevertheless it is not always possible to cast the constraints as an LMI. Frequently the problems are represented by bilinear matrix inequalities (BMI). The next section provides on overview of problems involving these constraints.

3.3.4 Optimisation problem involving BMI

Problems involving bilinear matrix inequalities are in general non convex, and consequently algorithms to solve them were developed much later than the LMI problems [SGL94]. Intense research has been carried out in this domain, and solvers are available for this kind of problem. The framework of the algorithm [KS03] is based on the augmented Lagrangian method in which the Lagrangian function is defined using a special penalty or barrier function.

A BMI problem can be described in the form:

Definition 3.3.10 (BMI optimisation problem) *A BMI optimisation problem consists of*

$$\begin{aligned} &\textit{minimise} \quad \upsilon^T x \\ &\textit{subject to} \quad F_0 + \sum_{i=1}^{m} x_i F_i + \sum_{j=1}^{q} p_j H_j + \sum_{i=1}^{m}\sum_{j=1}^{q} x_i p_j F_i H_j \succ 0 \end{aligned} \tag{3.28}$$

where $x \in \mathbb{R}^m$ *and* $p \in \mathbb{R}^q$ *are the decision variables and* $\upsilon \in \mathbb{R}^n$, $F_i = F_i^T \in \mathbb{R}^{n\times n}$ *with* $i = 1, ..., m$ *and* $H_j = H_j^T \in \mathbb{R}^{n\times n}$ *with* $j = 1, ..., q$

It represents the search of x and p among all values that satisfy constraints (3.28) such that the objective function $\upsilon^T x$ is minimised.

The modelling language Yalmip [Löf04] also supports the solver PENBMI [KS03] which is able to handle BMI constraints.

3.4 Hybrid systems

In this section, an introduction of hybrid systems, more precisely the switched linear systems is presented. It is followed by the historical achievements relating to piecewise affine systems and finally, some tools for analysis and control synthesis for this class of hybrid systems are also discussed.

3.4.1 An introduction to hybrid systems

Mathematical models are used to represent the physical behaviour of systems. Different models may be used to represent the same phenomena, depending on the objectives of the study and application. The choice of an adequate model is based on the tradeoff between the complexity of the model and its efficiency to solve analysis and synthesis problems. In other words, if the model is too simple, it may not capture the essential phenomena, but if it's too detailed, it may be very difficult to analyse and control it.

Traditionally, systems were modelled either by continuous dynamics or discrete dynamics. Continuous dynamics are described by differential or difference equations, for example the torque and power provided by an automobile engine and the heat transfer on an electrical resistance. Discrete dynamics are described by logical components, such as a finite state machine, if-then-else rules, propositional and temporal logic, for example the set of gear shift position in an automobile gearbox and the on-off switch from a thermostat. However, a large proportion of physical phenomena encountered in practice has an heterogeneous nature including both characteristics, such as an automobile powertrain system, a temperature regulator and many other applications.

The increasing demand on efficiency in the development of products and on performance of industrial processes has motivated engineers to research and develop tools for analysis and

synthesis of more complex models than the purely continuous or purely discrete. The advances on computer science allow the use of software and mathematical process models to test systems thoroughly in simulation before prototypes are built or experimental tests are carried out, which can provide a significant reduction in cost and time to release or implement new applications.

The need for more adequate modelling, analysis and design tools has driven scientists to investigate the dynamical systems that describe the interactions between continuous dynamics and discrete dynamics, which are usually called "hybrid systems". Examples of system that are hybrid in nature may include mechanical systems with collisions, diodes and switches, chemical processes controlled by valves or pumps, and embedded computation systems, where digital devices interact with an analogue environment.

Although some systems clearly have a hybrid nature, some classes of hybrid model can also be used to represent nonlinear behaviour of purely continuous dynamical systems [Joh02b]. Moreover, the tools for analysis and synthesis of hybrid systems may be used to circumvent the difficulties of working directly with the nonlinear model.

An overview of dynamics modelling, the elements of stability theory and the basics of control for hybrid systems are presented in [GST09], and many applications can be found, for example, air traffic control [TPS98], automotive control [BBdB$^+$00, PL06, MEMNL10], bioengineering [LTEP96, Bro93, YESG08], process control [EKSS00, KH08] , highway systems [HV00] and manufacturing [PC00].

The interdisciplinary field of hybrid systems, has led to the development of different communities with different viewpoints. Computer science researchers tend to focus their studies on the discrete behaviour of the system, while continuous dynamics are assumed to be relatively simple. On the other hand, researchers on system and control theory, tend to emphasise more the properties of continuous states, regarding hybrid systems as continuous systems with switching. Continuous-time systems with discrete switching events are referred to as switched systems.

Hence, hybrid systems can be classified in several specific categories. Regarding the switching events in switched systems, they can be [Lib03]:

- State-dependent or time-dependent switching,
- Autonomous (non-controlled) or controlled switching.

Each of these classes is briefly described below.

State-dependent switching

State-dependent switching is characterised by the continuous state-space partitioned into a finite or infinite number of operating regions, by means of a family of switching surfaces or guards. A continuous dynamical system is associated with each region. Whenever the system trajectory reaches a switching surface, the continuous state jumps instantaneously to a new value according to a reset map. This is illustrated in Fig. 3.3 by the dashed lines, while the bold lines represent the switching surfaces. When the reset map for a given transition is the identity, the state does not instantaneously change to a new value, but usually it loses differentiability when crossing the switching surface. This case is illustrated in Fig. 3.3 for the first switching of the trajectory.

Time-dependent switching

The time-dependent switching is a class of hybrid system in which the switches are activated according to time functions. These functions have a finite number of discontinuities, called switching times, on every bounded time interval, and take constant values on every interval

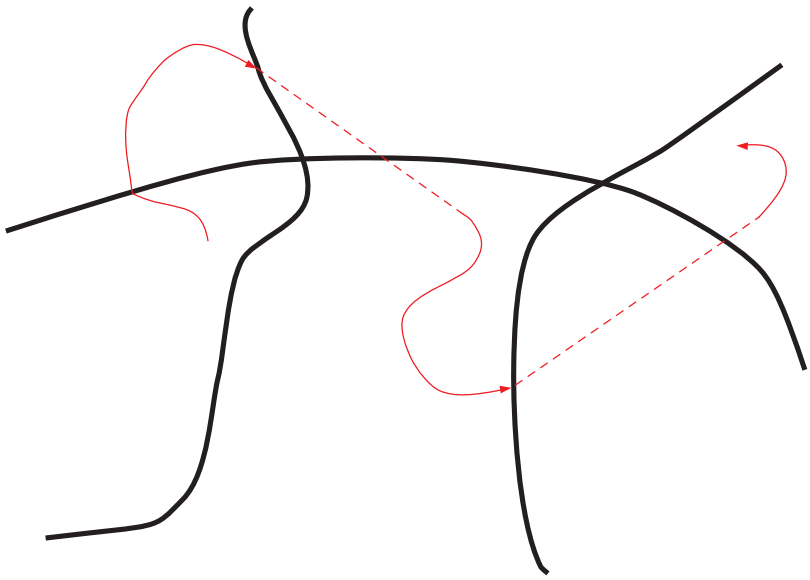

Figure 3.3: State-dependent switching, represented by the state trajectory (red) with reset maps (dashed) and switching surfaces (black thick lines)

between two consecutive switching times. The image of the time function is a finite index set. The role of this function is to specify, at each time instant, the index of the active subsystem (continuous dynamics). These switching instants can be prescribed a priori and fixed, or designed arbitrarily by engineers. Fig. 3.4 illustrates a switching signal (the time function) which is mapped in two index values, p_1 and p_2.

Autonomous and controlled switching

Autonomous switching refers to the situations where there is no direct control over the switching mechanisms that trigger the discrete switching. State-dependent switching systems with predetermined switching surfaces and time-dependent switching systems with unknown rules to define the switching signals are classified into the category of autonomous switching.

Controlled switching is represented by the situations in which the designer has control over the switching mechanism (either in state- or time-dependent systems) as they may be adjusted as the system evolves in order to achieve a desired behaviour.

The class of hybrid systems used in this thesis to model the vehicle dynamics consists of an autonomous state-dependent switching system, also called piecewise affine system, which is described in detail in the following section.

3.4.2 Piecewise affine systems

Piecewise affine systems consist of systems that have affine dynamics in different and non-overlapping regions of the state-space. These systems are able to capture many of the frequent nonlinearities and saturations from engineering systems (*e.g.* models for transistors and diodes), and can also be efficient in approximating general nonlinearities arbitrarily closely [Joh02b]. Two further characteristics ease the deployment of PWA systems: firstly, PWA functions can be efficiently implemented on inexpensive hardware; secondly, PWA systems and the corresponding

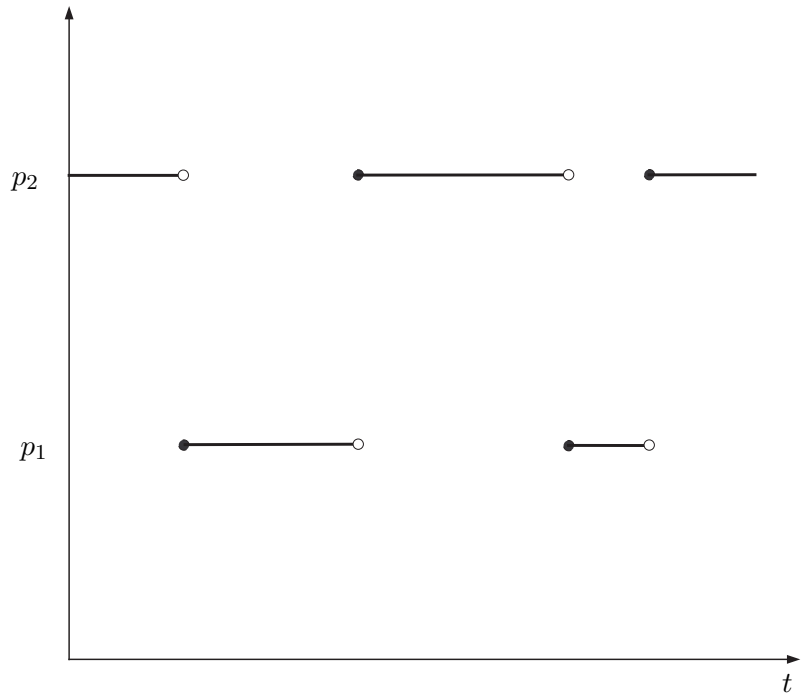

Figure 3.4: Time-dependent switching

control laws have a simple form, that is similar to linear or affine control laws, and that engineers in the industry are familiar with [BHL10].

Mathematically, continuous-time PWA systems can be described by:

$$\begin{aligned} \dot{x}(t) &= A_i x(t) + B_{ui} u(t) + B_{wi} w(t) + a_i \\ y(t) &= C_i x(t) + D_{ui} u(t) + D_{wi} w(t) \end{aligned} \tag{3.29}$$

where, similarly to (3.1), $x(t) \in \mathbb{R}^n$ is the state, $u \in \mathbb{R}^{n_u}$ is the control input, $w(t) \in \mathbb{R}^{n_w}$ is the exogenous input, a_i is an affine constant term and $y(t) \in \mathbb{R}^{n_y}$ is the output. The state-space is divided into M regions, denoted R_i for which the associated dynamics are described by the index $i \in \mathcal{I} = \{1, ..., M\}$.

These regions are usually described in terms of the state-space variables. More detailed information about the cell description and their boundaries is presented in the sequel.

Boundary descriptions

Although the regions of a piecewise affine system can be of any shape, restrictions on their geometry are often imposed in order to make it possible to analyse and control these systems. Mainly convex sets are used to describe the regions, polytopes and ellipsoids being very powerful for the analysis. These two shapes for the region boundaries are defined as follows

Definition 3.4.1 (Polytopic regions) *Assuming that the partitions R_i of the state-space for system* (3.29) *are polytopic cells, they can be described by the intersection of a finite number (p_i) of half-spaces [HB98, JR98], as follows:*

$$R_i = \{x | H_i^T x - g_i < 0\}, \tag{3.30}$$

where $H_i = [h_{i1}\ h_{i2}\ ...\ h_{ip_i}]$ *and* $g_i = [g_{i1}\ g_{i2}\ ...\ g_{ip_i}]^T$

When the polytopic regions are slab, they can be expressed as degenerated ellipsoids [HB98, RB05], because they exactly describe the polytopic regions and often require fewer parameters than (3.30), which is advantageous from a computational perspective.

Definition 3.4.2 (Ellipsoidal regions) *The (degenerated) ellipsoids for the operating regions can be described by:*

$$R_i = \{x|\ ||E_i x + f_i||_2 \leq 1\} \tag{3.31}$$

Following the description in [RB05], if $R_i = \{x \mid \underline{d}_i < c_i^T x < \bar{d}_i\}$ then the degenerated ellipsoid can be obtained by $E_i = 2c_i^T/(\bar{d}_i - \underline{d}_i)$ and $f_i = -(\bar{d}_i + \underline{d}_i)/(\bar{d}_i - \underline{d}_i)$.

Remark 3.4.1 *For the unbounded regions in the direction of the state variables that explicitly define the subsystem boundaries, the values of* $\bar{d}_i$ *and* $\underline{d}_i$ *must be specified such that they are beyond the physical limitation of the system. More details are provided in [HB98].*

The following example shows how to convert the slab polytopic regions into ellipsoidal regions.

Example 3.4.1 (Converting slab polytopic cell boundaries to ellipsoidal cell boundaries) *Considering a second order PWA systems with* $M = 3$ *and operating regions described by:*

$$\begin{aligned}
R_1 &= \{x \mid H_1^T x - g_1 < 0\}, \quad H_1^T = \begin{bmatrix} 1 & -1 \end{bmatrix}, \quad g_1 = -b \\
R_2 &= \{x \mid H_2^T x - g_2 < 0\}, \quad H_2^T = \begin{bmatrix} -1 & 1 \\ 1 & -1 \end{bmatrix}, \quad g_2 = \begin{bmatrix} b \\ b \end{bmatrix} \\
R_1 &= \{x \mid H_3^T x - g_3 < 0\}, \quad H_3^T = \begin{bmatrix} -1 & 1 \end{bmatrix}, \quad g_3 = -b
\end{aligned} \tag{3.32}$$

as shown by the dashed green lines in Fig. 3.5.

The hyperplanes defining the regions are parallel, and it can be noticed that region R_2 *is bounded on the direction of the vectors normal to the hyperplane and unbounded on the tangent direction. Considering* $c_2^T = [1\ -1]$*, given by the direction of the normal vector, with bounds at the values* $\underline{d}_2 = -b$ *and* $\bar{d}_2 = b$*. According to* $E_i = 2c_i^T/(\bar{d}_i - \underline{d}_i)$ *and* $f_i = -(\bar{d}_i + \underline{d}_i)/(\bar{d}_i - \underline{d}_i)$*, it is possible to obtain* $E_2 = [1/b\ \ -1/b]$ *and* $f_2 = 0$*, according to* $E_i = 2c_i^T/(\bar{d}_i - \underline{d}_i)$ *and* $f_i = -(\bar{d}_i + \underline{d}_i)/(\bar{d}_i - \underline{d}_i)$*. Only a lower and an upper bound exists respectively for region For regions* R_1 *and* R_3 *on the direction of* $c_1 = c_3 = c_2$*. In order to obtain an ellipsoid with finite volume in the direction of* $c_1 = c_3$*, it is necessary to choose the values of* $\bar{d}_1$ *and* $\underline{d}_3$ *(see Remark 3.4.1). Supposing that in practise, the system is limited to the dashed blue lines in Fig. 3.5, one can choose for* R_1*:* $\underline{d}_1 = b$ *and* $\bar{d}_1 = a$*, resulting in* $E_1 = \frac{2[1\ -1]}{a-b}$ *and* $f_1 = -\frac{a+b}{a-b}$*. For* R_3*,* $\bar{d}_3 = -b$ *and* $\underline{d}_3 = -a$*, resulting in* $E_3 = \frac{2[1\ -1]}{-b+a}$ *and* $f_3 = -\frac{-b-a}{-b+a}$*.*

The cell boundaries can be parametrised as a subset of the state-space:

Definition 3.4.3 (Cell boundary parametric description) *Each facet boundary between the neighbouring regions* R_i *and* R_j *is contained in the hyperplanes described by:*

$$\{x|c_{ij}^T x - d_{ij} = 0\}. \tag{3.33}$$

and the boundary parametric description can be obtained by:

$$\bar{R}_i \cap \bar{R}_j \subseteq \{l_{ij} + F_{ij} s\ /\ s \in R^{n-1}\} \tag{3.34}$$

where $F_{ij} \in R^{n \times n-1}$ *(full rank) is the matrix whose columns span the null space of* c_{ij}*, and* $l_{ij} \in R^n$ *is given by* $l_{ij} = c_{ij}(c_{ij}^T c_{ij})^{-1} d_{ij}$

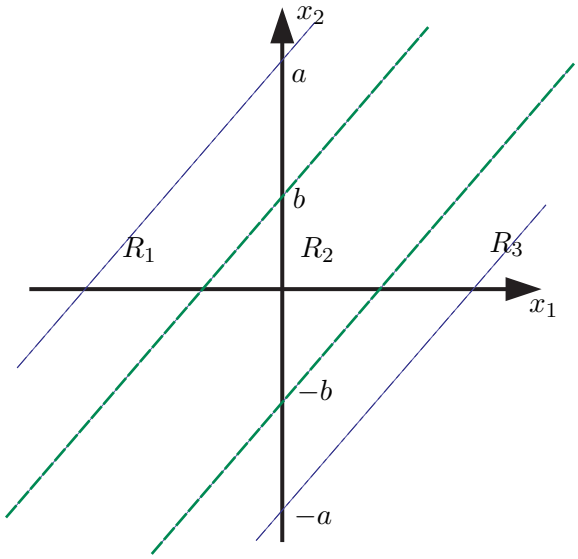

Figure 3.5: Cell boundaries (dashed green lines) for a second order PWA system and physical limit of the system (dash-dotted blue lines)

.

Having defined a PWA system and its operating regions, PWA system analysis and control are discussed in the next section.

3.5 Tools for analysis and control of piecewise affine systems

In this section a historical background of PWA systems is presented, with emphasis on the Lyapunov based methods. Theoretical tools for PWA systems analysis and control synthesis based on quadratic and piecewise quadratic Lyapunov functions are also described.

3.5.1 Previous work on Piecewise affine systems

The research and application of piecewise affine systems dates from the late 40's. In the work of [AC49] tools from Poincaré were used in the investigation of oscillations in nonlinear systems. Practical benefits of piecewise affine systems were noticed in [Sch53] which provides a discussion on piecewise linear servomechanisms. Saturation of linear systems has been considered in the work [Kal54]. In this work the saturated systems were considered as a series of linear regions in state-space, which were separated by switching boundaries. The same concept was used some decades later in [Joh02b] and other researchers, which has provided significant contribution for the control theory community.

In the 60's some research was devoted to piecewise affine systems, for instance [Pop61] on absolute stability, [Fil88] on differential equations with discontinuous right-hand side and [FL68] on optimal control. However it was not until the 70's that piecewise affine systems were considered as a class of model by the circuit community [CK77, Bok81] with the increasing need to efficiently simulate and analyse large scale circuits with diodes and other piecewise affine elements.

In the early 80's, [Son81] presented some pioneering work in the analysis of discrete-time

piecewise affine systems, exploiting properties of affine mappings and polyhedral sets. Similar ideas were employed later in [Kan97] for the analysis of robustness of discrete-time PWA systems.

Lyapunov based techniques have been applied to analysis and control synthesis of discrete-time PWA systems. In the article [LJ09], a methodology is presented to relax the conditions of finding a control Lyapunov function that renders the discrete-time system stable. Instead of computing off-line global Lyapunov function, the focus is on the synthesis of time-variant Lyapunov functions, by solving an online optimisation problem. Such trajectory-dependent Lyapunov functions, which are allowed to be locally non-monotone, can be thus derived. Still considering time-discrete systems, analysis and control design tools based on Lyapunov methods can be found in [MFTM00, FTCMM02, DRI02, dBBvdM$^+$08, LHT09].

Another widespread technique to construct state feedback controllers for discrete-time piecewise affine systems is through the use of MPC theory. A compact overview of the state-of-the-art for MPC methods for synthesis of PWA control law is provided in [BHL10] and references therein. It presents the equivalence of different hybrid automata descriptions, such as mixed logical dynamical (MLD) systems, linear complementarity (LC) systems, extended linear complementarity (ELC) systems, piecewise affine (PWA) systems, and max-min-plus scaling (MMPS) systems (more details in [HSB01]). Moreover, it also shows the computational techniques for solving hybrid MPC problem involving Mixed-Integer Quadratic Problems (details in [BM99]), when quadratic cost is considered, or Mixed-Integer Linear Problems (details in [BBM00]) when $1-$ or $\infty-$norms are used.

Regarding the PWA systems with continuous-time dynamics, [Pet97] proposed a technique based on vector fields to provide a qualitative analysis of the overall system dynamics, indicating sliding modes, probable limit cycles and instabilities.

In the late 90's, [BT99] showed that the analysis of even some simple PWA systems is either a *N-P* hard problem or undecidable. For this reason, it is not expected that algorithms for the exact solution of PWA systems analysis can be employed within polynomial time. On the other hand, analysis methods have been developed to cast the search of a Lyapunov function (to prove stability and verify invariant sets) as a convex optimisation program. These problems typically involve Linear Matrix Inequalities (LMIs) [BGFB94] and bilinear matrix inequalities (BMIs) [SGL94, GSP94]. The LMI problems can be efficiently solved using polynomial-time algorithms. These methods do not guarantee that a Lyapunov function can be found, however, if one is found then it guarantees a certain system performance.

Some applied research has been devoted to the use of piecewise affine systems for automotive applications, as presented in the sequence.

Piecewise affine control applied in automotive systems

Some applications of piecewise affine control can be found in the automotive domain. Discrete-time piecewise affine models are used in control strategies to minimise the effects of oscillations and vibrations (Bonanza effect) in automotive powertrains with backlash [HWBK06]. Also related to powertrain, in [GRB$^+$06] model predictive control techniques based on mixed-integer quadratic optimisation are used to manage the air-to-fuel ratio and torque in advanced technology gasoline direct-injection stratified-charge engines.

In the framework of driving assistance systems, [CDS07] presents a comparison of control methods based on tuned proportional-integral action and on model predictive control, developed for linear and piecewise affine systems for an adaptive cruise controller application.

The longitudinal tyre forces are approximated by piecewise affine functions in [BBFH01] for traction control using an MPC control strategy. The discrete-time piecewise affine model is

converted into an equivalent mixed-logical-dynamics system [BM99, HSB01], and the algorithms in [BBM00] are used to implement an explicit PWA form of the MPC law.

Similarly, the lateral tyre forces have been modelled as piecewise affine systems in [BCBT09] and in [PMB10], as described in Section 2.2.1 (Combined active steering and differential braking) for the design of a yaw rate controller based on the actuation of a steer-by-wire active steering system and differential wheel braking.

The more recent research and the state-of-the-art for analysis and control of continuous-time PWA systems based on the Lyapunov technique are presented in the following.

Lyapunov based techniques for piecewise affine systems

The work of [PD91] is possibly the first attempt to apply Lyapunov based methods on piecewise affine systems. Analysis methods for PWA systems based on common quadratic Lyapunov function have been investigated by many researchers. Necessary and sufficient conditions for the existence of a common quadratic Lyapunov function for two stable linear systems in the plane are discussed in [SN99]. These results were extended in [SNM03] for a finite number of stable linear-time-invariant systems. In [Lib03], Lie-algebraic conditions are presented for the existence of a common Lyapunov function for switched linear systems, and if they are solved the system is stable under arbitrary switching.

Extending these results on piecewise linear systems to systems containing affine terms, [HB98, Joh99] provided methods based on LMI optimisation algorithms for the computation of a common Lyapunov function for piecewise affine systems whose regions are described by polyhedral cells. A synthesis method for a piecewise linear state feedback controller is provided in [HB98] when the operating regions are slab, and [RB05] extends the results for a piecewise affine controller.

The discontinuous nature of hybrid systems has lead researchers to investigate the existence of multiple Lyapunov functions. Similarly to the case for the common Lyapunov function, in [HB98, Joh99] LMI based methods are provided for system analysis based on a piecewise quadratic Lyapunov function. The Lyapunov conditions are exploited in each of the polyhedral operating regions through the S-Procedure, and constraints are added to enforce continuity on the boundaries.

Control synthesis possibilities have also been proposed based on piecewise quadratic Lyapunov functions. Considering only piecewise linear systems, the authors in [DY08] proposed a method based on the Reciprocal Projection Lemma which is able to recover the linearity for the PWA systems that have a single equilibrium. For more general piecewise affine systems, a piecewise linear state feedback control law can be designed using convex optimisation with piecewise quadratic cost functions [RJ00]. In this procedure, Hamilton-Jacobi-Bellman inequalities are used to obtain lower bounds on the optimal cost, which serve as a suboptimal solution to the control problem. The control laws performance can be improved by further refinements of the partitioning. An extension of this work is proposed by [MH04] to take into account switching laws that depend not only on the system states, but also on exogenous inputs.

Piecewise affine state and output feedback controllers are proposed by [RH03] in which the control synthesis can be casted as an optimisation problem with BMI constraints once the equilibrium point of the closed-loop systems for each operating region has been previously chosen.

A specific technique for state feedback control of piecewise affine systems on simplices and rectangles is proposed in [HvS01].

As an alternative to the quadratic forms of Lyapunov function candidates, [Joh99] presents a stability analysis for piecewise affine systems based on piecewise linear Lyapunov functions,

which can be computed using linear programing.

PWA analysis and control synthesis based on quadratic and piecewise quadratic Lyapunov functions are presented below.

3.5.2 Lyapunov stability of piecewise affine systems

Throughout the methods for analysis and control synthesis presented in this section, it is assumed that the origin is the equilibrium point of the PWA system (3.29). A coordinate change as shown in Remark 3.2.2 is also possible if the origin is not the equilibrium point of the system.

It is important to note that switching plays a key role in the stability of PWA systems. If the dynamics of each subsystem are stable, it does not necessarily imply that the dynamics of the whole system are also stable. The following example shows how switching may influence the stability of the PWA system.

Example 3.5.1 (Influence of switching on the system stability) *[Lib03] Considering the Hurwitz matrices A_1 and A_2 (with the same eigenvalues) as follows:*

$$A_1 = \begin{bmatrix} -0.1 & 5 \\ -1 & -0.1 \end{bmatrix} \text{ and } A_2 = \begin{bmatrix} -0.1 & 1 \\ -5 & -0.1 \end{bmatrix} \tag{3.35}$$

and the piecewise linear systems:

$$\dot{x} = \begin{cases} A_1 x, & x_1 x_2 < 0 \\ A_2 x, & x_1 x_2 \geq 0 \end{cases} \tag{3.36}$$

where the state vector is $x = [x_1,\ x_2]^T$. The system trajectories for the same initial state of the autonomous linear systems $\dot{x} = A_1 x$ and $\dot{x} = A_2 x$ are shown in the plots of Fig. 3.6 (a,b). It can be noticed from the trajectory of the PWL system (3.36)*, plotted in Fig. 3.6 (c), that the switching is stable.*

On the other hand, by interchanging the operating regions of the PWA system, the resulting system becomes:

$$\dot{x} = \begin{cases} A_1 x, & x_1 x_2 \geq 0 \\ A_2 x, & x_1 x_2 < 0 \end{cases} \tag{3.37}$$

The system trajectory of (3.37) *from the same initial state is displayed in Fig. 3.6 (d), and it can noted that under this switching rule the stable dynamics A_1 and A_2 render the PWA system* (3.37) *unstable.*

The stability of piecewise affine systems can be proved by the existence of a Lyapunov function. Often, quadratic forms for Lyapunov function candidates are used in the control discipline [BGFB94] and also applied for piecewise affine systems.

Quadratic Lyapunov stability

Considering (3.29) with $u = 0$ and $w = 0$, a quadratic Lyapunov function candidate can be described as:

$$V(x) = x^T P x, \text{ with } P \in \mathbb{R}^{n \times n},\ P = P^T, \text{ and } P \succ 0. \tag{3.38}$$

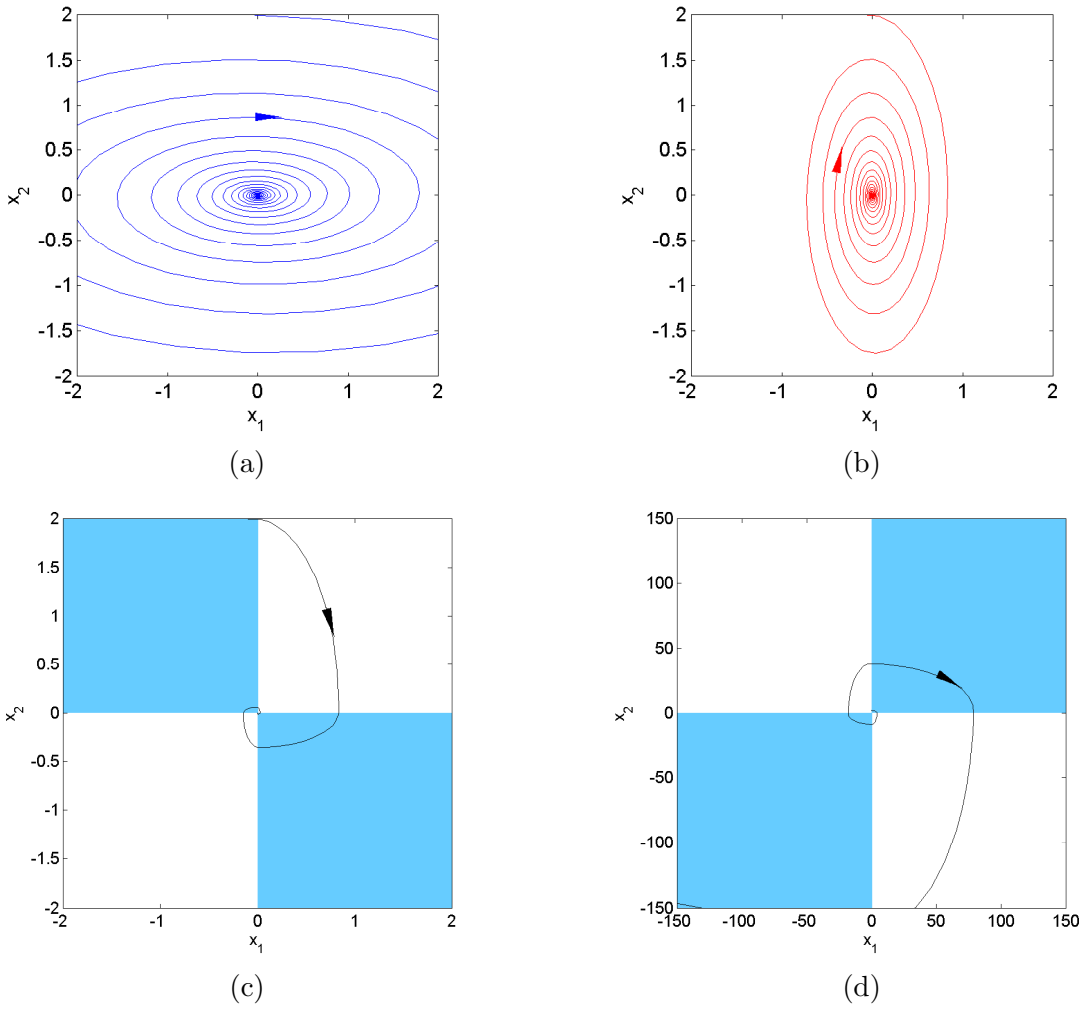

Figure 3.6: System trajectories from the same initial conditions for the stable linear autonomous systems (a) $\dot{x} = A_1 x$, (b) $\dot{x} = A_2 x$ and for (c) the PWA system (3.36) under stable switching and (d) the PWA system (3.37) under unstable switching. The shaded regions represent the operating regions of A_1.

Moreover it is required that V decreases along the trajectories of (3.29), equivalent to $\frac{dV(x)}{dt} < 0$. Supposing that $u = 0$ and $w = 0$, then $\frac{dV(x)}{dt}$ becomes:

$$\begin{aligned} \frac{dV(x)}{dt} &= (A_i x + a_i)^T P x + x^T P (A_i x + a_i) \\ &= \begin{bmatrix} x \\ 1 \end{bmatrix}^T \begin{bmatrix} A_i^T P + P A_i & P a_i \\ a_i^T P & 0 \end{bmatrix} \begin{bmatrix} x \\ 1 \end{bmatrix}, \end{aligned} \tag{3.39}$$

In order to take into account the switching boundaries, it is required that the Lyapunov conditions are valid on each of the operating regions of (3.29), described either by ellipsoidal cell boundaries (3.31) or polytopes (3.30). Expressing these conditions in quadratic forms allows the use of the S-procedure (3.3.2) to describe these constraints as an LMI feasibility problem.

Lemma 3.5.1 (Local quadratic stability for PWA systems) *Considering system* (3.29) *with* $u = 0$, $w = 0$, *its equilibrium point located at the origin, i.e.* $x_{eq} = 0$ *and its regions described*

as (3.31)*. If there exists a symmetric matrix* $P = P^T$*, and negative scalars* λ_i *such that:*

$$\begin{cases} P \succ 0,\ \lambda_i < 0,\ i = 1, ..., M \\ \begin{bmatrix} PA_i + A_i^T P + \lambda_i E_i^T E_i & Pa_i + \lambda_i E_i^T f_i \\ (Pa_i + \lambda_i E_i^T f_i)^T & -\lambda_i \left(I - f_i^T f_i\right) \end{bmatrix} \prec 0 \end{cases} \tag{3.40}$$

Then the PWA system is locally asymptotically stable [HB98].

Remark 3.5.1 *For the regions containing the origin, the condition of negative decay rate simplify to the standard Lyapunov condition,* $PA_i + A_i^T P \prec 0$

If it is not possible to obtain the ellipsoidal description of the regions (3.31), and only the polytopic description (3.30) is available, the same procedure can be used to cast the search of a quadratic Lyapunov function as an LMI problem. In this case, the conditions (3.40) must be replaced by:

$$\begin{cases} P \succ 0,\ i = 1, ..., M \\ \begin{bmatrix} PA_i + A_i^T P + \bar{H}_i^T \Lambda_i \bar{H}_i & Pa_i - \bar{H}_i^T \Lambda_i \bar{g}_i \\ (Pa_i - \bar{H}_i^T \Lambda_i \bar{g}_i)^T & \bar{g}_i^T \Lambda_i \bar{g}_i \end{bmatrix} \prec 0 \end{cases} \tag{3.41}$$

where Λ_i is a matrix with non-negative entries, $\bar{H}_i = [0\ h_{i1}\ h_{i1}\ ...\ h_{ip_i}]^T$ and $\bar{g}_i = [1\ g_{i1}\ g_{i1}\ ...\ g_{ip_i}]^T$ [HB98].

See Appendix A for details on how to describe the polytopic cell boundaries in a quadratic form. The polytopic description of cells allows the operating regions to be unbounded. In this case, the regions may cover the whole state-space and global stability conditions can be checked. Remark 3.5.1 is also valid for the proof of stability using polytopic cell boundaries.

Lemma 3.5.2 (Global quadratic stability for PWA systems) *Considering system* (3.29) *with* $u = 0$*,* $w = 0$ *and cell polytopic description* (3.30)*. If* $\mathcal{R} = \left\{ \bigcup_{i=1}^{M} R_i = \mathbb{R} \right\}$ *and* (3.41) *holds, then the system is globally asymptotically stable.*

Example 3.5.2 (Global quadratic stability) *Solving the feasibility problem* (3.41) *on the PWL system* (3.36) *leads to the quadratic Lyapunov function:*

$$V(x) = x^T P x,\ \textit{with}\ P = \begin{bmatrix} 10.2310 & 0.0000 \\ 0.0000 & 10.2310 \end{bmatrix} \tag{3.42}$$

Since the regions cover the whole state-space, recalling Lemma 3.5.2, it can be concluded that system (3.36) *is globally asymptotically stable*

However when attempting to solve the LMI (3.41) *for the PWL system* (3.37)*, no feasible solution could be found.*

These conditions may be very conservative, as a single Lyapunov function candidate must satisfy the stability conditions for all the piecewise affine dynamics simultaneously. One possibility to circumvent this limitation is the search for piecewise quadratic Lyapunov functions.

Piecewise quadratic stability

Considering a piecewise quadratic function:

$$V(x) = x^T P_i x + 2q_i^T x + r_i,\ P_i \in \mathbb{R}^{n\times n},\ P_i = P_i^T, q_i \in \mathbb{R}^n,\ r_i \in \mathbb{R}. \tag{3.43}$$

with the index i representing the regions of the piecewise affine system.

In order to ensure the continuity of the piecewise quadratic Lyapunov function across the boundaries of the regions R_i, the parametric boundary description from Definition 3.4.3 can be used [HB98].

The continuity is enforced by the equality constraints.

$$\begin{cases} F_{ij}^T(P_i - P_j)F_{ij} &= 0 \\ F_{ij}^T(P_i - P_j)l_{ij} + F_{ij}^T(q_i - q_j) &= 0 \\ l_{ij}^T(P_i - P_j)l_{ij} + 2(q_i - q_j)^T l_{ij} + (r_i - r_j) &= 0 \end{cases} \tag{3.44}$$

In order to satisfy the conditions for Lyapunov stability, it is required that $P_i \succ 0$ and $\frac{dV(x)}{dt} < 0$, in each of the regions, R_i. Considering ellipsoidal cell description (Definition 3.4.2) and applying the S-procedure, these conditions correspond to the LMIs:

$$\begin{cases} \lambda_i > 0,\ \gamma_i < 0,\ i = 1, ...M \\ \begin{bmatrix} P_i + \lambda_i E_i^T E_i & q_i + \lambda_i E_i^T f_i \\ (q_i + \lambda_i E_i^T f_i)^T & r_i + \lambda_i (f_i^T f_i - 1) \end{bmatrix} \succ 0 \\ \begin{bmatrix} A_i^T P_i + P_i A_i - \gamma_i E_i^T E_i & P_i a_i + A_i^T q_i - \gamma_i E_i^T f_i \\ (P_i a_i + A_i^T q_i - \gamma_i E_i^T f_i)^T & 2a_i^T q_i - \gamma_i (f_i^T f_i - 1) \end{bmatrix} \prec 0 \end{cases} \tag{3.45}$$

If the cells are described by polytopes, the corresponding LMIs are:

$$\begin{cases} i = 1, ...M \\ \begin{bmatrix} P_i - \bar{H}_i^T \Lambda_i \bar{H}_i & q_i + \bar{H}_i^T \Lambda_i^T \bar{g}_i \\ (q_i + \bar{H}_i^T \Lambda_i \bar{g}_i)^T & r_i - \bar{g}_i^T \Lambda_i \bar{g}_i \end{bmatrix} \succ 0 \\ \begin{bmatrix} A_i^T P_i + P_i A_i + \bar{H}_i^T \Gamma_i \bar{H}_i & P_i a_i + A_i^T q_i - \bar{H}_i^T \Gamma_i \bar{H}_i \\ (P_i a_i + A_i^T q_i - \bar{H}_i^T \Gamma_i \bar{H}_i)^T & 2a_i^T q_i + \bar{g}_i^T \Gamma_i \bar{g}_i \end{bmatrix} \prec 0 \end{cases} \tag{3.46}$$

where Λ_i and Γ_i are matrices containing non-negative entries.

Theorem 3.5.1 (Piecewise quadratic stability) *Considering system* (3.29) *with* $u = 0$, $w = 0$ *and regions described as* (3.31)*, if there exist symmetric matrices* $P_i = P_i^T$*, for* $i = 1, ..., M$*, such that conditions* (3.44) *and* (3.45) *or* (3.44) *and* (3.46) *hold, then the system is asymptotically stable.*

Remark 3.5.2 (Global piecewise quadratic stability of PWA system) *If the regions of the PWA system are unbounded, covering the whole state-space, and theorem 3.5.1 is verified, then the PWA system is globally asymptotically stable.*

Changing the boundaries of the PWA system from example 3.5.1, it is possible to find a case, shown in the following example, in which the dynamics are stable but the quadratic stability fails. On the other hand, a piecewise quadratic Lyapunov function can be found to prove the stability

Example 3.5.3 (Piecewise quadratic stability) *[Joh99] Considering the PWA affine systems*

$$\dot{x} = \begin{cases} A_1 x, & x \in \mathcal{R}_1 \text{ or } \mathcal{R}_3 \\ A_2 x, & x \in \mathcal{R}_2 \text{ or } \mathcal{R}_4 \end{cases} \tag{3.47}$$

where A_1 and A_2 as in equation (3.35) *and operating regions as illustrated on Fig. 3.7. The same figure depicts the trajectory from an initial state. Applying conditions* (3.41) *on system* (3.47) *leads to an infeasible problem. Nevertheless the theorem 3.5.1 holds, resulting in:*

$$P_1 = P_3 = \begin{bmatrix} 14.1924 & 0.0000 \\ 0.0000 & 70.6969 \end{bmatrix} \text{ and } P_2 = P_4 = \begin{bmatrix} 70.6969 & 0.0000 \\ 0.0000 & 14.1924 \end{bmatrix} \tag{3.48}$$

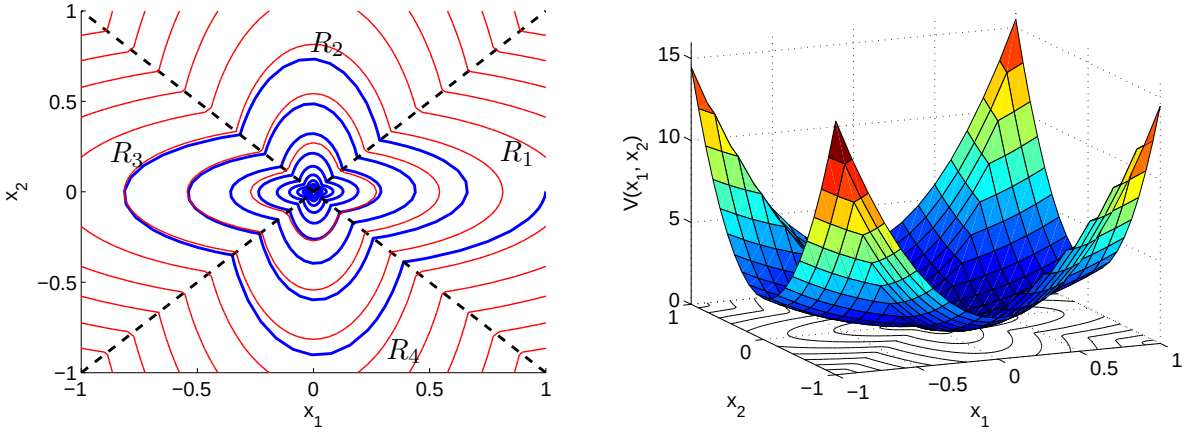

(a) (b)

Figure 3.7: (a) Trajectory of the PWA system (3.47) (in blue) and invariant sets corresponding to the piecewise quadratic Lyapunov function level curves (in red dotted); (b) Piecewise quadratic Lyapunov function.

It can be noticed in Fig. 3.7, that it is not possible to find ellipsoidal invariant sets (obtained from the quadratic Lyapunov function) that ensure that once the trajectory reaches the set, the system state will remain in it. However the level curves of the piecewise quadratic Lyapunov function (plotted in red dotted lines in Fig. 3.7) satisfy the invariant set properties.

Having described some tools for analysis of PWA systems, some methods for control synthesis are described in the sequel.

3.5.3 State feedback control for piecewise affine systems

Two methods for synthesis of state feedback controllers based on Lyapunov functions are presented in this section. The first method, introduced by [HB98] allows the design of a piecewise linear controller based on a single quadratic Lyapunov function through an LMI optimisation procedure. The second method presented was developed by [RH03]. It considers a piecewise affine controller based on a piecewise quadratic Lyapunov function. It is formulated as a BMI optimisation problem which can be transformed into two LMIs that are solved in iterative fashion, when some terms are fixed a priori.

The exogenous input $w(t)$ (see (3.29)) is not explicitly taken into account in neither of these methods. Nevertheless, differential inclusions [BGFB94, Joh99] and norm bounds on approximation errors [Joh99, Rod02] can be used to guarantee the robustness of the synthesis.

State feedback control based on quadratic Lyapunov function

Considering a PWA system such as (3.29) with $w = 0$ and slab operating regions described as (3.31), a PWL full state feedback controller of the from ($u = K_i x$) can be designed based on a quadratic Lyapunov function (3.38) using LMI optimisation procedure [HB98]. In this case the closed-loop dynamics become:

$$\dot{x}(t) = (A_i + B_i K_i)\, x(t) + a_i \tag{3.49}$$

Using the results from (3.40) and performing the variable change $Q = P^{-1}$ and $Y_i = K_i Q$, the following theorem can be derived.

Theorem 3.5.2 (Piecewise linear state feedback control) *if there exists a matrix $Q = Q^T > 0$; negative scalars $\mu_i < 0$ such that:*

$$\begin{gathered} Q = Q^T \succ 0 \\ \mu_i < 0 \quad (scalar) \\ \left[\begin{array}{cc} A_i Q + Q A_i^T + B_i Y_i + Y_i^T B_i^T - \mu_i a_i a_i^T & Q E_i^T + \mu_i a_i f_i^T \\ \left(Q E_i^T + \mu_i a_i f_i^T\right)^T & -\mu_i \left(I - f_i f_i^T\right) \end{array} \right] \prec 0, \end{gathered} \tag{3.50}$$

then the feedback $u = K_i x$ with $K_i = Y_i Q^{-1}$ renders the PWA system (3.49) *exponentially stable [HB98].*

Remark 3.5.3 *The same problem can be changed in order to have a common state feedback gain for all regions. For that, the term Y_i is replaced by a single variable Y. On the other hand, it may restrain the set of feasible solutions, rendering the problem more conservative.*

Remark 3.5.4 *An objective function can be included in the LMI, in order to obtain more satisfactory performance of the controller, rather than simply solving the feasibility problem. For example, maximise the decay rate of the Lyapunov function.*

Similarly to the analysis of stability, the control synthesis may become less conservative if piecewise quadratic Lyapunov functions are used, as described below.

State feedback control based on piecewise quadratic Lyapunov function

For the control synthesis based on a piecewise quadratic Lyapunov function, it is important to note that it is not evident to perform the variable changes applied in theorem 3.5.2 to recover convexity. The difficulty lies in finding a parametrisation for the inverse of the piecewise quadratic Lyapunov function in order to ensure its continuity (see equations (3.44)).

In the method developed in [RH03], a generic piecewise affine state feedback controller, such as:

$$u = K_i x + m_i \tag{3.51}$$

is considered in the controller design based on a piecewise quadratic Lyapunov function for the piecewise affine system (3.29), without perturbations

Remark 3.5.5 (Piecewise affine control input) *The affine term in* (3.51) *is used to control the PWA systems to arbitrary equilibrium points, rather than the origin. Although a coordinate change can be performed (as described in Remark 3.2.2) so that the equilibrium point is located at the origin, for PWA systems it would require a change in coordinates for each subsystem and changing also the boundaries of the operating regions, which can render the system analysis and control synthesis quite cumbersome.*

The closed-loop equations become:

$$\dot{x} = (A_i + B_i K_i)x + (a_i + B_i m_i) = \bar{A}_i x + \bar{b}_i \tag{3.52}$$

The matrix $\bar{A}_i$ of the closed loop system must be designed such that each region has a single equilibrium point denoted x^i_{eq}. This condition is mathematically expressed by:

$$(A_i + B_i K_i)x^i_{eq} + (a_i + B_i m_i) = 0 \tag{3.53}$$

The piecewise quadratic function (3.43) is a Lyapunov function if conditions (3.7) are verified. Alternatively, these conditions can be expressed as:

$$x \in R_i, \begin{cases} V_i(x) > \epsilon ||x - x_{eq}||_2 \\ \frac{d}{dt} V_i(x) < -\alpha_i V_i(x), \end{cases} \tag{3.54}$$

where x_{eq} is the closed-loop system equilibrium point, α_i is the Lyapunov function decay rate for region R_i, and $\epsilon \geq 0$ is fixed.

Applying the S-Procedure (lemma 3.3.2), the conditions of stability, for a system with ellipsoidal boundaries (3.31), can be written as:

$$\lambda_i > 0,\ \gamma_i > 0$$

$$\begin{bmatrix} P_i - \epsilon I_n + \lambda_i E_i^T E_i & q_i + \epsilon x_{eq} + \lambda_i E_i^T f_i \\ * & r_i - \epsilon x_{eq}^T x_{eq} + \lambda_i (f_i^T f_i - 1) \end{bmatrix} \succ 0 \tag{3.55}$$

$$\begin{bmatrix} \bar{A}_i^T P_i + P_i \bar{A}_i - \gamma_i E_i^T E_i + \alpha_i P_i & P_i \bar{b}_i + \bar{A}_i^T q_i - \gamma_i E_i^T f_i + \alpha_i q_i \\ * & 2\bar{b}_i^T q_i - \gamma_i (f_i^T f_i - 1) + \alpha_i r_i \end{bmatrix} \prec 0 \tag{3.56}$$

Since the equilibrium point of each region must be the extrema of the candidate piecewise quadratic Lyapunov function [HB98], when $x^i_{eq} \in R_i$, the following replacements must take place in constraints (3.44), (3.55) and (3.56):

$$\begin{aligned} q_i &\leftarrow -P_i x^i_{eq} \\ r_i &\leftarrow r_i + {x^i_{eq}}^T P_i x^i_{eq} \end{aligned} \tag{3.57}$$

Considering as an objective function the maximisation of the decay rates α_i, the controller synthesis can be cast as an optimisation problem, as follows:

$$\begin{array}{ll} \text{maximise:} & \min\limits_i \alpha_i \\ \text{subject to:} & (3.53),\ (3.44),\ (3.55),\ (3.56) \\ & \epsilon > 0, \quad \gamma_i > 0, \quad \lambda_i > 0, \quad \alpha_i > 0, \\ & -l_1 < K_i < l_1, \quad -l_2 < m_i < l_2 \end{array} \tag{3.58}$$

where l_1 and l_2 are vector bounds.

Such optimisation problem is not convex, due to terms such as $P_i B_i K_i$ in constraint (3.55) and $P_i x_{eq}^i$ in equality constraint (3.57). By choosing the equilibrium points of each subsystem a priori, constraints (3.57) become linear and the constraints of the optimisation problem (3.58) simplify to BMI.

Theorem 3.5.3 (PWA state feedback control synthesis, from [RH03]) *Assume the Lyapunov function* (3.43) *is defined in* $\mathcal{X} \subseteq \mathbb{R}^n$. *If there is a solution to the design problem* (3.58), *the closed-loop system is locally asymptotically stable inside any subset of the largest level set of the control Lyapunov function* (3.43) *that is contained in* $\mathcal{X} \in \mathbb{R}^n$. *If* $\epsilon > 0$, *then the convergence is exponential. If, furthermore,* $\mathcal{X} = \mathbb{R}^n$ *then the exponential stability is global.*

Proof 3.5.1 (Proof of Theorem 3.5.3) *Any level set of a Lyapunov functio is an invariant set for the system. Since the derivative of the Lyapunov function (well defined in the interior of the polytopic regions) is made strictly negative in the optimization problem in* (3.58), *the invariant sets of the system are also regions of attraction. Thus if* $\epsilon > 0$ *then* $|x - x_{eq}| \leq \epsilon^{-1} V(0) e^{-\iota}$, *where* $\iota = \min_i \alpha_i$, *which proves local exponential convergence when* $\mathcal{X} \subset \mathbb{R}^n$. *If,* $\mathcal{X} = \mathbb{R}^n$ *then the esxponential stability is global, because* (3.43) *is radially unbounded.*

Remark 3.5.6 (Choice of equilibrium points of R_i [RHH00]) *In order to ensure that the closed loop system has a single equilibrium point,* x_{eq}, *all other equilibrium points* (x_{eq}^i) *must be chosen outside their respective regions. A method for choosing the equilibrium points is proposed in [Rod02].*

Although algorithms to solve BMI problems for the optimal solution exists [GTS+94], they usually run in non-polynomial time, and are very restrictive for medium/large number of polytopic regions. Alternatively, algorithms that eqch iteration run in polynomial-time can be used for local solutions, and the problem may be solved in a reasonable computational time, as for instance the V-K iteration [BH98].

Remark 3.5.7 (V-K iteration method) *It is possible to convert this BMI problem into an LMI when some parameters are fixed constant.*

V-step*: Given a fixed controller, and a fixed* α_i, *solve:*

$$\begin{aligned} &\textit{Find:} && P_i,\ q_i,\ r_i \\ &\textit{subject to:} && (3.44), (3.55),\ (3.56), \\ & && \epsilon > 0, \quad \gamma_1 > 0, \quad \lambda_1 > 0, \end{aligned} \tag{3.59}$$

K-step*: For* P_i, q_i *and* r_i *fixed at the previous step, solve:*

$$\begin{aligned} &\textit{maximise:} && \min_i \alpha_i \\ &\textit{subject to:} && (3.53),\ (3.55),\ (3.56), \\ & && \epsilon > 0, \quad \gamma_1 > 0, \quad \lambda_1 > 0, \quad \alpha_i > l_0 > 0, \\ & && -l_1 < K_i < l_1, \quad -l_2 < m_i < l_2, \end{aligned} \tag{3.60}$$

For each iteration of the K-step, the decay rates, α_i must be greater than the value computed in the previous iteration. The loop must be repeated until there is no significant improvement on the cost or the LMIs become infeasible.

Remark 3.5.8 (Continuity of control input along system boundaries) *The control input can be forced to be continuous along the boundaries using the constraint:*

$$\begin{aligned} (K_i - K_j)\, F_{ij} &= 0 \\ (K_i - K_j)\, l_{ij} + (m_i - m_j) &= 0 \end{aligned} \tag{3.61}$$

for all neighbour regions R_j of each operating region R_i.

In many practical cases, not all the system states are available for measurement, either because the variable cannot be measured or because the existing sensors are too costly to be employed. In this case, output feedback control techniques provide possibilities to circumvent this drawback. A efficient method for synthesis of output feedback control for PWA system, introduced by [RH03] is presented below.

3.5.4 Output feedback control for piecewise affine systems

A PWA dynamic output feedback controller can also be designed to control system (3.29) in the absence of perturbations $w(t)$. For this, the state-space representation of the controller in each region has the form:

$$\left\{ \begin{array}{rl} \dot{x}_c(t) & = A_{ci}x_c + L_i y + b_{ci} \\ u & = K_i x_c + m_i \end{array} \right. \tag{3.62}$$

The closed loop system can be expressed in the same form as in (3.52), by defining an augmented state $\tilde{x} \stackrel{\Delta}{=} [x,\ x_c]^T$, hence:

$$\dot{\tilde{x}} = \tilde{A}_i \tilde{x} + \tilde{b}_i \tag{3.63}$$

where:

$$\tilde{A}_i = \left[\begin{array}{cc} A_i & B_i K_i \\ L_i C_i & A_{ci} \end{array} \right] \quad \text{and} \quad \tilde{b}_i = \left[\begin{array}{c} a_i + B_i m_i \\ b_{ci} \end{array} \right] \tag{3.64}$$

Similarly to the state feedback case, the matrix $\tilde{A}_i$ must be designed so that (3.63) has a single equilibrium point, denoted $\tilde{x}^i_{eq}$, for each of the operation regions of the PWA system. The corresponding constraint is:

$$\tilde{A}_i \tilde{x}^i_{eq} + \tilde{b}_i = 0 \tag{3.65}$$

The candidate PWQ Lyapunov function for the augmented system (3.63) has the form:

$$V_i(x) = \tilde{x}^T \tilde{P}_i \tilde{x} + 2\tilde{q}_i^T \tilde{x} + \tilde{r}_i. \tag{3.66}$$

where $\tilde{P}_i = \tilde{P}_i^T$, $\tilde{P}_i \in R^{2n \times 2n}$, $\tilde{q}_i \in R^{2n}$ and $\tilde{r}_i \in R$.

The conditions of positive definiteness and negative first derivative along the system trajectories (3.54) can be rewritten using the S-procedure (lemma 3.3.2), and are expressed as:

$$\lambda_i > 0,\ \gamma_i > 0$$

$$\left[\begin{array}{cc} \tilde{P}_i - \epsilon I_n + \lambda_i \tilde{E}_i^T \tilde{E}_i & \tilde{q}_i + \epsilon \tilde{x}_{eq} + \lambda_i \tilde{E}_i^T f_i \\ * & \tilde{r}_i - \epsilon \tilde{x}_{eq}^T \tilde{x}_{eq} + \lambda_i (f_i^T f_i - 1) \end{array} \right] \succ 0 \tag{3.67}$$

$$\left[\begin{array}{cc} \tilde{A}_i^T \tilde{P}_i + \tilde{P}_i + \tilde{A}_i - \gamma_i \tilde{E}_i^T \tilde{E}_i + \alpha_i \tilde{P}_i & \tilde{P}_i \tilde{b}_i + \tilde{A}_i^T \tilde{q}_i - \gamma_i \tilde{E}_i^T f_i + \alpha_i \tilde{q}_i \\ * & 2\tilde{b}_i^T \tilde{q}_i + \alpha_i \tilde{r}_i - \gamma_1 (f_1^T f_1 - 1) \end{array} \right] \prec 0 \tag{3.68}$$

where $\tilde{E}_i = [E_i,\ 0]$.

The conditions to ensure the continuity of (3.66) across the boundaries become:

$$\begin{cases} \tilde{F}_{ij}^T(\tilde{P}_i - \tilde{P}_j)\tilde{F}_{ij} &= 0 \\ \tilde{F}_{ij}^T(\tilde{P}_i - \tilde{P}_j)\tilde{l}_{ij} + \tilde{F}_{ij}^T(\tilde{q}_i - \tilde{q}_j) &= 0 \\ \tilde{l}_{ij}^T(\tilde{P}_i - \tilde{P}_j)\tilde{l}_{ij} + 2(\tilde{q}_i - \tilde{q}_j)^T\tilde{l}_{ij} + \tilde{r}_i - \tilde{r}_j &= 0 \end{cases} \tag{3.69}$$

where $\tilde{F}_{ij}$ and l_{ij} are the parametric description of the boundaries (see Definition (3.4.3)), adjusted to the augmented system as follows:

$$\tilde{F}_{ij} = \begin{bmatrix} F_{ij} & 0 \\ 0 & I \end{bmatrix} \quad \text{and} \quad \tilde{l}_{ij} = \begin{bmatrix} l_{ij} \\ 0 \end{bmatrix} \tag{3.70}$$

The constraints (3.57) are adapted for the augmented system, in order to ensure that the equilibrium point of each region, $\tilde{x}_{eq}^i$, is the extrema of the Lyapunov function, when $\tilde{x}_{eq}^i \in R_i$, they become:

$$\begin{aligned} \tilde{q}_i &\leftarrow -\tilde{P}_i\tilde{x}_{eq}^i \\ \tilde{r}_i &\leftarrow \tilde{r}_i + {\tilde{x}_{eq}^i}^T\tilde{P}_i\tilde{x}_{eq}^i \end{aligned} \tag{3.71}$$

for constraints (3.67), (3.68) and (3.69).

Considering a performance criterion as: $J = \min_i \alpha_i$, The goal is to find A_{ci}, K_i L_i, m_i, b_{ci}, and a PWQ Lyapunov function (3.66) that maximise the performance criterion J. Such optimisation problem can be written as:

$$\begin{aligned} &\text{maximise:} && \min_i \alpha_i \\ &\text{subject to:} && (3.65),\ (3.67),\ (3.68),\ (3.69), \\ & && \epsilon > 0 \quad \gamma_i > 0 \quad \lambda_i > 0 \quad \alpha_i > l_0 > 0 \\ & && -l_1 < K_i < l_1 \quad -l_2 < m_i < l_2 \end{aligned} \tag{3.72}$$

where l_0 is a scalar bound, l_1 and l_2 are vector bounds.

Similarly to the state feedback case, when $\tilde{x}_{eq}^i$ are chosen beforehand, (3.72) becomes a BMI optimisation procedure for which the V-K method can be employed. If continuity of the control input is desired, Remark 3.5.8 can also be considered in the output feedback control synthesis.

Remark 3.5.6 must also be taken into account for the output feedback case, in order to ensure that the closed loop has a single equilibrium point.

Corollary 3.5.1 (PWA output feedback control synthesis, from [RH03]) *Assume the Lyapunov function* (3.66) *is defined in* $\mathcal{X} \subseteq \mathbb{R}^{2n}$. *If there is a solution to the design problem* (3.72), *then the closed-loop system is locally asymptotically stable inside any subset of the largest level set of the control Lyapunov function* (3.66) *that is contained in* $\mathcal{X}$. *If* $\epsilon > 0$ *then the convergence is exponential. If, furthermore* $\mathcal{X} = \mathbb{R}^{2n}$ *then the exponential stability is global.*

Proof 3.5.2 (Proof of Corollary 3.5.1) *Similar to the proof of Theorem 3.5.3 replacing* x *by* $\tilde{x}$, x_{eq} *by* $\tilde{x}_{eq}$ *and the state space* $\mathbb{R}^n$ *by* $\mathbb{R}^{2n}$.

Remark 3.5.9 (Switching based on state estimate) *It is assumed in this approach that the switching between the controllers is driven only by the system outputs. In order to enable*

switches based on state estimates, a structure of a regulator and an estimator is required. Therefore the following constraint must be added:

$$\begin{cases} A_{ci} &= A_i + B_i K_i - L_i C_i \\ b_{ci} &= B_i m_i + b_i + (A_i - L_i C_i) x_{eq}^i \end{cases} \tag{3.73}$$

Other algorithms are also presented in [RH03] to solve the BMI optimisation procedure. Nevertheless the V-K method has shown to be adequate for the design of the ADAS proposed in this document.

3.6 Conclusion

In this chapter the theoretical tools used in the development of the vehicle lateral control assistance have been presented. Firstly, the continuous-time dynamical systems have been reviewed, as well as the Lyapunov stability concept and invariant set properties used to analyse such systems. Heed has been taken of the optimisation problems involving Linear and Bilinear matrix inequalities, as these are key in the system analysis.

The Piecewise affine system has been introduced as a class of hybrid system which is not only able to model saturation but also to arbitrarily approximate nonlinearities, being therefore adequate to model the lateral tyre forces. Another advantage of PWA systems is that they have a simple form which can be easily implemented and most industrial engineers are familiar with.

It has been shown that the use of piecewise affine systems has been investigated in some automotive systems in order to approximate nonlinearities. The formal description and theoretical tools for analysis and control synthesis of these systems based on Lyapunov stability have also been presented in this chapter. The possibility of control synthesis based on state feedback is useful for the lane keeping application and the output feedback is particularly interesting in order to avoid the use of high cost sensors.

A PWA vehicle model is introduced in the next chapter.

Chapter 4

Vehicle model

Contents

In this chapter the vehicle model used in the design of the lane keeping assist systems is developed. Firstly, a simple single track nonlinear vehicle model is presented alongside the nonlinear tyre forces acting on the vehicle. In the second section, an analysis of the nonlinear vehicle model is carried out, showing the effects of vehicle speed and road adherence on the vehicle stability. The PWA approximation of the nonlinear model is introduced in this chapter. A model for the road is described in the fourth section and the dynamics of the additional variables to describing the vehicle position with respect to the centre of the lane are introduced in the fifth section completing the PWA model used in the design of lane keeping assist systems. The simulation environment and prototype vehicles used in the evaluation of the assistance systems are also described in this chapter.

4.1 Vehicle Model

A very extensive variety of vehicle models exists in literature (see [Ack02, Pac04, Raj06b, GoAE92, MM95, MSC09]). The models differ in terms of the level of abstraction with respect to

the real system depending how the sprung mass, wheel spin, suspensions, brakes, aerodynamics, tyres, powertrain and driveline are considered in the model. A single track model (also known as bicycle model) for lateral dynamics may consist of 2 degrees of freedom, while advanced vehicle simulators may use models with more than 30 degrees of freedom. The choice of an adequate model is then related to its underlying assumptions and the intent of use.

A widely used simplified single track vehicle model [Ack02], which is considered to capture the essential vehicle lateral steering dynamics, is approximated by a PWA system which is used to design the controllers for driving assistance.

The commercial simulator for vehicle dynamics CarSim [MSC09] is used in the simulations in order to verify the controller performance with respect to unmodelled effects, such as combined lateral and longitudinal tyre forces, pitch, roll and driver dynamics.

A more detailed description of these models is provided in the sequel, while the modelling of tyre forces is discussed in section 4.1.2.

4.1.1 2-DOF nonlinear vehicle model

A simplified single track vehicle model for lateral dynamics, often referred to as "bicycle model" is obtained from the following assumptions:

- Absence of lateral load transfer (i.e. The two wheels of each axle are lumped into one located at its centre).
- Absence of longitudinal load transfer.
- Absence of pitch and roll dynamics.
- Constant longitudinal velocity.
- Chassis or suspension compliance effects are neglected.

Writing the cinematic equations for a vehicle under these assumptions leads to [Ack02]:

$$\begin{cases} m(\dot{v}_y + r v_x) &= F_{yf}\cos\delta_f + F_{yr} \\ J\dot{r} &= l_f F_{yf}\cos\delta_f - l_r F_{yr} \end{cases} \tag{4.1}$$

where r is the vehicle yaw rate, v_x and v_y are the longitudinal and lateral vehicle speed, δ_f is the steering angle, m is the vehicle mass, l_f (l_r) is the distance from the front (rear) axle to the centre of gravity (CG), J is the vehicle inertia respect to the vertical axle through the CG, F_{yf} and F_{yr} are the front and rear lateral forces which are discussed in the next section. Fig. 4.1 illustrates these variables and parameters.

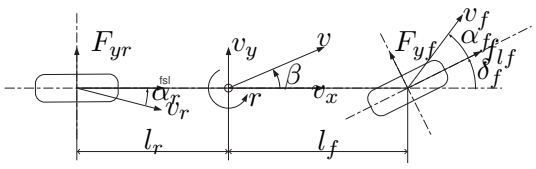

Figure 4.1: Single track vehicle model.

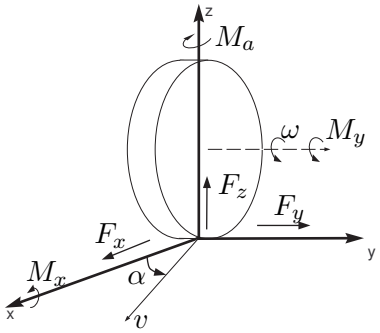

Figure 4.2: Forces and moments from the road acting on tyres

4.1.2 Tyre forces

The forces and moments from the road acting on each tyre, as illustrated on Fig. 4.2, have an important influence on the vehicle dynamics.

The longitudinal and lateral forces (F_x and F_y respectively) are generated by the deformation of the rubber compounds. Experimental results show that the longitudinal force depends on the slip ratio, defined as:

Definition 4.1.1 (Wheel slip ratio) *The longitudinal slip is the difference between the longitudinal velocity at the axle of the wheel, v_x and the equivalent rotational velocity of the tyre, $\omega_w r_e$. The longitudinal slip ratio is defined as:*

$$\begin{array}{ll} \sigma_x = \frac{\omega_w r_e - v_x}{v_x} & \textit{during braking,} \\ \sigma_x = \frac{\omega_w r_e - v_x}{\omega_w r_e} & \textit{during acceleration,} \end{array} \tag{4.2}$$

Analogously, the lateral force depends on the wheel sideslip angle, defined as:

Definition 4.1.2 (Wheel sideslip angle) *The wheel sideslip angle is defined as the difference between the orientation of the wheel (steering angle) and the orientation of the wheel longitudinal velocity. The wheel sideslip angle is illustrated by the angle α in Fig. 4.2.*

The velocity angle in each wheel can be calculated by the ratio of the lateral velocity to the longitudinal velocity. The resulting sideslip angles for the front and rear wheels are:

$$\begin{aligned} \alpha_f &= \delta_f - \tan^{-1}\left(\tfrac{v_y + l_f r}{v_x}\right) \\ \alpha_r &= -\tan^{-1}\left(\tfrac{v_y - l_r r}{v_x}\right) \end{aligned} \tag{4.3}$$

Under the assumption that the angles remain small the following approximation is valid:

$$\begin{aligned} \alpha_f &= \delta_f - \tfrac{v_y + l_f r}{v_x} \\ \alpha_r &= -\tfrac{v_y - l_r r}{v_x} \end{aligned} \tag{4.4}$$

It is also possible to express the front and rear wheels sideslip angles with respect to the vehicle sideslip angle, denoted by β and depicted in Fig. 4.1. Still under the assumption that the angles remain small, β replaces v_y (since $v_y = v \sin\beta$), which yields;

$$\begin{aligned} \alpha_f &= \delta_f - \beta - \tfrac{l_f r}{v} \\ \alpha_r &= -\beta + \tfrac{l_r r}{v} \end{aligned} \tag{4.5}$$

Having defined the wheel slip ratio and the wheel sideslip angles, the next section shows how they are related to the tyre forces.

Pacejka's tyre model

The Magic Formula tyre model [Pac04] provides a method to calculate the longitudinal and lateral tyre forces as well as the aligning moment, for a very large domain of validity, including large values of slip ratio and sideslip angles.

Considering a decoupled case, in which only either lateral or longitudinal force is being generated on the tyre, the force is given by:

$$y(\kappa) = D\sin\{C\arctan[(1-E)B\kappa + E\arctan(B\kappa)]\}, \tag{4.6}$$

where κ is one of the input variables: slip ratio σ or sideslip angle α. The output y is respectively the longitudinal force F_x, or lateral force F_y, or aligning moment M_z. Fig. 4.3 illustrates the shape of the Pacejka model either for lateral or longitudinal tyre forces (only for positive sideslip angles for sake of clarity). Three distinct zones can be identified. The first region, comprising modest values of sideslip angle (or slip ratio) correspond to regular driving situation, where the lateral dynamics are not so demanding. In this region, the relation between the sideslip angle and the force can be considered linear, and systems such as LDWS and LKAS are designed to operate in this domain. As the sideslip angle is increased, reaching the sliding behaviour, the tyre force does not respond linearly and slip starts to occur. ESC systems operate mainly in these conditions attempting to reduce the sideslip angle. Once the tyre force reaches its extremum, the forces saturate completely and even a decrease on the tyre forces may be noticed. The same analysis is valid for the longitudinal motion.

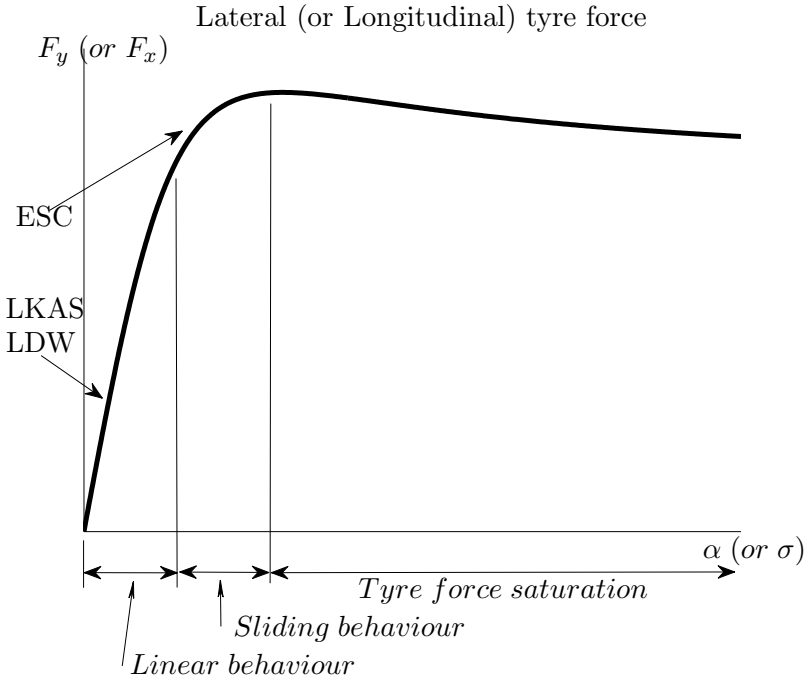

Figure 4.3: Pacejka model for tyre forces and region of operation of LKS and ESC

The parameters B (stiffness factor), C (shape factor), D (peak value) and E (curvature factor) are determined experimentally. It is important to remark on the meaning of these factors [Raj06b]:

Remark 4.1.1 *The coefficient D, as its nomenclature says, represents the peak value of the tyre force (or aligning moment).*

Remark 4.1.2 *The shape factor, C controls the limits of the sine function in* (4.6)*, and thereby determines the shape of the resulting curve.*

$$C = \frac{2}{\pi} sin^{-1}\left(\frac{y_s}{D}\right) \tag{4.7}$$

where y_s is the asymptotic value of the output y at large values of κ.

Remark 4.1.3 *The cornering (or longitudinal) stiffness of the tyre can be obtained by the product BCD, representing the slope of the curve at the origin, $\alpha = 0$, (or $\sigma = 0$). It is usually adjusted by the stiffness factor B as D and C are set as previously mentioned.*

Remark 4.1.4 *The curvature factor E is used to control the curvature near the peak of the curve, as well as the value $\kappa = \kappa_m$, in which the peak of the curve occurs.*

$$E = \frac{B\kappa_m - tan\left(\frac{\pi}{2C}\right)}{B\kappa_m - tan^{-1}\left(b\kappa_m\right)} \tag{4.8}$$

Remark 4.1.5 *Ply-steer and conicity effects (possibly rolling resistance also) can be taken into account with horizontal and vertical offsets, S_h and S_v respectively. In this case, a variable change is performed,*

$$\bar{\kappa} = \kappa - S_h \tag{4.9}$$

and the output function becomes:

$$Y(\kappa) = y(\bar{\kappa}) + S_v \tag{4.10}$$

Figure 4.4(a) illustrates the influence of the coefficients in an example of a lateral tyre force.

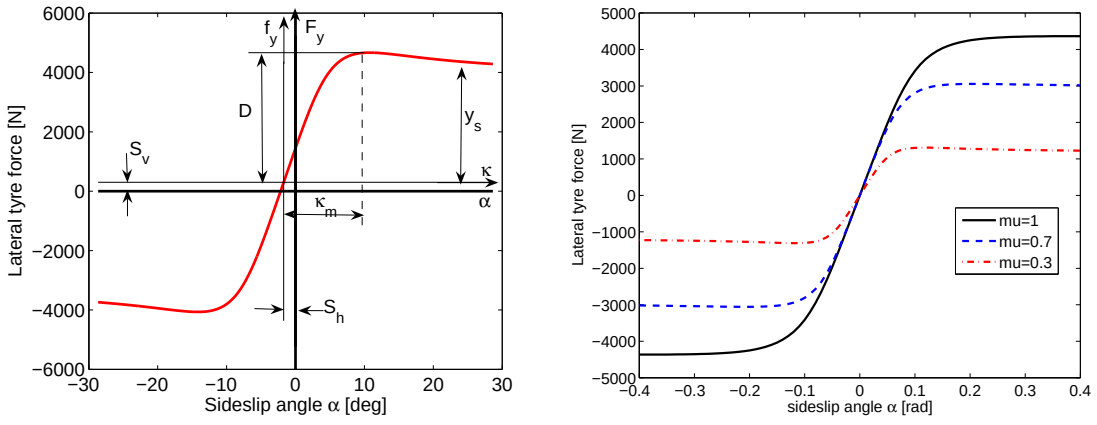

(a) (b)

Figure 4.4: (a) Pacejka magic formula parameters and (b) Effects of road adhesion on tyre lateral force.

The adhesion coefficient and normal force acting on the tyre are embedded inside the parameters.

Effects of the adherence

The effect of the road adherence on the lateral tyre forces, either for the front or rear wheels can be expressed for the Pacejka model (4.6) by the following changes in the parameters [MK02]:

$$\begin{aligned} B &\leftarrow (2-\mu)B, \\ C &\leftarrow \tfrac{(5-\mu)C}{4}, \\ D &\leftarrow \mu D, \\ E &\leftarrow E. \end{aligned} \tag{4.11}$$

Figure 4.4 (b) shows the reduction of the tyre force for different adhesion coefficients.

Combined effect of longitudinal and lateral force

The friction circle (also referred to as friction ellipse, traction circle) can be used to qualitatively illustrate the limits of horizontal frictional forces interacting between the tyre and the road when combined lateral and longitudinal forces are considered [Pac04], as shown in Fig. 4.5.

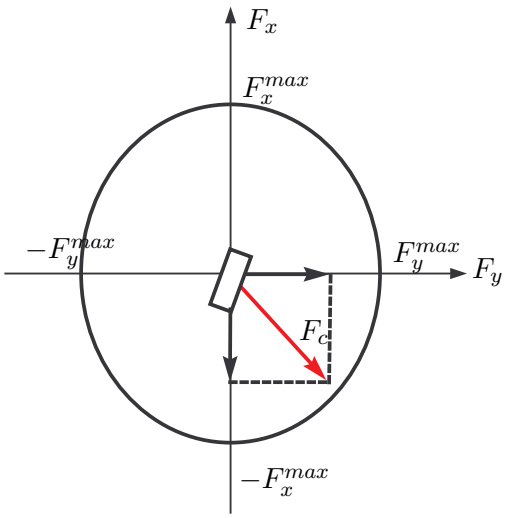

Figure 4.5: Friction ellipse showing the limit of the combined of longitudinal and lateral tyre forces

The resulting force from the cornering and braking action, F_c, depicted in Fig. 4.5 by the red arrow, cannot exceed the ellipse which determines the maximum magnitude of the combined longitudinal and lateral forces.

Although some recent research states that the representation of the combined effects of longitudinal and lateral forces is not a true ellipse [BB11], the friction circle/ellipse is still useful to highlight some important considerations in the design of the ADAS.

Considering, for instance, a case of pure cornering at the lateral force extrema. The resulting force lie on the horizontal axis of Fig. 4.5 and $F_c = F_y^{max}$ (or $F_c = -F_y^{max}$), therefore actions such as braking or accelerating the wheel will have no effects on the vehicle dynamics, since the tyre force will saturate. A reduction in the lateral component is required, in order to enable the action on the longitudinal force. Similarly, if a tyre is at the extrema of longitudinal tyre force, the torque must released before a steering action is performed.

4.1.3 Nonlinear model analysis

It is well known from literature (see for example [OHTD98]) that the nonlinear vehicle model (4.1) presents a limited region of stability, including a stable equilibrium point and two saddle points. The region of stability also depends on the vehicle steering angle, longitudinal velocity and road adherence. In order to show how these parameters influence the stability region, simulations have been carried out with the nonlinear vehicle model (4.1) with tyre forces given by the Pacejka model according to (4.6) and wheel sideslip angles given by (4.3). The numerical values of the parameters from the Pacejka tyre model and the vehicle parameters used in the simulations are described in Table 4.2.

Effects of road adhesion

The effects of the changes in the road adhesion on the vehicle stability can be seen from the simulations performed with the nonlinear vehicle model (4.1) at constant speed $v_x = 20\ [m/s]$. The vehicle model has been simulated from different initial conditions and a constant steering input for three different road adhesion coefficients. The resulting state trajectories can be seen in Figure 4.6. The model shows unstable behaviour for trajectories starting from high yaw rate and sideslip angle, even in ideal adherence conditions (Fig. 4.6-a). As the adhesion conditions are degraded the stable region is reduced, as it can be observed from Fig. 4.6 (b) and (c), representing wet and icy asphalt respectively.

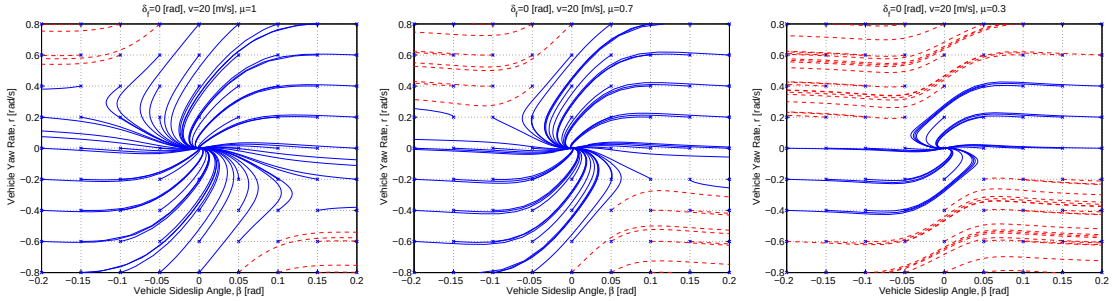

(a) (b) (c)

Figure 4.6: Effects on the state trajectory for nonlinear vehicle model at constant steering $\delta_f = 0$, considering the different road adhesion (a) $\mu = 1$, dry asphalt, (b) $\mu = 0.7$, wet asphalt, (c) $\mu = 0.3$, icy asphalt.

Effects of the steering angle

The stability of the nonlinear vehicle model (4.1), as well as its equilibrium point, also depends on the steering angle. Fig. 4.7 depicts system trajectories for a constant steering angle $\delta_f = 0.04\ [rad]$. The set of initial conditions and longitudinal velocity of $v = 20\ [m/s]$ are the same as above and the different conditions of road adherence are also considered.

It can be noticed that in ideal adherence condition shown in Fig. 4.7-(a) the steering input does not alter significantly the set of initial condition from which the state trajectories are stable. Although the same behaviour can be noticed for the trajectories on wet asphalt shown in Fig. 4.7-(b), the extrema values of sideslip angle of the stable trajectories tend to increase and reach values that are beyond the vehicle's physical limits encountered in regular driving conditions. When comparing the effects of steering on icy asphalt, depicted in Fig. 4.7-(c), the

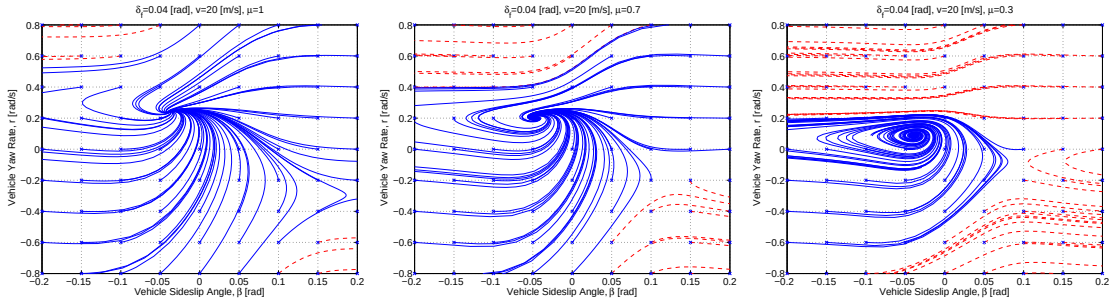

(a) (b) (c)

Figure 4.7: Effects on the state trajectory for nonlinear vehicle model at constant steering angle $\delta_f = 0.04\ [rad]$, considering the different road adhesion (a) $\mu = 1$, dry asphalt, (b) $\mu = 0.7$, wet asphalt, (c) $\mu = 0.3$, icy asphalt.

reduction of the stability region for the initial conditions of positive sideslip angle is evident. An even larger increase on the extrema values of attained sideslip angle for the stable trajectories can also be seen.

Effects of the longitudinal speed

The vehicle longitudinal speed also influences the stability of the dynamic system and its convergence to the equilibrium point. The simulations performed on the nonlinear vehicle model (4.1) show that instability occurs as the vehicle longitudinal speed increases. The same initial condition was considered in the simulations, as the analyses have been carried over for the three different road conditions. Figures 4.8 and 4.9 show the simulation results for steering angles $\delta_f = 0\ [rad]$ and $\delta_f = 0.04\ [rad]$, respectively.

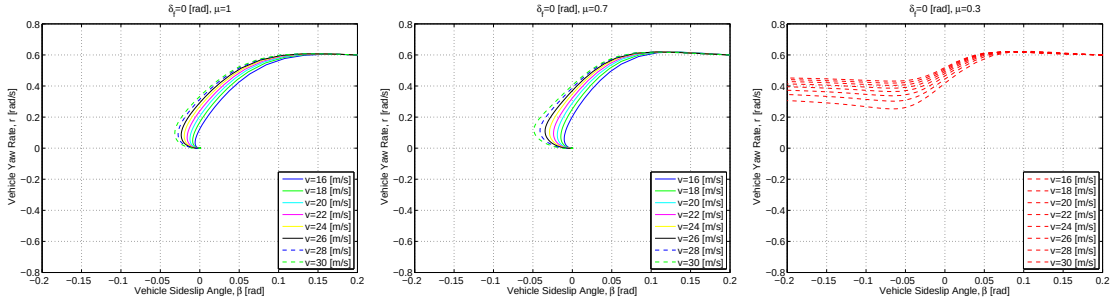

(a) (b) (c)

Figure 4.8: Effects of the vehicle longitudinal speed on nonlinear vehicle model for constant steering angle $\delta_f = 0$ in different adhesion conditions.

The state trajectories for the simulations with zero steering angle on dry and wet asphalt, illustrated respectively in Fig. 4.8-(a) and (b), are not significantly different for increasing speed. For all longitudinal velocities tested, the state trajectories are stable but larger values of sideslip angle are attained when the adherence is reduced from $\mu = 1$ to $\mu = 0.7$. Considering icy asphalt, shown in Fig. 4.8-(c), none of the tested conditions were stable. It has already been demonstrated that the trajectory from this initial condition is not stable for $v = 20\ [m/s]$, from the analysis depicted in Fig. 4.7-(c), but even the reduction of the longitudinal velocity is not enough to recover the stability from such initial conditions.

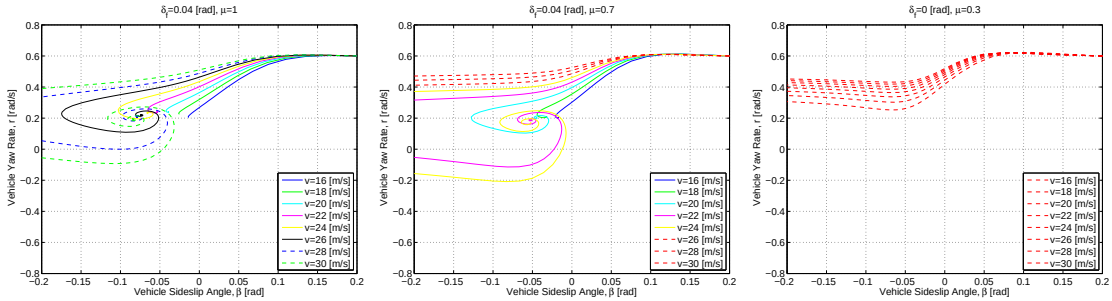

(a) (b) (c)

Figure 4.9: Effects of the vehicle longitudinal speed on nonlinear vehicle model for constant steering angle $\delta_f = 0.04\ [rad]$ in different adhesion conditions.

When a steering angle of $\delta_f = 0.04\ [rad]$ is considered in the simulations, it can be noticed a significant increase on the extrema values of sideslip angle in the stable trajectories for higher longitudinal velocities. Such effect is noticeable on dry asphalt by the results plotted on Fig. 4.9)-(a) for the trajectories corresponding to vehicle speed beyond 26 $[m/s]$. The same effect occurs at lower speed (20 $[m/s]$) for reduced road adherence, as shown in the subplot (b). Moreover, the trajectories become unstable for longitudinal velocities larger than 24 $[m/s]$. Similarly to the case without steering angle, none of the trajectories from this initial condition are stable on icy asphalt, as depicted Fig. 4.9-(c)

Having presented the nonlinear vehicle lateral dynamics and its behaviour through the simulations, its approximation by a PWA model can be introduced, as shown in the next section.

4.2 Piecewise affine vehicle model

In order to approximate system (4.1) by a piecewise affine system, the lateral tyre forces domain can be partitioned into polyhedral sets so that for each of the regions an affine system is used to describe the corresponding linearised dynamics.

Considering that the front and rear tyre forces described by (4.6) are approximated by the following PWA functions:

$$\begin{cases} F_{yf}(\alpha_f) = e_{fi} + d_{fi}\alpha_f \\ F_{yr}(\alpha_r) = e_{ri} + d_{ri}\alpha_r \end{cases} \tag{4.12}$$

where d_{fi}, d_{ri}, e_{fi} and e_{ri} depend on the front and rear tyre forces and the index (i) corresponding to the partitioning of the tyre force domain, based on the tyre sideslip angles. An illustration of the affine functions is depicted in Fig. 4.10 by the continuous lines for the front and rear wheel.

System (4.1) is linearised around uniform rectilinear motion ($v_x = v = \text{constant}$, $r = 0$, $v_y = 0$, $\delta_f = 0$) taking into account the PWA functions (4.12) adopted to approximate the nonlinear tyre forces and the sideslip angles considered as in (4.5). The vehicle dynamics can be represented by the PWA system:

$$\dot{x}^b = A_i^b x^b + B_i^b u + a_i^b, \tag{4.13}$$

and the corresponding dynamics are:

$$A_i^b = \begin{bmatrix} -2\frac{d_{fi}+d_{ri}}{mv} & -1 - 2\frac{d_{fi}l_f - d_{ri}l_r}{mv^2} \\ 2\frac{d_{ri}l_r - d_{fi}l_f}{J} & -2\frac{d_{fi}l_f^2 + d_{ri}l_r^2}{Jv} \end{bmatrix}, \quad B_i^b = \begin{bmatrix} \frac{2d_{fi}}{mv} \\ \frac{2d_{fi}l_f}{J} \end{bmatrix}, \quad a_i^b = \begin{bmatrix} 2\frac{e_{fi}+e_{ri}}{mv} \\ 2\frac{e_{fi}l_f - e_{ri}l_r}{J} \end{bmatrix}. \tag{4.14}$$

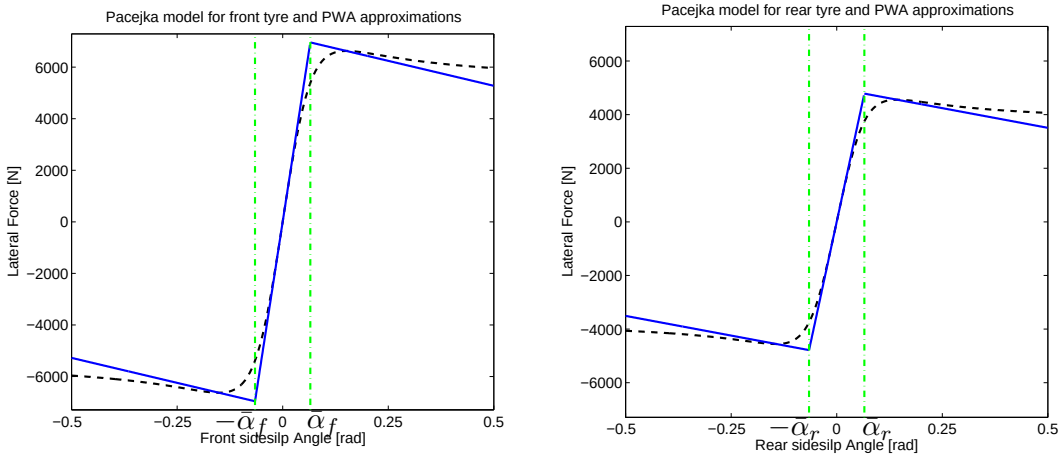

(a) (b)

Figure 4.10: Lateral force according to Pacejka model (dashed) and corresponding PWA approximations (solid) and partitions (dash-dot) for the (a) front tyres and (b) rear tyres.

where the control input is the front wheel steering angle $u = \delta_f$, the vehicle sideslip angle β (which replaces v_y since $v_y = v \sin\beta$) and the yaw rate r are the state variables $x^b = [\beta, r]^T$.

Considering the front sideslip angle as in (4.5), the operating regions of the PWA system (4.13) depend on the state (β and r) and control input (δ_f). Throughout the theoretical tools presented in Section 3.5 it has been assumed that the switching should depend only on the state, therefore, the control input should not directly affect the operating mode if one intends to apply the analysis and control tools. For a steer-by-wire configuration, in which the actuators are coupled directly to the front wheels, a first-order dynamics for the actuator with large enough bandwidth can be included in the system, in order to avoid the feed-through from u in the model. It is also useful to enforce continuity of the control input at the boundaries. Therefore, the steering angle is included as an additional state to the system as follows:

$$\dot{\delta}_f = -\tau\delta_f + \tau u_c, \tag{4.15}$$

The resulting PWA model for the vehicle dynamics becomes:

$$\dot{x}^d = A_i^d x^d + B_i^d u_c + a_i^d, \tag{4.16}$$

and the corresponding dynamics are:

$$A_i^d = \begin{bmatrix} -2\frac{d_{fi}+d_{ri}}{mv} & -1 - 2\frac{d_{fi}l_f - d_{ri}l_r}{mv^2} & \frac{2d_{fi}}{mv} \\ 2\frac{d_{ri}l_r - d_{fi}l_f}{J} & -2\frac{d_{fi}l_f^2 + d_{ri}l_r^2}{Jv} & \frac{2d_{fi}l_f}{J} \\ 0 & 0 & -\tau \end{bmatrix}, \quad B_i^d = \begin{bmatrix} 0 \\ 0 \\ \tau \end{bmatrix}, \quad a_i^d = \begin{bmatrix} 2\frac{e_{fi}+e_{ri}}{mv} \\ 2\frac{e_{fi}l_f - e_{ri}l_r}{J} \\ 0 \end{bmatrix}. \tag{4.17}$$

where $x^d = [\beta, r, \delta_f]^T$ and u_c becomes the control input of the augmented plant.

Remark 4.2.1 (Linear vehicle model) *A linear vehicle model can be obtained from* (4.13) *considering that the linearisation is valid for the whole domain of the tyre forces. In this case, the model has only one operating region, $i = 1$. The commonly used linear tyre forces approximation*

is obtained by setting $e_{f1} = 0$, $e_{r1} = 0$, $d_{f1} = c_f$ *and* $d_{r1} = c_r$ *where* c_f *and* c_r *are related to the parameters in the Pacejka's formula as indicated in Remark 4.1.3 as follows:*

$$c_f = B_f C_f D_f, \qquad c_r = B_r C_r D_r. \tag{4.18}$$

It is important to ensure that the PWA model (4.13) keeps the essential lateral dynamics of a vehicle expressed by the model (4.1). In the subsequent section, different analyses are presented in order to assess the compatibility of behaviours.

4.2.1 Analysis of PWA vehicle model

In order to investigate the behaviour of the PWA vehicle model, several simulations have been carried out considering the same aspects as mentioned in Section 4.1.3, such as different road adhesion, longitudinal speed and steering angle. Additionally, the effects of the PWA approximations of the lateral tyre force have also been evaluated.

Firstly, the front and rear lateral tyre forces are approximated by the piecewise affine functions (4.12), as shown in 4.10 (a) and (b), respectively. The approximations for the linear region are obtained as described in Remark 4.2.1. This region is limited by the values denoted $\pm\bar{\alpha}_z$, where the index $z = (f, r)$ represents the front or rear tyre, respectively. These values are computed with respect to the extrema value of the Pacejka model as follows:

$$\alpha_z = (1 + \varsigma)\frac{\mu D_z}{c_z}, \tag{4.19}$$

where ς is the gain in percentage of the extrema of the linear region with respect to the extrema of the Pacejka model.

The affine approximations have been defined by the equation of the linear approximation at $\pm\alpha_z$ and the extrema points of the Pacejka model. Such single partitioning of the front and rear tyre force domain leads to $M = 9$ operating regions, as illustrated in Fig. 4.11. Even though the partitioning can be refined, the simulations shown below confirm that this simple partitioning is capable of capturing the essential behaviour of the nonlinear model.

The effects of the road adhesion, steering angle and longitudinal velocity for the PWA vehicle model are presented in the sequel.

Effects of the road adhesion on the PWA vehicle model

Considering a constant steering input $\delta_f = 0$ and a constant longitudinal speed $v = 20$ $[m/s]$, the PWA vehicle model (4.13) has been simulated at different road adhesion conditions ($\mu =$ 1, 0.7, 0.3). The PWA functions that approximate the tyre forces, depicted in 4.10, have been computed using $\varsigma = 5\%$ and the numerical values for the parameters of the vehicle and Pacejka model are shown in Table 4.3. The set of initial conditions is the same as the one used in Section 4.1.3.

The effect of the adhesion on the PWA model can be seen in Fig. 4.12 for zero steering angle and in Fig. 4.13 for steering angle at $\delta_f = 0.04$ $[rad]$. The boundaries of the operating regions are defined by the hyperplanes:

$$\begin{aligned} \pm\bar{\alpha}_f &= \delta_f - \beta - \tfrac{l_f r}{v} \\ \pm\bar{\alpha}_r &= -\beta + \tfrac{l_r r}{v}, \end{aligned} \tag{4.20}$$

and their projections on the $\beta - r$ plane are illustrated by the green dash-dot lines in both figures for the values of $\delta_f = 0$ and $\delta_f = 0.04$ $[rad]$ respectively.

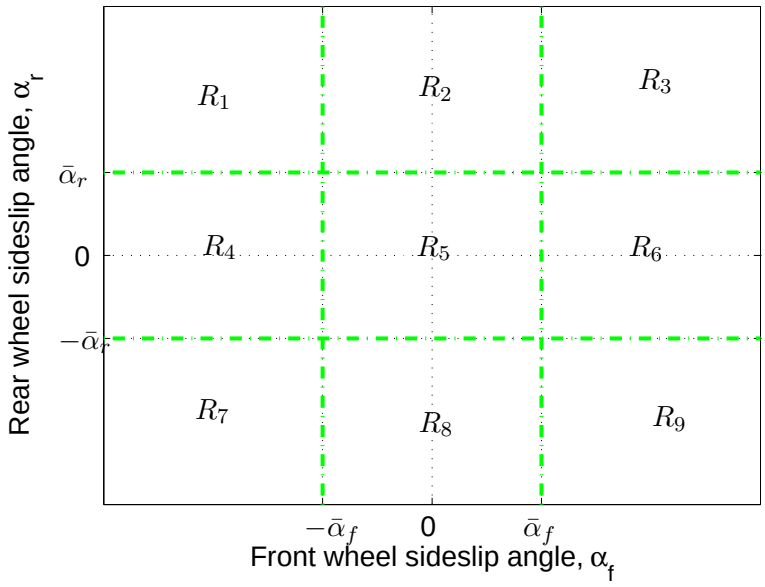

Figure 4.11: Operating regions of PWA vehicle model corresponding to single partitions of the domains from the front and rear tyre forces.

It can be seen from Fig. 4.12 that as the adhesion is reduced so is the stable region, similarly to the results obtained for the nonlinear model depicted in Fig. 4.6. The response of the PWA vehicle model is very similar to the nonlinear one, for a zero steering angle on the ideal road adhesion as shown respectively in the subplots Fig. 4.12-(a) and Fig. 4.6-(a). As the road adhesion is reduced, it can be noticed that the PWA vehicle model shows a larger stability region than the nonlinear one, presenting stable trajectories especially for changes on the yaw rate initial condition.

Concerning the influence of steering, the shifting of the stability region observed on the nonlinear vehicle (see Fig. 4.7) can also be noticed for the PWA vehicle model, as illustrated in Fig. 4.13. However, the PWA modelling does not reproduce the increase on the extreme values of sideslip angle on wet asphalt ($\mu = 0.7$). Nevertheless, this effect is noticeable on the trajectories of the PWA vehicle model when the road adhesion is reduced to $\mu = 0.3$, as shown in Fig. 4.13-(c).

Effects of longitudinal speed in PWA model

Similarly to the analysis with the nonlinear vehicle model, the PWA vehicle model (4.13) has been simulated at different longitudinal velocities. The results, considering the PWA approximations with $\varsigma = 5\%$ (see Fig. 4.10), are shown in Fig. 4.14 for zero steering angle and in Fig. 4.15 for a constant steering angle $\delta_f = 0.04$ $[rad]$.

When comparing the effect of longitudinal velocity on the PWA vehicle model with the nonlinear one at zero steering angle (see Fig. 4.14 and Fig. 4.8, respectively), very similar results are obtained for the dry and wet asphalt conditions. Nevertheless, the unstable behaviour of the nonlinear vehicle on low adherence ($\mu = 0.3$) is not reproduced by the PWA model, except for the longitudinal speed beyond 30 $[m/s]$.

Taking the steering angle into account, as shown in Fig. 4.9 for the nonlinear vehicle model,

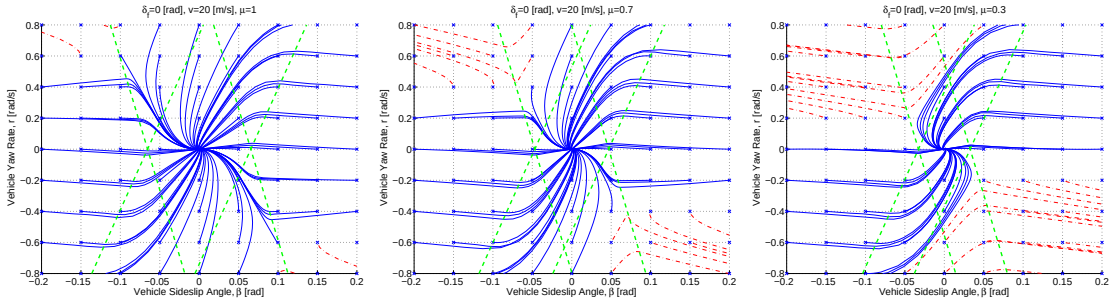

(a) (b) (c)

Figure 4.12: State trajectories for PWA vehicle model with steering angle $\delta_f = 0$ and tyre forces approximated as in Fig. 4.10 on (a) $\mu = 1$, dry asphalt, (b) $\mu = 0.7$, wet asphalt and (c) $\mu = 0.3$, icy asphalt.

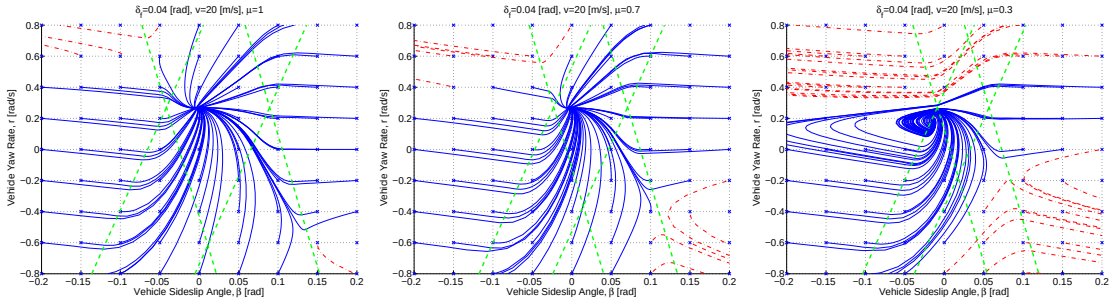

(a) (b) (c)

Figure 4.13: State trajectories for PWA vehicle model with steering angle $\delta_f = 0.04$ $[rad]$ and tyre forces approximated as in Fig. 4.10 on (a) $\mu = 1$, dry asphalt, (b) $\mu = 0.7$, wet asphalt and (c) $\mu = 0.3$, icy asphalt.

and in Fig. 4.15 for the PWA model, it can be seen that larger vehicle speed is required to render the PWA unstable. Considering the wet asphalt condition, for example, the nonlinear vehicle presents unstable behaviour for longitudinal velocities beyond 24 $[m/s]$, whereas no unstable trajectory is obtained for the PWA model in the range of investigated longitudinal velocities. For icy asphalt, a stable trajectory occurs at 16 $[m/s]$, contrarily to the nonlinear vehicle model. At higher speed, both models present unstable behaviour.

From the results obtained in these analyses, it can be noticed that the PWA vehicle model is able to capture the essential effects present on the nonlinear model. The differences of these models, presented mainly through the comparison of the effects of the longitudinal velocity can be mitigated by a finer approximation of the PWA functions.

The sign of slopes of the PWA functions used to approximate the tyre forces play an important role on the behaviour of the PWA model. Such effects are analysed below.

Effects of PWA functions

The PWA functions that approximate the lateral tyre forces have been modified in order to assess the influence of the coefficients d_{fi} and d_{ri} on the behaviour of the PWA model (4.13). Fig. 4.16 presents the PWA approximations of the front and rear tyre lateral forces obtained for $\varsigma = -5\%$ (note that in this case the slope of the affine approximations (d_{fi} and d_{ri}) are positive).

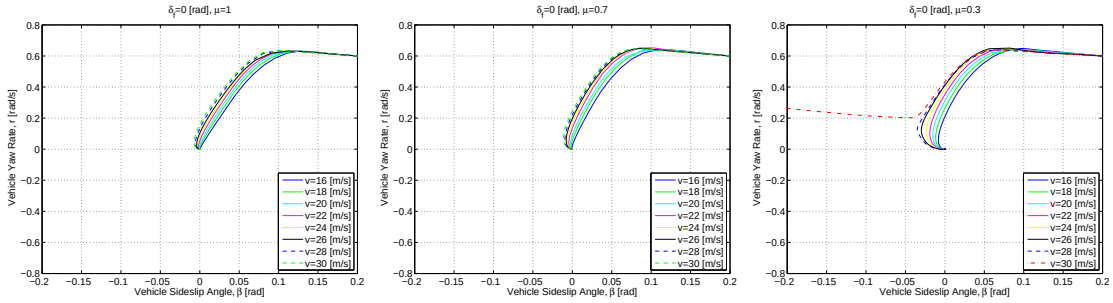

(a) (b) (c)

Figure 4.14: Effects of the longitudinal speed on PWA vehicle model with steering angle $\delta_f = 0$ and tyre forces approximated as in Fig. 4.10 in different adhesion conditions (a) $\mu = 1$, dry asphalt, (b) $\mu = 0.7$, wet asphalt and (c) $\mu = 0.3$, icy asphalt.

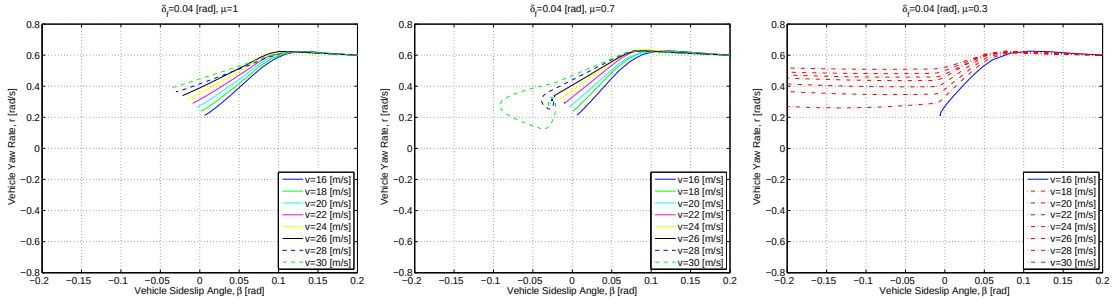

(a) (b) (c)

Figure 4.15: Effects of the longitudinal speed on PWA vehicle model with steering angle $\delta_f = 0.04\ [rad]$ and tyre forces approximated as in Fig. 4.10 in different adhesion conditions (a) $\mu = 1$, dry asphalt, (b) $\mu = 0.7$, wet asphalt and (c) $\mu = 0.3$, icy asphalt.

Similarly to the analysis presented above, the behaviour of the PWA vehicle model has been investigated for changes in the road adhesion and longitudinal speed for constant steering angles at $\delta_f = 0$ and $\delta_f = 0.04\ [rad]$.

The simulation results for the effects of road adhesion are presented for both steering angles in Fig. 4.17 and Fig. 4.19 respectively.

Contrarily to the results obtained with $\varsigma = +5\%$ (shown in Fig. 4.12 and Fig. 4.13), when the coefficients d_{fi} and d_{ri} are positive for all operating regions, all state trajectories are stable, regardless of the road adhesion condition. On the other hand, it can be noticed that the state trajectory from the initial conditions which lead to unstable trajectories for $\varsigma = +5\%$ (negative slopes) is not directly steered to the linear region, and a significant increase on the extreme value of sideslip angle occurs.

For instance, the trajectory starting at $\beta = -0.1$ and $r = 0.6$ for zero steering angle on wet asphalt is unstable for the PWA approximation with $\varsigma = +5\%$, as shown in Fig. 4.12-(b). For the same conditions and PWA approximation with $\varsigma = -5\%$, shown in Fig. 4.17-(b), the trajectory is stable but the sideslip angle diverges from the equilibrium point, as the gradient at initial condition is not oriented to the linear region, therefore the sideslip angle reaches it extremum at $\beta = -0.13\ [rad]$.

Such pronounced a shape of the state trajectories is not present in the trajectories from the initial conditions corresponding to the trajectories that are stable for $\varsigma = +5\%$. For instance,

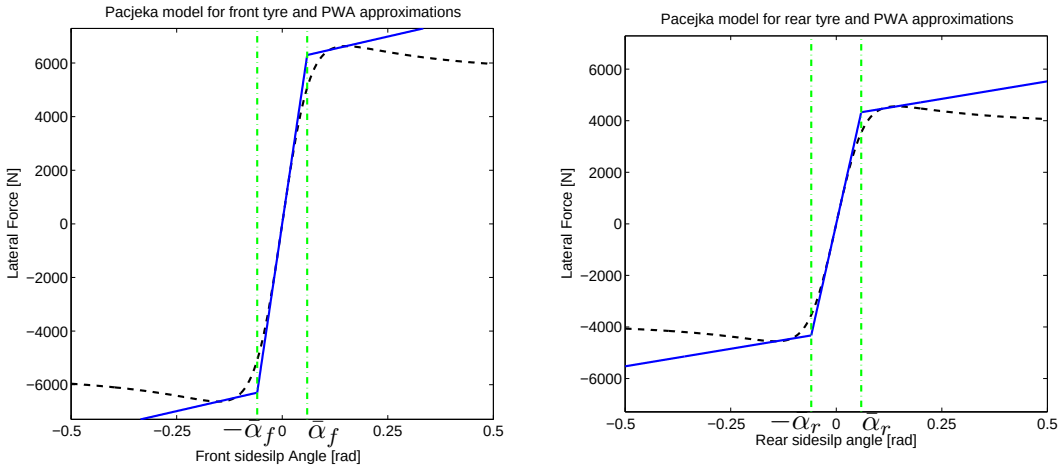

(a) (b)

Figure 4.16: Lateral force according to Pacejka model (dashed) and corresponding PWA approximations (solid) and partitions (dash-dot) for the (a) front tyres and (b) rear tyres.

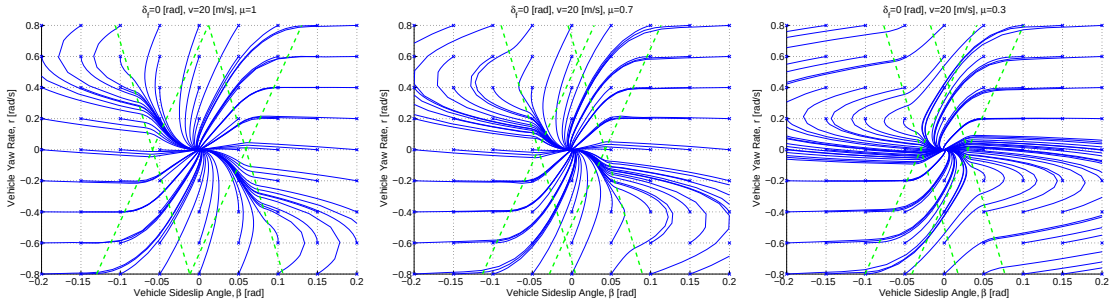

(a) (b) (c)

Figure 4.17: State trajectories for vehicle model with steering angle $\delta_f = 0$ $[rad]$ and tyre forces approximated with $\varsigma = -5\%$ on (a) $\mu = 1$, dry asphalt, (b) $\mu = 0.7$, wet asphalt and (c) $\mu = 0.3$, icy asphalt.

the trajectories starting at $\beta = -0.1$ and $r = 0.4$, for wet asphalt at zero steering angle (see Fig. 4.12 and Fig. 4.17) present a gradient in the direction of the linear region, being stable for both PWA approximations.

Fig. 4.19 and Fig. 4.20 depict the effects of the longitudinal speed on the behaviour of the PWA vehicle model with lateral tyre forces approximated with $\varsigma = -5\%$ (positive slopes only as shown in Fig. 4.16). The first corresponds to constant zero steering angle, while the latter refers to a constant steering angle $\delta_f = 0.04$ $[rad]$.

As for the evaluation of road adhesion effects, the PWA model obtained with $\varsigma = -5\%$ is not able to reproduce the unstable behaviour of the nonlinear vehicle model. Although all trajectories converge to the equilibrium point, the curves present pronounced values of sideslip angle as the longitudinal velocity increases, as shown in Fig. 4.19-(c) for $v = 30$ $[m/s]$. Taking into account the steering angle, the effect appears in Fig. 4.20-(b) and (c) for the vehicle speed $v \geq 26$ $[m/s]$ and $v \geq 16$ $[m/s]$ respectively. Such conditions correspond to the conditions leading to unstable behaviour for the PWA system obtained with $\varsigma = +5\%$ shown in Fig. 4.14 and Fig. 4.15.

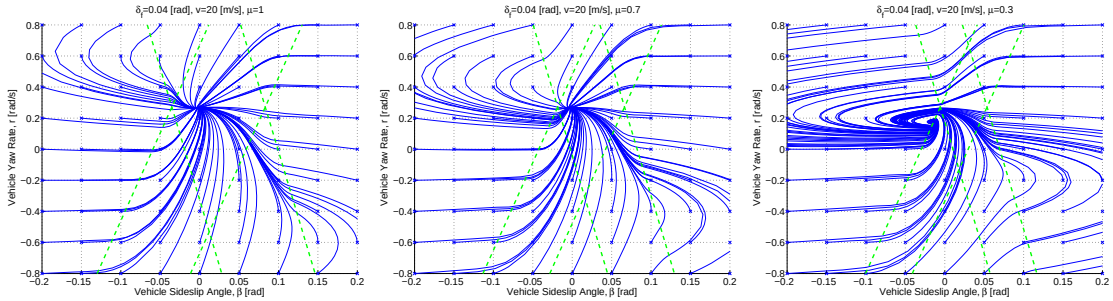

(a) (b) (c)

Figure 4.18: State trajectories for PWA vehicle model with steering angle $\delta_f = 0.04$ $[rad]$ and tyre forces approximated with $\varsigma = -5\%$ on (a) $\mu = 1$, dry asphalt, (b) $\mu = 0.7$, wet asphalt and (c) $\mu = 0.3$, icy asphalt.

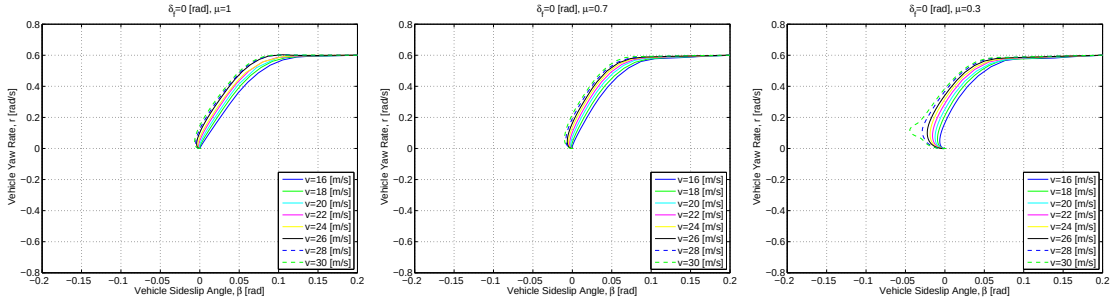

(a) (b) (c)

Figure 4.19: Effects of the longitudinal speed on PWA vehicle model with steering angle $\delta_f = 0$ and tyre forces approximated with $\varsigma = -5\%$ in different adherence conditions (a) $\mu = 1$, dry asphalt, (b) $\mu = 0.7$, wet asphalt and (c) $\mu = 0.3$, icy asphalt.

Remark 4.2.2 *Although the state trajectories in Figures 4.17-4.20 are apparently stable in the mathematical sense (they all converge to the equilibrium point), the values of vehicle sideslip angle are extremely high and do not correspond to physical values encountered in regular driving conditions.*

Remark 4.2.3 *Despite the stability observed in the simulations, Theorem 3.5.1 fails to obtain a piecewise quadratic Lyapunov function to prove the stability of* (4.13) *with the affine functions defined by* $\varsigma = -5\%$ *(see Fig. 4.16).*

It can be noticed that the regions of stability are increased when the vehicle dynamics is modelled with PWA systems (with either $\varsigma > 0\%$ or $\varsigma < 0\%$), which corresponds to a optimistic representation of the reality. Hence, the performance of the controllers designed for the PWA models must be carefully analysed in simulations and in practise, in order to avoid unstable behaviour that is not captured by the PWA model. More details about the model for validation and prototype vehicle will be presented in the end of this chapter.

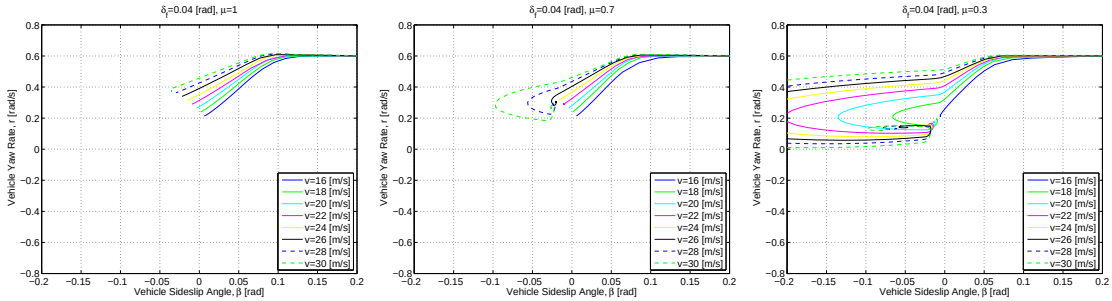

(a) (b) (c)

Figure 4.20: Effects of the longitudinal speed on PWA vehicle model with steering angle $\delta_f = 0.04$ $[rad]$ and tyre forces approximated with $\varsigma = -5\%$ in different adherence conditions (a) $\mu = 1$, dry asphalt, (b) $\mu = 0.7$, wet asphalt and (c) $\mu = 0.3$, icy asphalt.

4.2.2 Assumptions for PWA vehicle model for formal analysis and control synthesis

The theoretical tools for analysis and control synthesis of PWA systems presented in Section 3.5 are based on quadratic and piecewise quadratic Lyapunov functions. For these reasons, some simplifications of the PWA vehicle model have been considered in order to ensure the existence of Lyapunov functions and to be able to use these tools for the design of the lateral assistances.

The two assumptions considered for the PWA vehicle model are:

1. **Saturation of the front wheel is considered**. Since, in general, the vehicles have an understeering behaviour, only the vehicle saturation of the front wheel is considered. The PWA vehicle model (4.13) (or (4.16)) is obtained by taking into account the front tyre forces approximated by PWA functions, and assuming a simple linear approximation for the rear tyre forces *i.e.* $d_{ri} = c_f$ and $e_{ri} = 0$ (as shown in Remark 4.2.1).

2. **Positive slope for PWA approximations of lateral tyre force**. Based on Remark 3.5.6 about the choice of equilibrium points of the closed loop PWA subsystems, in order to synthesise the PWA controllers, only positive values for the slope of the PWA functions that approximate the front tyre lateral force are considered. A detailed description about this adaptation to the PWA vehicle model is provided in Appendix A.2. Under this assumption, $d_{fi} > 0 \ \forall i \in \mathcal{I} = \{1, ..., M\}$. Fig. 4.16 (a) depicts an example of front tyre lateral force approximation with positive slopes only. This assumption is important, not only to enable the use of system analysis and control synthesis based on quadratic Lyapunov functions, ensuring that the closed loop system has only one equilibrium point, but also to be able to provide PWA controllers in which the switches take place before the tyre saturation occurs, so that the assistance can anticipate a critical situation.

A drawback of these assumptions is that it is impossible to evaluate the region of stability, based on the PWA vehicle model, since it becomes globally stable considering the second assumption. The evaluation of the performance and region of stability must be analysed through simulations on the nonlinear model (with PWA controllers) or on the prototype vehicle.

The same simplifications of the PWA vehicle model could be considered in order to design assistances for oversteering vehicles. In this case, a linear model should be considered for the approximation of the lateral forces of front tyres, whereas PWA functions should be used to model the lateral forces of the rear tyres.

4.3 Road Geometry

The road curvature is defined by the inverse of the road radius:

$$\rho \triangleq \frac{1}{R} \tag{4.21}$$

It is modelled as straight, circular and clothoid sections. Clothoids ensure a smooth transition between different road curvature values (e.g. straight to circular roads), [Raj06c]. A clothoid is defined to be a spiral whose curvature is a linear function of it arc length. Mathematically it is defined in terms of the Fresnel integrals and its parametric equations are:

$$\begin{bmatrix} X(t) \\ Y(t) \end{bmatrix} = a \begin{bmatrix} \int_0^t \cos\left(\frac{\pi u^2}{2}\right) du \\ \int_0^t \sin\left(\frac{\pi u^2}{2}\right) du \end{bmatrix} \tag{4.22}$$

where $X(t)$ and $Y(t)$ are the longitudinal and lateral distances respectively. The constant a indicates the centre of the spiral, which has coordinates $\left(\frac{a}{2}, \frac{a}{2}\right)$ (supposing that it is in the first quadrant and starting from the origin at $t = 0$).

The distance travelled by a vehicle at constant speed increases linearly with time, therefore, for a chlothoidal road profile, the curvature is considered as increasing linearly with respect to time. Fig. 4.21 (a) shows a road built from straight, clothoidal and a circular sectors. The corresponding road curvature for a vehicle travelling at constant speed of $c = 20m/s$ is plotted at Fig. 4.21 (b).

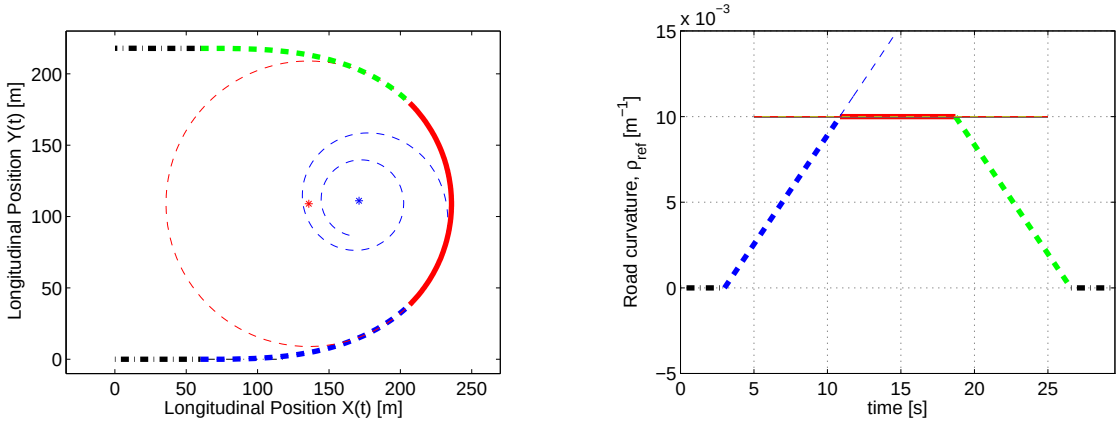

(a) (b)

Figure 4.21: (a) Road profile of straight (dash-dot line), clothoidal (dashed line) and circular (solid line) sectors. (b) Corresponding road curvature for a vehicle travelling at constant speed $v = 20$ $[m/s]$.

4.4 Additional dynamics for lane keeping

For lane keeping purposes, the model (4.13) (or (4.16)) has to be expanded with the dynamics of the relative yaw angle and the lateral displacement with respect to the lane centreline. These measurements are provided by a video sensor. Let $\psi_L = \psi - \psi_t$ be the yaw angle error which

is the angle between the vehicle orientation and the tangent to the road. The road reference curvature ρ_{ref} is defined by ($\dot{\psi}_t = v\rho_{ref}$), and the following equality can be derived:

$$\dot{\psi}_L = r - v\rho_{ref}. \tag{4.23}$$

Denoting l_s, the look-ahead distance, the equation giving the evolution of the measurement of the lateral offset y_L from the centerline at sensor location is obtained by

$$\dot{y}_L = v(\beta + \psi_L) + l_s r. \tag{4.24}$$

The vehicle model which takes into account the positioning of the vehicle can be described by:

$$\dot{x}^p = A_i^p x^p + B_i^p u + B_\rho^p \rho_{ref} + a_i^p \tag{4.25}$$

where $x^p = [\beta, r, \psi_L, y_L]^T$ and

$$A_i^p = \begin{bmatrix} -2\frac{d_{fi}+d_{ri}}{mv} & -1 - 2\frac{d_{fi}l_f - d_{ri}l_r}{mv^2} & 0 & 0 \\ 2\frac{d_{ri}l_r - d_{fi}l_f}{J} & -2\frac{d_{fi}l_f^2 + d_{ri}l_r^2}{Jv} & 0 & 0 \\ 0 & 1 & 0 & 0 \\ v & l_s & v & 0 \end{bmatrix}, \tag{4.26}$$

$$B_i^p = \begin{bmatrix} \frac{2d_{fi}}{mv} \\ \frac{2d_{fi}l_f}{J} \\ 0 \\ 0 \end{bmatrix}, \quad B_\rho^p = \begin{bmatrix} 0 \\ 0 \\ -v \\ 0 \end{bmatrix}, \quad a_i^p = \begin{bmatrix} 2\frac{e_{fi}+e_{ri}}{mv} \\ 2\frac{e_{fi}l_f - e_{ri}l_r}{J} \\ 0 \\ 0 \end{bmatrix}. \tag{4.27}$$

Fig. 4.22 illustrates the additional variables describing the vehicle positioning for lane keeping.

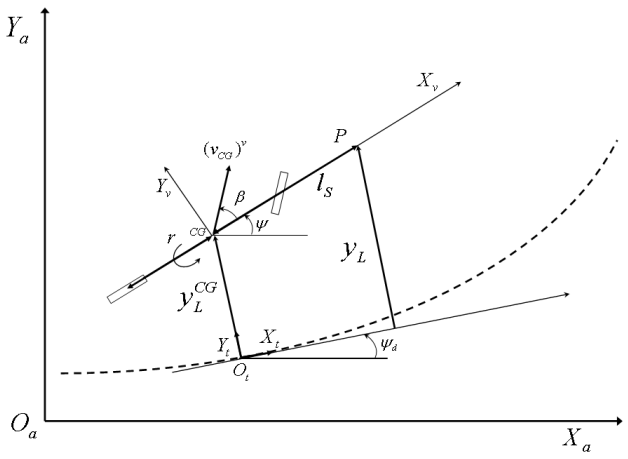

Figure 4.22: Dynamics and positioning for a single track vehicle model.

Remark 4.4.1 *Similarly to* (4.16)*, the steering angle can also be included in the state vector (see* (4.15)*) in order to have the partitions described in terms of state variables only. In this case the system becomes PWA of the form:*

$$\dot{x}^v = A_i^v x^v + B_i^v u + B_\rho^v \rho_{ref} + a_i^v \tag{4.28}$$

where $x^v = [\beta, r, \psi_L, y_L, \delta_f]^T$ *and*

$$A_i^v = \begin{bmatrix} -2\frac{d_{fi}+d_{ri}}{mv} & -1-2\frac{d_{fi}l_f-d_{ri}l_r}{mv^2} & 0 & 0 & \frac{2d_{fi}}{mv} \\ 2\frac{d_{ri}l_r-d_{fi}l_f}{J} & -2\frac{d_{fi}l_f^2+d_{ri}l_r^2}{Jv} & 0 & 0 & \frac{2d_{fi}l_f}{J} \\ 0 & 1 & 0 & 0 & 0 \\ v & l_s & v & 0 & 0 \\ 0 & 0 & 0 & 0 & -\tau \end{bmatrix}, \tag{4.29}$$

$$B_i^v = \begin{bmatrix} 0 \\ 0 \\ 0 \\ 0 \\ \tau \end{bmatrix}, \quad B_\rho^v = \begin{bmatrix} 0 \\ 0 \\ -v \\ 0 \\ 0 \end{bmatrix}, \quad a_i^v = \begin{bmatrix} 2\frac{e_{fi}+e_{ri}}{mv} \\ 2\frac{e_{fi}l_f-e_{ri}l_r}{J} \\ 0 \\ 0 \\ 0 \end{bmatrix}. \tag{4.30}$$

4.5 Electrically assisted steering column

The prototype vehicle, on which the developed assistances will be tested, has been equipped with a DC motor that provides the torque on the steering column (described in detail in Section 4.6.2). For this reason, it becomes interesting to consider the steering column dynamics in the PWA vehicle model used to design the lane keeping assistances, so that the torque on the steering column can be used as control input for the practical implementation.

The steering column can be modelled as a second order linear system [ME08] as follows:

$$\begin{bmatrix} \dot{\delta}_p \\ \ddot{\delta}_p \end{bmatrix} = \begin{pmatrix} 0 & 1 \\ 0 & -\frac{B_s}{I_s} \end{pmatrix} \begin{bmatrix} \delta_p \\ \dot{\delta}_p \end{bmatrix} + \begin{pmatrix} 0 & 0 \\ \frac{1}{I_s} & -\frac{1}{I_s} \end{pmatrix} \begin{bmatrix} \tau_p \\ \tau_{alg} \end{bmatrix} \tag{4.31}$$

where δ_p is the angle on the steering wheel, and the inputs are the torque on the steering wheel τ_p and the self-alignment torque τ_{alg} from the wheels at the steering wheel level. The parameters B_s and I_s stand for the damping coefficient and inertial moment of the steering column, respectively.

The self-alignment torque, at the front wheels level, can be modelled as the product between the length of the tyre contact η and the front tyre lateral force F_{yf}. Considering the PWA approximation for the front tyre lateral forces (4.12) and the front wheel sideslip angle as in (4.3), the self-alignment torque at steering wheel level becomes:

$$\tau_{alg} = \eta \frac{2F_{yf}}{R_s} = 2\frac{\eta}{R_s}\left(d_{fi}\left(\delta_f - \beta - \frac{l_f r}{v}\right) + e_{fi}\right), \tag{4.32}$$

where R_s is the gear ratio from the steering wheel to the front wheels, given by:

$$R_s = \frac{\delta_p}{\delta_f} \tag{4.33}$$

Rewriting the second equation from (4.31) in terms of δ_f and considering the self-alignment torque τ_{alg} as described in (4.32) yields:

$$\ddot{\delta}_f = 2\eta\frac{d_{fi}}{I_s R_s^2}\beta + 2\eta\frac{l_f d_{fi}}{I_s R_s^2 v}r - 2\eta\frac{d_{fi}}{I_s R_s^2}\delta_f - \frac{B_s}{I_s}\dot{\delta}_f + \frac{1}{I_s R_s}\tau_p - 2\eta\frac{e_{fi}}{I_s R_s^2} \tag{4.34}$$

The PWA vehicle model (4.25) can then be extended to take into account the dynamics of the electrically powered steering column, which becomes:

$$\dot{x} = A_i x + B_i u + B_\rho \rho_{ref} + a_i \tag{4.35}$$

where $x = [\beta, r, \psi_L, y_L, \delta_f, \dot{\delta}_f]^T$ and $u = \tau_p$

$$A_i = \begin{bmatrix} -2\frac{d_{fi}+d_{ri}}{mv} & -1-2\frac{d_{fi}l_f - d_{ri}l_r}{mv^2} & 0 & 0 & \frac{2d_{fi}}{mv} & 0 \\ 2\frac{d_{ri}l_r - d_{fi}l_f}{J} & -2\frac{d_{fi}l_f^2 + d_{ri}l_r^2}{Jv} & 0 & 0 & \frac{2d_{fi}l_f}{J} & 0 \\ 0 & 1 & 0 & 0 & 0 & 0 \\ v & l_s & v & 0 & 0 & 0 \\ 0 & 0 & 0 & 0 & 0 & 1 \\ 2\eta\frac{d_{fi}}{I_s R_s^2} & 2\eta\frac{l_f d_{fi}}{I_s R_s^2 v} & 0 & 0 & -2\eta\frac{d_{fi}}{I_s R_s^2} & -\frac{B_s}{I_s} \end{bmatrix},$$

$$B_i = \begin{bmatrix} 0 \\ 0 \\ 0 \\ 0 \\ 0 \\ \frac{1}{I_s R_s} \end{bmatrix}, \quad B_\rho = \begin{bmatrix} 0 \\ 0 \\ -v \\ 0 \\ 0 \\ 0 \end{bmatrix}, \quad a_i = \begin{bmatrix} 2\frac{e_{fi}+e_{ri}}{mv} \\ 2\frac{e_{fi}l_f - e_{ri}l_r}{J} \\ 0 \\ 0 \\ 0 \\ -2\eta\frac{e_{fi}}{I_s R_s^2} \end{bmatrix}. \tag{4.36}$$

This model is particularly advantageous when the partitions of the PWA system are described in term of front wheel sideslip angle, since they can be rewritten in terms of state-space variables.

Table 4.1 summarises the models used for the design of the assistances.

Table 4.1: Summary of PWA vehicle models used for assistance design

	Control Input		
Assistance type	δ_f	$\dot{\delta}_f$	τ_a
Vehicle Dynamics	(4.13)	(4.16)	
Vehicle Dynamics and Positioning	(4.25)	(4.28)	(4.35)

Although the models described for the design of the lateral assistances are able to capture the essentials of the vehicle lateral dynamics, several effects and dynamics have been neglected. For this reason, it is important to evaluate the assistance performance either on the real vehicle or using a more complete vehicle model in simulations. In the next section the simulation environment and the prototype vehicle used to validate the lateral assistances are presented.

4.6 Simulation environment and practical implementation

In order to evaluate the performance of the controllers, simulations and experiments on a prototype vehicle have been carried out. In this section the CarSim simulation environment is detailed as well as the equipment installed on the prototype vehicle.

4.6.1 CarSim simulation environment

CarSim vehicle model [Mac81] uses detailed nonlinear tyre models according to combined slip theory and takes into account the major kinematics and compliance effects of the suspensions (nonlinear spring models) and steering systems. It also considers the roll and pitch dynamics which were neglected at the control design stage. Fig. 4.23 shows the user interface of the simulator. The standard CarSim D-Class vehicle has a nonlinear second order speed depending rack and pinion ratio steering system; a realistic actuator with a bandwidth of 10Hz is considered for the active steering.

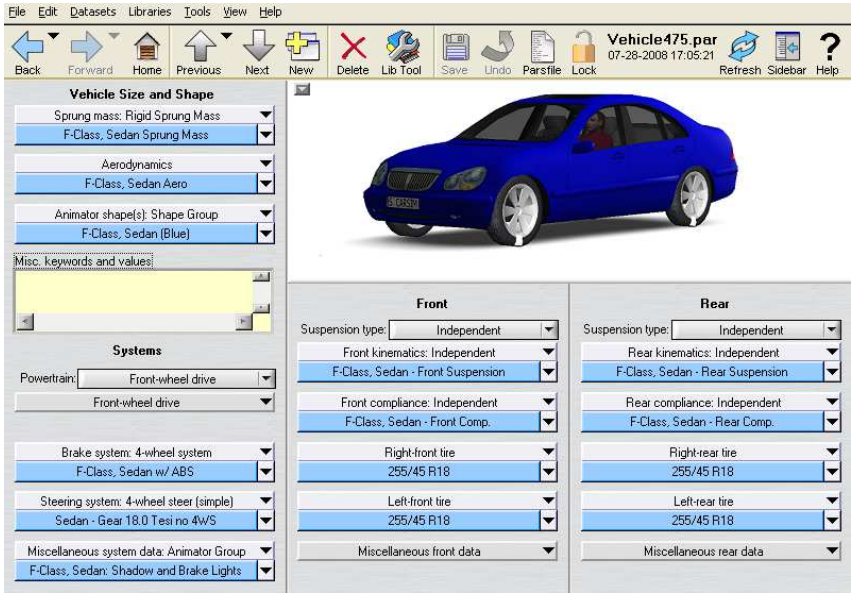

Figure 4.23: User Interface of CarSim simulator

Table 4.2 presents the numerical values of the parameters from the standard CarSim D-Class vehicle model and the Pacejka parameters obtained from the same vehicle model with 225/65R17 front and rear tyres.

4.6.2 Practical Implementation on prototype vehicle CARLLA

The experimental vehicle used in the practical implementation (Fig. 4.25) is a Peugeot-307 SW, named CARLLA[32], has been equipped and instrumented at LIVIC to test the driving assistance systems. The equipment used for lateral assistance includes proprioceptive and exteroceptive sensors, actuators and computing units. Each of these, is detailed below, and the system architecture can be seen in Fig. 4.24.

[32]Contrôleur d'Assistance Routière Longitudinale et Latérale

Table 4.2: Vehicle parameters for standard CarSim D-Class vehicle model:

Vehicle parameters			Pacejka parameters			
			Front tyres		Rear tyres	
m	1862	[kg]	B_{yf}	11.4592	B_{yr}	11.4592
J	2488	[kg m^2]	C_{yf}	1.4	C_{yr}	1.4
c_f	1.0633e+5	[N/rad]	D_{yf}	6628	D_{yr}	4556
c_r	7.3104e+4	[N/rad]	E_{yf}	-0.5	E_{yr}	-0.7
l_f	1.18	[m]				
l_r	1.77	[m]				

Proprioceptive Sensors

- **Odometer**: The odometer provides a periodic pulse, the width of which is inversely proportional to the vehicle longitudinal speed. Therefore, the measurement of the pulse width is sent to the computing unit in order to retrieve the vehicle longitudinal speed, by the inversion of this signal.

- **Inertial central**: A Crossbow VG400 three-axis inertial central is linked to the PC through the RS232 to provide along the three axes the measurements of acceleration (longitudinal, lateral and vertical) and rotational speeds (roll, pitch and yaw). The inertial central is shown in Fig. 4.26 (a).

- **Optical sensor CORREVIT**: A CORREVIT optical sensor type 2-axis S-400, shown in Fig. 4.26 (b), provides measurements of the longitudinal and lateral speeds of the vehicle, as well as an estimation of the vehicle sideslip angle, through an internal Kalman filter. The sensors is based on an optical system to treat the scrolling of the road surface. A translation of the measurements from the sensor location to the vehicle centre of gravity is required.

- **Angular optical sensor**: An angular optical sensor type CHM 510-13BT-002, produced by BEI IDEACOD is mounted on the steering column at the level of the steering wheel gear. The measured angles are encoded in 13 bits, which corresponds to an angle variation of 0.1266°. The wheel steering angle can also be retrieved from this measurement, due to the mechanical coupling between the steering wheel and the wheels. The steering angle sensor is illustrated in Fig. 4.26 (c).

- **Driver torque sensor**: The driver torque on the steering wheel is obtained by a torque sensor SCAIME type ZF, which is mounted on the connection of the steering wheel and steering column. The measurements are in the range $\{-31.5,\ +31.5\}$ $[Nm]$ encoded with 12 bits, such that each bit corresponds to a torque variation of $0.0154Nm$. This sensor can be seen in the schema representing the steering system in Fig. 4.28.

- **Wheel torque sensor**: The torque transmitted to the wheels is measured with a sensor SCAIME type DR2513, placed on the steering column under the pinion of the electric motor. the measurements range from $\{-50,\ +50\}$ $[Nm]$, encoded with 12 bits such that

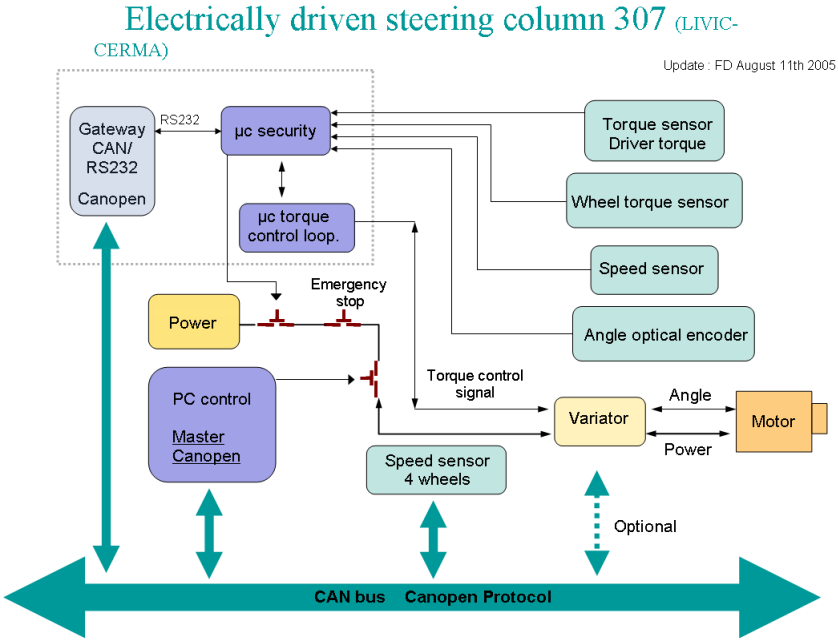

Figure 4.24: Archtecture of electric steering column

each bit correspond to a torque variation of $0.0244Nm$. The wheel torque sensor in the steering system is shown in Fig. 4.28.

Exteroceptive Sensors

- **Video camera**: a CCD camera model CNB WK-ZS260IR is mounted at the rear view mirror for frontal vision, as shown in Fig. 4.27. It works either in day light or at night, and delivers an 8-bit grey-scaled image with resolution of 752(H) x 582(V) pixels at a frequency of 25 frames per second.

  The images are treated with the algorithms described in [LDLC06] which are capable of

Figure 4.25: Aerial View from Satory-Versailles test track. Photo from: TGLR, Atelier Gérard Leroux, 13, rue Pierre Clavillier, 78800 Houilles, France and experimental vehicle.



(a) (b) (c)

Figure 4.26: Proprioceptive sensors used to equip the prototype vehicle CARLLA (a) Inertial central, (b) CORREVIT, (c) Optical encoder for steering angle.

detecting the lane marks. Moreover it computes the vehicle lateral offset at look-ahead distance and relative yaw angle, both with respect to the centre of the lane. The road curvature is also computed by the algorithm.

- **RTK GPS**: a RTK[33] GPS[34] model Thalès SAGITTA 02 has been used to log the vehicle position and yaw angle. A precise cartography of the test track is available which makes it possible to evaluate the vehicle trajectory.

Figure 4.27: CCD video camera for frontal view

Actuators

The original hydraulic steering column of the Peugeot 307 has been replaced by an electric DC motor driven by a PIC micro-controller. Two possibilities of usage are possible with the electric assisted steering column [Dup07]. It may work in a regular mode in which the micro controller ensures a regular electric steering assistance while driving. It can also be used in the experimental mode, in which the micro-controller receives reference signals of torque from the computing unit and ensures the low level control to track the reference signals. The validity of the reference signals are checked for safety reasons. The DC motor can be seen in the schema for the steering system in Fig. 4.28.

The reference signal may also be provided in terms of steering angle, in this case, a PID controller is used to track the reference.

[33] Real Time Kinetic
[34] Global Positioning System

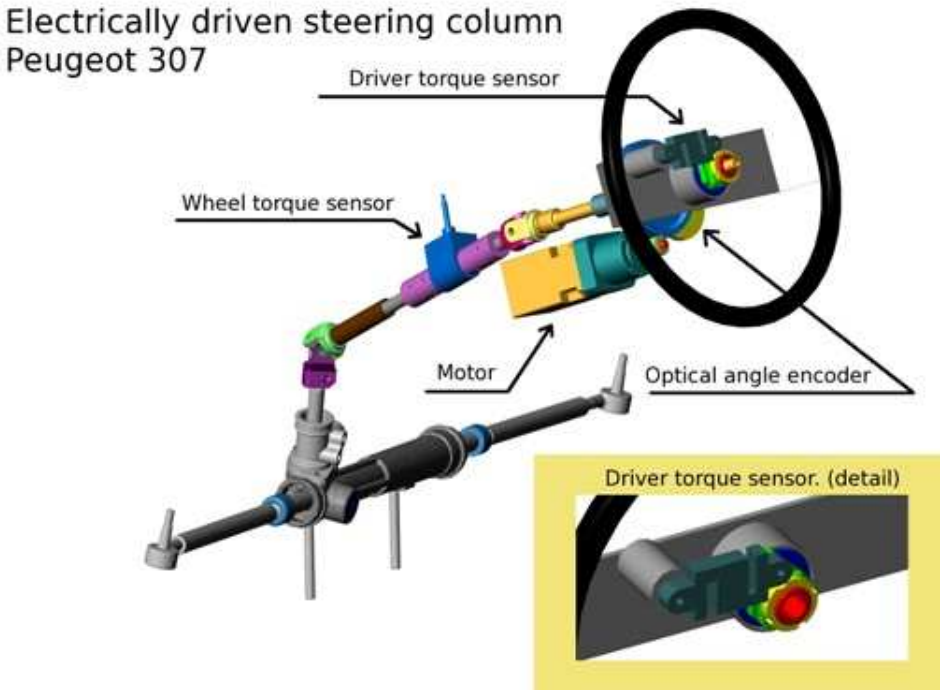

Figure 4.28: Steering system

Computing units

2 PCs are installed in the boot of CARLLA (shown in Fig. 4.29), one is dedicated for the image treatment algorithms, while the other is used for the control algorithms. Each of the PCs is equipped with 2 AMD Opteron 2.2 GHz processors and 1Gb RAM memory. They serve as Human-Machine Interface through the software *RTMaps*, developed by *Intempora*. *RTMaps* allows the acquisition of data from different channels (serial port, bus Can, video, etc) and also the creation of logs. The algorithms of image processing and control are coded in *C++* and integrated to *RTMaps* through *Microsoft Visual Studio*.

Parameters of prototype vehicle CARLLA

The numerical values of the vehicle parameters used are presented in Table 4.3,

4.6.3 Testing Track

The practical experiments took place on a test track located in Satory-Versailles, 20Km west of Paris, France. The track is 3.5km long, consisting of typical road profiles as straight lines and bends of various radii. The GPS coordinates of the centre of the test track are depicted in Fig. 4.30 (a) and the corresponding curvature for the track is shown in (b). The straight sectors are depicted in blue, the clothoidal in red and the circular in green. It is important to note that it is possible to attain saturation of the lateral tyre forces in some curves.

Fig. 4.25 depicts an aerial view of the test track.

Figure 4.29: Computing units for image processing and control algorithms

Table 4.3: Vehicle parameters for the Prototype vehicle CARLLA:

Vehicle parameters			Pacejka parameters			
			Front tyres		Rear tyres	
m	1600	[kg]	B_{yf}	8.3278	B_{yr}	8.3278
J	2454	[kg m^2]	C_{yf}	1.1	C_{yr}	1.1
c_f	39995	[N/rad]	D_{yf}	4366	D_{yr}	3820
c_r	34993	[N/rad]	E_{yf}	-1.661	E_{yr}	-1.661
l_f	1.22	[m]				
l_r	1.44	[m]				
B_s	14	$[m]$				
I_s	0.05	$[kgm^2]$				
η	0.13	$[m]$				
R_s	15					

4.7 Conclusion

In this chapter, the nonlinear vehicle model for lateral dynamics has been presented. It captures the essential lateral dynamics which includes the translational and yaw motion, assuming constant longitudinal speed and that the two wheels of each axle are lumped into one located at its centre. Roll and pitch dynamics, load transfers and chassis or suspension compliance effects have been neglected. The Pacejka model for tyre lateral forces has also been presented and simulations of the nonlinear vehicle model have been carried out in order to investigate the effects of road adhesion and longitudinal speed on the stability of the model.

The approximation of the tyre lateral forces by piecewise affine functions has been demonstrated and the PWA vehicle model for lateral dynamics has been developed. Simulations have

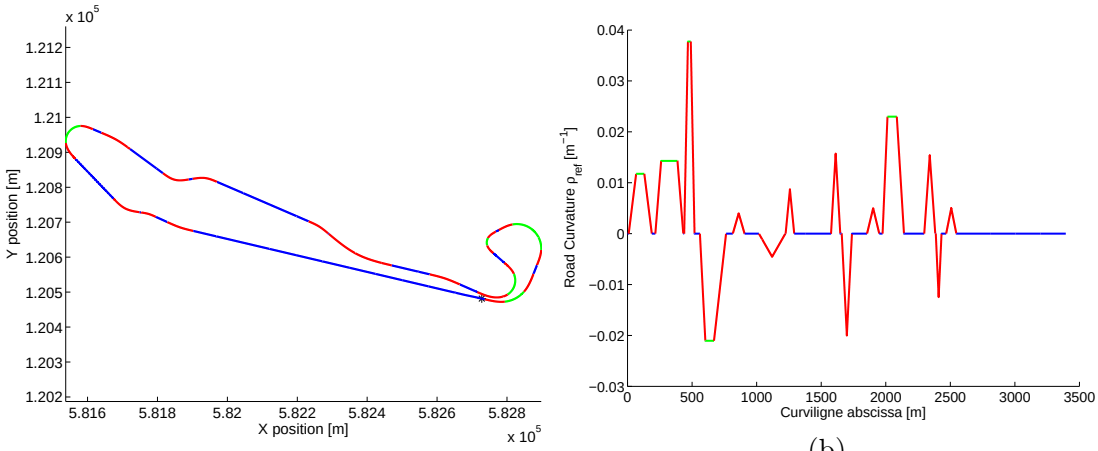

(a) (b)

Figure 4.30: (a) GPS coordinates (Lambert projection) of Satory test track and (b) Corresponding road curvature.

shown that the PWA vehicle model can reproduce the behaviour of the nonlinear system. Moreover, the effect of road adhesion, steering angle, and longitudinal velocity for different PWA approximations has been discussed.

Two important assumptions have been made in order to use the PWA vehicle model for the design of driving steering assistance systems based on (piecewise) quadratic Lyapunov functions. Firstly, only saturation of the front tyre forces has been considered, as most passenger cars have understeering behaviour. Secondly, the slopes of the piecewise affine functions that approximate the Pacejka tyre model are positive. Despite these simplifications, the PWA vehicle model still covers the whole domain of lateral tyre force, being therefore adequate for the development of the *Perceptive-ESC* .

The road geometry has been presented and modelled for a vehicle travelling at constant speed. Additional variables to take into account the vehicle positioning and electric powered steering column have also been introduced.

Finally, the simulation environment and prototype vehicle, which take into account the neglected dynamics and effects of the PWA single track vehicle model, have also been described. They are used to validate the lateral assistance systems, described in the next part.

Part III

Driving assistance for vehicle dynamics and positioning

Chapter 5

Active steering control for handling improvement

Contents

In this chapter, the design of active steering systems based on PWA controllers is investigated. A simple control structure, consisting of a single proportional-integral (PI) controller, has been extended to a PWL PI controller, in which the switches are driven by the measurement of the yaw rate, and the switching boundaries are specified by a parametrisation of the vehicle dynamics with respect to this variable. At a second stage, the structure is enhanced with a PWL feedback loop in order to improve the vehicle stability, and the switches are driven by estimation of the front wheel sideslip angle.

For both proposed PWL controllers, the stability is proved by piecewise quadratic Lyapunov functions. The performance of the PWL controllers is evaluated by simulations on a CarSim vehicle model and comparisons with respect to corresponding linear controllers are carried out.

The main objective of this chapter is the investigation of the potential advantages of active steering systems based on PWA controllers. Moreover it is intended to verify that the vehicle stability can be improved by taking into account the nonlinear behaviour of the tyre lateral forces in the control synthesis.

5.1 Piecewise linear control for reference yaw rate tracking

As mentioned in Section 2.2.1, an active steering system is designed to reject disturbances and enlarge the vehicle stability region, while the driver is responsible to provide the required

steering angle to follow the track. Such systems are usually included in steer-by-wire vehicles, and a reference model is used to convert the driver steering angle on the steering wheel into a yaw rate reference.

Many possibilities to design the reference model can be found in the literature. In [OBNY+11], a first order transfer function with the same steady state gain as the conventional car is used. The gain is derived from the single track linear model. In [MSC07] a nonlinear first order model is considered in which the lateral acceleration is also taken into account. In this work, as the objective is the evaluation of the PWL controllers, a more simple reference model, consisting only of the steady state gain is used. The yaw rate reference signal is computed from the driver input, based on the steering wheel angle, δ_p, as follows:

$$r_d = K_\delta(v)\delta_p \tag{5.1}$$

in which K_δ is computed as:

$$K_\delta(v) = \lim_{s\to 0} C_{lin}(v)\left[sI - A_{lin}(v)\right]^{-1} B_{lin}(v), \tag{5.2}$$

where $C_{lin} = [0 \quad 1]$, and the index *lin* represents the linear approximation of the tyre lateral forces (see Remark 4.2.1) for vehicle model (4.13). Most drivers are only familiar with the linear operating region of the tyre forces, hence the choice of this dynamics as a reference model makes sense.

Several control strategies for active steering systems can be found in the literature (as described in Section 2.2.1). In the patent [B+03], a PI (proportional-integral) controller has been used to ensure the tracking of constant yaw rate reference signal ($\dot{r}_d = 0$) in the design of an active steering system in which the integral term is used to reject perturbations on the lateral and yaw dynamics.

The linear PI controller on the basis of yaw rate error can be described as:

$$\begin{aligned} \delta_{fPI} &= -K_P(r - r_d) - K_I \textstyle\int_0^t (r - r_d)\, d\zeta \\ \delta_{fPI} &= -K_P\dot{\alpha}_0 - K_I\alpha_0 \end{aligned} \tag{5.3}$$

where α_0 is thus an additional state introduced by the dynamic controller (5.3) in the closed loop system.

Due to its simplicity, this controller has been chosen as a basis to be extended to a PWL structure.

In order to improve the vehicle handling without neglecting the nonlinear behaviour of the lateral tyre forces, two extensions of this active steering controller are proposed by considering the affine approximations of the lateral tyre forces in the design of piecewise linear proportional-Integral (PI_i) controllers.

Remark 5.1.1 (Anti windup) *It is important to note, mainly for the practical implementation of the PWL PI controllers, that the control input is computed only for the active operating region of the state-space. Therefore, when a switch from one operating region to another takes place, the current value of the error variable, α_0, is carried over and the only gains of the corresponding region are changed to conpute the control input. Such configuration avoids the accumulation of integration term for regions that are not active.*

The first control strategy, named *Controller-1*, involves the design of the PI gains for the affine regions of the PWA vehicle model. Moreover, a parametrisation of the vehicle dynamics

in terms of the yaw rate is carried over to have the switches driven only by the yaw rate. Such switching condition avoids the use of the high cost sensors for measurement of vehicle sideslip angle and estimators of wheel sideslip angles.

For second active steering assistance, referred to as *Controller-2*, a state feedback loop is included in order to enhance the vehicle dynamic stability. Both control strategies are discussed in the subsequent sections.

5.1.1 PWL PI with Parametrised vehicle dynamics - *Controller-1*

Controller-1 is based on a parametrisation of vehicle dynamics with respect to the yaw rate, which is a variable that can be measured without additional cost on the currently commercialised passenger cars. The switching conditions are redefined through an analysis of the steady state behaviour of the nonlinear vehicle model. The vehicle dynamics parametrisation in terms of yaw rate is shown below.

Parametrisation of vehicle dynamics in term of yaw rate

By solving the equation for the nonlinear vehicle model (4.1) equal to zero at constant speed and different constant inputs (steering angle, δ_f), the steady state values of the vehicle lateral speed, v_y^{ss} and yaw rate, r^{ss} are obtained. The values obtained are marked with $\times$ in Fig. 5.1.

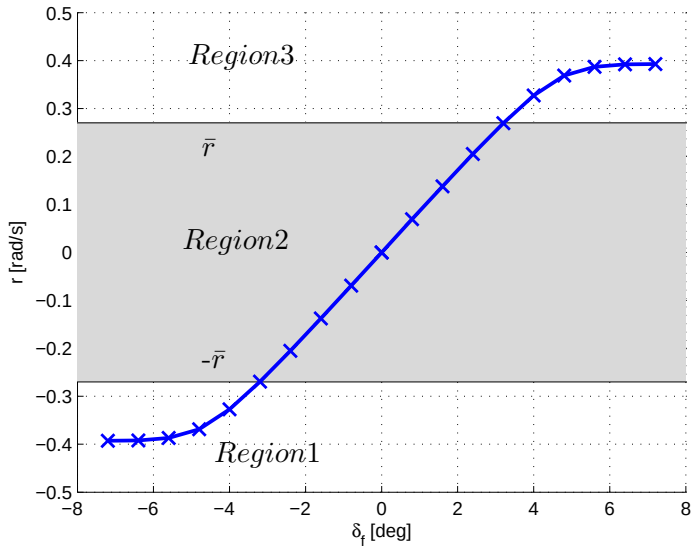

Figure 5.1: Steady state nonlinear vehicle yaw rate for different steering angles; the computed regions are emphasized by the gray box ($v = 30$ $[m/s]$).

For each triple $\{\delta_f,\ v_y^{ss},\ r^{ss}\}$, using equations (4.3), the front and the rear tyre sideslip angles at steady-state can be computed, which are denoted $\alpha_f^{ss}(\delta_f)$ and $\alpha_r^{ss}(\delta_f)$, respectively. Consequently, the front and rear tyre forces corresponding to the steady-state condition, can also be calculated by (4.6).

In Fig. 5.2, the Pacejka tyre model is plotted for the front tyre (solid line). The $\times$ marks on the diagram represent the lateral tyre force as a function of the computed front wheel sideslip angle from the steady-state analysis. For the sake of clarity, only the front tyre is plotted but the same is done for the rear tyre.

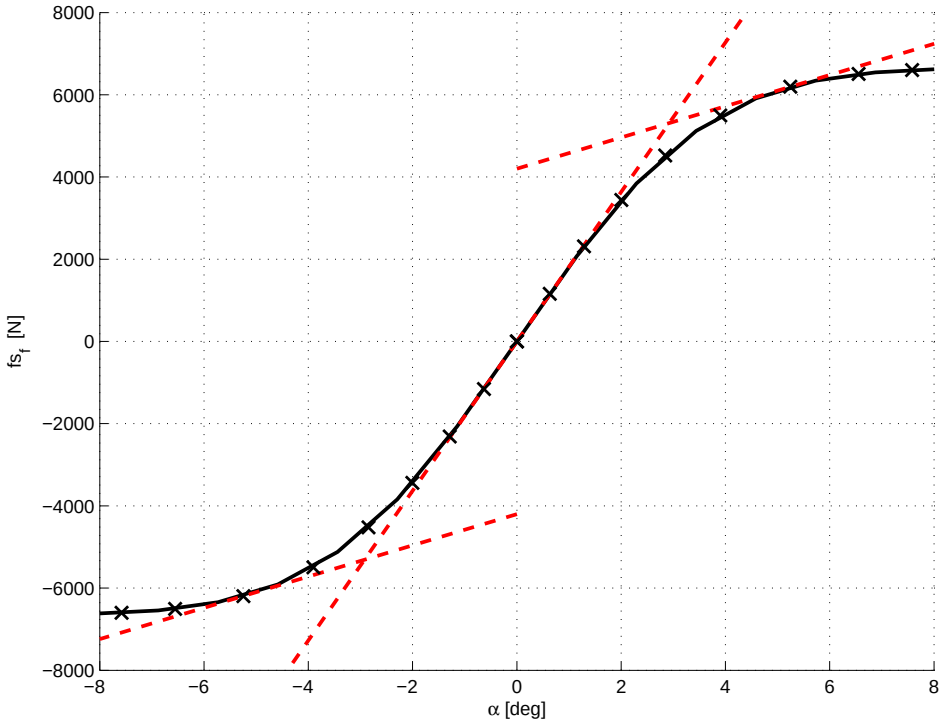

Figure 5.2: Front tyre force described by the Pacejka magic formula and corresponding PWA approximation.

Considering the PWA approximation of the lateral tyre forces, with the hyperplanes $\alpha_f = \bar{\alpha}_{f(ij)}$ and $\alpha_r = \bar{\alpha}_{r(ij)}$ delimiting the neighbouring operating regions R_i and R_j, it is possible to find, with arbitrary precision, values of wheel sideslip angle at steady state that correspond to each $\bar{\alpha}_{f(ij)}$ and $\bar{\alpha}_{r(ij)}$, *i.e*:

$$\begin{aligned} |\alpha_f^{ss}(\delta_f) - \bar{\alpha}_{f(ij)}| < \epsilon \\ |\alpha_r^{ss}(\delta_f) - \bar{\alpha}_{r(ij)}| < \epsilon \end{aligned} \tag{5.4}$$

where $\epsilon > 0$ is a scalar, determining the desired precision.

Since α_f^{ss} and α_r^{ss} are unique for each triple$\{\delta_f,\ v_y^{ss},\ r^{ss}\}$, the obtained values can be linked to the state-space variables, and consequently, be used to redefine the partitions $\alpha_f = \bar{\alpha}_{f(ij)}$ and $\alpha_r = \bar{\alpha}_{r(ij)}$ in terms of state-space variables.

A parametrisation in terms of yaw rate is chosen, because it can be measured in currently commercialised vehicles. By doing so, the partitions on the tyre sideslip angle determine the hyperplanes on the yaw rate.

Fig. 5.2 shows an example for the front wheel of a simple partitioning at $\alpha_f = \pm\bar{\alpha}_f$. The corresponding values of yaw rate in steady state are depicted in Fig. 5.1 by the values $r = \pm\bar{r}$.

Having redefined the switching boundaries in terms of yaw rate, the PWL PI controller is introduced below.

Structure of *Controller-1*

The redefinition of the partitions in terms of yaw rate enables the implementation of a simpler controller structure involving a PWL proportional-integral controller (PI_i), as an extension of

(5.3). A scheme of the proposed control system is shown in Fig. 5.3. It also illustrates the switch before the gains on the block diagram, corresponding to the configuration mentioned on Remarak 5.1.1.

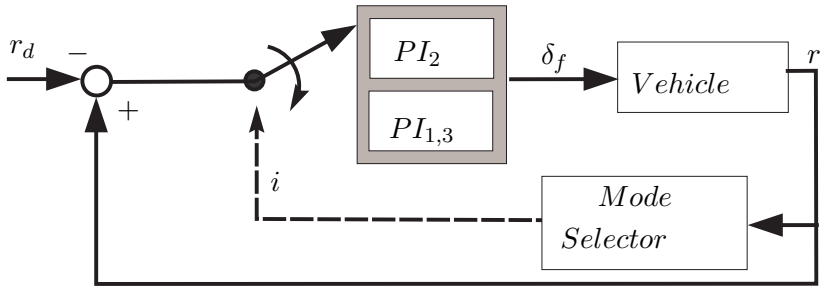

Figure 5.3: Schema from *Controller-1.*

The control input to ensure the tracking of constant yaw rate reference signal ($\dot{r}_d = 0$) is defined as:

$$\begin{array}{rcl} \delta_f & = & -K_{Pi}(r - r_d) - K_{Ii}\int_0^t (r - r_d)\, d\zeta \\ \delta_f & = & -K_{Pi}(r - r_d) - K_{Ii}\alpha_0.\ i \in \mathcal{I} \end{array} \tag{5.5}$$

where $\mathcal{I} = \{1, ..., M\}$ is the set of indexes of all operating regions of the PWA vehicle model (4.13).

Substituting (5.5) in (4.13) leads to the augmented vehicle state-space description in which the internal model of the constant reference is enclosed in the PWA system:

$$\dot{x}_a = A_{ai}x_a + B_{ai}u_a + a_{ai} \tag{5.6}$$

in which:

$$A_{ai} = \begin{bmatrix} -\frac{d_{fi}+d_{ri}}{vm} & \frac{l_r d_{ri} - d_{fi}l_f - v^2 m - K_{Pi}d_{fi}v}{v^2 m} & \frac{-K_{Ii}d_{fi}}{vm} \\ \frac{l_r d_{ri} - d_{fi}l_f}{J} & -\frac{{l_f}^2 d_{fi} + {l_r}^2 d_{ri} + K_{Pi}l_f d_{fi}v}{vJ} & \frac{-K_{Ii}l_f d_{fi}}{J} \\ 0 & 1 & 0 \end{bmatrix} \tag{5.7}$$

and

$$B_{ai} = \begin{bmatrix} \frac{K_{Pi}d_{fi}}{vm} \\ \frac{K_{Pi}l_f d_{fi}}{J} \\ -1 \end{bmatrix}, \qquad a_{ai} = \begin{bmatrix} \frac{e_{fi}+e_{ri}}{vm} \\ \frac{e_{fi}l_f - e_{ri}l_r}{J} \\ 0 \end{bmatrix}, \tag{5.8}$$

where $x_a = [\ \beta, \quad r, \quad \alpha_0\ ]$ and $u_a = r_d$.

The following algorithm describes the design steps of *Controller-1*

Algorithm 5.1.1 *:*

1. ***PWA approximation of tyre forces*** *The PWA affine functions that approximate the nonlinear tyre model are defined such that they take into account the nonlinear behaviour of the tyre lateral forces. The boundaries defining the validity of each approximation are also defined.*

2. ***Steady-State analysis*** *At this stage, the steady-state response of nonlinear vehicle model* (4.1) *is computed at constant longitudinal velocity for different steering angles. The yaw rate and wheel sideslip angles at steady-state corresponding to each steering angle must be computed.*

3. ***Parametrisation in terms of yaw rate*** *The boundaries for each PWA approximation, defined in Step-1, are compared to the computed values of wheel sideslip angle at steady state, considering a certain precision, and then linked to the corresponding value of yaw rate at steady-state. If conditions* (5.4) *are not satisfied, Step-2 must be repeated with a finer refinement of steering angles as input.*

4. ***PWA modelling*** *Considering the PWA approximations, defined in Step-1 and the boundaries in terms of yaw rate, the PWA vehicle model can be described and the PI gains for each subsystem have to be designed such that the closed loop system is stable and exhibits required performance. At the end of this stage, the closed loop system* (5.5) *can be obtained.*

5. ***PWQ Lyapunov stability*** *A piecewise quadratic Lyapunov function for the closed loop system can be searched using Theorem 3.5.1. If the LMI problem is infeasible, one can return to Step-4 to compute new PI gains for each subsystem, or return to Step-1 to simplify the approximations. The assumptions from Section 4.2.2 should be considered in order to use Theorem 3.5.1 to prove the stability of the PWA closed loop system.*

Controller-1 has been synthesised based on this algorithm, as described below.

Synthesis of *Controller-1*

The assumptions described in Section 4.2.2 have been considered in the design of this lateral assistance. Therefore, it is considered in the PWA model (4.13) for all operating regions that only the front wheel lateral tyre forces saturate, *i.e.* $d_{ri} = c_r$ and $e_{ri} = 0$, and that the PWA approximations contain only positive slopes for *i.e.* $d_{fi} > 0$,.

The vehicle longitudinal speed has been considered constant at $v = 30$ $[m/s]$ and the numerical values of the parameters describing the vehicle and Pacejka model of tyre forces are presented in Table 4.2.

The PWA functions (4.12) (for the front tyre) have been chosen such that they are able to take into account the linear and the nonlinear behaviour of the tyre force. They are depicted with dashed lines in Fig. 5.2. The values of wheel sideslip $\pm\bar{\alpha}_f$, establishing the boundaries of the operating regions, determine the two corresponding hyperplanes on the yaw rate, at threshold values $r = \pm\bar{r}$, as shown in Fig. 5.1, creating subsets that cover the whole state-space. According to (3.30), the boundaries of each operating region of the parametrised PWA systems are described by:

$$\begin{aligned} H_1^T &= \begin{bmatrix} 0 & 1 & 0 \end{bmatrix}, & g_1 &= -0.27, \\ H_2^T &= \begin{bmatrix} 0 & -1 & 0 \\ 0 & 1 & 0 \end{bmatrix}, & g_2 &= \begin{bmatrix} 0.27 \\ 0.27 \end{bmatrix}, \\ H_3^T &= \begin{bmatrix} 0 & -1 & 0 \end{bmatrix}, & g_3 &= -0.27, \end{aligned} \tag{5.9}$$

Even though the approximation of the tyre force (and corresponding yaw rate) could be refined, it is shown in the simulations (Section 5.3) that the performance can be improved by using this simple partitioning, $\mathcal{I} = \{1, 2, 3\}$.

The controller gains are shown in Table 5.1.

Table 5.1: Gains for yaw rate tracking based on yaw rate only - *Controller-1*

Regions	Gains	
	K_{Pi}	K_{Ii}
$i = 1, 3$	1	0.2
$i = 2$	1.5	5

The stability proof of *Controller-1* is presented in Section 5.2.1.

This control structure presents some advantages with respect to the linear controller 5.3, as shown in the simulation results in Section 5.3. Nevertheless, the parametrisation of the vehicle dynamics in terms of steady-state yaw rate implies that the assistance may not be satisfactory in some critical situations, such as skidding at low yaw rate. Such undesired effects can be mitigated by taking the vehicle sideslip angle into account in a feedback loop, which can also enhance the transient regime. Such an improvement is presented in the next section.

5.1.2 Piecewise linear state feedback for yaw rate tracking - *Controller-2*

Having proposed a first PWL linear controller for active steering, the structure can be improved by considering the vehicle sideslip angle, not only to define the switching boundaries, but also in the design of a state feedback loop to enhance the vehicle stability.

The proposed control strategy involves the design of two control loops as shown in Fig. 5.4, for which Remark 5.1.1 also holds. The control law can be written as follows:

$$\delta_f = -\begin{bmatrix} K_{\beta i} & K_{ri} \end{bmatrix} x^b + \delta_{fPI} \qquad i \in \mathcal{I} \tag{5.10}$$

where $x^b = [\beta, r]^T$ is the vector of state variables.

The first control loop is a piecewise linear state feedback, which is designed using the pole placement techniques, in order to improve the vehicle dynamics. It requires the measurement of the vehicle sideslip angle β which can be measured with the CORREVIT optical sensor (see Section 4.6.2), as done in [MENML09], or estimated (see [SCM07] and [DBL$^+$08]).

The second control loop, δ_{fPI}, is the PWL PI controller to track the yaw rate reference, as follows:

$$\begin{aligned} \delta_{fPI} &= -K_{Pi}(r - r_d) - K_{Ii} \int_0^t (r - r_d)\, d\zeta \\ \delta_{fPI} &= -K_{Pi}\dot{\alpha}_0 - K_{Ii}\alpha_0 \ , \quad \text{for i} \in \mathcal{I} \end{aligned} \tag{5.11}$$

Substituting (5.10) in (4.13) leads to the augmented vehicle state-space description in which the internal model of the constant reference is enclosed to the PWA system:

$$\dot{x}_a = A_{ai} x_a + B_{ai} u_a + a_{ai} \ , \tag{5.12}$$

where $x_a = [\beta,\ r,\ \alpha_0]$ and $u_a = r_d$.

As already mentioned, this control strategy requires the measurement of the vehicle sideslip angle for the PWL state feedback loop. However, this variable is not measurable by the current on-board sensors, therefore estimation algorithms or optical sensors would be required which are still very costly to be deployed by the automotive industry in commercialised vehicles. Despite this drawback, which might also seem incompatible with the objective of developing low-cost assistances, the investigation of such control structure is justified for being an intermediate

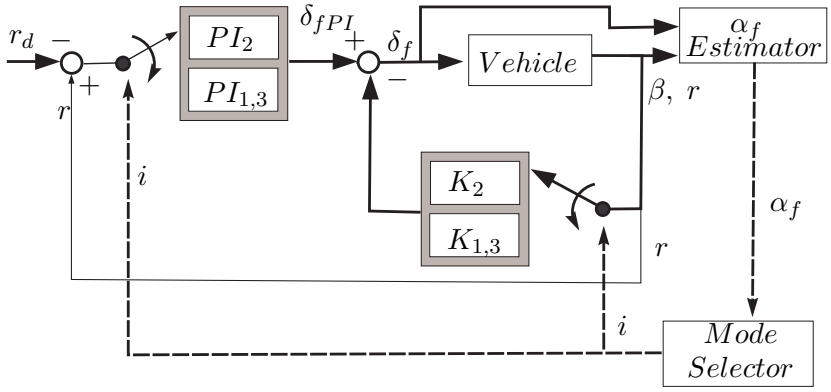

Figure 5.4: Schema from *Controller-2*.

stage in the design of the *Perceptive-ESC* . The main goal at this point is the evaluation of the potential advantages of PWA controllers to enhance the vehicle dynamics, as well as the comprehension of its limitations. For this reason, it has been decided not to devote further work to the development of observers for the proposed active steering systems, but to consider them in the design of the *Perceptive-ESC* assistance.

Since the control structure involves the measurement of the vehicle sideslip angle, β and yaw rate, r, the switching boundaries can be expressed directly in term of the wheel sideslip angles, which can be computed using (4.3), (4.4) or other estimation algorithm. Describing the switching boundaries in terms of state variables is particularly interesting to use the techniques for analysis of PWA system described in Section 3.5.2, therefore (4.4) is chosen to estimate the wheel sideslip angles, as described in the following discussion about the control synthesis.

The following algorithm provides the steps to the design of *Controller-2*.

Algorithm 5.1.2 *:*

1. ***PWA approximation of tyre forces*** *The PWA affine functions that approximate the nonlinear tyre model are defined such that they take into account the nonlinear behaviour of the tyre lateral forces. The boundaries defining the validity of each approximation are also chosen.*

2. ***PWA modelling*** *Considering the PWA approximations, defined in Step-1, the PWA vehicle model can be described. At this stage, the PI gains and state feedback gains must also be designed for each subsystem such that the closed-loop exhibits acceptable performance. Replacing the expression for the control input in the PWA vehicle model yields the closed loop system* (5.12).

3. ***PWQ Lyapunov stability*** *A piecewise quadratic Lyapunov function for the closed loop system can be searched using Theorem 3.5.1. For that the boundaries of the PWA closed loop system must be expressed in term of the state variables, a detailed description of this procedure is provided in Section 5.2.2. If the LMI problem is infeasible, Step-2 must be repeated to compute new PI gains for each subsystem or state feedback, or return to Step-1 to simplify the approximations. The assumptions from Section 4.2.2 should be considered in order to use Theorem 3.5.1 to prove the stability of the PWA closed loop system.*

This control strategy could also be described as a PWL dynamical state feedback, and more sophisticated procedures for the control synthesis could be used in order to avoid the possibly cumbersome search of adequate gains. Nevertheless, the structure with the PI_i gains has been privileged due to the heuristic knowledge gained from the design of the more simple structure of *Controller-1*.

In the sequel, the design of synthesis of *Controller-2*, following the previously presented algorithm is described.

Synthesis of *Controller-2*

Similarly to the synthesis of *Controller-1*, the assumptions from Section 4.2.2 have been kept for the design of this steering assistance The PWA affine approximation for the front tyre force is shown in Fig. 5.2. Consequently, the switching between the controllers is driven by the estimate of the front wheel sideslip angle, as shown in Fig. 5.4. This variable is computed as in (4.5).

Even though a finer partitioning of the tyre force domain could be employed, the simulation results, presented in Section 5.3, show that using only 3 regions ($M = 3$) the resulting PWL controller can already enhance the vehicle handling.

Similarly to *Controller-1*, the numerical values of the vehicle parameters of (4.13) are presented in Table 4.2. The vehicle longitudinal speed is considered constant at $v = 30$ $[m/s]$.

The gains have been chosen so that the closed loop system is stable in each of the operating regions. The numerical values for the gains are described in Table 5.2

Table 5.2: Gains for yaw rate tracking based on front sideslip angle - *Controller-2*

	Gains			
Regions	$K_{\beta i}$	K_{ri}	K_{Pi}	K_{Ii}
$i = 1, 3$	0.001	0.001	0.3	0.1
$i = 2$	1.9	0.6	1.5	2

The gains of *Controller-1* and *Controller-2*, proposed respectively in Sections 5.1.1 and 5.1.2, were designed such that each subsystem is stable, however it does not imply that the whole closed loop systems (5.12) and (5.6) are also stable. The next section presents the proof of stability of the PWA closed loop systems.

5.2 Stability Analysis

The stability proof of the proposed control schemas is based on the search of a continuous piecewise quadratic Lyapunov function, as described in Theorem 3.5.1. For both controllers the LMIs are solved using the toolbox for PWL systems [HJ99]. The application of this theorem for the PWA closed loop systems (5.6) and (5.12) is presented in the following.

5.2.1 Stability analysis for switching based on yaw rate

The PWA model of the vehicle under action of *Controller-1* (equation (5.6)) already has its partitions described in terms of state variables (parametrisation in terms of yaw rate). Therefore, Theorem 3.5.1 can be directly used to verify the overall system stability.

Using the vehicle parameters as shown in Table 4.2, the gains described in Table 5.1 and the boundaries of the parametrised PWA systems described by equations (5.9), a piecewise quadratic Lyapunov function has been computed and its projection for $\alpha_0 = 0$ is shown in Fig 5.5.

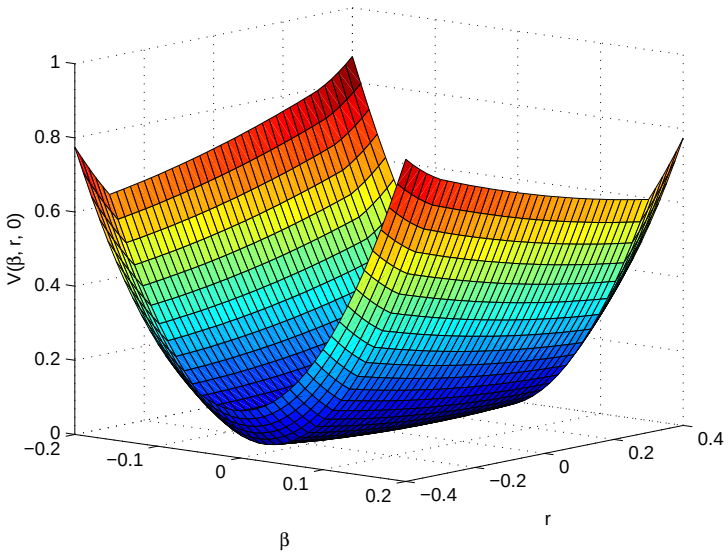

Figure 5.5: Piecewise quadratic Lyapunov function for the PWA system (5.6), representing the vehicle equipped with *Controller-1*.

5.2.2 Stability analysis for switching based on front tyre sideslip angle

In order to use Theorem 3.5.1 in the vehicle model under *Controller-2* (5.12), it is required to reformulate the overall dynamics such that the partitions of the PWA systems are described in terms of state-space variables. For that, a coordinate change is performed such that a new state-space vector is composed of the front and rear tyre sidelip angles α_f, α_r and the variable α_0.

Evoking (4.5), a transformation matrix can be defined:

$$T = \begin{bmatrix} -1 & -\frac{l_f}{v} & 0 \\ -1 & \frac{l_r}{v} & 0 \\ 0 & 0 & 1 \end{bmatrix}, \tag{5.13}$$

such that:

$$\bar{x} = \begin{bmatrix} \alpha_f \\ \alpha_r \\ \alpha_0 \end{bmatrix} = Tx_a + \begin{bmatrix} \delta_f \\ 0 \\ 0 \end{bmatrix} \tag{5.14}$$

Replacing the expression for δ_f from (5.10) into equation (5.14) leads to

$$\bar{x} = \begin{bmatrix} \alpha_f \\ \alpha_r \\ \alpha_0 \end{bmatrix} = Sx_a + \begin{bmatrix} K_{Pi} \\ 0 \\ 0 \end{bmatrix} r_d, \tag{5.15}$$

where:

$$S = \begin{bmatrix} -K_\beta - 1 & -\frac{l_f}{v} - K_r - K_{Pi} & -K_{Ii} \\ -1 & \frac{l_r}{v} & 0 \\ 0 & 0 & 1 \end{bmatrix} \tag{5.16}$$

The derivative of expression (5.15) results in:

$$\dot{\bar{x}} = S\dot{x_a} + \begin{bmatrix} K_{Pi} \\ 0 \\ 0 \end{bmatrix} \dot{r}_d \tag{5.17}$$

Since it was assumed that $\dot{r}_d = 0$, and considering

$$x_a = S^{-1} \left(\bar{x} - \begin{bmatrix} K_{Pi} \\ 0 \\ 0 \end{bmatrix} r_d \right), \tag{5.18}$$

system (5.12) can be rewritten in the new coordinates as:

$$\dot{\bar{x}} = \bar{A}_i \bar{x} + \bar{B}_i r_d + \bar{a}_i, \tag{5.19}$$

where:

$$\bar{A}_i = SA_{ai}S^{-1} \tag{5.20}$$

$$\bar{B}_i = -SA_{ai}S^{-1} \begin{bmatrix} K_{Pi} \\ 0 \\ 0 \end{bmatrix} + SB_{ai} \tag{5.21}$$

$$\bar{a}_1 = Sa_{ai} \tag{5.22}$$

According to (3.30), the operating regions of (5.19), described in terms of front wheel sideslip angle, can be simply describe by:

$$R_i = \{\bar{x} \mid H_i^T \bar{x} - g_i < 0\}, \tag{5.23}$$

where for each region:

$$\begin{aligned} H_1^T &= \begin{bmatrix} 1 & 0 & 0 \end{bmatrix}, \quad g_1 = -0.09, \\ H_2^T &= \begin{bmatrix} -1 & 0 & 0 \\ 1 & 0 & 0 \end{bmatrix}, \quad g_2 = \begin{bmatrix} 0.09 \\ 0.09 \end{bmatrix}, \\ H_3^T &= \begin{bmatrix} -1 & 0 & 0 \end{bmatrix}, \quad g_3 = -0.09, \end{aligned} \tag{5.24}$$

Considering the vehicle parameters as shown in Table 4.2, the gains provided in Table 5.2 and applying Theorem 3.5.1, a piecewise quadratic Lyapunov function has been found for the system (5.19). Fig. 5.6 depicts a projection of the PWQ Lyapunov function computed for $\alpha_0 = 0$ and input $r_d = 0$.

The stability of both active steering systems could be proved using piecewise quadratic Lyapunov functions, however it is important to verify the performance of the controlled vehicle and its behaviour with respect to unmodelled dynamics. Such analysis are presented in the following section.

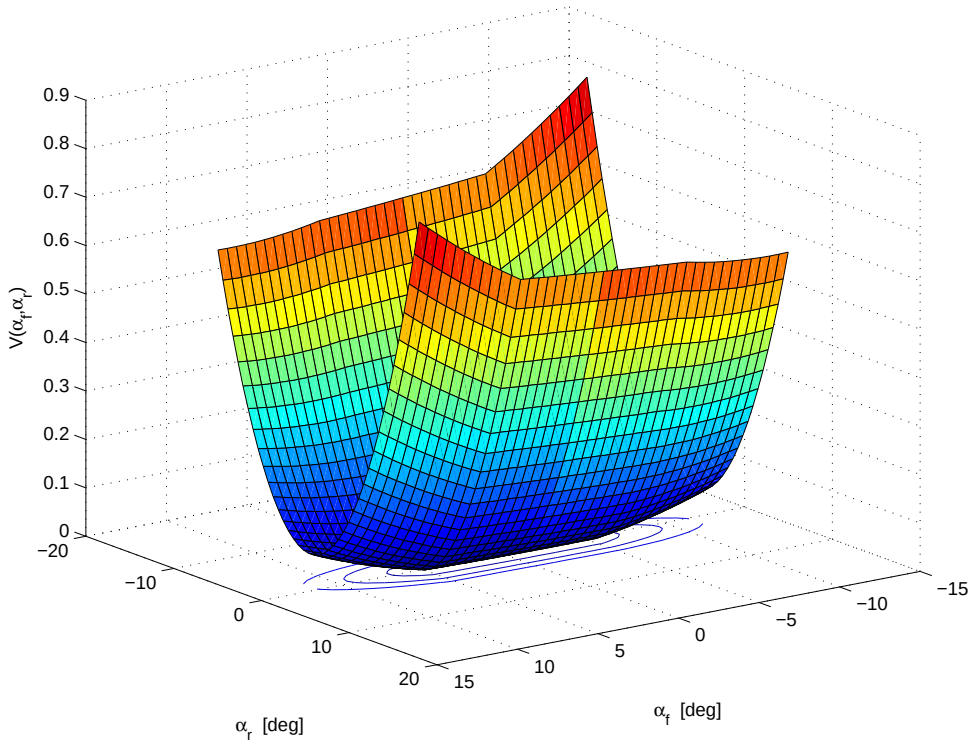

Figure 5.6: Piecewise quadratic Lyapunov function computed for the PWA system (5.12) representing the vehicle equipped with *Controller-2*.

5.3 Simulation results

Several simulations in the CarSim environment have been performed in order to:

- validate the proposed control systems with respect to additional dynamics and nonlinear combined lateral and longitudinal tyre force effects which were neglected at the control design stage,
- evaluate the improvements of each of the proposed PWL controllers (*Controller-1* and *Controller-2*), by comparison with the standard PI controller (as in [B$^+$03]) designed in the linear region only.

Each of the proposed controllers have been tested separately and the simulations were performed on the same vehicle in three different configurations:

- the uncontrolled vehicle (unc);
- a vehicle equipped with the designed controllers in the linear region, equation ((5.5) and (5.10)) with $i = 2$, (lin. contr) only;
- a vehicle equipped with the proposed PWL control strategies, equation ((5.5) and (5.10)) with $i = 1, 2, 3$, (PWL contr).

The scenarios of the simulations consisted of two kinds. Firstly, disturbances on the lateral and yaw dynamics are applied to the vehicle in order to verify the ability of the controlled system to reject perturbations. The second scenario consists of a sudden change in direction. In both cases, the manoeuvres are conducted such that the tyre forces reach the nonlinear regions in order to show the improvements provided by the piecewise linear control strategies. Table 5.3 relates the configuration of each simulation with the figures depicting the obtained results.

Table 5.3: Summary of simulation results for active steering systems:

	Controller-1			*Controller-2*		
Scenarios	*unc*	*lin contr.*	*PWL contr.*	*unc*	*lin contr.*	*PWL contr.*
Disturbances	Fig. 5.8 to Fig. 5.11			Fig. 5.12 to Fig. 5.15		
Direction change	Fig. 5.16 to Fig. 5.17			Fig. 5.18 to Fig. 5.19		

The standard CarSim D-Class vehicle, described in Section 4.6.1 has been used to analyse the responses of both the uncontrolled and the controlled vehicles. The simulations are performed at a vehicle speed of $v = 33\ m/s$.

The ratio between the steering wheel and the yaw rate reference, K_δ, which depends on the vehicle speed, $K_\delta(v)$, is chosen to be the same as in the uncontrolled vehicle (5.2). To take into account the nonlinearities of the Carsim vehicle, used in the simulation section, the gain $K_\delta(v)$ is obtained from the uncontrolled vehicle measurements by storing the steady state yaw rate values in a look-up table for different steering angles and vehicle velocities ($K_\delta(v, \delta_p)$).

5.3.1 Response to Sudden Disturbances

To analyse the improved performance of the active steering system, the vehicles are subjected to sudden disturbances on both the lateral and the yaw dynamics. Two sets of disturbances are applied to the vehicle, as depicted in Fig. 5.7 (a) and (b). The left subplots of both pictures show that the driver intends to ride straight forward. The right subplots show the disturbances as external lateral force and yaw moment. The disturbances on Fig. 5.7 (b) have greater magnitudes.

Response of *Controller-1* subjected to sudden disturbances

The response for each vehicle configuration equipped with *Controller-1* is shown in Fig. 5.8, which depicts the vehicle sideslip angle and yaw rate on the top and bottom subplots respectively. The controlled vehicle sideslip and yaw rate are improved by both the performed control actions (shown in the third subplot of Fig. 5.9) in comparison to the uncontrolled vehicle. It is also important to note that in this case the disturbances are relatively small such that the vehicle does not reach the region in which $-\bar{r} < r < \bar{r}$, as shown in the first and second subplots of Fig. 5.9, the proposed PWL control action is equal to the action performed by the controller designed for the linear region, which can be seen in the third subplot of Fig. 5.9.

However, when the disturbances are sufficiently large, as indicated in Fig. 5.7 (b), the vehicle yaw rate reaches values beyond the defined thresholds $\pm\bar{r}$, as shown in the second subplot of Fig. 5.10. Consequently, the operation region of the vehicle *PWL contr* switches from the linear region R_2 to the affine regions R_1 and R_3, as shown in the second subplot of Fig. 5.11. Due

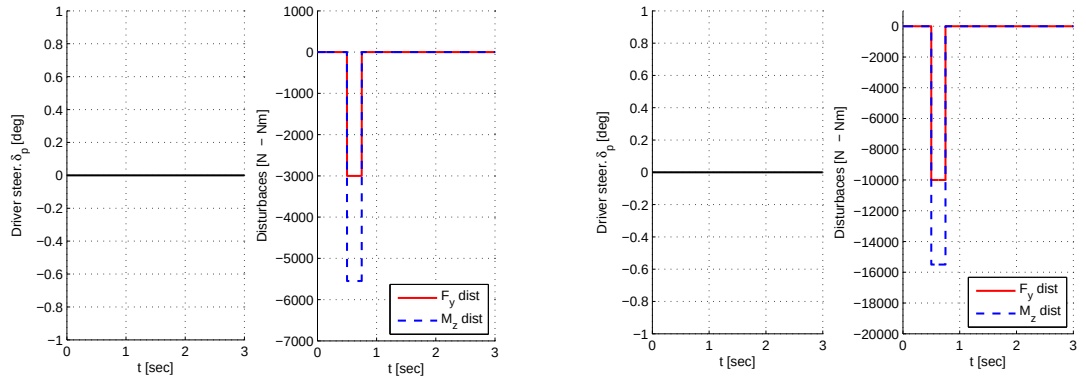

Figure 5.7: sudden disturbance on the uncontrolled (unc) and both controlled ((lin. contr), (PWL contr)) cars. (a) small disturbance, (b) large disturbance

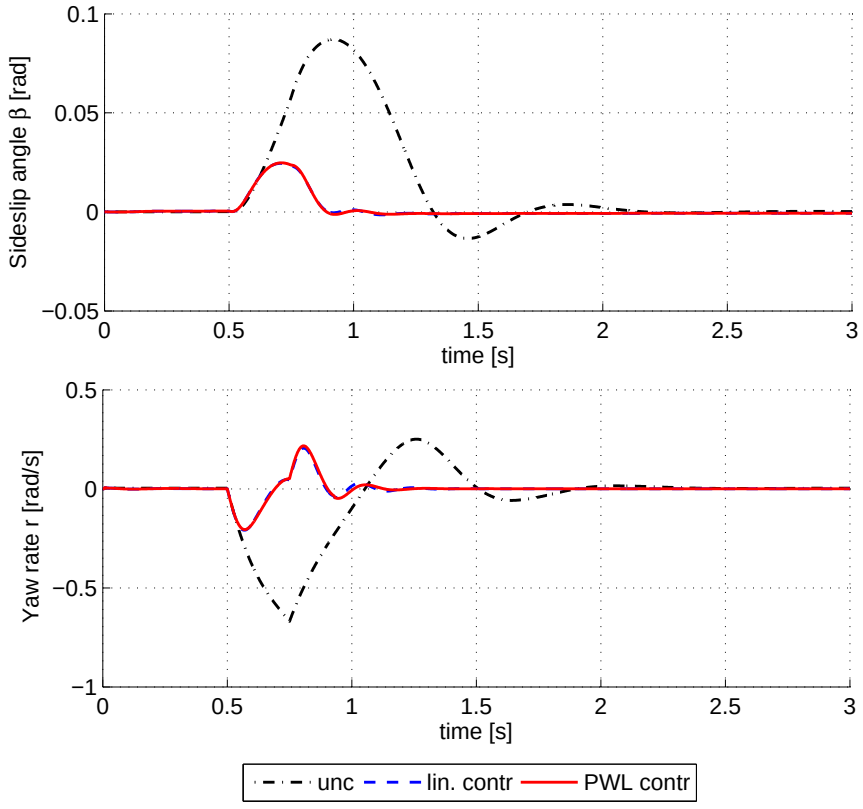

Figure 5.8: Response to a small sudden disturbance on the uncontrolled (unc) and both controlled ((lin. contr), (PWL contr)) cars (*Controller-1*).

to the switching, the resulting control input from *Controller-1* differs from the vehicle equipped with the linear control only (*lin. contr*), as indicated in the bottom subplot of Fig. 5.11. The

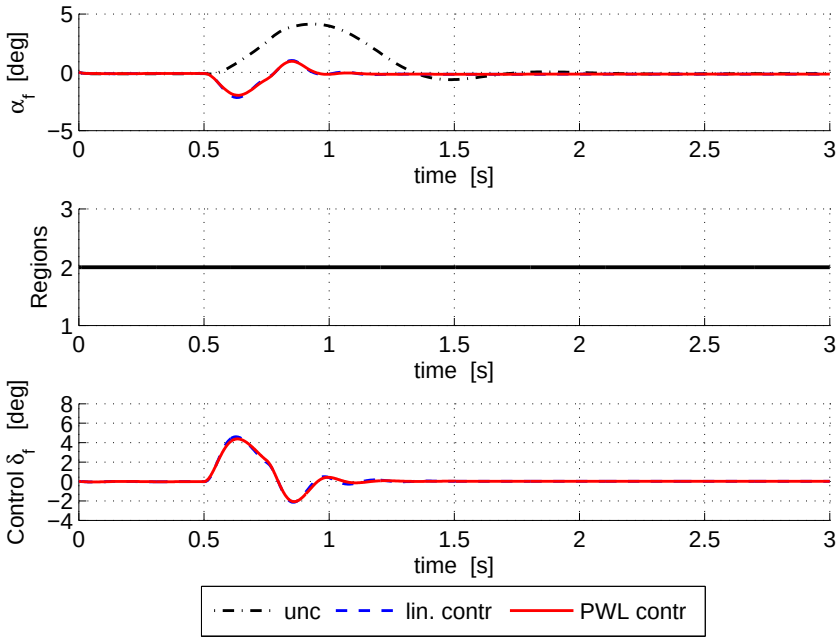

Figure 5.9: Operating regions and control input as response to a small sudden disturbance on the uncontrolled (unc) and both controlled ((lin. contr), (PWL contr)) cars (*Controller-1*).

corresponding vehicle dynamics is plotted in Fig. 5.10 showing smaller values of vehicle sideslip angle and yaw rate and therefore, a improved performance of the PWL controller.

It can be noted that the PWL controller based on the parametrisation of yaw rate, has improved performance with respect to the linear PI controller. The first subplot of Fig. 5.11 indicates that the wheel sideslip angle of *PWL contr* reaches values smaller than the *lin contr*, indicating that the PWL controller avoids the saturation of tyre forces.

Response of *Controller-2* subjected to sudden disturbances

The same disturbances were applied to vehicle equipped with *Controller-2*. Similarly to the results present for *Controller-1*, when the disturbances are small (Fig. 5.7 (a)) the control of the vehicle *lin contr* and *PWL contr* are identical, as the front wheel sideslip angle is in the interval $-\bar{\alpha}_f < \alpha_f < \bar{\alpha}_f$. The vehicle sideslip angle and yaw rate are shown in Fig. 5.12 and the control input and front wheel sideslip angle are shown in Fig. 5.13.

Submitting the vehicles equipped with *Controller-2* to the disturbances Fig. 5.7 (b), the distinct control action of the *PWL contr* with respect to the *lin contr* can be noticed, as illustrated in the bottom subplot of Fig. 5.11. The values of front wheel sideslip angle outside the interval $-\bar{\alpha}_f < \alpha_f < \bar{\alpha}_f$, depicted in the first subplot cause the switching between controller as it can be seen in the second subplot of the same figure.

The vehicle sideslip angle and yaw rate corresponding to this manoeuvre are depicted in Fig. 5.11.

Similarly to the results obtained for *Controller-1*, it can be noticed that the PWL control strategy is more adequate in avoiding the saturation of the tyre force, due to the smaller values of front wheel sideslip angle obtained during the manoeuvre.

The enhanced performance of both PWL controllers is also tested for a sudden direction

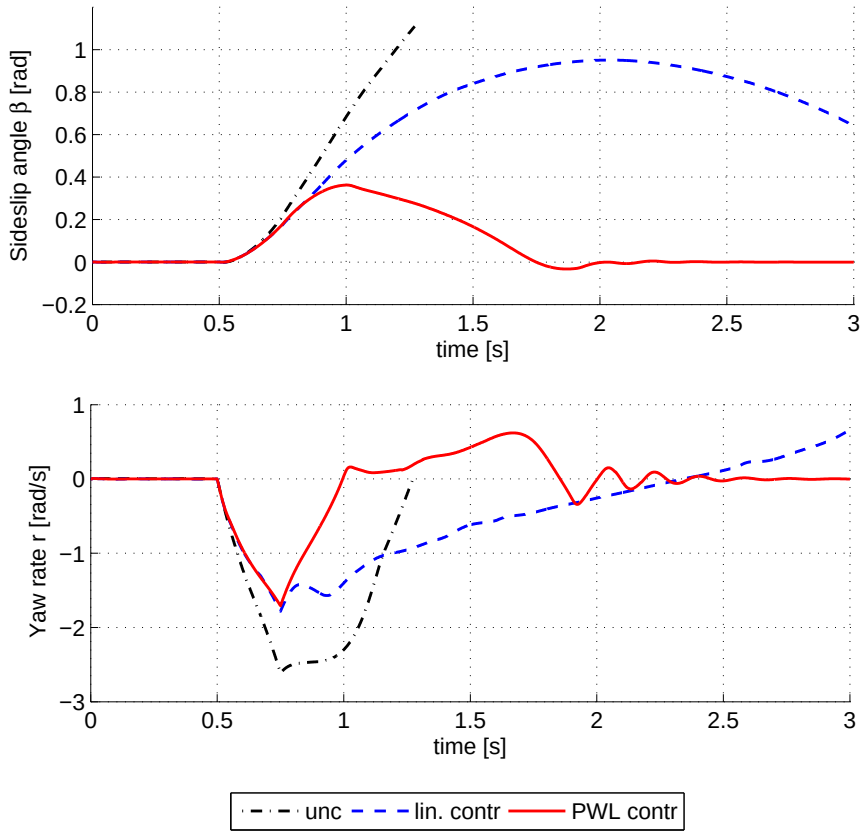

Figure 5.10: Response to a sudden disturbance on the uncontrolled (unc) and both controlled ((lin. contr), (PWL contr)) cars (*Controller-1*).

change. The results are described below.

5.3.2 Response to Sudden Direction changes

Several sudden direction changes are simulated to show the tracking of the desired yaw rate, the faster response of the controlled vehicles and their improved performance. In order to verify the enhanced performance of the PWL controllers, the same driver input is applied and compared to the *unc* and *lin contr* vehicles.

Response of *Controller-1* subjected to sudden direction changes

A sudden direction change performed by the driver action on the steering wheel (δ_p), as shown in the first subplot of Fig. 5.16. The manoeuvre is very demanding, as it can be seen by the lateral acceleration shown in the second subplot of Fig. 5.16. In this case, only the PWL control approach performs satisfactorily, as shown in the third and fourth subplots of Fig. 5.16 depicting the vehicle sideslip and the yaw rate respectively. The PWL control action shown in the third subplot of Fig. 5.17 switches, according to the chosen partitions, maximising the lateral acceleration (second subplot of Fig. 5.16) while reducing the yaw rate error.

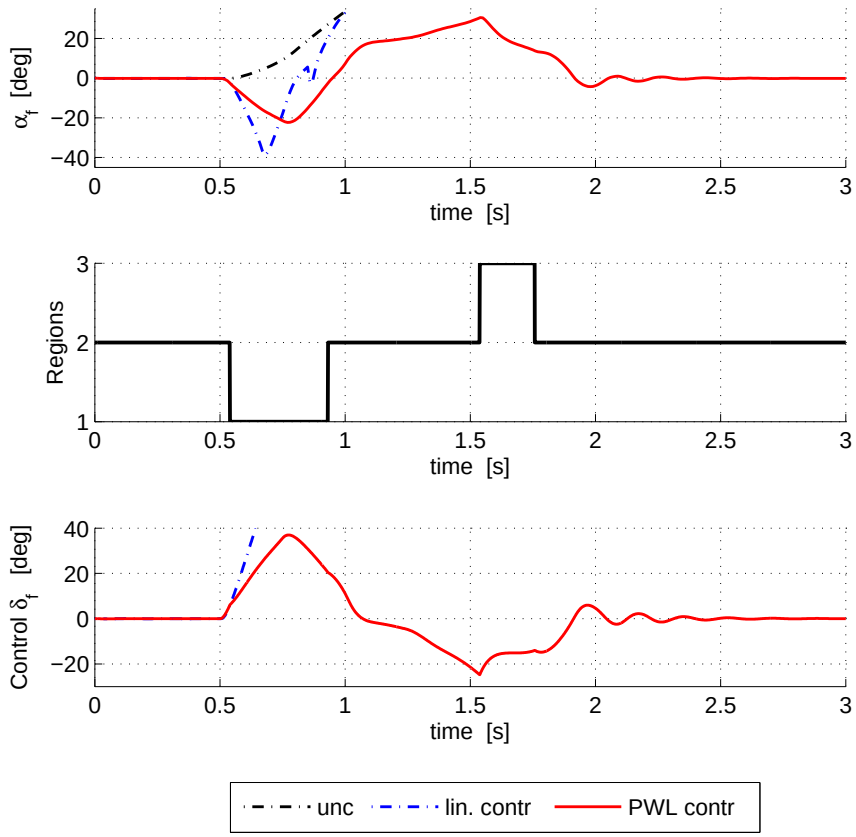

Figure 5.11: Operating regions and control input as response to sudden disturbance on the uncontrolled (unc) and both controlled ((lin. contr), (PWL contr)) cars (*Controller-1*).

Response of *Controller-2* subjected to sudden direction changes

The same direction change is applied in the vehicle equipped with, *Controller-2*, which is compared to the performance of the linear controller only and uncontrolled vehicles. Fig. 5.18 displays the driver input and the corresponding yaw rate reference signal. Also in this situation only the PWL controller is able to respond satisfactorily to the driver input.

Fig. 5.19 shows in its first subplot the tyre sideslip angle. It can be seen that the values reached for vehicle *PWL Contr* are much smaller than the other two vehicles, indicating that the PWL strategy is able to avoid tyre saturation in demanding manoeuvres. The switching between the operating regions, driven by the front wheel sideslip angle, is shown in the second subplot of Fig. 5.19. The third subplot illustrates the control input.

It is interesting to compare the response of both vehicles equipped with the PWL controllers, since they are submitted to the same sudden direction change. It can be seen that the response vehicle equipped with *Controller-1* presents more oscillations during the manoeuvre for the vehicle sideslip angle as well as the yaw rate, as depicted in the top and bottom left subplots of Fig. 5.16. Analysing the response of the vehicle equipped with *Controller-2*, it can be seen that the response of the vehicle sideslip angle (top left subplot of Fig. 5.18) is slightly faster than for *Controller-1*, and less oscillation is produced in steady state. Similarly for the yaw rate, as shown in the top left subplot of Fig. 5.18. Such results confirm the enhancement provided by

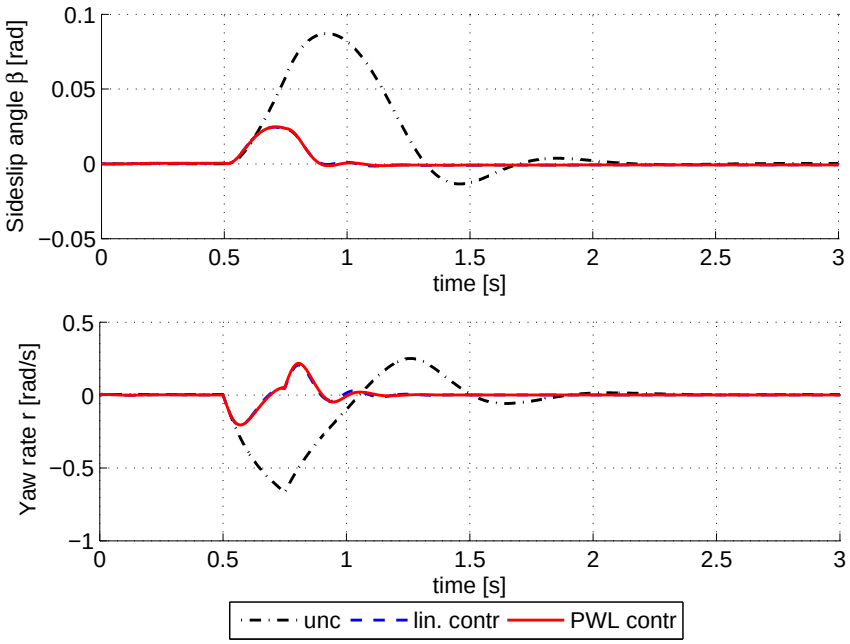

Figure 5.12: Response to a small sudden disturbance on the uncontrolled (unc) and both controlled ((lin. contr), (PWL contr)) cars (*Controller-2*).

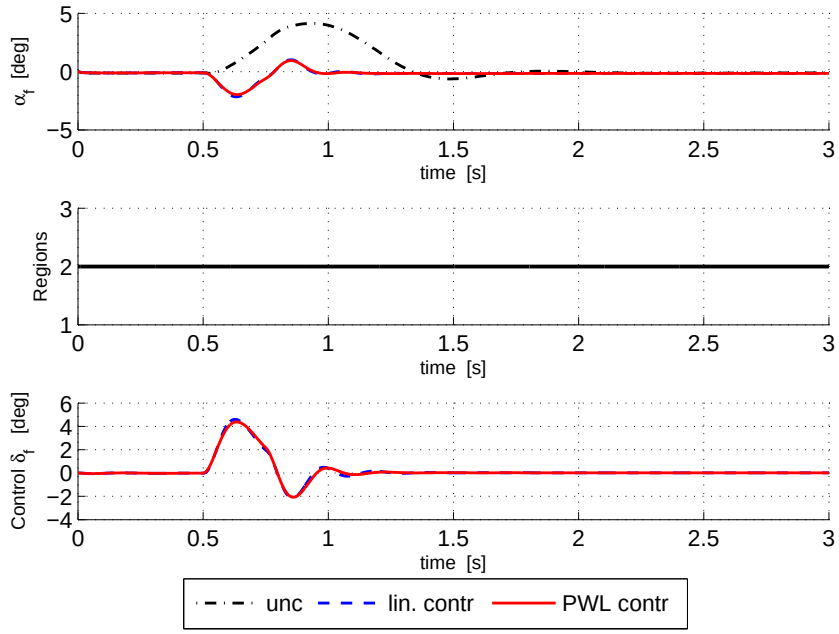

Figure 5.13: Operating regions and control input as response to small sudden disturbance on the uncontrolled (unc) and both controlled ((lin. contr), (PWL contr)) cars (*Controller-2*).

the additional state feedback loop, as well as the switching based on the front wheel sideslip angle.

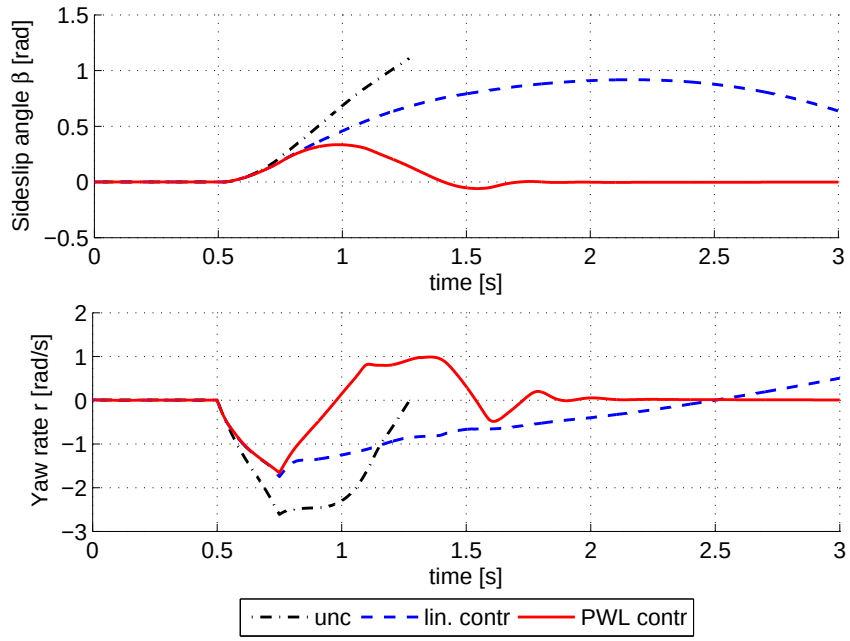

Figure 5.14: Response to sudden disturbance on the uncontrolled (unc) and both controlled ((lin. contr), (PWL contr)) cars (*Controller-2*).

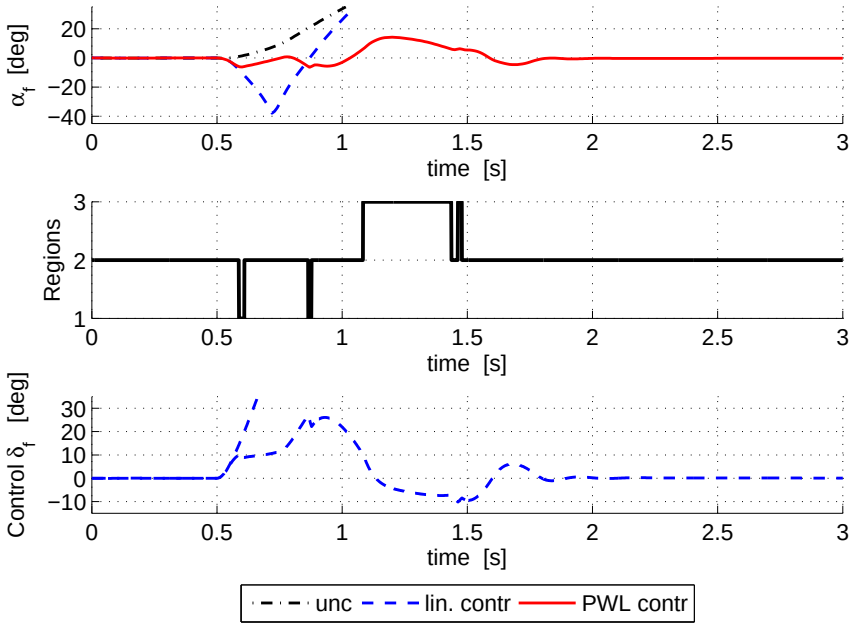

Figure 5.15: Operating regions and control input as response to sudden disturbance on the uncontrolled (unc) and both controlled ((lin. contr), (PWL contr)) cars (*Controller-2*).

5.4 Conclusions

In this chapter two control strategies based on the PWA vehicle model have been presented. Both control laws belong to the class of PWL controllers, as they do not contain affine terms.

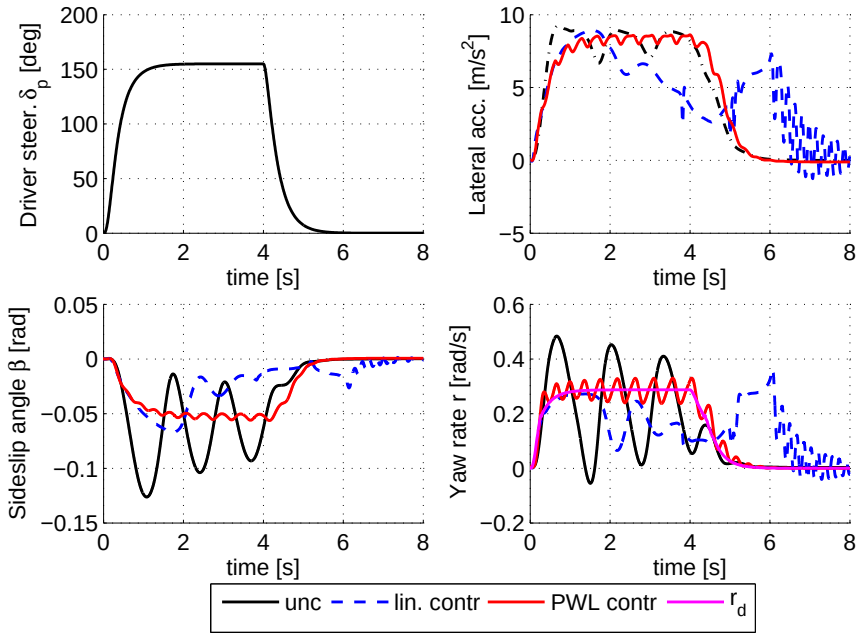

Figure 5.16: Response to a sudden direction change on the uncontrolled (unc) and both the controlled ((lin. contr), (PWL contr)) vehicles (*Controller-1.*)

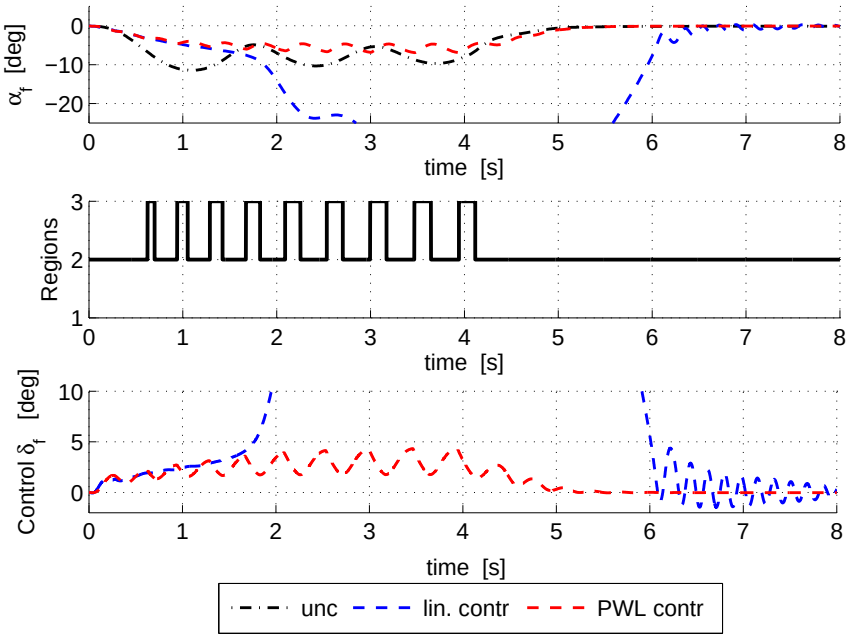

Figure 5.17: Wheel sideslip angle, operating region and control input for a sudden direction change on the uncontrolled (unc) and both the controlled ((lin. contr), (PWL contr)) vehicles (*Controller-1*).

They have been designed as an extension of a simple PI controller on the yaw rate error. For the first control strategy, the PI has been simply extended to a PWL PI. The switching

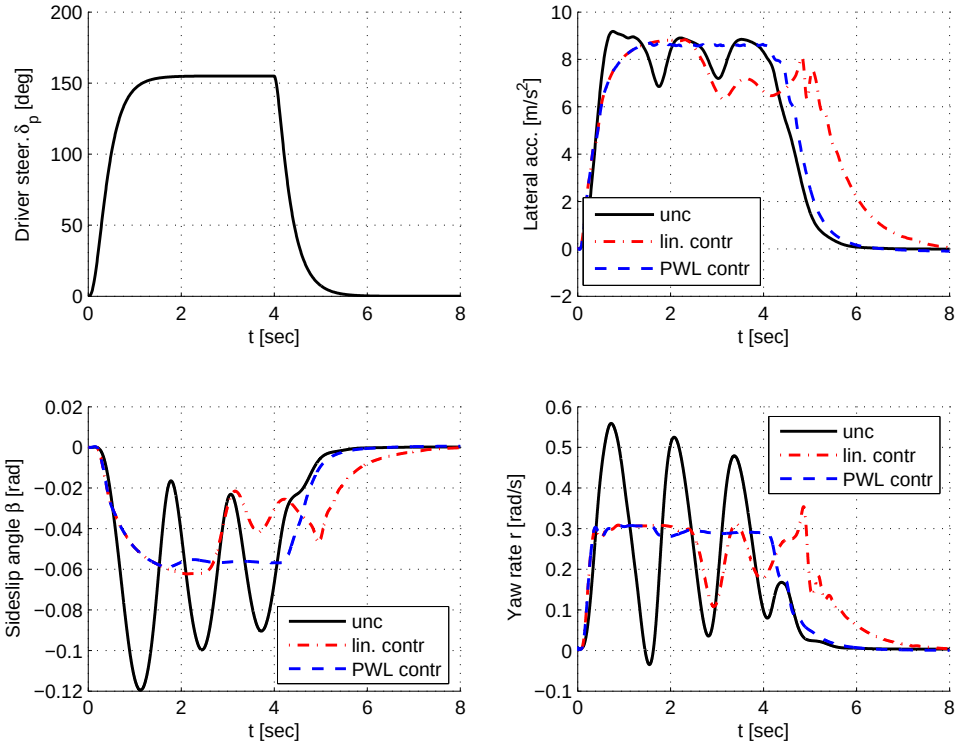

Figure 5.18: Response to the driver input on steering wheel causing a sudden direction change on the uncontrolled (unc) and both controlled ((lin. contr), (PWL contr)) cars (*Controller-2*).

boundaries of the controller have been obtained from a parametrisation of the vehicle dynamics in steady-steate in terms of yaw rate, which is easily measurable.

For the second control strategy a PWL state feedback loop has been included to improve the vehicle dynamics and the switches between the PWL controllers are driven by estimates of the front wheel sideslip angle. Despite requiring the measurement of the vehicle sideslip angle, the development of *Controller-2* has been important to the investigation of the advantages of PWL controller to stabilise the vehicle dynamics.

Piecewise quadratic Lyapunov functions have been used to prove the stability of both systems. The S-procedure is applied to restrict the Lyapunov conditions to each operating region and equality constraints are employed to force continuity along the boundaries. The search of a piecewise quadratic Lyapunov function is then casted as an LMI feasibility problem.

Despite the simple structure of these assistances, the advantages of using the PWL controllers with respect to simple linear controllers in very demanding manoeuvres have been presented through the simulations in different scenarios.

Moreover, it has been shown that satisfactory performance of *Controller-1* may be limited due to oscillations caused by the switches based on the parametrisation of the vehicle dynamics in term of yaw rate. The switches based on the front wheel sideslip angle, as for *Controller-2*, have proven to be more adequate, consequently the vehicle sideslip angle may not be neglected in the design of PWL controllers to enhance the vehicle dynamics which suggests that the control structures must take into account observers to estimate this variable, and avoid the high cost of optical sensors, such as CORREVIT.

These two main achievements accomplish the objective of this stage regarding the develop-

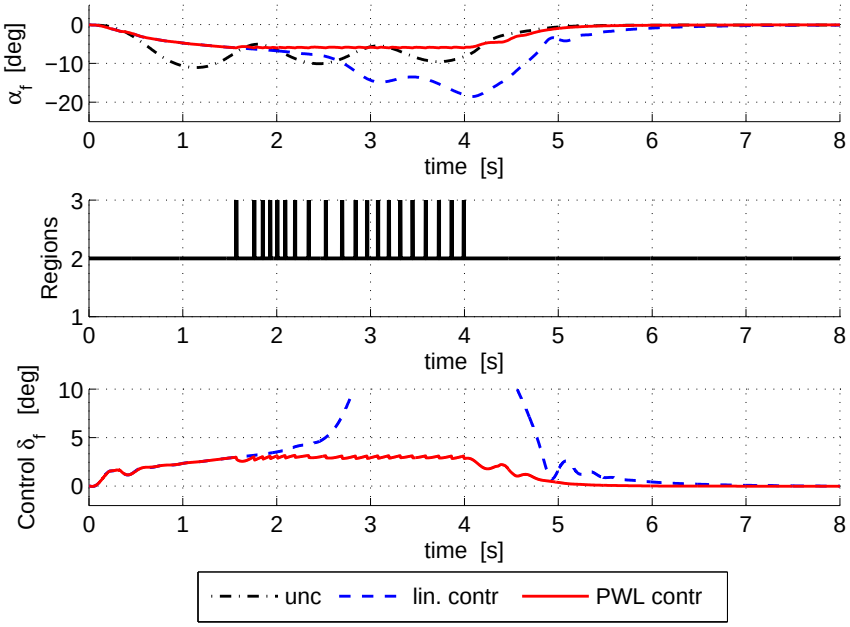

Figure 5.19: Wheel sideslip angle, operating region and control input for a sudden direction change on the uncontrolled (unc) and both controlled ((lin. contr), (PWL contr)) cars (*Controller-2*).

ment of the *Perceptive-ESC* .

The proposed steering assistances are directly linked with the driver awareness as he/she is responsible for providing an adequate reference value, hence inadequate to avoid unintended lane departure. In the next chapter, exteroceptive signals are taken into account in the design of a lane departure avoidance systems.

Chapter 6

Internal model based control for lane keeping assistance

Contents

This chapter presents two control strategies for lane keeping. They take into account the road geometry in order to reject the road curvature considered as a disturbance.

The controller that introduces the chapter is an extension of a control synthesis technique developed at LIVIC [MELMN09]. The control synthesis is based on the minimisation of invariant sets from a quadratic Lyapunov function, to outer approximate a polytope describing the normal driving conditions. The extension, named *Controller-3*, consists of the addition of an internal model for the disturbances so that the vehicle converges to a zero lateral offset condition in steady-state. Moreover, constraints for pole clustering are added to the BMI problem to ensure good damping performance and also asymptotic stability.

The development of the second controller presented in this chapter is aimed at the evaluation of the PWL controller for lane keeping. For this purpose, a simple structure is chosen which consists of a PWL Proportional-double-Integral-derivative ($PIID_i$) based on the lateral offset. In order to keep a simple structure, based on the results obtained for *Controller-1*, the switching is driven only by the yaw rate, considering the parametrisation of the yaw rate from the steady-state analysis. Similarly to the algorithms proposed in the previous chapter, the stability proof is performed on the closed loop system once the gains are defined.

The first section describes the effect of the internal model on the vehicle model for a state feedback and $PIID_i$ controllers. The structure and synthesis of *Controller-3* and *Controller-4*

are described in detail in the second and third sections respectively. The results obtained from practical implementation and simulations on CarSim environment are presented in Section 6.4 while the conclusions wrap-up the chapter.

6.1 Internal model

An adequate strategy for the design of control laws, considering parameter uncertainties or perturbations consists in integrating the perturbations, in the controller by means of an internal model, which represents the disturbances as a family of known functions [FW76].

Road building standards define, as presented in section 4.3, that the clothoids are to be used to interconnect straight roads to constant curvature roads [Raj06d] (chapter-2) and, at constant speed, this implies that the road curvature increases linearly with respect to curviligne abscissa and thus to time:

$$\rho = \frac{1}{F^2} s \tag{6.1}$$

where F is a fixed scale parameter and s is the length measured along the clothoid which increases linearly at constant vehicle speed. Using the lateral offset y_L as input, the internal model is described by the the state variables $\varphi = [\varphi_1, \ \varphi_2]^T$, as follows:

$$\begin{cases} \dot{\varphi}_1 &= y_L, \\ \dot{\varphi}_2 &= \varphi_1, \end{cases} \tag{6.2}$$

Considering a PWA vehicle model (4.25), which includes the variables describing the positioning of the vehicle, the internal model can be added to the state, which yields:

$$x^{im} \triangleq [\beta, r, \psi_L, y_L, \varphi_1, \varphi_2]^T, \tag{6.3}$$

and the augmented system becomes:

$$\dot{x}^{im} = A_i^{im} x^{im} + B_{ui}^{im} u + B_\rho^{im} \rho_{ref} \tag{6.4}$$

where $u = \delta_f$ and the system matrices become:

$$A_i^{im} = \begin{bmatrix} -2\frac{d_{fi}+d_{ri}}{mv} & -1 - 2\frac{d_{fi}l_f - d_{ri}l_r}{mv^2} & 0 & 0 & 0 & 0 \\ 2\frac{d_{ri}l_r - d_{fi}l_f}{J} & -2\frac{d_{fi}l_f^2 + d_{ri}l_r^2}{Jv} & 0 & 0 & 0 & 0 \\ 0 & 1 & 0 & 0 & 0 & 0 \\ v & l_s & v & 0 & 0 & 0 \\ 0 & 0 & 0 & 1 & 0 & 0 \\ 0 & 0 & 0 & 0 & 0 & 1 \end{bmatrix},$$

$$B_{ui}^{im} = \begin{bmatrix} \frac{2d_{fi}}{mv} \\ \frac{2d_{fi}l_f}{J} \\ 0 \\ 0 \\ 0 \\ 0 \end{bmatrix}, \quad B_\rho^{im} = \begin{bmatrix} 0 \\ 0 \\ -v \\ 0 \\ 0 \\ 0 \end{bmatrix}, \quad a_i^{im} = \begin{bmatrix} 2\frac{e_{fi}+e_{ri}}{mv} \\ 2\frac{e_{fi}l_f - e_{ri}l_r}{J} \\ 0 \\ 0 \\ 0 \\ 0 \end{bmatrix}. \tag{6.5}$$

Applying in system (6.4) a state feedback of the form:

$$u = Kx^{im}, \tag{6.6}$$

with $K = [k_1, k_2, k_3, k_4, k_5, k_6]$, the closed loop system becomes:

$$\dot{x}^{im} = (A_i^{im} + B_{ui}^{im} K)x^{im} + B_\rho^{im}\rho_{ref} + a_i^{im}. \tag{6.7}$$

Denoting by a_{ij}, b_{ij} and c_{ij} the elements of the i^{th} row and j^{th} column of the matrices A_i^{im}, B_{ui}^{im} and a_i^{im} respectively, in order to ease the notation, the equilibrium point of (6.7) is:

$$x_{eq} = \begin{bmatrix} -\frac{a_{12}b_{21}-b_{11}a_{22}}{b_{21}a_{11}-b_{11}a_{21}} v\rho_{ref} + \frac{b_{11}c_{21}-b_{21}c_{11}}{b_{21}a_{11}-b_{11}a_{21}} \\ v\rho_{ref} \\ \left(\frac{a_{12}b_{21}-b_{11}a_{22}}{b_{21}a_{11}-b_{11}a_{21}} v - l_s\right)\rho_{ref} - \frac{b_{11}c_{21}-b_{21}c_{11}}{b_{21}a_{11}-b_{11}a_{21}} \\ 0 \\ x_{eq5} \\ 0 \end{bmatrix} \tag{6.8}$$

in which

$$\begin{aligned} x_{eq5} = \; & -\rho_{ref}(vb_{21}k_3a_{12} - b_{21}k_3l_sa_{11} + va_{11}b_{21}k_2 - vb_{21}k_1a_{12} - vb_{11}k_3a_{22} + b_{11}k_3l_sa_{21} \\ & +vb_{11}k_1a_{22} - va_{21}a_{12} + va_{11}a_{22} - va_{21}b_{11}k_2)/(k_5v(-b_{21}a_{11} + b_{11}a_{21}))v \\ & -((b_{21}k_3 - b_{21}k_1 - a_{21})c_1 + (a_{11} + b_{11}k_1 - b_{11}k_3)c_2)/(k_5(b_{21}a_{11} - b_{11}a_{21})) \end{aligned}$$

From (6.8) it can be observed that in steady-state the yaw rate is equal to $v\rho_{ref}$ and the lateral offset is equal to zero. Therefore, by choosing adequately the state feedback gains, it is possible to stabilise (6.7) and steer the vehicle to a zero lateral offset condition even in the presence of the curvature perturbation.

Although using a full state feedback may be advantageous to improve the vehicle dynamics and enlarge stability margins, the disturbances can also be rejected by use of proportional and integral gains on the variable to be regulated. For the constant road curvature in circular sections, an integral term (denoted I_{1i}) is needed to reject this disturbance. In a clothoid, ρ_{ref} is considered as increasing linearly with respect to time (as a ramp function), thus an additional integral term (denoted I_{2i}) is required to obtain zero lateral-offset. Considering the control PWL PII input:

$$\begin{aligned} \delta_f = \; & -P_i y_L - I_{1i}\int_0^t y_L\, d\nu - I_{2i}\int_0^t\int_0^\nu y_L d\eta d\nu \\ \delta_f = \; & -P_i y_L - I_{Ii}\varphi_1 - I_{2i}\varphi_2, \; for\; i \in \mathcal{I}. \end{aligned} \tag{6.9}$$

The equilibrium point of the PWA vehicle model (6.4) for control input (6.9) is:

$$x_{eq} = \begin{bmatrix} -\frac{a_{12}b_{21}-b_{11}a_{22}}{b_{21}a_{11}-b_{11}a_{21}} v\rho_{ref} + \frac{b_{11}c_{21}-b_{21}c_{11}}{b_{21}a_{11}-b_{11}a_{21}} \\ v\rho_{ref} \\ \left(\frac{a_{12}b_{21}-b_{11}a_{22}}{b_{21}a_{11}-b_{11}a_{21}} v - l_s\right)\rho_{ref} - \frac{b_{11}c_{21}-b_{21}c_{11}}{b_{21}a_{11}-b_{11}a_{21}} \\ 0 \\ x_{eq5} \\ 0 \end{bmatrix} \tag{6.10}$$

where:

$$x_{eq5} = \frac{a_{11}a_{22} - a_{12}a_{21}}{I_{1i}(a_{11}b_{21} - a_{21}b_{11})} v\rho_{ref} + \frac{a_{11}c_{21} - a_{21}c_{11}}{I_{1i}(a_{11}b_{21} - a_{21}b_{11})}$$

It can be noted that the PII_i controller also rejects the disturbances and only the internal model variable φ_1 in steady-state differs from the equilibrium point obtained for the state feedback controller.

Having described the effect of the internal model, the structures and synthesis of *Controller-3* and *Controller-4* are discussed in the next sections.

6.2 Linear state feedback with internal model, *Controller-3*

Taking into account the internal model described in Section 4.3, the controller synthesis developed in LIVIC [MELMN09] has been extended in order to ensure zero lateral offset in steady-state and also to include constraints for pole clustering.

A linear vehicle model of system (6.4) (see Remark 4.2.1) has been used to design the assistance. The road curvature is considered to be bounded by $|\rho_{ref}| < \rho_{ref}^{max}$, therefore system is rewritten as:

$$\dot{x} = Ax + B_u u + B_w w \tag{6.11}$$

where the superscripts ^{im} have been intentionally not written in order to ease the notation and w is considered an exogenous input $w = \frac{\rho_{ref}}{\rho_{ref}^{max}}$ and $B_w = \rho_{ref}^{\max} B_\rho^{im}$

Since it is intended to apply a control law that enables the vehicle to perform curves, $\rho_{ref} \neq 0$, the equilibrium point is no longer fixed at the origin (as in the case of straight lines). Therefore, to make use of the Lyapunov theory of stability, it is necessary to ensure that the state trajectories converge to an invariant set containing all the equilibrium points.

As presented in [MELMN09], by means of BMI optimisation procedure, it is possible to find simultaneously a state feedback gain and a quadratic Lyapunov function, which guarantee the invariant set properties even in the presence of disturbances.

This algorithm for control synthesis is extended in this work by the additional dynamics from the internal model which ensure zero lateral offset in steady-state behaviour. Moreover a constraint is included for poles clustering, in order to enhance the damping characteristic of the closed-loop response as shown below.

An ellipsoidal invariant set of the form:

$$\varepsilon(P) \stackrel{\Delta}{=} \{x \in \mathbb{R}^n : x^T P x \leq 1\}, \text{ with } P = P^T \text{ and } P \succ 0, \tag{6.12}$$

can be obtained from a quadratic Lyapunov function:

$$V(x) = x^T P x, \text{ with } P \succ 0 \text{ and } \dot{V}(x) < 0. \tag{6.13}$$

The invariant set must contain all trajectories starting from a subset which represents the states at the activation of the assistance system. This subset of initial conditions is a polytope $L(T^N)$ defined as:

$$x \in L(T^N) \stackrel{\Delta}{=} \{x \in \mathbb{R}^6 : |T^N x| \leq 1\}, \tag{6.14}$$

where $T^N \in \mathbb{R}^{6x6}$ is a diagonal matrix with the following elements:

$$T^N \triangleq \begin{bmatrix} (\beta^N)^{-1} & 0 & 0 & 0 & 0 & 0 \\ 0 & (r^N)^{-1} & 0 & 0 & 0 & 0 \\ 0 & 0 & (\psi_L^N)^{-1} & 0 & 0 & 0 \\ 0 & 0 & 0 & (y_L^N)^{-1} & 0 & 0 \\ 0 & 0 & 0 & 0 & (\varphi_0^N)^{-1} & 0 \\ 0 & 0 & 0 & 0 & 0 & (\varphi_1^N)^{-1} \end{bmatrix} \tag{6.15}$$

where the values β^N and r^N can be set as the equilibrium point of (6.7) for $\rho_{ref} = \rho_{ref}^{\max}$ and the remaining parameters are chosen based on safety conditions such as maximum vehicle positioning on the road.

Minimising the ellipsoid that contains the polytope (6.14) at the same time as satisfying the conditions $\dot{V} < 0$, $V(x) \geq 1$, $w^T w \leq 1$ can be expressed in terms of a bilinear matrix inequality optimisation problem, by using the S-procedure [BGFB94] as follows:

$$\begin{array}{ll} \text{Minimise:} & tr(Q), \quad det(Q) \quad \text{or} \quad \lambda_{max}(Q) \\ \text{Subject to:} & \gamma \succ 0, \\ & Q \succ 0, \\ & \begin{pmatrix} QA^T + Y^T B_u^T + AQ + B_u Y + \gamma Q & B_w \\ B_w^T & -\gamma \end{pmatrix} \preceq 0, \\ & \begin{pmatrix} 1 & z_j^T \\ z_j & Q \end{pmatrix} \succeq 0, \quad j = 1, ..., g/2, \end{array} \tag{6.16}$$

where γ is a real constant, $Q = P^{-1}$, $Y = KP^{-1}$, and z_j represents each of the $g = 64$ vertices of the polytope (6.14).

Bounds on the control input can also be included in the optimisation problem. This constraint is important not only to limit the control input with respect to the actuator physical limitations but also to keep the vehicle dynamics within the linear behaviour, avoiding excessive lateral accelerations and saturation of the lateral tyre forces. The constraint can be expressed as:

$$\begin{pmatrix} 1 & \frac{1}{\delta_f^{max}} Y \\ \frac{1}{\delta_f^{max}} Y^T & Q \end{pmatrix} \succeq 0, \tag{6.17}$$

where δ_f^{max} is the maximum steering input used in the control design phase.

In order to enhance the damping characteristic of the closed loop response, constraints can be included to specify regions where the poles have to be located. A constraint for pole clustering defining a conic sector of angle θ centred at the origin [CG96], as shown in Fig. 6.1 can be described as:

$$\begin{pmatrix} \sin\theta \begin{bmatrix} AQ + QA^T \\ +B_w Y + Y^T B_w^T \end{bmatrix} & \cos\theta \begin{bmatrix} AQ - QA^T \\ +B_w Y - Y^T B_w^T \end{bmatrix} \\ \cos\theta \begin{bmatrix} -AQ + QA^T \\ -B_w Y + Y^T B_w^T \end{bmatrix} & \sin\theta \begin{bmatrix} AQ + QA^T \\ +B_w Y + Y^T B_w^T \end{bmatrix} \end{pmatrix} \prec 0 \tag{6.18}$$

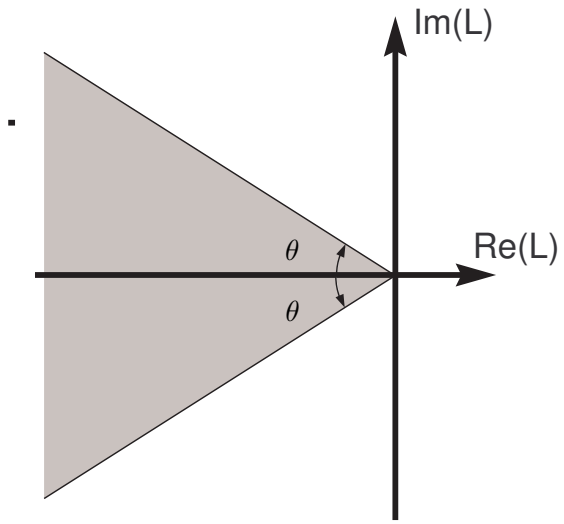

Figure 6.1: Conic region for pole clustering within angle θ

If the optimisation problem composed of (6.16), (6.17) and (6.18) is feasible, the resulting controller is able to reject the disturbances of road curvature and it ensures that all the state trajectories are contained in the invariant set $\varepsilon(P)$. Moreover, the pole clustering condition (6.18) ensures that all eigenvalues have negative real parts, therefore the closed loop linear system (6.7) is asymptotically stable even in the presence of disturbances.

6.2.1 Controller synthesis

The software PENBMI [KS03] was used to solve the BMI problem (6.16), including constraints (6.17) and (6.18). The maximum road curvature was considered $\rho_{ref}^{max} = 0.005m^{-1}$. The polytopic region T^N was defined with the following values:

$$T^N = [0.013,\ 0.174,\ 0.017,\ 0.2,\ 0.005,\ 0.005]\,. \tag{6.19}$$

The numerical values of the vehicle parameters used in the design are presented in Table 4.3, and the vehicle longitudinal speed has been considered constant at $v = 15\ [m/s]$.

The bound for control input was defined as $|\delta_f^{max}| = 5°$ and the angle for poles clustering was chosen $\theta = 30°$. The computed gain from the optimisation problem (6.16) is ensured to stabilise asymptotically the system for bounded disturbances $|\rho_{ref}| \leq \rho_{ref}^{max}$, since constraint (6.18) is satisfied and consequently all real parts of the eigenvalues of the closed loop system (6.7) are negative, as shown bellow.

$$\lambda = \begin{bmatrix} -6.7218 + 1.3347i \\ -6.7218 - 1.3347i \\ -2.1680 \\ -1.5181 \\ -0.4520 \\ -0.2470 \end{bmatrix}, \tag{6.20}$$

The corresponding gain is given by:

$$K = [-0.1813, \quad -0.0955, \quad -0.9418, \quad -0.0781, \quad -0.0045, \quad -0.0341] \tag{6.21}$$

This control law has been implemented and tested on a prototype vehicle to verify the performance of the proposed lane keeping assistance system. Moreover, simulations in the CarSim environment have been carried out in order to explore the use of such a controller in lane change and/or obstacle avoidance systems. These results are presented in Sections 6.4.1 and 6.4.2 respectively.

Possibilities of exploring the use of PWA models to handle the tyre saturation, are presented in the next sections.

6.3 PWL PIID on lateral offset - *Controller-4*

Based on the results obtained for *Controller-1*, an extension has been proposed for a lane keeping system. For this, vehicle model (4.25) is considered and the switching conditions are based only on the yaw rate, according to the steady-state analysis which was developed for *Controller-1*. Despite the improvements in the vehicle dynamics shown by *Controller-2* due to the inclusion of the state feedback and the switching driven by the wheel sideslip angle, the most simple structure has been privileged at this first stage, with the goal restricted to the evaluation of the potential advantages of the PWL controller with respect to the corresponding linear controller for lane keeping purposes.

Taking into account the considerations about the road geometry and correspondent internal model to reject road curvatures, shown in 6.1, a simple control strategy involving a piecewise linear proportional double integrator and derivative ($PIID_i$) on the lateral offset is used in order to design this preliminary *Perceptive-ESC* . The control strategy is described below.

6.3.1 Control strategy for PWL PIID on lateral offset

It has been shown in Section 6.1, that the use of a proportional-double-integral controller may be adequate to reject disturbances such as the road curvature, to ensure zero lateral offset condition in steady-state. Therefore, the internal model (6.2), and an additional derivative term (denoted D_i) are included in the state vector of the PWA vehicle model (4.25). The dynamics due to the integral and derivative terms are:

$$\begin{array}{rcl} \dot{\varphi}_1 & = & y_L, \\ \dot{\varphi}_2 & = & \varphi_1, \\ \dot{\varphi}_3 & = & -\frac{1}{\tau}\varphi_3 + y_L, \end{array} \tag{6.22}$$

where τ is the filter time constant. Defining:

$$y_{Ld} \;=\; -\tfrac{1}{\tau^2}\varphi_3 + \tfrac{1}{\tau}y_L, \tag{6.23}$$

the regulator becomes:

$$\begin{array}{rl} \delta_f = & -P_i y_L - I_{1i}\int_0^t y_L\, d\nu - I_{2i}\int_0^t\int_0^\nu y_L d\eta d\nu - D_i y_{Ld} \\ \delta_f = & -P_i y_L - I_{Ii}\varphi_1 - I_{2i}\varphi_2 - D_i y_{Ld},\ for\ i = 1, 2,\ 3. \end{array} \tag{6.24}$$

Replacing the expression (6.24) for the control input ($u = \delta_f$) in the vehicle model (4.25) and including the dynamics (6.22) the PWA closed loop system becomes:

$$\dot{x} = A_i x + B_\rho \rho_{ref} + a_i \tag{6.25}$$

where $x = [\beta, r, \psi_L, y_L, \varphi_1, \varphi_2, \varphi_3]^T$ and

$$A_i = \begin{bmatrix} -2\frac{d_{fi}+d_{ri}}{mv} & -1-2\frac{d_{fi}l_f-d_{ri}l_r}{mv^2} & 0 & -b_{1i}(P_i+\frac{D_i}{\tau}) & -b_{1i}I_{1i} & -b_{1i}I_{2i} & b_{1i}\frac{D_i}{\tau^2} \\ 2\frac{d_{ri}l_r-d_{fi}l_f}{J} & -2\frac{d_{fi}l_f^2+d_{ri}l_r^2}{Jv} & 0 & -b_{2i}(P_i+\frac{D_i}{\tau}) & -b_{2i}I_{1i} & -b_{2i}I_{2i} & b_{2i}\frac{D_i}{\tau^2} \\ 0 & 1 & 0 & 0 & 0 & 0 & 0 \\ v & l_s & v & 0 & 0 & 0 & 0 \\ 0 & 0 & 0 & 1 & 0 & 0 & 0 \\ 0 & 0 & 0 & 0 & 1 & 0 & 0 \\ 0 & 0 & 0 & 1 & 0 & 0 & -\frac{1}{\tau} \end{bmatrix},$$

$$B_\rho = \begin{bmatrix} 0 \\ 0 \\ -v \\ 0 \\ 0 \\ 0 \\ 0 \end{bmatrix} \quad \text{and} \quad a_i = \begin{bmatrix} 2\frac{e_{fi}+e_{ri}}{mv} \\ 2\frac{e_{fi}l_f-e_{ri}l_r}{J} \\ 0 \\ 0 \\ 0 \\ 0 \\ 0 \end{bmatrix}, \tag{6.26}$$

where $b_{1i} = \frac{2d_{fi}}{mv}$ and $b_{2i} = \frac{2d_{fi}l_f}{J}$.

Fig. 6.2 shows the schema for the PWL control structure. The Remark 5.1.1 is also valid for this configuration.

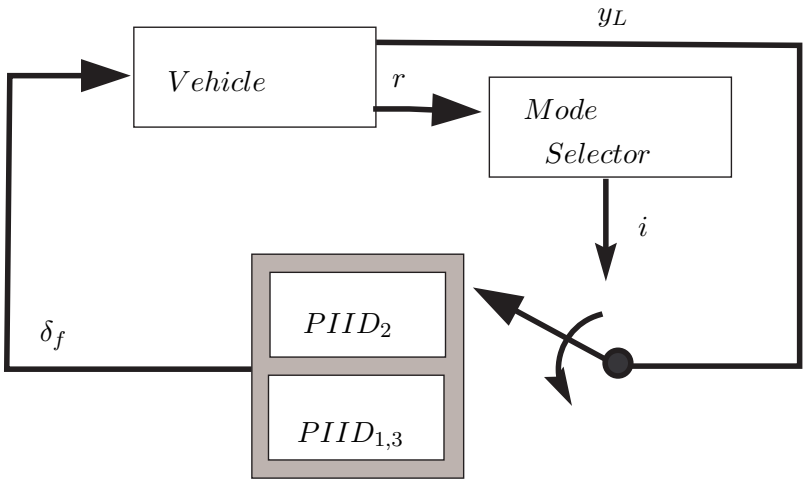

Figure 6.2: Schema from *Controller-4*.

The controller synthesis for this lane keeping assistance is described below.

Synthesis of *Controller-4*

Algorithm 5.1.1 has been employed in the design of *Controller-4*, since it also involves the parametrisation of the vehicle dynamics in terms of yaw rate and a proof of stability based on piecewise quadratic Lyapunov function. The LMIs to proof stability were solved using the toolbox for PWL systems [HJ99]

For each subsystem, the Simulink Response Optimisation toolbox was used to tune the design parameters through numerical optimisation; the design requirements are expressed in terms of rise time, settling time and overshoot. The gains from each $PIID_i$ are obtained from a Sequential Quadratic Programming method as described in [GMW81].

The same PWA approximation of the Pacejka tyre force used for *Controller-1*, (see Fig. 5.2) has been employed for the design of *Controller-4*, consequently the boundaries of the PWA vehicle model have been defined for the same values of yaw rate, $r = \pm\bar{r}$, (see Fig. 5.1). Considering a vehicle speed of $v = 30$ $[m/s]$, and CarSim vehicle parameters as shown in Table 4.2, the obtained gains are:

Table 6.1: Gains for lane keeping based on yaw rate only - *Controller-4*

	Gains			
Regions	P_i	I_{1i}	I_{2i}	D_i
$i = 1, 3$	0.4363	0.3879	0.1842	0.0271
$i = 2$	0.7272	0.6787	0.2812	0.0368

They are computed such that each subsystem is stable, however the stability of the whole system considering the switches between each subsystem is presented below.

6.3.2 Stability proof and invariant set analysis for *Controller-4*

The PWA model of the vehicle under action of *Controller-4* (6.25) has already its partitions described in term of state variables (parametrisation in terms of yaw rate), Theorem 3.5.1 can be directly used to verify the overall system stability. The boundaries of the parametrised PWA systems described by:

$$\begin{aligned} H_1^T &= \begin{bmatrix} 0 & 1 & 0 & 0 & 0 & 0 & 0 \end{bmatrix}, \quad g_1 = -0.27, \\ H_2^T &= \begin{bmatrix} 0 & -1 & 0 & 0 & 0 & 0 & 0 \\ 0 & 1 & 0 & 0 & 0 & 0 & 0 \end{bmatrix}, \quad g_2 = \begin{bmatrix} 0.27 \\ 0.27 \end{bmatrix}, \\ H_3^T &= \begin{bmatrix} 0 & -1 & 0 & 0 & 0 & 0 & 0 \end{bmatrix}, \quad g_3 = -0.27, \end{aligned} \tag{6.27}$$

Considering the gains according to Table 6.1, the LMIs of Theorem 3.5.1 applied for system (6.25) are feasible, therefore the system is stable admitting a piecewise quadratic Lyapunov function of the form (3.43).

Although the system is stable, it is important to investigate the invariant sets corresponding to the piecewise quadratic function to ensure that the vehicle stays in the lane. The two parallel lines in Fig. 6.3 represent the projection on the $\psi_L - y_L$ plane of a fixed strip of width $2d$ in the centre of the lane (B.3). The set defined by $\epsilon = \bigcup_{i=1}^{3} \epsilon_i$ where $\epsilon_i = \left\{x \in R^7 / x^T P_i x \leq c\right\}$, where c

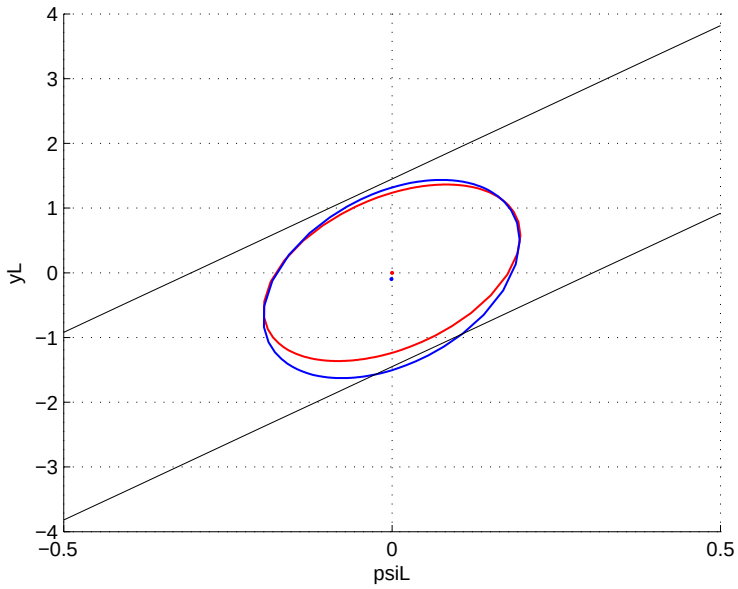

Figure 6.3: Hyperlanes describing the set $\mathcal{T}$ (for $a = 1.5m$ and $2d = 4.4m$) and the ellipsoidal invariant sets corresponding to P_1 and P_2

is a constant, is invariant for (6.25). Therefore every trajectory that starts in ϵ remains in the set for $t \to \infty$. The maximum invariant set obtained from the Lyapunov function is computed such that the front wheel positions do not exit the lane $\epsilon \subset T$. The ellipsoids in Fig. 6.3 correspond to the projection of ϵ_i on the ψ_L-y_L plane.

The advantages of *Controller-4* in comparison to the same control strategy designed for the linear region only can be seen in section 6.4.3, after the presentation of the results from practical implementation and simulations of the assistance systems *Controller-3*.

6.4 Results

In this section the simulation and practical implementation results of the proposed controller for lane departure avoidance systems are presented.

Controller-3 has been implemented on the prototype vehicle CARLLA and tested as a lane departure avoidance system considering the activation strategy described in Appendix-B. The results are presented in Section 6.4.1.

Simulations in CarSim environment, presented in Section 6.4.2, have also been carried out in order to assess the use of *Controller-3* in lane change manoeuvres, according to the standard ISO-3888-1.

Controller-4 has been evaluated in CarSim environment and compared to the response of the corresponding controller for the linear region only, in order to investigate the advantages of the PWL control structure. The scenarios consisted of disturbance rejection, and sudden direction changes. The results are shown in Section 6.4.3.

Table 6.2 summarises the simulations and practical experimentation carried out with each controller.

Table 6.2: Summary of practical implementation and simulation results for internal model based LKAS:

Controller	CarSim Environment	CARLLA	Purpose
Controller-3		Fig. 6.4 - Fig. 6.9	Lane departure avoidance
	Fig. 6.10 - Fig. 6.11		Obstacle avoidance
Controller-4	Fig. 6.12 - Fig. 6.17		Autonomous vehicle

6.4.1 Practical Implementation of *Controller-3*

An activation strategy for the lane departure avoidance system using *Controller-3* is described in Appendix-B. It takes into account the driver awareness and risk of lane departure based on the position of the front wheels. The practical tests have been carried out with the prototype vehicle CARLLA (described in Section 4.6.2).

The experiment scenario consists of departure from the lane, supposing that the driver is not attentive. Fig. 6.4 shows the positioning of the vehicle on the lane. The first subplot shows the relative yaw angle while in the second it is shown the position of the front wheels with respect to the lane, which is shown by the dashed-dot line. The activation occurs at $51s$ approximately when the right wheel crosses the fixed centred strip of $\pm d$, depicted by the dashed line. The front wheels remain in the lane during the whole control action. The driver recovers attention at $63s$, and the controller is deactivated.

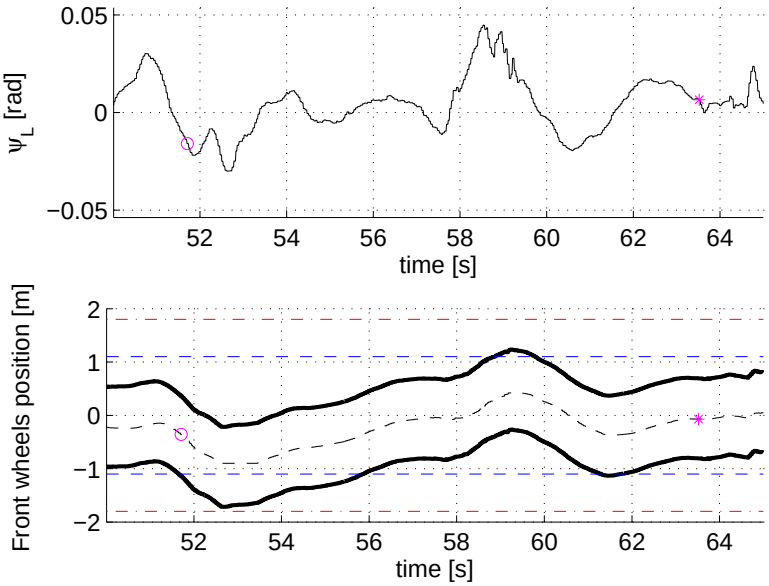

Figure 6.4: Relative yaw angle, ψ_L and position of the front wheels with respect to lane for practical implementation of *Controller-3*.

The dynamics of the vehicle during the intervention of the lane keeping system can be seen

in Fig. 6.5. The vehicle sideslip angle, yaw rate and longitudinal speed are depicted. The

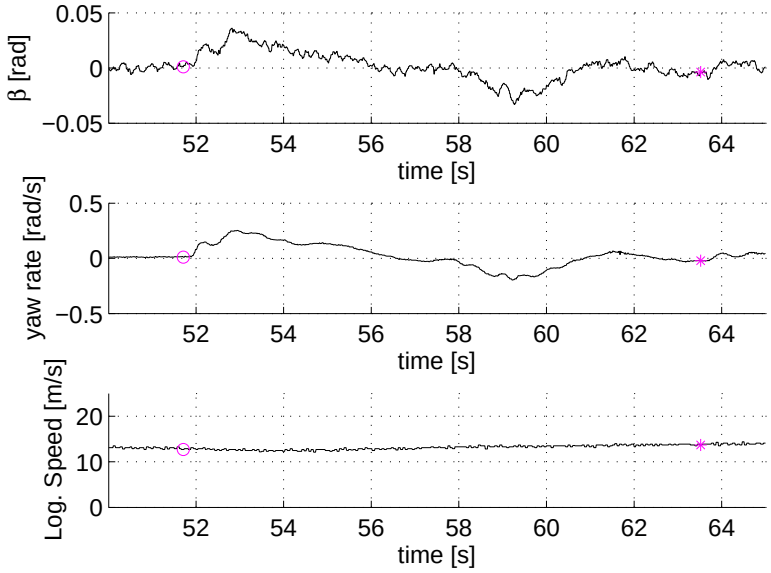

Figure 6.5: Vehicle sideslip angle, yaw rate and longitudinal speed during control action of *Controller-3* to avoid lane departure.

required control input is shown in the top subplot of Fig 6.6. In the bottom subplot, the road curvature for the corresponding part of the track, can be seen. Even though the values of the road curvature are larger than the bound chosen in the design phase ($\rho_{ref}^{max} = 0.005\ m^{-1}$), the controller performs satisfactorily keeping the vehicle within the lane limits.

Another manoeuvre is performed in order to show the lane keeping controller performance. As it can be seen by the road curvature of the test track depicted in Fig. 6.9, this scenario corresponds to an inattentive driver on a curve to the right side, which is also sharper than the considered bound ρ_{ref}^{max} in the design stage.

The activation, shown in the bottom subplot of Fig. 6.7, takes place due to the positioning of the right front wheel, which reaches the centred strip on the interior side of the curve. Even though the correction induces a longer excursion of the vehicle near the exterior side of the lane, the performance is satisfactory, as the front wheels do not exit the lane. The relative yaw angle is plotted on the top subplot of Fig. 6.7.

The dynamics of vehicle during the control action are illustrated on Fig. 6.8. The subplot shows the vehicle sideslip angle, yaw rate and longitudinal speed, respectively. Finally, the required control input is shown in the top subplot of Fig. 6.9.

Due to the satisfactory performance of the lane keeping system, obstacle avoidance manoeuvres (doule lane change) with the same controller have been performed in the CarSim simulation environment on a vehicle model similar to the experimental vehicle. The results are shown in the next section.

6.4.2 Simulation results of *Controller-3* as obstacle avoidance assistance

In order to test *Controller-3* as an obstacle avoidance assistance (double lane change), it has been supposed that a system, as in [VGMG09], is available to provide a reference trajectory

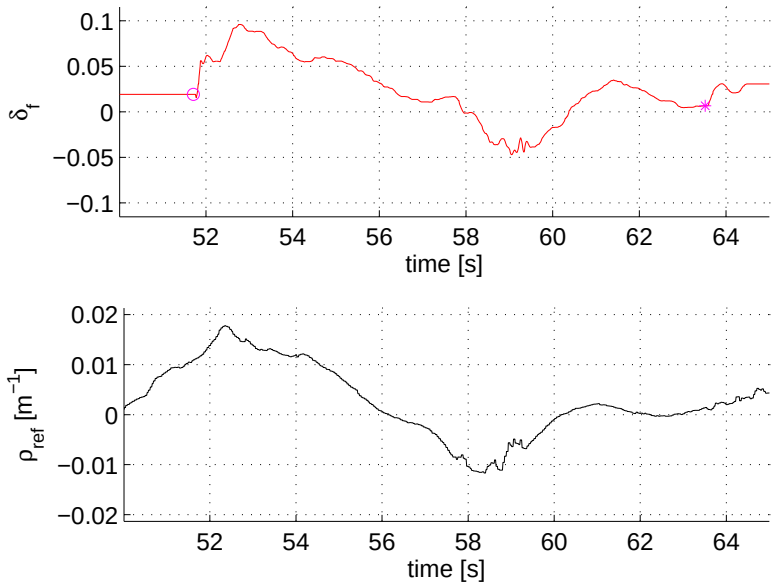

Figure 6.6: Control input for lane departure avoidance manoeuvre of *Controller-3* and road curvature.

which is capable of avoiding an obstacle. The objective is to investigate the performance of *Controller-3* to follow the reference trajectory. For this, a double lane change manoeuvre, following the standard ISO-3888-1, at a vehicle speed of 25 $[m/s]$ has been carried out in the CARSIM environment. The test is defined by a pre-determined placement of cones on the road and the manoeuvre is performed on a dry surface. The reference trajectory is shown in the top subplot of Fig. 6.10. The corresponding vehicle sideslip angle and the yaw rate are shown in the middle and bottom subplots of Fig. 6.10.

In Fig. 6.11 the lateral offset, y_l, and the proposed control action are shown. The controller achieves the path following with a reduced path following error in the lateral direction (0.4 [m] as can be observed in the first subplot of Fig. 6.10). The second subplot depicts the control input required for such manoeuvre.

6.4.3 Simulation results of *Controller-4*

Several simulation tests in the CarSim environment have been performed in order to evaluate the improvements of the proposed Piecewise Linear $PIID_i$ control (*Controller-4*) strategy by comparison with the same controller designed in the linear region only ($i = 2$).

The same vehicle in two different configurations was used in the simulations. The first consisted of the vehicle equipped with the designed controller in the linear region only, equation (6.24) with $i = 2$, named *lin.-ctrl*; The second configuration consisted of the vehicle equipped with the proposed PWL control strategy, equation (6.24) with $i = 1, 2, 3$, named *PWL-ctrl*. Two different scenarios are presented in the following: response to sudden disturbances as external lateral force and yaw moment, and response to sudden direction changes (in dry and wet pavement). Both vehicles were tested at a longitudinal speed of $v = 30\,[m/s]$.

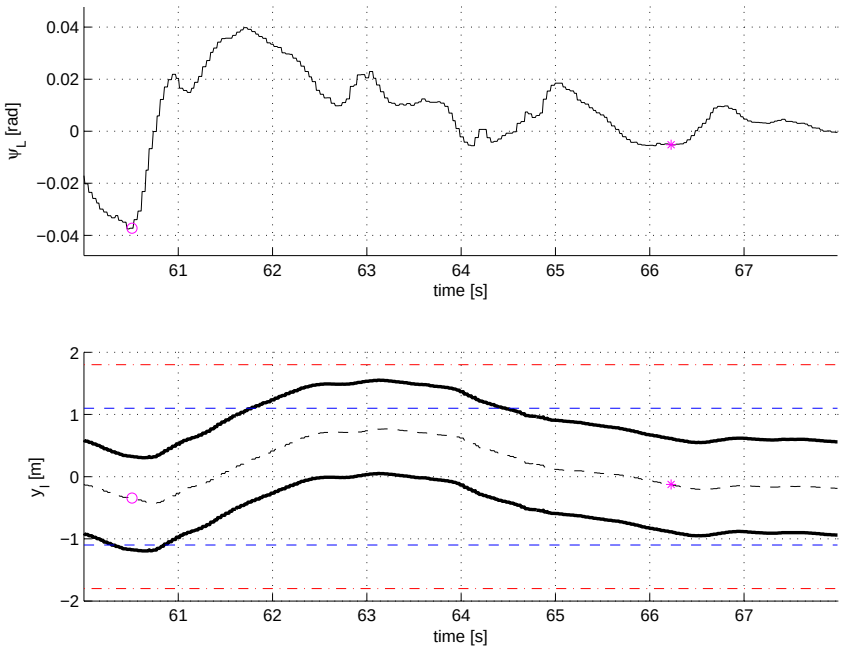

Figure 6.7: Vehicle relative yaw angle , ψ_L and position of the front wheels with respect to lane during lane departure avoidance manoeuvre in curve of *Controller-3*.

Sudden Disturbances

To analyse the improved performance, the vehicle is subject to a sudden disturbance on both the lateral and the yaw dynamics as shown in the upper-left subplot of Fig. 6.12. The disturbances, and the required manoeuvre for correction are strong enough to make the vehicle lateral dynamics enter the nonlinear region, as it can be seen in the bottom-left subplot of Fig. 6.13, showing the active regions of the *PWL-ctrl* vehicle. It is important to note that the control input of the PWL controller is reduced when the vehicle yaw rate exits the linear region ($i = 1$), as shown in the bottom-right subplot of Fig. 6.13. Consequently, the tyre sideslip angles, depicted on the upper-right subplot of Fig. 6.13, do not increase as much as for the vehicle *lin.-ctrl*. The upper-right subplots of Fig. 6.12 and Fig. 6.13 show the vehicle trajectories and the lateral-offset, respectively. The reduction by about 50% of the overshot in lateral-offset for the *PWL-ctrl* confirms its improved performance for lane keeping purposes.

Sudden Change in Direction

Several manoeuvres are performed to analyse the response of the lane keeping controller with respect to change in directions. The results presented consist of a demanding lane change manoeuvre, as the vehicles reach a lateral acceleration of 8.9 $[m/s^2]$, in two different road adhesion conditions, while no external disturbances are applied.

Considering firstly good adhesion conditions, characterised by the road adhesion coefficient ($\mu = 1$), the enhanced performance of the proposed control strategy for lake keeping is clear when compared to the response of *lin.-ctrl*, for the manoeuvre shown in the upper-left subplot of Fig. 6.14. Analysing Fig 6.15, it can be seen that by the switch of *PWL-ctrl* between the regions $i = 1, 2$, in the bottom-left subplot, the control action depicted on the bottom-right, is reduced when the vehicle yaw rate reaches the partition limits. Consequently, the vehicle

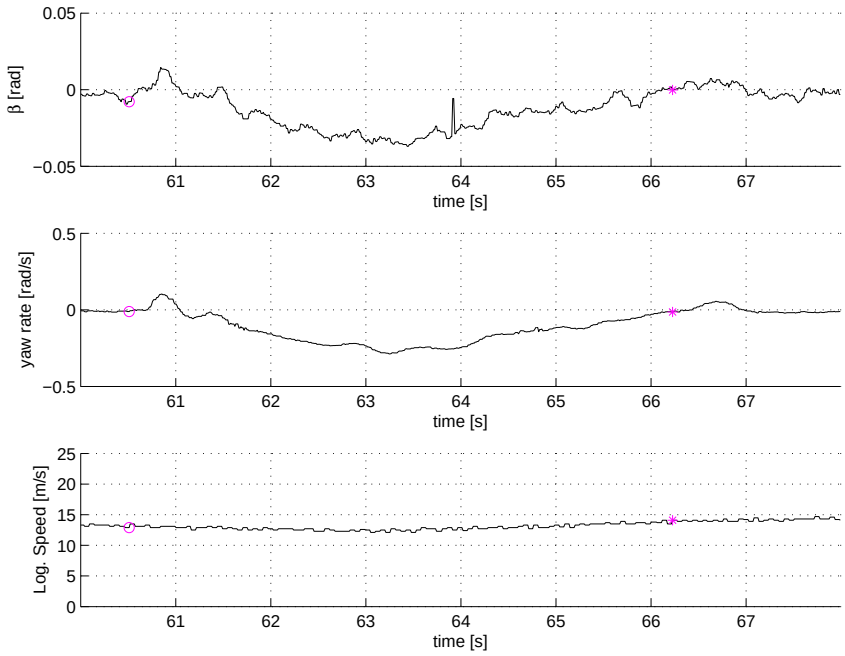

Figure 6.8: Vehicle sideslip angle, yaw rate and longitudinal speed during lane departure avoidance manoeuvre in curve for *Controller-3*.

remains in a controllable condition, avoiding the tyre forces saturation which can be seen by the smaller values of front wheel sideslip angle in the upper-right subplot. Moreover the lateral-offset is steered to zero faster than for the *lin.-ctrl* vehicle. The vehicle lateral dynamics (vehicle sideslip angle and yaw rate) are shown in the bottom subplots of Fig. 6.14. In order to evaluate the robustness with respect to different road adhesion coefficients, the same manoeuvre is performed for a deteriorated road adhesion ($\mu = 0.7$), corresponding to wet pavement. The results are shown in Fig. 6.16 and 6.17. Even though the lateral-offset reaches more significant values, as the manoeuvre is very demanding, it can be seen that, also in this case, the proposed PWL controller performance is improved with respect to the *lin.-ctrl*, which is at its stability limit.

6.5 Conclusion

In this chapter, the synthesis of two controllers for lane keeping purposes have been presented. Both controllers incorporate an internal model in order to reject the disturbances, such as the road curvature, considered an exogenous input.

The first proposed assistance, named *Controller-3*, has been developed using a linear vehicle model, whereas for the second, named *Controller-4*, a simple PWL control structure has been chosen in order to develop a preliminary *Perceptive-ESC* from which the advantages of the PWL modelling can be verified.

The control synthesis employed for the design of the assistance *Controller-3* is based on the minimisation of quadratic invariant set to outer approximate a polytope representing the regular driving conditions and to ensure the boundedness of the state trajectories. This technique for the design of lane keeping assistance had already been developed at LIVIC [MELMN09]. The novelty of *Controller-3* lies in the inclusion of the internal model in the state vector in order

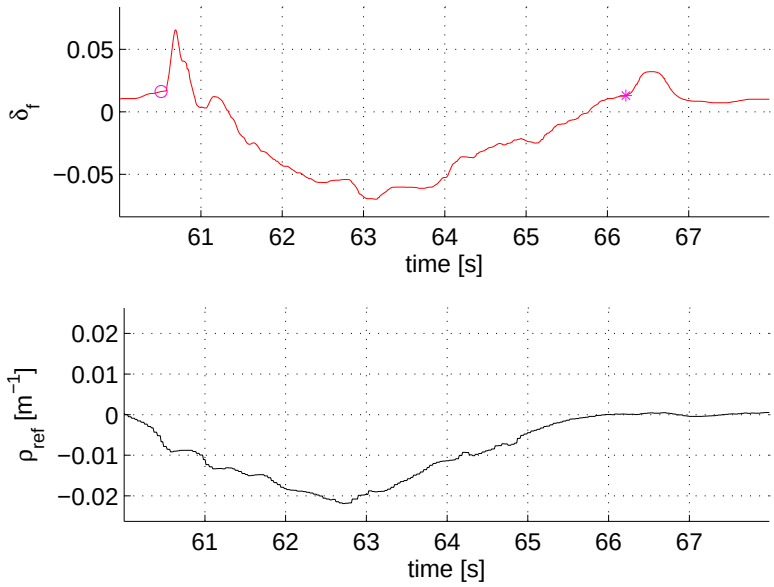

Figure 6.9: Control input of *Controller-3* in lane departure avoidance manoeuvre and road curvature.

to ensure zero lateral offset in steady-state. Another extension consists of the inclusion of pole clustering constraints not only to enhance the damping conditions but also to guarantee asymptotic stabilisation.

Practical implementation on the prototype vehicle CARLLA confirms the asymptotic stabilisation, and invariant set properties from the Lyapunov functions, even on roads with sharper curves than the design parameters. Therefore, it can be concluded that *Controller-3* performs satisfactorily as a lane departure avoidance system.

The influence of the dynamical controller has also been tested on more demanding manoeuvres. The tests carried out on CarSim environment have showed that *Controller-3* can potentially be used as collision avoidance assistance as well, since it has performed the standard manoeuvre ISO-3888-1 satisfactorily.

Motivated by the previous results obtained for the PWL controllers of the proposed steering assistance systems, a similar structure has been chosen for the development of *Controller-4*, consisting of a PWL PIID on the lateral offset.

It has been shown that the use of PWA controllers can satisfactorily handle demanding situations with respect to the lateral dynamics. Simulations in CarSim environment with *Controller-4*, consisting of disturbance rejection and of sudden direction changes, have confirmed the potential of PWL controller to enhance the vehicle manoeuvrability with respect to the single linear controller, even with the switching based simply on yaw rate.

Based on these results, the choice of using a simple structure for a preliminary version of the *Perceptive-ESC* has proven to be adequate, accomplishing the goal of demonstrating the advantages of the PWL controller and its potential for lane keeping purposes.

The main drawback of this synthesis lies in the fact that tuning the gains may be an arduous task since the stability proof of the whole system can only be performed afterwards. This disadvantage motivates the search of PWA affine controllers in which the synthesis provides the gains and ensures the stability simultaneously.

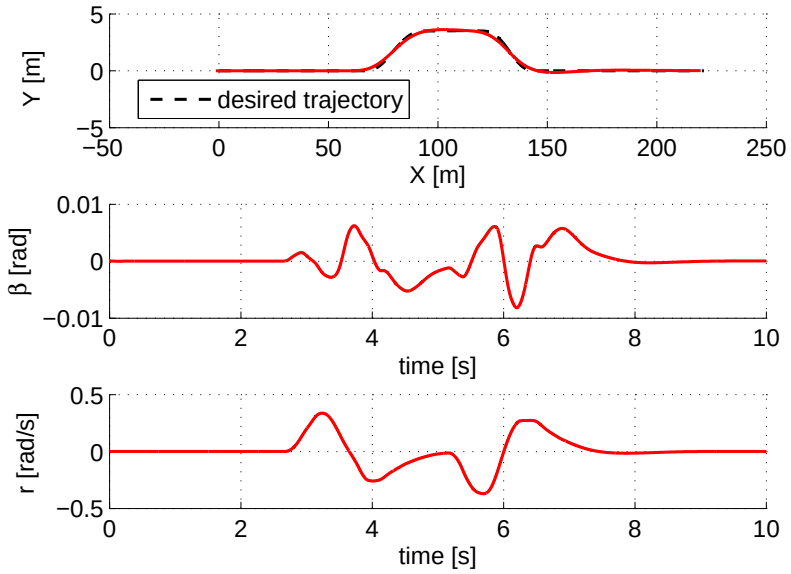

Figure 6.10: Path of standard CarSim Moose test and vehicle under *Controller-3* following manoeuvre performed at a vehicle speed $v = 25\ [m/s]$.

In the next chapter, these aspects are taken into account in the design of a lane departure avoidance systems.

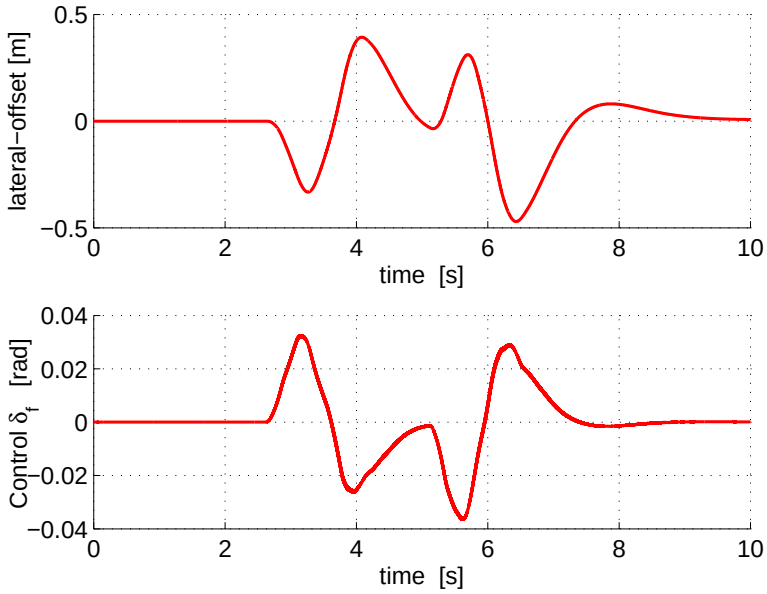

Figure 6.11: Lateral offset and control input of vehicle equipped with *Controller-3* performing the standard CarSim Moose test at a vehicle speed $v = 25\ [m/s]$.

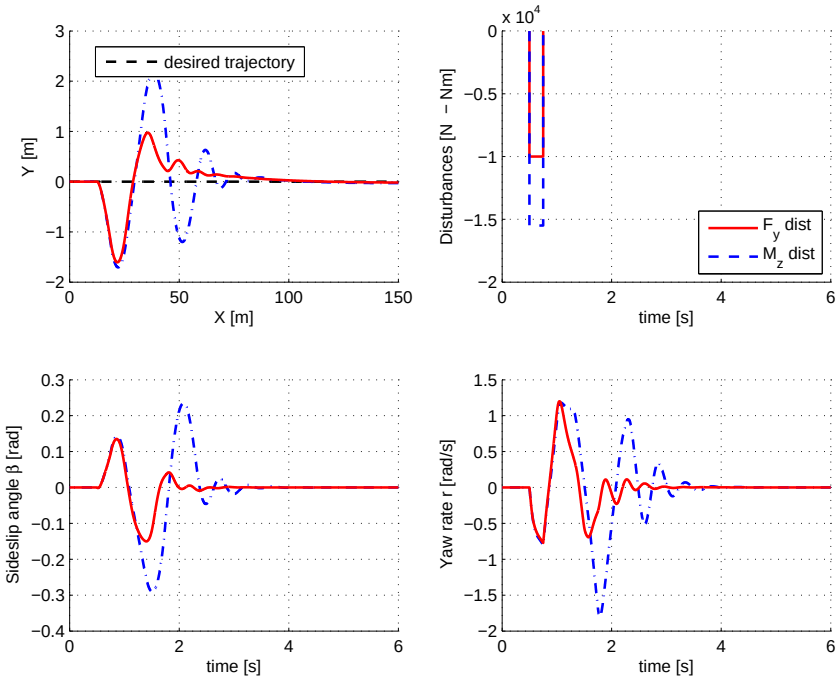

Figure 6.12: Response to a sudden disturbance on vehicles *lin.-ctrl* (dashed line) and *PWL-ctrl* (continuous line) with *Controller-4* at $v = 30\ [m/s]$.

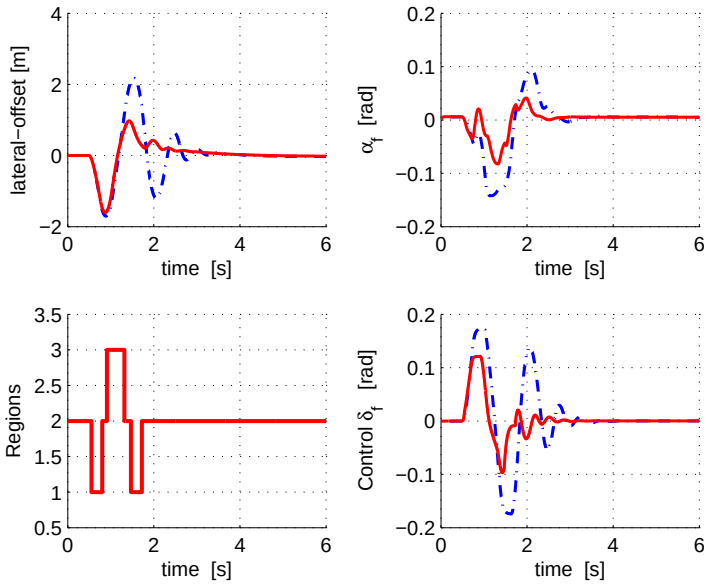

Figure 6.13: Response to a sudden disturbance on vehicles *lin.-ctrl* (dashed line) and *PWL-ctrl* (continuous line) with *Controller-4* at $v = 30\ [m/s]$.

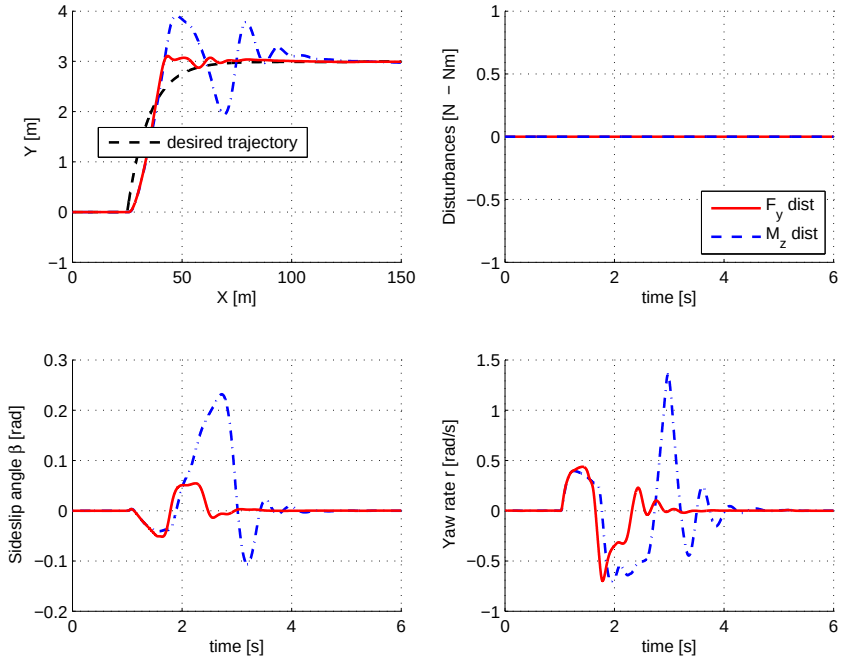

Figure 6.14: Response to a lane change on vehicles *lin.-ctrl* (dashed line) and *PWL-ctrl* (continuous line) with *Controller-4* at $v = 30\ [m/s]$ on dry road.

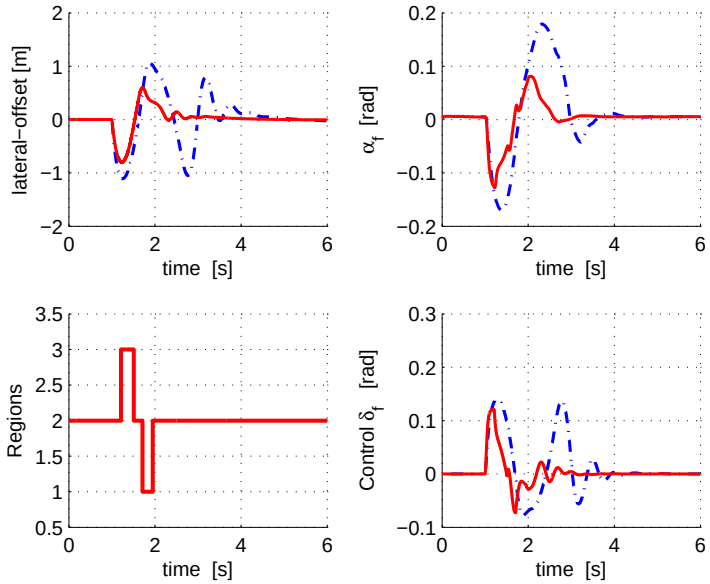

Figure 6.15: Response to a lane change on vehicles *lin.-ctrl* (dashed line) and *PWL-ctrl* (continuous line) with *Controller-4* at $v = 30\ [m/s]$ on dry road.

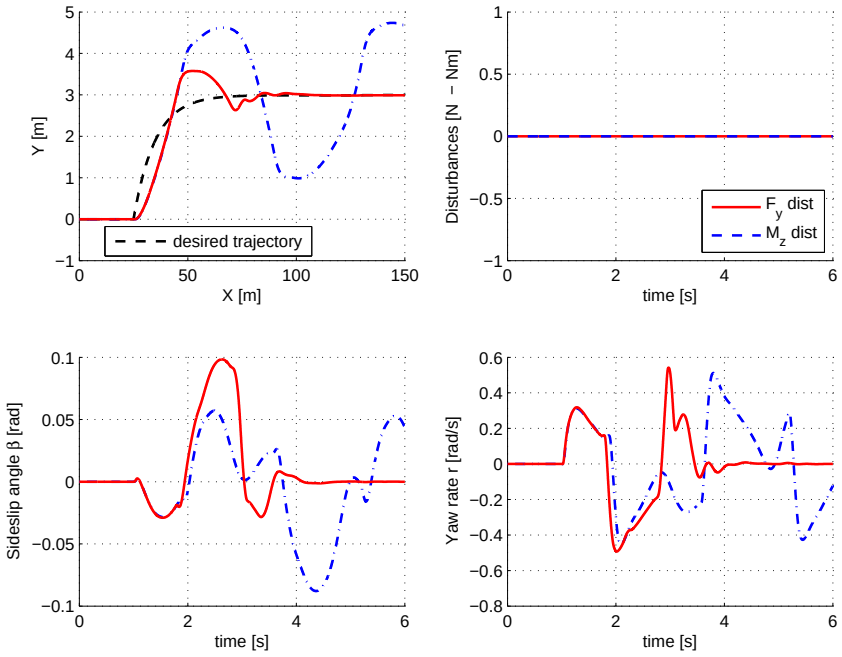

Figure 6.16: Response to a lane change on vehicles *lin.-ctrl* (dashed line) and *PWL-ctrl* (continuous line) with *Controller-4* at $v = 30\ [m/s]$ on wet road.

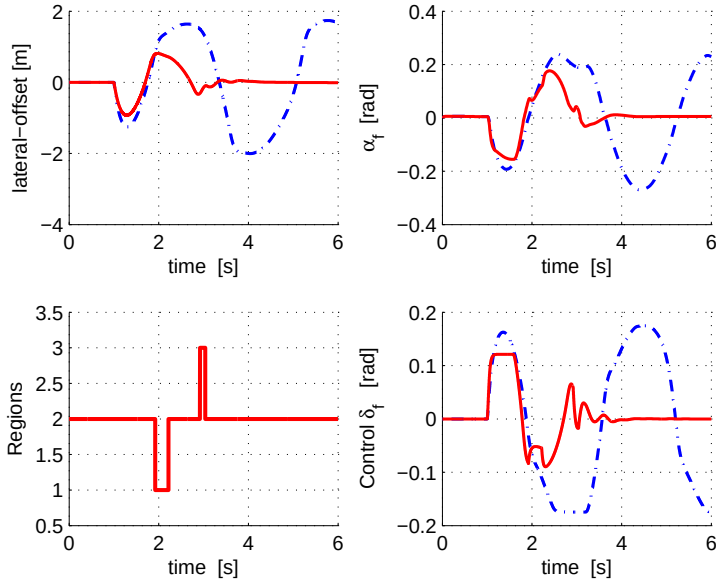

Figure 6.17: Response to a lane change on vehicles *lin.-ctrl* (dashed line) and *PWL-ctrl* (continuous line) with *Controller-4* at $v = 30\ [m/s]$ on wet road.

Chapter 7

Lyapunov based PWA control for lane departure avoidance

Contents

This chapter presents the development of lane departure avoidance assistances that use PWA controllers to cope with the lateral tyre force nonlinear behaviour. The syntheses employed to compute the PWA controllers allow the gains to be set while the stability is ensured by the quadratic Lyapunov function through optimisation procedures involving LMI and BMI.

The first section presents a PWL state feedback control, named (*Controller-5*), based on quadratic Lyapunov. The control synthesis is cast as an LMI optimisation and the influence of the PWA approximations from the Pacejka tyre force on the feasibility of the LMIs is also analysed.

As an attempt to circumvent the conservativeness of the synthesis based on a single quadratic Lyapunov function, the synthesis of a PWA state feedback controller (*Controller-6*) considering a piecewise quadratic Lyapunov function is described in Section 7.2.

In order to provide a *Perceptive-ESC* which can be produced only with the sensors available on currently commercialised passenger cars, this controller is extended to a lane departure avoidance assistance in which the measurement of the vehicle sideslip angle is avoided. This assistance, named *Controller-7* and presented in Section 7.4, is based on the PWA output feedback control synthesis.

The results from simulation and/or practical implementation of the controllers for lane departure avoidance are presented in Section 7.5, followed by the conclusions that wrap-up this chapter.

7.1 PWL state feedback based on quadratic Lyapunov function - *Controller-5*

For the development of the following lane departure avoidance systems, the control syntheses employed for the PWA vehicle model ensure the stability while the gains are designed. These approaches are particularly interesting when the number of parameters to be tuned and operating regions increase.

Controller-5 has been designed considering the switching of the PWA vehicle model (4.28) based on the tyre sideslip angle, as in (4.5). Since these partitions are slab, they can be exactly approximated by degenerated ellipsoids (see Definition 3.4.2), and Theorem 3.5.2 can be used for the synthesis of a PWL state feedback based on a quadratic Lyapunov function, as shown below.

7.1.1 Control synthesis - *Controller-5*

Several PWA approximations, according to (4.12), of the tyre forces have been used in the control synthesis using Theorem 3.5.2. Following the assumption described in Section 4.2.2, the understeering behaviour of most passenger cars is privileged, hence saturation of the tyre forces has been considered only for the front tyre and a linear model has been used to describe the rear tyre forces ($d_{ri} = c_f$ and $e_{ri} = 0$). Concerning the tyre force approximation for the front tyres, the same slope was considered for the linear region ($d_{flin} = c_f$ and $e_{flin} = 0$) in all PWA vehicle models that were analysed, whereas two distinct investigations have been carried out for the affine approximations. Firstly, the domain of the front tyre lateral force was divided into three regions only, and secondly, several regions at different intervals of front tyre sideslip angle have been considered.

The numerical values of the vehicle parameters are provided in 4.3 and the vehicle speed is considered constant at $v = 15$ $[m/s]$, since the controller was intended to be implemented on the prototype vehicle CARLLA and evaluated on the test track in Satory (Versailles-France). The LMIs were solved using LMI Lab [Mat11].

PWA approximation with single partitioning

The partitioning of the tyre forces for the PWL state feedback control problem is illustrated in Fig. 7.1. As it can be seen, only three PWA functions have been considered resulting in a PWA model with 3 operating regions $\mathcal{I} = 1, 2, 3$. The thresholds that limit the linear region are named $\pm\bar{\alpha}_f$ and a second point $\pm\alpha_f^{end}$, marked as $\times$ in Fig. 7.1, is used to determine the PWA approximation for operating regions R_1 and R_3.

The ellipsoidal cell description for each region can be obtained as indicated in the example 3.4.1. It follows:

$$\begin{aligned} E_1 &= [-1, -\tfrac{l_f}{v}, 0, 0, 1]\tfrac{2}{-\bar{\alpha}_f - \underline{d}}, \quad & f_1 &= -\tfrac{-\bar{\alpha}_f + \underline{d}}{-\bar{\alpha}_f - \underline{d}}, \\ E_2 &= [-1, -\tfrac{l_f}{v}, 0, 0, 1]\tfrac{1}{\bar{\alpha}_f}, & f_2 &= -\tfrac{\bar{\alpha}_f - \bar{\alpha}_f}{\bar{\alpha}_f + \bar{\alpha}_f} = 0, \\ E_3 &= [-1, -\tfrac{l_f}{v}, 0, 0, 1]\tfrac{2}{d - \bar{\alpha}_f}, & f_3 &= -\tfrac{\bar{d} + \bar{\alpha}_f}{d - \bar{\alpha}_f}, \end{aligned} \tag{7.1}$$

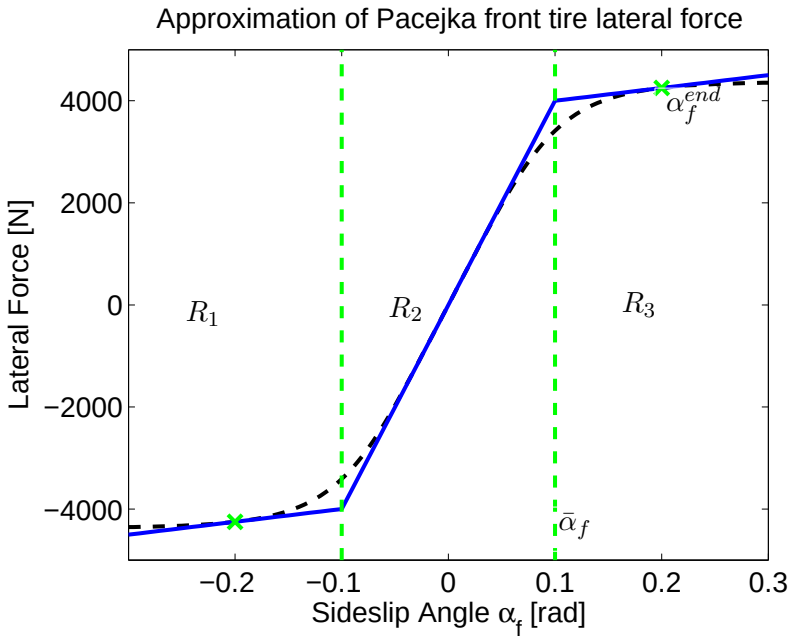

Figure 7.1: Single PWA approximation of front tyre lateral force.

where $\underline{d}$ and $\bar{d}$ can be arbitrarily set, such that $\underline{d} < -\bar{\alpha}_f$ and $\bar{d} > \bar{\alpha}_f$.

Table 7.1 summarises the results obtained for the PWL state feedback control synthesis based on a single Lyapunov function for different values of $\bar{\alpha}_f$ and α_f^{end}. Due to the symmetry of PWA functions used to approximate the lateral tyre force, only the values for positive sideslip angle are shown.

It can be seen from Table 7.1 that the problem becomes unfeasible when the difference between the slopes of the PWA functions $(c_f - d_3)$ is larger than approximately $20000N/m$. In order to obtain a gradual slope difference from one region to another, the PWA approximation has been refined and its influence on the feasibility of the LMIs has been investigated in the sequel.

PWA approximation with multiple partitioning

The partitioning of the tyre force domain has been refined, as illustrated in Fig. 7.2, such that the linear region is limited between the values of $\pm\bar{\alpha}_f$, and the affine regions are defined by the increment α_f^{step} until the value α_f^{end}, as illustrated in Fig. 7.2, resulting in the set of operating regions $\mathcal{I} = 1, ..., M$.

The LMI conditions of Theorem 3.5.2 to find a PWL state feedback for the vehicle model (4.28) have been tested for several coefficients determining the PWA approximations. The linear regions have been defined by the values $\bar{\alpha}_f \in \mathcal{P}$, where $\mathcal{P} = \{0.01,\ 0.02, ...,\ 0.15\}\ [rad]$. To define the affine approximations of the Pacejka model for lateral tyre force, increments of $0.01\ [rad]$ for α_f^{step} in the range $\{0.01,\ 0.15\}\ [rad]$ have been considered, *i.e.* $\alpha_f^{step} \in S$, where $S = \{0.01,\ 0.02, ...,\ 0.15\}\ [rad]$. The values α_f^{end}, delimiting the boundary between the operating regions R_{M-1} and R_M are obtained from the expression $\alpha_f^{end} = \bar{\alpha}_f + k\alpha_f^{step}$, for $k \in \{1, 2, 3, ...\}$ and $\alpha_f^{end} \leq 0.3$, for each $\bar{\alpha}_f \in \mathcal{P}$ and $\alpha_f^{step} \in \mathcal{S}$.

Similarly to the results obtained for a single partitioning, whenever the difference between

Table 7.1: Feasibility of Quadratic Stabilisation for simple partition

Attempt	$\bar{\alpha}_f$ $[rad]$	α_f^{end} $[rad]$	d_3 $[N/m]$	e_3 $[N]$	$c_f - d_3$ $[N/m]$	Result
1	0.05	0.06	32489.92	375.26	7505.17	Feasible
2	0.05	0.07	32610.18	369.25	7384.91	Feasible
3	0.05	0.08	31469.7	426.27	8525.39	Feasible
4	0.05	0.09	29941.16	502.7	10053.93	Feasible
5	0.05	0.1	28259.18	586.8	11735.91	Feasible
6	0.05	0.11	26541.24	672.69	13453.85	Feasible
7	0.05	0.12	24858.31	756.84	15136.78	Feasible
8	0.05	0.13	23253.42	837.08	16741.67	Feasible
9	0.05	0.14	21750.32	912.24	18244.77	Feasible
10	0.05	0.15	20359.51	981.78	19635.58	Feasible
11	0.05	0.16	19082.74	1045.62	20912.35	no
12	0.05	0.17	17916.36	1103.94	22078.74	no
⋮	0.05	⋮	⋮	⋮	⋮	no
25	0.05	0.3	9416.02	1528.95	30579.07	no
26	0.06	0.07	25225.27	886.19	14769.82	Feasible
27	0.06	0.08	27207	767.29	12788.09	Feasible
28	0.06	0.09	26589.85	804.31	13405.24	Feasible
29	0.06	0.1	25325.21	880.19	14669.88	Feasible
30	0.06	0.11	23850.47	968.68	16144.62	Feasible
31	0.06	0.12	22335.52	1059.57	17659.58	Feasible
32	0.06	0.13	20861.75	1148	19133.34	Feasible
33	0.06	0.14	19469.73	1231.52	20525.36	no
⋮	0.06	⋮	⋮	⋮	⋮	no
51	0.07	0.09	19887.23	1407.55	20107.86	no
52	0.07	0.1	20435.25	1369.19	19559.85	Feasible
53	0.07	0.11	19814.31	1412.65	20180.78	no
⋮	⋮	⋮	⋮	⋮	⋮	no
220	0.15	0.3	-10970.02	7644.77	50965.11	no

the slopes of the linear and the affine region $i = M\ c_f - dfM$ is larger than approximately $20000N/m$ the LMIs are not feasible, even if the differences of slopes of two subsequent regions are smaller than this value.

It can be noticed from these results, and those presented in Appendix C, that the chosen refinement of the partition does not improve the feasibility of LMIs from Theorem 3.5.2.

Some simulations (presented in section 7.5.1) have been carried out to evaluate the improvements on the performance from the computed PWL state feedback with respect to the gains designed for the linear region only. Nevertheless, it can be seen that the approximations for which the LMIs are feasible, are very close to the linear behaviour of the tyre forces, and therefore not adequate to represent the saturation of the tyre forces. For this reason, a control synthesis based on piecewise quadratic Lyapunov functions has been investigated as an attempt

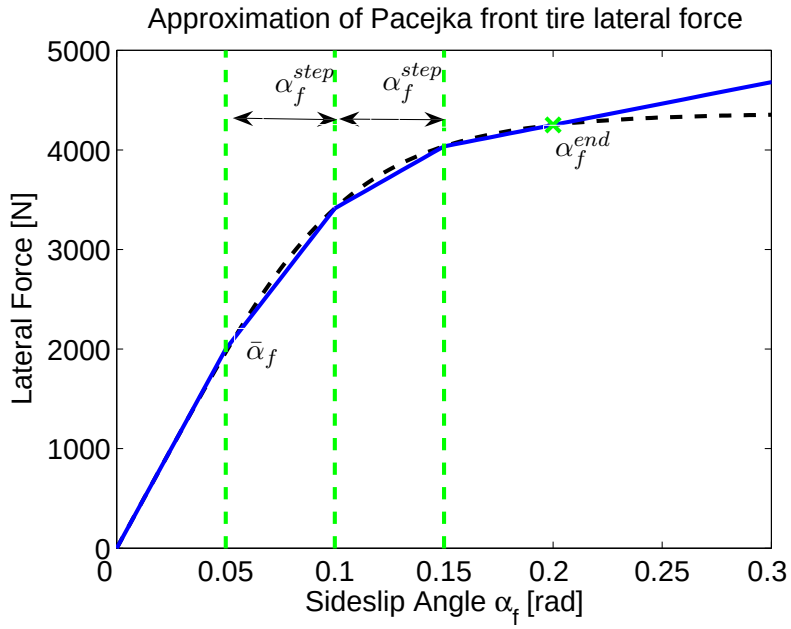

Figure 7.2: Multiple PWA approximation of front tyre lateral force.

to circumvent the conservativeness of Theorem 3.5.2, as presented in the next section.

7.2 PWA state feedback controller - *Controller-6*

As presented in Section 3.5.3, it is possible to design a PWA state feedback control $u_c = K_i x + m_i$ for a PWA system with a previously chosen equilibrium point for its closed loop system and each of the subsystems by solving the BMI problem (3.58). This control synthesis is employed to design a lane departure avoidance controller as shown below.

7.2.1 PWA state feedback control for lane departure avoidance

Lane departure avoidance systems have as main objective to steer the vehicle to the centre of the lane. Considering roads with reduced curvatures, when riding in the centre of the lane the vehicle state variables (model (4.35)) belong to a small set including the origin. Therefore, the action of steering the vehicle to the centre of the lane may be interpreted as designing a controller such that trajectories of the closed loop system converge to the equilibrium point located at the origin.

The PWA vehicle model (4.35) has been used for the design of this assistance. Taking into account the assumptions described in Section 4.2.2, the PWA vehicle model from (4.35) is obtained considering the understeering behaviour. In consequence, only the front tyre forces are approximated by PWA functions according to (4.12) and a single linear approximation is assumed for the rear tyre, as follows:

$$\begin{cases} f_{sf}(\alpha_f) = e_{fi} + d_{fi}\alpha_f, & \text{for } \underline{\alpha}_f^i \leq \alpha_f \leq \bar{\alpha}_f^i, \\ f_{sr}(\alpha_r) = c_r \alpha_r, & \forall\ \alpha_r, \end{cases} \tag{7.2}$$

where the values $\underline{\alpha}_f^i$ and $\bar{\alpha}_f^i$ represent respectively the lower and upper boundary of the operating region R_i in terms of front wheel sideslip angle.

The choice of using (4.35) as a PWA vehicle model is motivated mainly by two reasons. Firstly, by including the model of the steering column in the state-space vector, the partitioning of the operating regions can be written in terms of state-space variables (see equations (4.4)), hence, it avoids feed-through from the control input to the nonlinearity. Secondly, this model of the actuator is more realistic than the first order dynamics employed in (4.28).

The operating regions are slab and can be described by degenerated ellipsoids (see Definition 3.4.2), as follows:

$$E_i^T = [-1,\ -\tfrac{l_f}{v},\ 0,\ 0,\ 1,\ 0]\tfrac{2}{\bar{\alpha}_f^i - \underline{\alpha}_f^i}, \quad f_i = -\tfrac{\bar{\alpha}_f^i + \underline{\alpha}_f^i}{\bar{\alpha}_f^i - \underline{\alpha}_f^i}, \tag{7.3}$$

where lower and upper bounds must be chosen respectively for R_1 and R_M, taking into account the physical limitations of the wheel sideslip angle.

Considering the hyperplane between R_i and R_j, $\alpha_f - \alpha_f^{ij} = 0$, or in terms of state-space variables, $[-1,\ -\frac{l_f}{v},\ 0,\ 0,\ 1,\ 0]x - \alpha_f^{ij} = 0$, then the matrices expressing the parametric description of this boundary (see Definition 3.4.3) are given by:

$$F_{i,j} = \begin{bmatrix} \frac{l_f}{v} & 0 & 0 & 1 & 0 \\ 1 & 0 & 0 & 0 & 0 \\ 0 & 1 & 0 & 0 & 0 \\ 0 & 0 & 1 & 0 & 0 \\ 0 & 0 & 0 & 1 & 0 \\ 0 & 0 & 0 & 0 & 1 \end{bmatrix}, \tag{7.4}$$

$$l_{i,j} = \begin{bmatrix} -\frac{\alpha_f^{ij}}{2+l_f^2/v^2}, & -\frac{\alpha_f^{ij} l_f}{v\left(2+l_f^2/v^2\right)}, & 0, & 0, & \frac{\alpha_f^{ij}}{2+l_f^2/v^2}, & 0 \end{bmatrix}.$$

Disturbances and exogenous inputs, such as the road curvature, are not taken into account in the PWA control synthesis.

Having defined the PWA model, the PWA state feedback controller for the lane departure avoidance assistance can be computed, using the following algorithm, based on the BMI optimisation problem 3.58.

Algorithm 7.2.1 *:*

1. ***PWA approximation of tyre forces*** *The PWA affine functions, that approximate the nonlinear tyre model, are defined such that they take into account the nonlinear behaviour of the tyre lateral forces. The boundaries defining the validity of each approximation are also defined. The assumptions from Section 4.2.2 should be considered in order to obtain a solution for the BMI optimisation problem 3.58.*

2. ***Definition of the closed-loop equilibrium points****. The equilibrium point of the closed loop system (x_{eq}) must be defined a priori. The origin is chosen for the lane departure avoidance assistance system. The equilibrium points of all other affine dynamics (x_{eq}^i) must be chosen such that they do not belong to the respective operating regions (see Remark 3.5.6).*

3. ***Initial controller design*** *In order to use the V-K method (see Remark 3.5.7) to solve 3.58, design, for each operating region of the PWA vehicle model an initial state feedback controller $K_i^{k=0}$ and $m_i^{k=0}$ where k indicates the iteration of the V-K method. The affine term on the control input $m_i^{k=0}$ may be used to force the equilibrium points of the affine regions to the desired locations.*

4. ***V-Step*** *Using the gains and decay rate obtained in the previous step i.e.* $K_i^k \leftarrow K_i^{k-1}$, $m_i^k \leftarrow m_i^{k-1}$ *and* $\alpha_i^k \leftarrow \alpha_i^{k-1}$, *apply the V-step to find a piecewise quadratic Lyapunov function. If the LMIs* (3.59) *are not feasible at the first iteration, retake the algorithm from Step-2. From the second iteration onwards, if LMIs* (3.59) *are not feasible, stop the iterations and the controller is given by the result obtained at the last feasible iteration, i.e.* $K_i \leftarrow K_i^{k-1}$ *and* $m_i \leftarrow m_i^{k-1}$.

5. ***K-Step*** *Apply the K-Step (LMIs* (3.60)*) using the values obtained from the previous step for the piecewise quadratic Lyapunov function. If LMIs* (3.60) *are feasible, return to Step-4 (V-Step). If LMIs* (3.60) *are not feasible, stop the iterations and the controller is given by the result obtained at the last feasible iteration, i.e.* $K_i \leftarrow K_i^{k-1}$ *and* $m_i \leftarrow m_i^{k-1}$. *If no significant improvement on the cost is obtained, stop the algorithm and the controller is given by* $K_i \leftarrow K_i^k$ *and* $m_i \leftarrow m_i^k$.

It is important to be reminded, that the replacements (3.57) must be taken into account in *Step-4* of the Algorithm 7.2.1 for the operating region corresponding to the linear approximation of the tyre forces, since the closed loop equilibrium point $x_{eq} = 0$ belongs to this region. Besides, continuity of the control input along the switching boundaries may be enforced in *Step-5* of the Algorithm 7.2.1 using the equality constraints (3.61).

Details of the synthesis of the PWA state feedback for the lane departure avoidance assistance *Controller-6* are provided below.

7.2.2 PWA state feedback control synthesis

The numerical values of parameters describing the vehicle and Pacejka tyre force models are shown in Table 4.3. A longitudinal speed of $v = 21\ [m/s]$ has been considered. Since it was intended to implement *Controller-6* on the prototype vehicle CARLLA, such speed is adequate to evaluate the controller on sections of the test track with road curvature $\rho_{ref} > 0.01\ [m^{-1}]$.

The PWA functions used to approximate the Pacejka tyre model have been defined, as illustrated in Fig. 7.1, with threshold values $|\bar{\alpha}_f| = 0.07\ [rad]$ and $|\alpha_f^{end}| = 0.2\ [rad]$, resulting in the following partitioning:

$$\begin{cases} \begin{cases} f_{sf}(\alpha_f) = e_{f1} + d_{f1}\alpha_f, & \text{for } \alpha_f < -\bar{\alpha}_f, \\ f_{sf}(\alpha_f) = c_f\alpha_f, & \text{for } -\bar{\alpha}_f \leq \alpha_f \leq \bar{\alpha}_f, \\ f_{sf}(\alpha_f) = e_{f3} + d_{f3}\alpha_f, & \text{for } \alpha_f > \bar{\alpha}_f, \end{cases} \\ \{\ f_{sr}(\alpha_r) = c_r\alpha_r \quad \forall \alpha_r, \end{cases} \tag{7.5}$$

The numerical values of the piecewise affine approximations for the tyre lateral forces, considering such threshold values are indicated in Table 7.2.

Remark 7.2.1 (Choice of boundaries for the linear region) *Although the bounds for the linear region are relatively small, these values do not represent a limitation of the method. Similar syntheses have also been successfully achieved with bounds at higher levels, as* $|\bar{\alpha}_f| = 0.1\ [rad]$, *for instance. The use of lower values for the boundaries has been necessary in order to evaluate the behaviour of the PWA controller in safe conditions during the practical implementation.*

Table 7.2: Numerical values of PWA approximations of tyre lateral forces for *Controller-6*

Region	d_{fi}	e_{fi}	d_{ri}	e_{ri}
R_1	11162	−2018.3	3.4993	0
R_2	3.9995	0	3.4993	0
R_3	11162	2018.3	3.4993	0

Consequently the ellipsoidal cell description (7.3) of the operating regions becomes:

$$\begin{aligned} E_1^T &= [-1,\ -\tfrac{l_f}{v},\ 0,\ 0,\ 1,\ 0]\tfrac{2}{-\bar{\alpha}_f-\underline{d}}, \quad f_1 = -\tfrac{-\bar{\alpha}_f+\underline{d}}{-\bar{\alpha}_f-\underline{d}}, \\ E_2^T &= [-1,\ -\tfrac{l_f}{v},\ 0,\ 0,\ 1,\ 0]\tfrac{1}{\bar{\alpha}_f}, \qquad f_2 = -\tfrac{\bar{\alpha}_f-\bar{\alpha}_f}{\bar{\alpha}_f+\bar{\alpha}_f} = 0, \\ E_3^T &= [-1,\ -\tfrac{l_f}{v},\ 0,\ 0,\ 1,\ 0]\tfrac{2}{d-\bar{\alpha}_f}, \quad f_3 = -\tfrac{\bar{d}+\bar{\alpha}_f}{d-\bar{\alpha}_f}, \end{aligned} \tag{7.6}$$

where the numerical values for the bounds are: $\bar{d} = -\underline{d} = 0.3$.

Although the partitioning could be refined, the results obtained in practical implementation, presented in Section 7.5.2, show that the controller computed using this simple partitioning is able to handle the nonlinear behaviour of the tyre forces satisfactorily.

Due to the symmetry of the lateral tyre force with respect to the origin, and consequently also the dynamics of the PWA vehicle model, only regions R_1 and R_2 are considered in the control synthesis. The gains obtained for region R_1 can be applied in region R_3, *e.g.* $K_1 = K_3$ and $m_1 = -m_3$. This procedure reduces the number of LMIs to be solved.

The control synthesis proposed in [MELMN09] (previously developed at LIVIC) has been used for the design of the initial controller $K_i^{k=0}$ in order to initialise the V-K method. The following two advantages motivated the use of the controller developed in [MELMN09] in the design of the *Perceptive-ESC* . Firstly, since the disturbances, such as the road curvature, are not explicitly taken into account in algorithm 7.2.1, the method proposed in [MELMN09] is able to compute invariant sets for the lateral assistance given that the road curvatures are bounded. Secondly, the gains obtained from [MELMN09] have already been validated for the prototype vehicle CARLLA in the linear domain of tyre lateral forces and in the presence of non zero road curvature. Therefore, for the linear region, R_2:

$$K_2^{k=0} = [-351.9,\ -68.37,\ -728.44,\ -56.69,\ -620.60,\ -1.81]\,, \quad m_2 = 0 \tag{7.7}$$

For the first iteration, the same controller has been chosen for region R_1, therefore $K_1^{k=0} = K_2^{k=0}$. Due to the chosen partitioning and PWA approximation of the tyre forces, the equilibrium point of the closed loop dynamics in R_1 is already outside this region, *i.e* $x_{eq}^1 \notin R_1$, therefore $m_1^{k=0} = m_2^{k=0} = 0$ can be set for the first iteration.

In order to enforce that the equilibrium point of the closed loop system must be the extrema of the piecewise quadratic Lyapunov function candidate, the replacements (3.57) are applied taking into account that equilibrium point of the closed loop system belongs to the linear region ($x_{eq} = 0 \in R_2$). In consequence, the terms q_2 and r_2 from the piecewise quadratic Lyapunov function (3.43) become:

$$q_2 = 0_{6\times 1}, \quad r_2 = 0, \tag{7.8}$$

for all iterations (V-Step), which ensures $V(0) = 0$.

It is known from [MELMN09], that the performance of the state feedback gain $K_2^{k=0}$ is satisfactory, therefore the following constraint is included in the *K-step* to avoid that the behaviour of the vehicle in the linear region is much altered during the optimisation process, limiting the variation of K_2 in the range $K \pm 5\%$. The additional constraint is:

$$0.95|K_2^0| < |K_2^k| < 1.05|K_2^0| \tag{7.9}$$

Moreover, the constraints (3.61) are added to the K-step in order to guarantee the continuity of the control input. The bounds on the controller gain and affine terms have been set as $l_1 = l_2 = 10^3$ and the constant $\epsilon = 10^{-6}$.

The V-K method using this initial controller has been carried out using CVX [GB11], and after 19 iterations the increase on the decay rate was smaller than a fixed threshold $s_c = 0.001$, (*i.e.* $\alpha_i^k - \alpha_i^{k-1} < s_c$), therefore it was considered that no significant improvement was obtained from the optimisation procedure. The resulting gains are as follows:

$$\begin{aligned} K_1 &= [-334.3651,\ -71.7693,\ -764.8334,\ -53.8590,\ -651.2582,\ -1.7312]\,, \quad m_1 = 3.1111 \\ K_2 &= [-378.8095,\ -74.3513,\ -764.8334,\ -53.8590,\ -606.8138,\ -1.7312]\,, \quad m_2 = 0 \\ K_3 &= K_1, \qquad\qquad\qquad\qquad\qquad\qquad\qquad\qquad\qquad\qquad\qquad\quad m_3 = -m_1 \end{aligned} \tag{7.10}$$

The decay rate of the piecewise quadratic Lyapunov function after the 19^{th} iteration is, for each operation region:

$$\alpha_1 = \alpha_3 = 0.8383, \qquad \alpha_2 = 1.3301 \tag{7.11}$$

The main drawback of this control structure is the need to measure the vehicle sideslip angle, which cannot be done with the sensor on the currently commercialised vehicles. For these reasons a solution based on observers is investigated in the subsequent section.

7.3 PWA output feedback controller - *Controller-7*

This section presents the design of a *Perceptive-ESC* , named *Controller-7* which is based only on variables that can be measured with the sensors on currently commercialised cars.

As described in Section 3.5.4, a PWA output feedback controller based on piecewise quadratic Lyapunov functions can be designed for PWA systems. This section presents the application of these theoretical tools for the design of lane departure avoidance systems.

7.4 PWA output feedback controller for lane departure avoidance

In order to use the piecewise quadratic Lyapunov based control technique for the design of *Controller-7*, the assumptions described in Section 4.2.2 have been applied to the PWA vehicle model (4.35). Moreover, it is assumed that the vehicle sideslip angle is not available for measurement, therefore the outputs from the system are defined by the vector y as:

$$\left\{ \begin{array}{rcl} \dot{x} & = & A_i x + B_i u + a_i \\ y & = & C_i x \end{array} \right. \tag{7.12}$$

where $x = [\beta, r, \psi_L, y_L, \delta_f, \dot{\delta}_f]^T$ and $u = \tau_a + \tau_d$,

$$C_i = \begin{bmatrix} 0 & 1 & 0 & 0 & 0 & 0 \\ 0 & 0 & 1 & 0 & 0 & 0 \\ 0 & 0 & 0 & 1 & 0 & 0 \\ 0 & 0 & 0 & 0 & 1 & 0 \\ 0 & 0 & 0 & 0 & 0 & 1 \end{bmatrix} \quad \forall i \in \mathcal{I}, \tag{7.13}$$

and A_i, B_{ui} and a_i are as described in (4.36), with $d_{fi} > 0$, $d_{ri} = c_r$ and $e_{ri} = 0$ for all $i \in \mathcal{I}$.

Recalling (3.62), the controller takes the form:

$$\begin{cases} \dot{x}_c(t) &= A_{ci}x_c + L_i y + b_{ci} \\ u &= K_i x_c + m_i \end{cases} \tag{7.14}$$

and the closed loop system can be written as:

$$\dot{\tilde{x}} = \tilde{A}_i \tilde{x} + \tilde{b}_i \tag{7.15}$$

where:

$$\tilde{A}_i = \begin{bmatrix} A_i & B_i K_i \\ L_i C_i & A_{ci} \end{bmatrix} \quad \text{and} \quad \tilde{b}_i = \begin{bmatrix} a_i + B_i m_i \\ b_{ci} \end{bmatrix} \tag{7.16}$$

The ellipsoidal cell descriptions (7.3) must be adjusted to the piecewise affine output feedback closed loop system (7.15). Hence,

$$\tilde{E}_i = [E_i,\ 0] \tag{7.17}$$

.

Similarly, the parametric cell boundaries (7.4) become:

$$\tilde{F}_{ij} = \begin{bmatrix} F_{ij} & 0 \\ 0 & I \end{bmatrix} \quad \text{and} \quad \tilde{l}_{ij} = \begin{bmatrix} l_{ij} \\ 0 \end{bmatrix} \tag{7.18}$$

As the switches of the controller can be driven only by the system outputs, the controller has to be designed with the structure of a regulator and an estimator (see remark: 3.5.9), so that the switch can be based on the front wheel sideslip angle, computed from the estimate of the vehicle sideslip angle and the measurements of yaw rate and steering angle as in (4.4). For this, the constraint (3.73) is included in the BMI inequalities (3.72)

Similarly to *Controller-6*, the origin is considered as the equilibrium point of the PWA closed loop system, and the following algorithm can be employed to synthesise the controller.

Algorithm 7.4.1 *:*

1. ***PWA approximation of tyre forces*** *Taking into account the assumptions from Section 4.2.2, define the PWA functions to approximate the tyre nonlinear lateral forces, as well as the region of validity for each approximation.*

2. ***Definition of the closed-loop equilibrium points****. The equilibrium point of the closed loop system ($\tilde{x}_{eq}$) must be defined a priori. The origin is chosen for the lane departure avoidance assistance system. The equilibrium points of all other affine dynamics ($\tilde{x}^i_{eq}$) must be chosen such that they do not belong to the respective operating regions (see Remark 3.5.6).*

3. ***Initial controller design*** *An initial controller ($A_{ci}^{k=0}$, $L_i^{k=0}$, $b_{ci}^{k=0}$, $K_i^{k=0}$ and $m_i^{k=0}$) has to be defined for each region in order to use the V-K method (see Remark 3.5.7). It is intended to switch based on the estimate of front wheel sideslip angle, which is rewritten in terms of state variables (β, r and δ_f), however the sideslip angle is not available for measurement. Therefore a observer regulator structure is required.*

   Considering an initial state feedback controller with gain $K_i^{k=0}$, such that the eigenvalues of the closed loop system dynamics $(A_i + B_{ui}K_i^{k=0})$ are located at λ_i. The gains for the observer can be obtained by pole placement, such that they are located at $\sigma\lambda_i$, for $\sigma \in \mathbb{R}$ and $5 \leq \sigma \leq 10$. The values of m_i are chosen so that the closed loop equilibrium point for each region is at the desired location.

   The matrices A_{ci}^k, and b_{ci}^k, are obtained from (3.73)*, as follows:*

$$\begin{cases} A_{ci}^k &= A_i + B_i K_i^k - L_i^k C_i \\ b_{ci}^k &= B_i m_i^k + b_i + (A_i - L_i^k C_i) x_{eq}^i \end{cases} \tag{7.19}$$

4. ***V-Step*** *Using the gains and decay rate obtained in the previous step i.e. $K_i^k \leftarrow K_i^{k-1}$, $m_i^k \leftarrow m_i^{k-1}$, $L_i^k \leftarrow L_i^{k-1}$, and $\alpha_i^k \leftarrow \alpha_i^{k-1}$, write the closed loop equations* (7.15) *using* (7.19)*. Perform the replacements* (3.71) *for the region corresponding to the linear dynamics in order to ensure that the equilibrium point of the closed loop system $\tilde{x}_{eq}$ is the extrema of the piecewise quadratic Lyapunov function. Solve the feasibility problem considering the LMIs* (3.67)*,* (3.68)*,* (3.69)*, $\epsilon > 0$, $\gamma_i > 0$ and $\lambda_i > 0$.*

   If the LMIs are not feasible at the first iteration, retake the algorithm from Step-2. From the second iteration onwards, if LMIs are not feasible, stop the iterations and the controller is given by the result obtained at the last feasible iteration, i.e. $K_i \leftarrow K_i^{k-1}$ and $m_i \leftarrow m_i^{k-1}$, $L_i \leftarrow L_i^{k-1}$, and $A_{ci} \leftarrow A_{ci}^{k-1}$, and $b_{ci} \leftarrow b_{ci}^{k-1}$.

5. ***K-Step*** *fixing the piecewise quadratic Lyapunov function obtained at the previous Step, solve*

$$\begin{aligned} &\textit{maximise:} && \min_i \alpha_i \\ &\textit{subjected to:} && (3.65),\ (3.67),\ (3.68),\ (7.19) \\ & && \epsilon > 0 \quad \gamma_i > 0 \quad \lambda_i > 0 \quad \alpha_i > l_0 > 0 \\ & && -l_1 < K_i < l_1 \quad -l_2 < m_i < l_2 \end{aligned} \tag{7.20}$$

   If LMIs (7.20) *are feasible, return to Step-4 (V-Step). If LMIs* (7.20) *are not feasible, stop the iterations and the controller is given by the result obtained at the last feasible iteration, i.e. $K_i \leftarrow K_i^{k-1}$ and $m_i \leftarrow m_i^{k-1}$. If no significant improvement on the cost is obtained, stop the algorithm and the controller is given by $K_i \leftarrow K_i^k$ and $m_i \leftarrow m_i^k$, $L_i \leftarrow L_i^{k-1}$, $A_{ci} \leftarrow A_{ci}^{k-1}$ and $b_{ci} \leftarrow b_{ci}^{k-1}$.*

Based on 7.4.1, the synthesis of the *Perceptive-ESC* using only sensors available on the currently commercialised vehicles is presented below.

7.4.1 PWA output feedback control synthesis

Similarly to *Controller-6*, the numerical values from the prototype vehicle CARLLA, described in Table 4.3 have been used, considering a longitudinal speed of $v = 21$ $[m/s]$ as well as the

PWA functions to approximate the Pacejka tyre model defined in Table 7.2, with threshold values $|\bar{\alpha}_f| = 0.07$ $[rad]$ and $|\alpha_f^{end}| = 0.2$ $[rad]$. Remark 7.2.1 is equally considered in this control synthesis.

Still based on the development of *Controller-6*, the initial controller for the operating region corresponding to linear dynamics was obtained from [MELMN09], and the same controller was extended to the affine regions, hence:

$$K_i^{k=0} = [-351.9,\ -68.37,\ -728.44,\ -56.69,\ -620.60,\ -1.81] \text{ and } m_i = 0 \text{ for } i = 1, 2, 3. \tag{7.21}$$

The observer was computed according to $Step - 3$ of Algorithm 7.4.1 with $\sigma = 7.6.$ and the same gains have been considered for all regions, *i.e.* $L_1^{k=0} = L_2^{k=0}$.

The constraints to enforce continuity of the control input (3.61) as well as the bounds on the controller K_2 according to (7.9) have been included in the K-step.

After 3 iterations, the LMIs solved with CVX [GB11] became unfeasible, the computed controller at the $3^r d$ iterations:

$$\begin{aligned} K_1 &= [-415.0616,\ -81.1789,\ -806.3640,\ -50.5724,\ -591.5498,\ -1.6332]\,, \quad m_1 = 6.8571 \\ K_2 &= [-317.1029,\ -75.4880,\ -806.3640,\ -50.5724,\ -689.5085,\ -1.6332]\,, \quad m_2 = 0 \\ K_3 &= K_1, \quad m_3 = -m_1, \end{aligned} \tag{7.22}$$

and the resulting gains for the observer are:

$$\begin{aligned} L_1 = L_3 &= 10^4 \begin{bmatrix} 0.3076 & 0.9144 & 0.5649 & -1.1432 & 1.0388 \\ -0.1782 & -0.5599 & -0.4354 & 0.8375 & -0.8309 \\ 0.1662 & 0.5005 & 0.3144 & -0.6335 & 0.5798 \\ 0.9786 & 2.9595 & 1.8830 & -3.8019 & 3.4587 \\ -0.4465 & -1.3493 & -0.8514 & 1.7212 & -1.5662 \\ 1.1999 & 3.9064 & 3.6210 & -6.8277 & 7.2030 \end{bmatrix}, \\ L_2 &= 10^3 \begin{bmatrix} 0.9589 & 2.5050 & 0.1537 & -0.8708 & 0.0297 \\ -0.2040 & -0.6620 & -0.0936 & 0.2362 & -0.1872 \\ 0.4824 & 1.3151 & 0.0860 & -0.4493 & 0.0377 \\ 2.6273 & 7.1835 & 0.5271 & -2.7802 & 0.0949 \\ -1.2489 & -3.4238 & -0.2314 & 1.2670 & -0.0453 \\ 0.6049 & 2.7614 & 0.7531 & -1.8031 & 3.9319 \end{bmatrix}. \end{aligned} \tag{7.23}$$

7.5 Results

In this section, the simulation and practical implementation results of the proposed Lyapunov-based controllers for lane departure avoidance systems (*Controller-5* to *Controller-7*) are presented. The main goal is to validate the controllers with respect to nonlinear combined lateral and longitudinal tyre forces and additional dynamics, such as combined lateral and longitudinal tyre forces, pitch, roll and driver dynamics, which were neglected at the control design stage.

The activation strategy employed for the lane departure avoidance assistance systems is described in detail in Appendix B. It incorporates an assessment of the driver awareness through the measurement of his/her input torque on the steering wheel, as well as the risk of lane departure computed by the position of the front wheels with respect to the lane.

The PWL state feedback *Controller-5* has not been implemented on the prototype vehicle CARLLA. It has been evaluated through simulations carried out with the PWA vehicle model (4.28). These results are presented in Section 7.5.1.

Both *Controller-6* and *Controller-7* have been implemented in CARLLA and throughout the practical experiments the driver was considered inattentive at different segments of the road and at different driving at longitudinal speeds. Forcing the instability of the vehicle to test the assistances may become very critical in terms of safety. For this reason, the prototype vehicle CARLLA has been equipped with composite rings (Skid-concept [Bou11]) that are mounted on the front tyres, in order to reproduce a degraded road adhesion condition. A picture of the ring mounted on the front wheel of CARLLA is shown in Fig. 7.3. The use of this rings ease the occurrence of instability which occur at relatively low speeds, due to the degraded road adhesion. Therefore they enable the evaluation of these assistances without jeopardising the safety of the vehicle and passengers.

Figure 7.3: Skidconcept ring mounted on front wheel.

The results presented for *Controller-6* and *Controller-7* correspond to a lane departure avoidance manoeuvre performed at approximately $v = 15$ $[m/s]$ on the S-curve located approximately at the coordinates $(X_{GPS} = 5.817,\ Y_{GPS} = 1.207)\times 10^5$ $[m]$ from Fig. 4.30. More details about the experiment scenarios and the results obtained for each assistance are presented in Sections 7.5.2 and 7.5.3 respectively.

Table 7.3 summarises the presentation of the results from simulations and practical experimentation carried out with each controller.

Results from *Controller-5* are discussed below.

7.5.1 Simulation results for *Controller-5*

Simulations on a PWA vehicle model (4.28) have been carried out with the Piecewise linear state feedback, *Controller-5*, as well as a linear state feedback designed for the linear region only, for comparison purposes.

Table 7.3: Summary of evaluation of the controller performance

Controller	Simulation	CARLLA	Purpose
Controller-5	Fig. 7.4 - Fig. 7.8		Lane departure avoidance
Controller-6		Fig. 7.9 - Fig. 7.15	Lane departure avoidance
Controller-7		Fig. 7.16 - Fig. 7.22	Lane departure avoidance

The controller tested corresponds to the results of Theorem 3.5.2 for the piecewise approximation of front tyre lateral forces shown in *Attempt* 52 of Table 7.1, since it is the partitioning closest to the saturation of the lateral tyre force among the feasible solutions.

$$\begin{aligned} K_1 = K_3 &= [-118.9353,\ -8.5598,\ -128.7984,\ -3.4168,\ 33.0271] \\ K_2 = K_{lin} &= [-586.6699,\ -40.5169,\ -571.4703,\ -15.1552,\ -28.4450] \end{aligned} \tag{7.24}$$

The activation strategy used in the simulation is described in Appendix B. The scenario consists of a vehicle moving straight at $v = 15\ [m/s]$ and exiting the lane with a relative yaw angle $\psi_L = 0.07\ [rad]$.

The results are depicted in Fig. 7.4 to Fig. 7.8. The vehicle sideslip angle and yaw rate, representing the vehicle dynamics, are shown in Fig. 7.4, while the vehicle positioning is shown in Fig. 7.5 by the relative yaw angle and lateral offset at look-ahead distance. Although the response of the vehicle controlled with *Controller-5*, denoted *PWL* in the figures, is very similar to the vehicle equipped with the controller for the linear region only (denoted *lin*), it can be noticed that the control input and, in consequence, the steering angle are significantly different, as shown in Fig. 7.6.

The front and rear sideslip angles corresponding to the lane departure avoidance manoeuvre are plotted in Fig. 7.7. It can be seen that for both vehicles the value of the front sideslip angle is larger than the threshold value established for the operating region corresponding to the linear behaviour of the front tyres lateral force (i.e. $|\alpha_f| > \bar{\alpha}_f$). Therefore the switching of PWL state feedback takes place for the vehicle equipped with *Controller-5*, which is able to reduce the front tyre sideslip angle.

The front and rear tyre lateral forces are depicted in Fig. 7.8. It can be noticed that despite the control action for both vehicles, the front tyre forces are saturated.

The results imply that the use of a single quadratic Lyapunov function is not adequate for the synthesis of PWL controllers for lane departure avoidance systems. The use of the piecewise affine approximation that better takes into account the nonlinear behaviour of the tyre forces, results in a controller that is very reactive, as it can be seen in Fig. 7.4 to Fig. 7.8. The positioning of the vehicle with respect to the lane is quickly restored, as the assistance is activated, and excursion of the lane is avoided as presented in Fig. 7.5. On the other hand, the vehicle dynamics are too excited reaching relatively high values of sideslip angle ($\beta = \pm 0.02\ [rad]$) and yaw rate ($r = -0.4\ [rad/s]$) for a manoeuvre on a straight line. Consequently the lateral tyre forces saturate for both vehicles *lin* and *PWL*.

The vehicle dynamics response under the action of the controller could be enhanced by including constraints for pole clustering or to bound the control input, for instance. However, the conservativeness of the control synthesis based on a single quadratic Lyapunov function

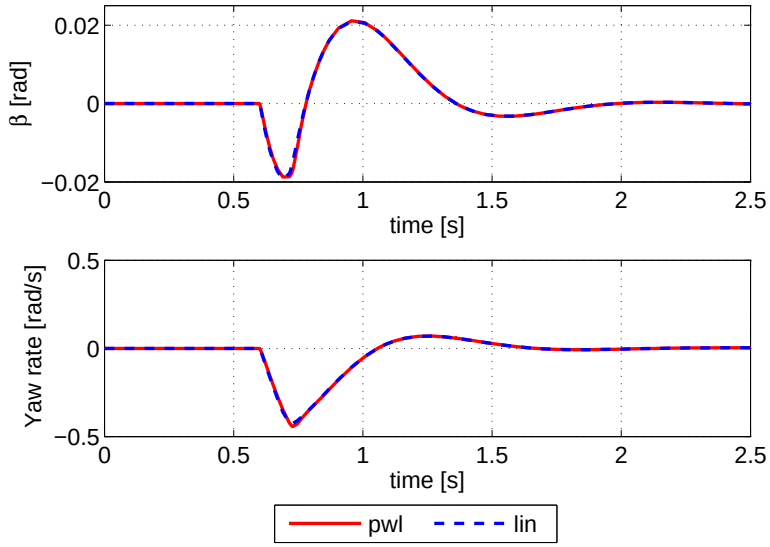

Figure 7.4: Dynamics of vehicles *lin* (dashed line) and *PWL* (continuous line) with *Controller-5* at $v = 15\ [m/s]$.

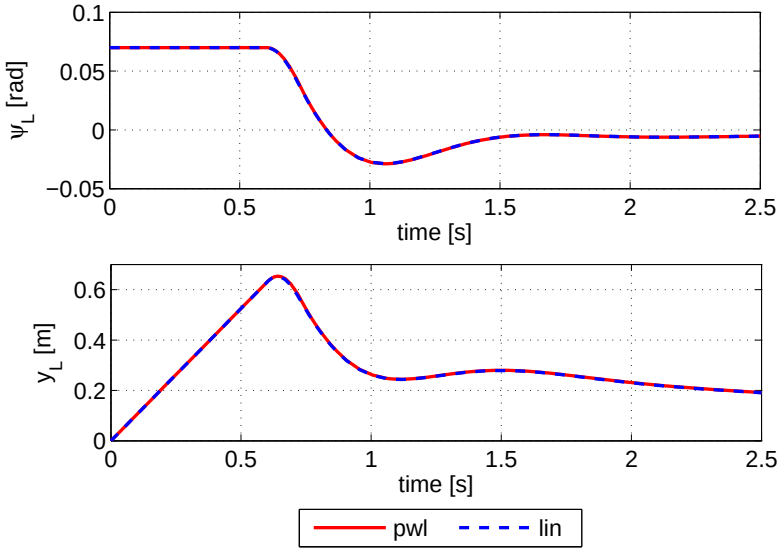

Figure 7.5: Positioning of vehicles *lin* (dashed line) and *PWL* (continuous line) with *Controller-5* at $v = 15\ [m/s]$.

results in very restrained feasible sets, so that there is not much room for additional constraints while keeping the LMIs feasible.

Controller-6, based on piecewise quadratic Lyapunov function provides an adequate possibility to overcome this shortcoming, as shown from the results discussed below.

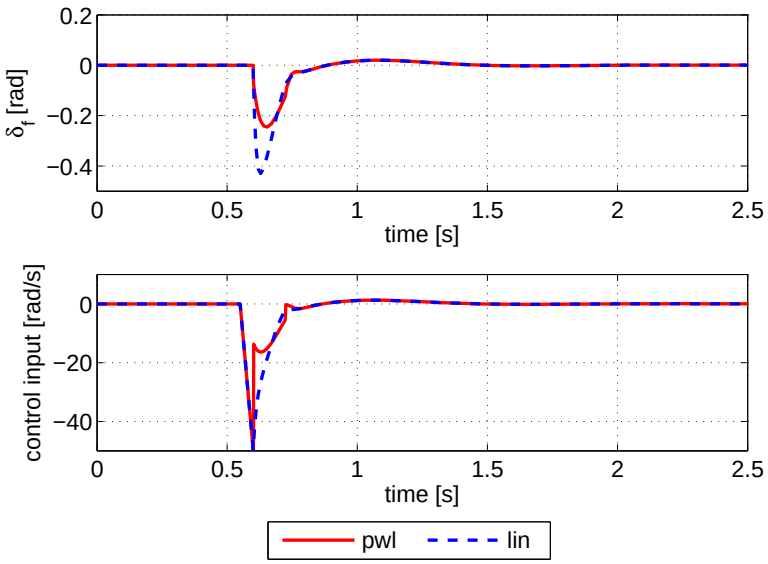

Figure 7.6: Steering angle and control input of vehicles *lin* (dashed line) and *PWL* (continuous line) with *Controller-5* at $v = 15$ $[m/s]$.

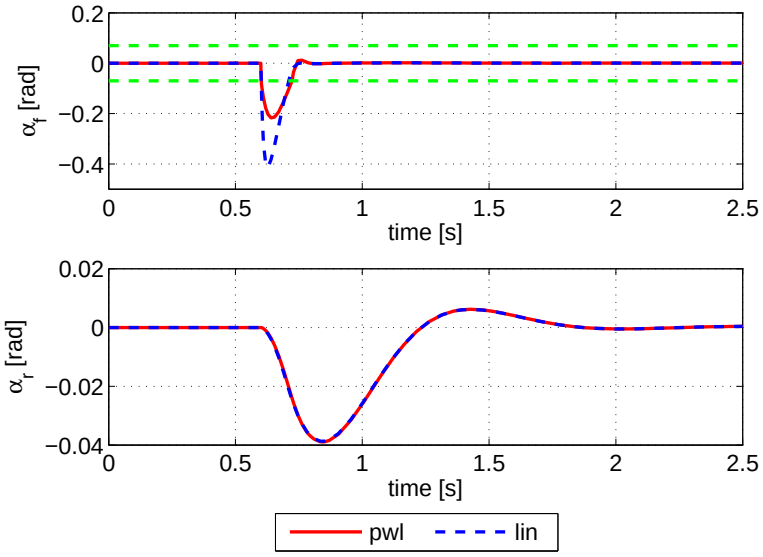

Figure 7.7: Front and rear tyre sideslip angle of vehicles *lin* (dashed line) and *PWL* (continuous line) with *Controller-5* at $v = 15$ $[m/s]$.

7.5.2 Results from practical implementation of *Controller-6*

The controller synthesised in Section 7.2.2 for the lane keeping assistance system *Controller-6* has been implemented in the prototype vehicle CARLLA, which has been equipped with the composite rings (Skid-concept [Bou11]) around the front tyres to reproduce degraded road conditions.

The results from the lane departure avoidance manoeuvre are illustrated in Fig. 7.9 to Fig. 7.15.

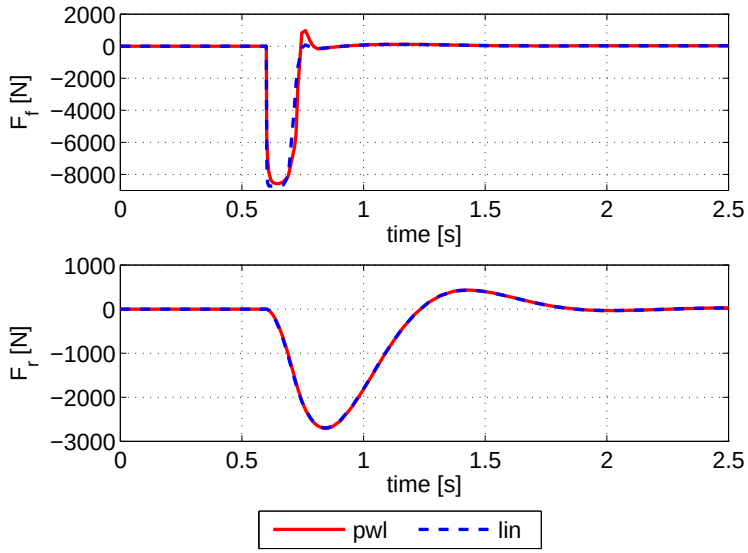

Figure 7.8: Front and rear lateral tyre forces of vehicles *lin* (dashed line) and *PWL* (continuous line) with *Controller-5* at $v = 15\ [m/s]$.

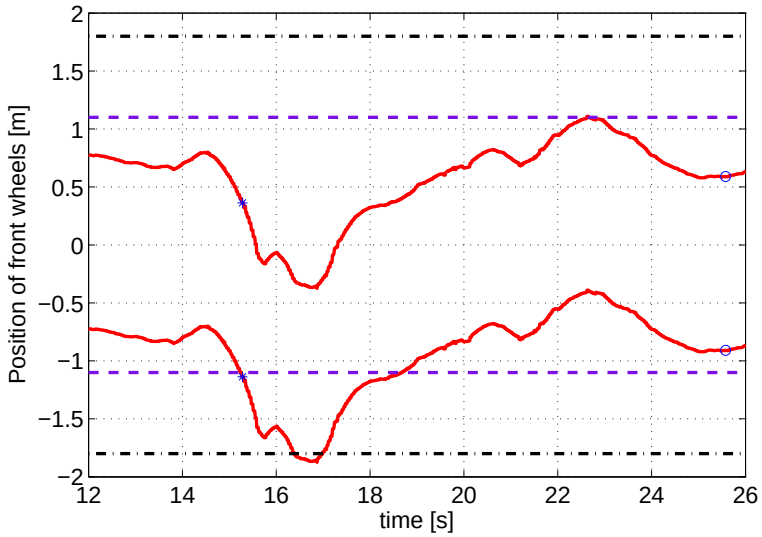

Figure 7.9: Position of front wheels with respect to lane markings for *Controller-6* with skip-concept rings.

The road profile can be seen in the bottom subplot of Fig. 7.15 which depicts the road curvature estimated by the lane detection algorithm. It consists of an S-turn with the first curve to the left hand side.

The vehicle is located at the centre of the lane as it approaches the curve, and tends to continue forward, since there is no action of the driver on the steering wheel, as depicted in Fig. 7.14. The activation takes place as the front right wheel crosses the centre strip with width $2d = 2.2\ [m]$ (see activation strategy in Appendix B), shortly after $t = 15\ [s]$ and it is indicated by the red symbol "$*$" on the figures.

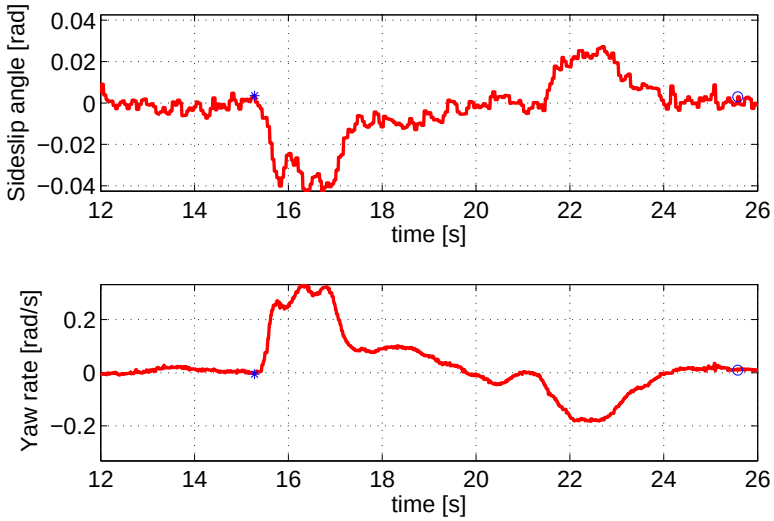

Figure 7.10: Vehicle Sideslip Angle and yaw rate for *Controller-6* with skip-concept rings.

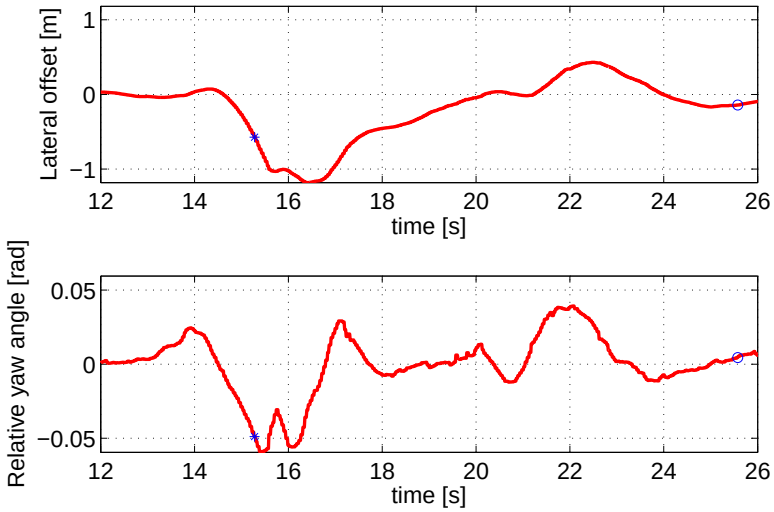

Figure 7.11: Vehicle positining from video sensor: Lateral offset and relative yaw angle for *Controller-6* with skip-concept rings.

The position of the front wheels with respect to the lane is reconstructed from the exteroceptive signals representing the positioning of the vehicle and illustrated in Fig. 7.11, with the lateral offset at look ahead distance and the relative yaw angle on the top and bottom subplots respectively (see Appendix B for details).

The control input, corresponding to the activation of the assistance is shown in Fig. 7.14. The state variables representing the dynamics of the car are shown in Fig. 7.10 describing the measurements of sideslip angle and yaw rate.

These two variables, the front wheel steering angle, shown in Fig. 7.12 and the vehicle longitudinal speed shown in Fig. 7.13, are used to compute an estimate of the wheel sideslip

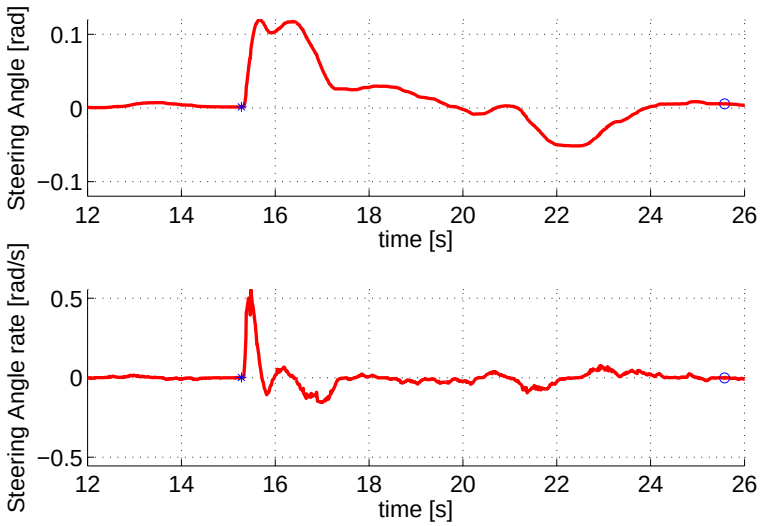

Figure 7.12: Steering angle and steering angle derivative for *Controller-6* with skip-concept rings.

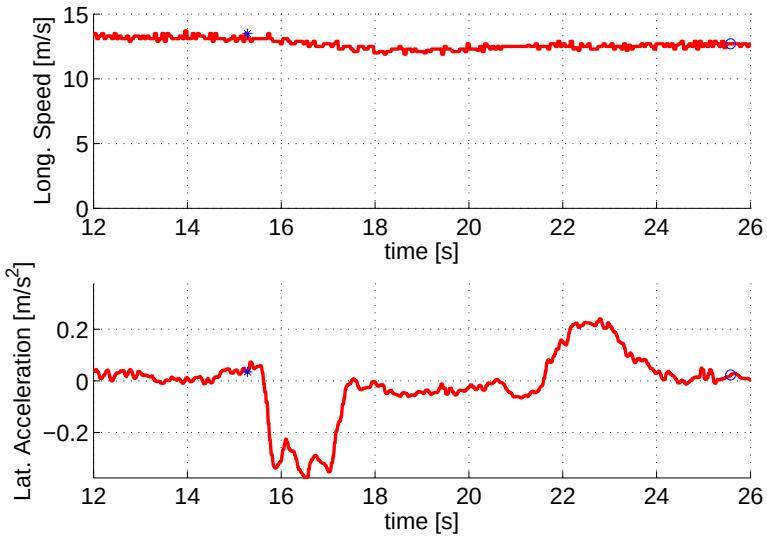

Figure 7.13: Vehicle longitudinal speed and lateral acceleration for *Controller-6* with skip-concept rings.

angle, according to (4.5). The resulting front wheel sideslip angle is illustrated in Fig. 7.15. The switching between the PWA state feedback controllers is driven by this variable. The thresholds limiting the linear region of operation are depicted by the green dash-dot line. The switching takes place, as shown in the bottom plot of Fig. 7.14 from R_2 to R_3 shortly after the assistance is activated.

It can be noticed that the control input (top plot of Fig. 7.14) is reduced when the switching takes place, as an attempt to drive the state variables to the linear operating region of the tyre lateral force, under the action of K_3 and m_3. Consequently the reduction on the steering action,

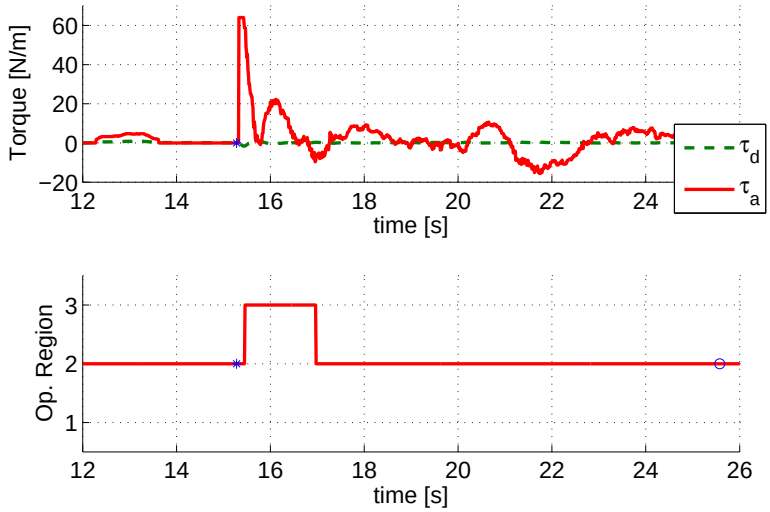

Figure 7.14: Control Input and corresponding operation regions for *Controller-6* with skip-concept rings.

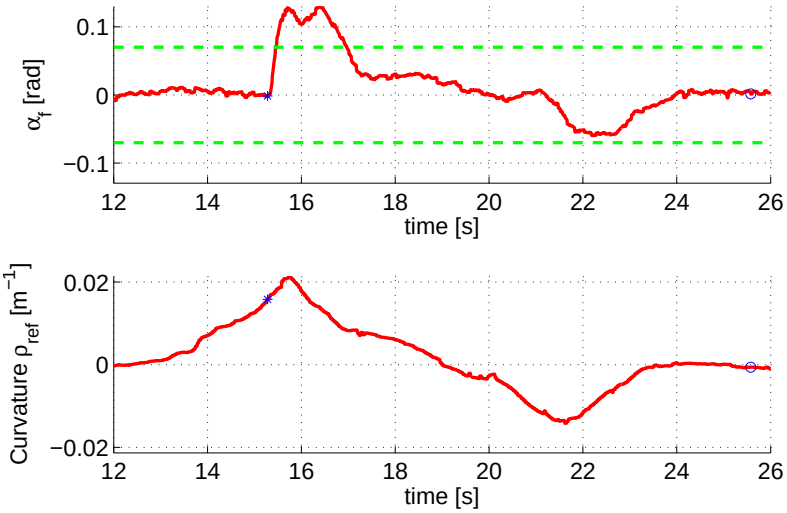

Figure 7.15: Estimated front wheel sideslip angle and measured road curvature for *Controller-6* with skip-concept rings.

shown in Fig. 7.12, shortly before $t = 16$ $[s]$ induces a reduction of the front wheel sideslip angle.

Since the vehicle is still negotiating the left-hand side curve, the control input is forced to increase again to keep the vehicle in the lane in spite of the brief excursion from the lane exhibited in Fig. 7.9 around $t = 17$ $[s]$.

The manoeuvre is successfully performed and the vehicle is repositioned at the centre of the lane while it negotiates the right hand side turn until the driver retakes the control, as indicated by the red symbol "o" in the presented plots.

Having presented the results from practical implementation of the PWA feedback controller,

the results of the PWA output feedback synthesised for *Controller-7* are discussed in the sequel.

7.5.3 Results from practical implementation of *Controller-7*

The PWA ouuput feedback controller obtained in Section 7.4.1 for the *Perceptive-ESC* (*Controller-7*) has been implemented on the prototype vehicle CARLLA with the composite rings (skid-concept) mounted on the front wheel tyres. It has been evaluated as a lane departure assistance system, with activation described in Appendix B.

The results shown in Fig. 7.16 to Fig. 7.22 correspond to the lane departure avoidance manoeuvre on the same S-curve as the previous presented results

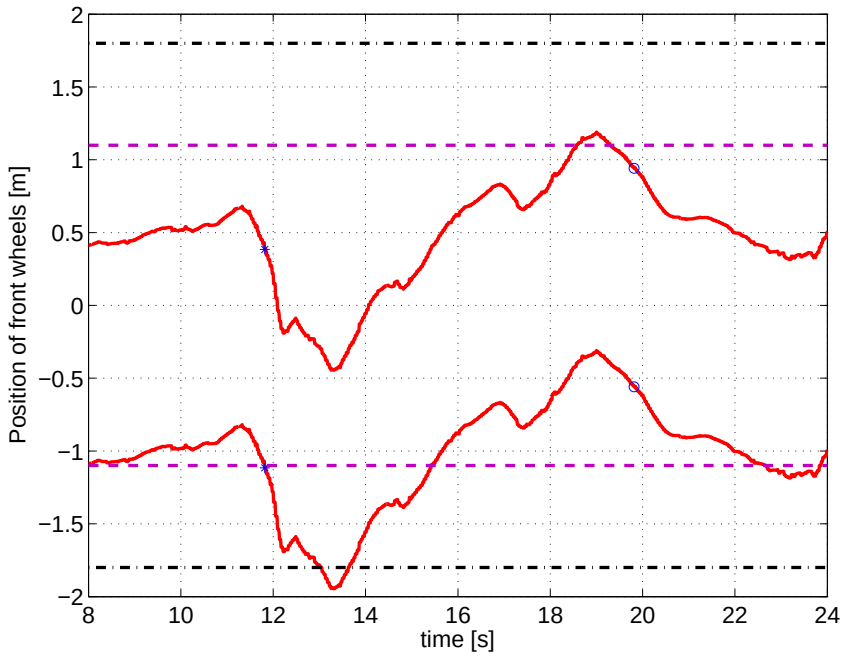

Figure 7.16: Position of front wheels with respect to lane markings for *Controller-7* with skid-concept rings.

The activation takes place at about $t = 12$ $[s]$ as the vehicle tends to drift out of the right lane without action of the driver ($|\tau_d| < \tau_{on}$ in Fig. 7.21). Fig. 7.16 shows the activation as the front right wheel crosses the centred strip on the lane of width $2d = 2.2$ $[m]$, depicted by the blue dotted lines.

The switching of the PWA output control structure of *Controller-7* is based on the estimate of the front wheel sideslip angle. As the vehicle sideslip angle is assumed to be unavailable for measurement, its estimate is used in the computation of the front wheel sideslip angle, using also the measurements of yaw are, steering angle and longitudinal velocity, as follows:

$$\alpha_{f(est)} = \delta_f - \beta_{(est)} - \frac{l_f r}{v} \tag{7.25}$$

The estimated vehicle sideslip angle ($\beta_{(est)}$) is plotted in the top of Fig. 7.17. Its measurement, provided by the CORREVIT optical sensor (β_{meas}), is also depicted only to enable a comparison and evaluation of the synthesised observer. The vehicle yaw rate (r) is shown in the same figure, while the steering angle (δ_f) is provided in the top plot of Fig. 7.19 and longitudinal velocity v is shown in Fig. 7.20.

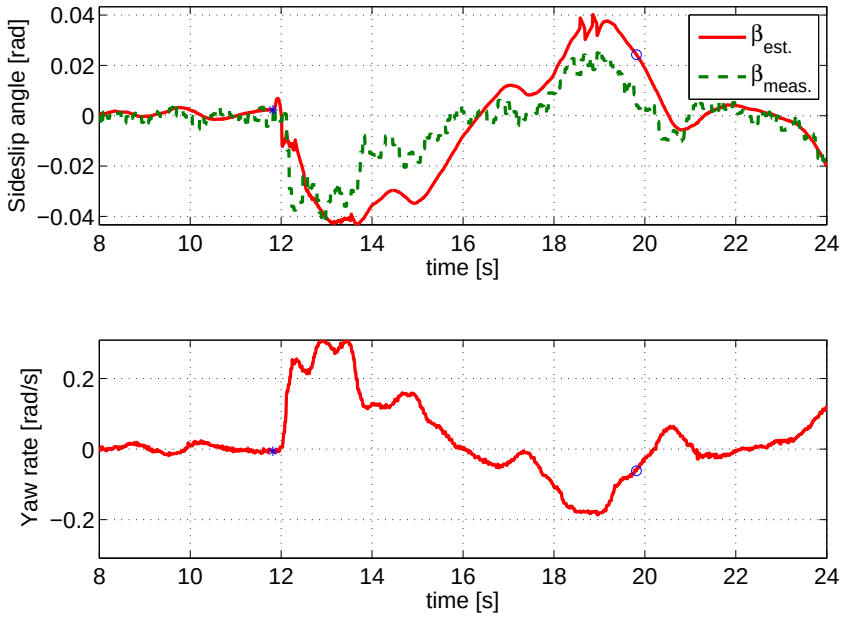

Figure 7.17: Vehicle Sideslip Angle and yaw rate for *Controller-7* with skid-concept rings.

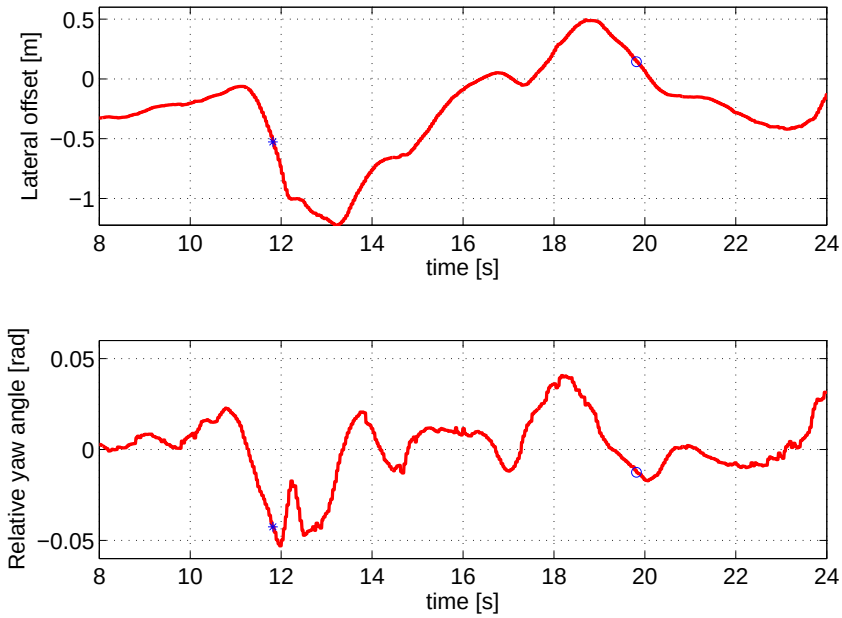

Figure 7.18: Vehicle positining from video sensor: Lateral offset and relative yaw angle for *Controller-7* with skid-concept rings.

The computed wheel sideslip angle ($\alpha_{f(est)}$) based on the estimation of the vehicle sideslip angle is shown by the blue solid line in Fig. 7.22. For comparison purposes, the computed front wheel sideslip angle computed using the measurement of the vehicle sideslip angle is also shown in the same figure, represented by the dashed line.

It can be seen that the observer obtained from the control synthesis tends to overestimate the vehicle sideslip angle, which induces also an overestimation effect on the computed front wheel

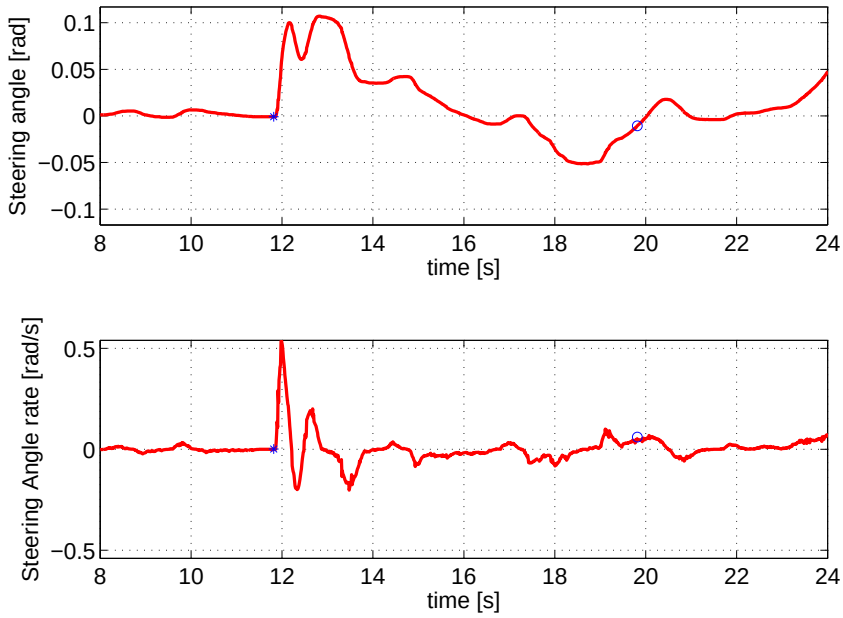

Figure 7.19: Steering angle and steering angle derivative for *Controller-7* with skid-concept rings.

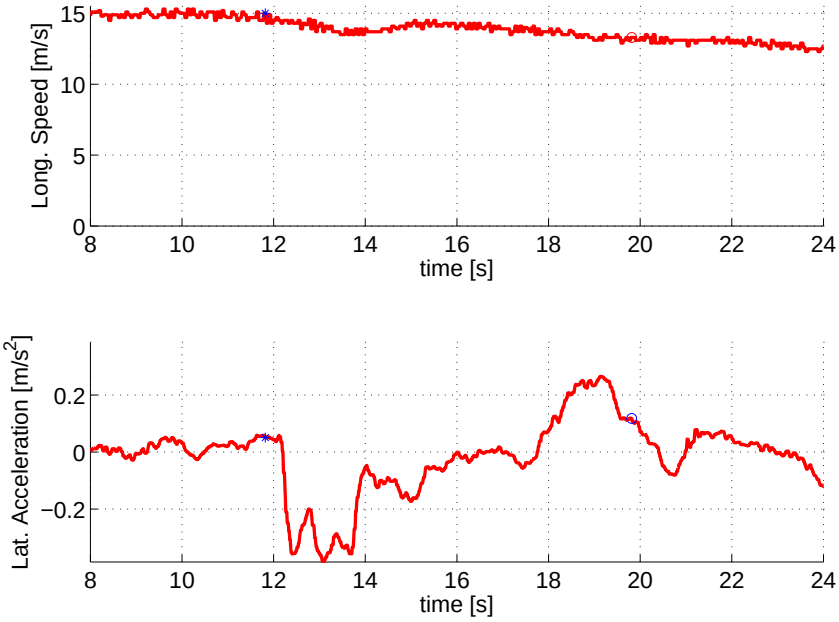

Figure 7.20: Vehicle longitudinal speed and lateral acceleration for *Controller-7* with skid-concept rings.

sideslip angle. Designing a better observer for the state vector turned out to be challenging, considering the proposed method. Since there are no constraints on the observer, the poles of its dynamics tend to become faster at each iteration of the K-Step, as an attempt to maximise the decay rate of the piecewise quadratic Lyapunov function. Thus it potentiates the errors between the vehicle and its model. Fixing the gains for the observer at the K-Step does not seem to

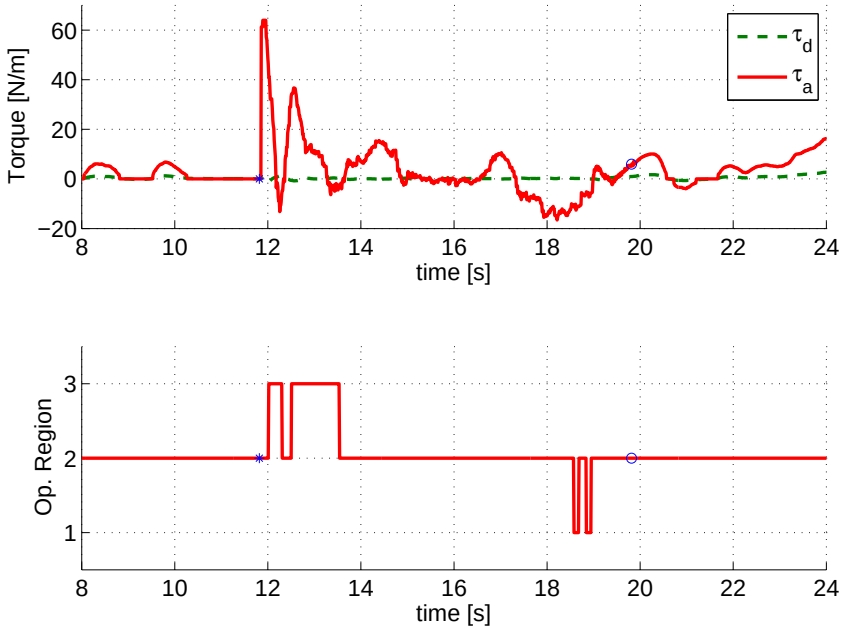

Figure 7.21: Control Input and corresponding operation regions for *Controller-7* with skid-concept rings.

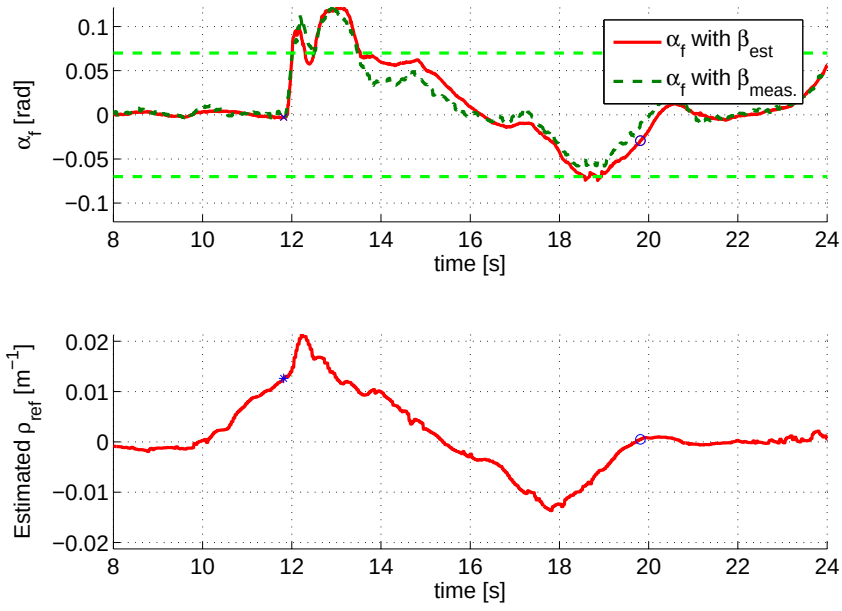

Figure 7.22: Estimated front wheel sideslip angle and measured road curvature for *Controller-7* with skid-concept rings.

overcome the problem as the LMIs become infeasible, probably due to the lack of flexibility for the decision variables.

Despite the errors on the estimated variables, no significant changes in the performance of the PWA output feedback controller with respect to *Controller-6* can be noticed.

It is interesting to note the reduction on the steering action after the first switch from R_2 to R_3 at approximately $t = 12$ $[s]$ as shown in the bottom plot of Fig. 7.21. On the top plot of the same figure, it can be seen that the reduction of the control input τ_a due to the action of K_3 and m_3, is able to reduce the vehicle sideslip angle, as an attempt to avoid the saturation of the lateral tyre force that can be seen in Fig. 7.22. The controller even switches back to R_2, but since it is still negotiating the curve, a more pronounced input torque is required to avoid the lane departure.

Similarly to the results presented for *Controller-6*, an excursion of the lane occurs briefly in the time interval $13 < t < 14$ $[s]$.

While negotiating the following curve to the right hand side (for $t > 17$ $[s]$), some switches can also be noticed. In this case, it is mainly due to the overestimation of the front wheel sideslip angle as can be seen in Fig. 7.22. Nevertheless, the action of the overall controller is able to negotiate the S-turn and steer the vehicle back to the centre of the lane, when the driver retakes control of the vehicle, deactivating the assistance.

7.6 Conclusion

In this chapter, control techniques for the design of a lane keeping assistance systems have been developed. The analysis and synthesis are based on quadratic and piecewise quadratic Lyapunov functions.

An approach based on a single quadratic Lyapunov function has been employed for the design of *Controller-5*. Despite the advantage of the PWL state feedback compared to the linear state feedback, as shown in the simulation results, the design procedure of *Controller-5* could be further improved by the inclusion of an objective function instead of solving an LMI feasibility problem. Moreover, other constraints could be added to the LMIs, in order to obtain a controller that better fits the design requirements, and avoid the high gains which render the system too reactive. Nevertheless, the limitations regarding the PWA approximation of the nonlinear model for lateral tyre force could not be circumvented, since the synthesis based on a single quadratic Lyapunov function that must be valid for all subsystems is very conservative. Techniques based on piecewise quadratic Lyapunov function have therefore been sought.

It has been demonstrated that the use of a PWA controller provides more flexibility to obtain a piecewise quadratic Lyapunov function for the closed loop system. The use of the V-K method to obtain a suboptimal solution for the BMI has been particularly advantageous due to the availability of a state feedback controller for linear model. Consequently, the main challenges have become the adequate modelling and the optimisation of the controllers for the affine operating regions. The PWA state feedback controller designed for *Controller-6* has been deployed as lane departure assistance system and evaluated in practical implementation. The results have shown satisfactory performance and adequate action to avoid the tyre forces saturation on degraded road adhesion.

Nevertheless, the reduction on the steering action may deteriorate the vehicle trajectory and, depending on the road profile, this control action may not be sufficient to keep the vehicle in the lane which implies that a combined control action may required to generate the adequate yaw moment.

The vision algorithm has shown some limitations that prohibited the evaluation of the controller for more demanding manoeuvres. Being designed for the detection of a single lane, it was not able to restore and treat the images adequately when sudden direction changes or lane excursions took place.

As currently commercialised vehicles are not equipped with sideslip angle sensors (CORRE-VIT), and their costs render it impracticable to be introduced in production, a solution avoiding the used of such sensors has been implemented. *Controller-7* uses an estimator-regulator structure to estimate the vehicle sideslip angle, and the PWA output feedback controller can be designed, based on a piecewise quadratic Lyapunov function.

The lack of bounds for the observer gains combined with the objective function of maximising the Lyapunov decay rate has caused the poles of the observer dynamics to become very fast, which is not desirable when discretisation is needed for practical implementation.

The results from the practical implementation are equivalent to those of *Controller-6*, from which it can be concluded that the observer-based control synthesis is adequate for the design of a driving assistance system that takes into account the nonlinear tyre forces and is based only on sensors currently in use.

Part IV

Conclusions and Perspectives

Chapter 8

Conclusions and perspectives

8.1 Conclusions

In this thesis, the development and practical validation of a *Perceptive-ESC* is presented. It is a driver assistance system to avoid unintended lane departure even in situations of strong lateral solicitation. Besides, the proposed assistance is based on measurements provided only by sensors that are available in currently commercialised vehicles.

During the preceding three parts of this thesis, the motivation, mathematical tools and preliminary systems have been thoroughly described in order to achieve the *Perceptive-ESC* .

In the first part, the motivations have been described and the thesis objectives have been set. A methodology has also been described, consisting of several stages in which the complexity of the proposed assistances has been progressively augmented and for which the benefits could be evaluated at each step.

By analysing the trends of road ITS projects, it has been shown that efforts have been concentrated to provide solutions that require relatively low investment and that can be implemented in a short time. Moreover, recent projects tend to focus on highly automated systems that do not replace the driver completely, but share the driving task, helping the driver in critical and tedious situations. These two tendencies have propelled the research towards a solution based only on sensors currently in use and on a strategy to share the control with the driver.

During the bibliographic study, attention has also been given to the already existing ADAS for vehicle lateral control and the research activities on this topic. It has been noticed that the most efficient systems to handle vehicle instability are based on proprioceptive signals, such as ESC. On the other hand, systems based on exteroceptive signals, such as LDWS and LKAS, are generally designed to operate in relatively low lateral acceleration, and are not adequate when demanding manoeuvres are required. A lack of assistance systems that are able to perceive the environment and simultaneously handle vehicle instability has been identified as an open field of research, which confirms the novelty of this application and theoretical approach adopted in this work.

The mathematical tools and description of the vehicle model used in the design of the lateral control assistances have been presented in the second part. The careful study of PWA systems has enabled the comprehension not only of their behaviour but also their limitations. The analysis and control synthesis are based on Lyapunov quadratic stability, for which LMI and BMI are essential tools.

The first part of the thesis has also covered the analysis of the vehicle lateral dynamics and its modelling through PWA systems. It has been shown that PWA systems can adequately

reproduce the vehicle nonlinear dynamics, but in order to use the Lyapunov based control synthesis, two assumptions have been made. Firstly, only the tyre force saturation of the front wheels are taken into account in the PWA model, and secondly only PWA functions with positive slopes are considered to approximate the tyres lateral force. It has been shown that these simplifications render PWA vehicle models less accurate in reproducing the instabilities of the vehicle nonlinear lateral dynamics. On the other hand, they allow the risk of instability to be detected and enable the controller to act in advance in order to avoid the tyre force saturation, being thus satisfactorily for the design of driving assistance systems.

The third part presents the evolution of the controllers designed for the driver assistance systems. The simplest control structures have been privileged in the early stages of the development and complexity has been gradually increased. Such design methodology has proved adequate for the achievement of the *Perceptive-ESC* , as it enabled, at each stage, the evaluation and thorough comprehension of the advantages of the PWA controllers.

For the first two driving assistance systems only the vehicle dynamics have been considered. The proposed active steering systems consist of PWL Proportional-Integral controllers on the basis of the yaw rate error. For the first, the switching of the PWL controllers is driven by the yaw rate, and the boundaries have been obtained from a parametrisation of the vehicle dynamics in terms of the same variable. The second active steering system is extended with a PWL state feedback loop in order to enhance the vehicle dynamics with the switching based on an estimation of the vehicle sideslip angle. The stability of both systems has been proved by piecewise quadratic Lyapunov functions. Simulations have proved that the PWL controller is advantageous in demanding manoeuvres when compared to the same corresponding linear controller. Moreover, it has been noticed that the vehicle sideslip dynamics should not be neglected in the design of the controller and definition of the switching conditions in order to obtain satisfactory responses from the controlled system.

The exteroceptive signals have been taken into account in two stages. The first technique explored is based on the inclusion of internal models to reject the disturbances such as the road curvatures. An extension of a driver assistance system developed at LIVIC has been proposed and the advantages of considering the internal model in the design of the controller has been confirmed in the practical experiments and even as an obstacle avoidance system through the ISO-3888-1 (double lane change manouevre) in simulations in CarSim environment.

In order to take into account the nonlinear behaviour of the lateral tyre forces, a PWL controller has been designed for lane keeping purposes. It incorporates the internal model in a PIID structure on the basis of lateral offset. Similarly to the active steering systems, the stability has been proved by a piecewise quadratic Lyapunov. The purpose of analysing the advantages of the PWL controller for lane keeping has been achieved with this simple control strategy, confirming the feasibility of lane departure avoidance systems for emergency situations based on this class of hybrid system.

At a second stage in the development of lane departure avoidance systems, the efforts have been focused on the Lyapunov based control syntheses that provide the gains and ensure stability simultaneously.

The conservativeness of using a single quadratic Lyapunov function has become evident in the development of the PWL state feedback controller for lane departure avoidance. On the other hand, it has been shown that this drawback can be circumvented by the use of piecewise quadratic Lyapunov function for the syntheses of PWA state and output feedback controllers. For the output feedback structure, only the sensors currently in use have been considered, which avoids the measurement of sideslip angle. The results obtained from the practical implementation of the PWA state feedback have demonstrated its potential to handle the vehicle instabilities

and its satisfactorily performance in lane departure avoidance manoeuvres, even in degraded road adhesion. It can also be noticed that the trajectory of the vehicle may deteriorate due to the reduction of the steering action to recover vehicle stability, which implies that the single control action on the steering wheel may not be sufficient to keep the vehicle on track. A positive aspect of this limitation lies in the fact that the reduction of the tyre lateral force may enable the longitudinal component to increase and generate the adequate yaw moment, either by independent wheel braking or differential torque, if a combined control action is implemented.

The practical experiments of the PWA output feedback have shown that it avoids the lane departure satisfactorily, but the trade-off between the quality of the trajectory and keeping the wheel sideslip low is equally present. Such results confirm that the observer-based control structure which is able to estimate the vehicle sideslip angle, can be implemented without additional costs, since it is based on sensors already available in currently commercialised passenger cars. Table 8.1 summarises the assistances proposed.

Table 8.1: Summary of proposed assistances

	Assistance	Control Strategy	Validation
Controller-1	Yaw control	PWL PI	CarSim
Controller-2	Yaw control	PWL PI and state feedback	CarSim
Controller-3	LKAS / LCA	Linear state feedback	CARLLA/CarSim
Controller-4	LKAS	PWL PIID	CarSim
Controller-5	LKAS	PWL state feedback	Nonlinear Model (4.28)
Controller-6	LKAS	PWA state feedback	CARLLA
Controller-7	LKAS	PWA output feedback	CARLLA

The main contributions of this thesis can be thus summarised as:

- Proposition and analysis of a PWA vehicle model for lateral dynamics
- Proposition of active steering systems that take into account the nonlinear behaviour of the tyre forces.
- Proposition of a lane departure avoidance systems that take into account the nonlinear behaviour of the tyre forces in order to be able to handle vehicle instability in emergency situations.
- Development of a lane departure avoidance system, based only on sensors currently in use, which is able to deal with strong lateral solicitations.

8.2 Perspectives

During the development of the thesis some hints about the future research on this field have been given. Among them, attention could be focused on the following topics:

- Use of loop shaping techniques to optimise and ensure the robustness of the active steering PI controllers.
- The inclusion of bounds for the observer in the PWA output feedback control synthesis and use of more sophisticated observers for wheel sideslip angle to drive the switching of the PWA controllers.
- Combined control action of steering angle with either differential braking or torque distribution.
- Strategies of activation and share of the driving tasks.

Despite the contributions of this thesis, the research in this field can still be further explored, and some important aspects should be investigated in more depth, such as ways to render the assistance more intuitive for drivers, as well as its acceptance.

The development of vision algorithms adapted for harsh direction changes, as in critical situations, may also be an interesting aspect to render these assistances feasible and commercially practicable. Moreover, the current development of electric vehicles with 4-wheel drive also presents an interesting opportunity to combine the actions on steering angle distributed wheel torque.

Appendix A

Polytopic cells and equilibrium points

A.1 Quadratic form for polytopic cell description

Considering a matrix $\Lambda_i \in \mathbb{R}^{p_i \times p_i}$, defined as:

$$\Lambda_i \stackrel{\Delta}{=} \begin{bmatrix} \lambda_{00} & \cdots & \lambda_{0p_i} \\ \vdots & \ddots & \vdots \\ \lambda_{p_i 0} & \cdots & \lambda_{p_i p_i} \end{bmatrix} > 0 \tag{A.1}$$

Since the elements of Λ_i are all non-negative, it can be affirmed, using the polytopic cell description (3.30), that the state belongs to a given operating region, *i.e.* $x \in R_i$, only if:

$$-\lambda^i_{0j}\left(h^t_{ij}x - gij\right) > 0, \quad \lambda^i_{0j} > 0, \quad j = 1, ..., p_i \tag{A.2}$$

and therefore only if

$$-\lambda^i_{jk}\left(h^t_{ij}x - gij\right)\left(h^t_{ik}x - gik\right) > 0, \quad \lambda^i_{jk} > 0, \quad \forall j = 1, ..., p_i \; and \; k = 1, ..., p_i \tag{A.3}$$

Consequently, $x \in R_i$ if

$$\begin{bmatrix} x \\ 1 \end{bmatrix}^T \begin{bmatrix} \bar{H}_i^T \Lambda_i \bar{H}_i & -\bar{H}_i^T \Lambda_i \bar{g}_i \\ -(\bar{H}_i^T \Lambda_i \bar{g}_i)^T & \bar{g}_i^T \Lambda_i \bar{g}_i \end{bmatrix} \begin{bmatrix} x \\ 1 \end{bmatrix} > 0, \tag{A.4}$$

where $\bar{H}_i = [0 \; h_{i1} \; h_{i1} \; ... \; h_{ip_i}]^T$ and $\bar{g}_i = [1 \; g_{i1} \; g_{i1} \; ... \; g_{ip_i}]^T$. Inequality (A.4) corresponds to a quadratic form so that the S-procedure can be applied.

A.2 Piecewise affine approximations and equilibrium points

The equilibrium point of the closed-loop system (4.28) under the PWA state feedback $u_c = K_i x + m_i$ and $\rho_{ref} = 0$ is given by:

$$x_{eq}^i = \begin{bmatrix} \frac{e_{ri}}{d_{ri}} \\ 0 \\ -\frac{e_{ri}}{d_{ri}} \\ -\frac{d_{fi}k_5e_{ri} - d_{fi}k_3e_{ri} + k_1d_{fi}e_{ri} - d_{ri}k_5e_{fi} + m_id_{fi}d_{ri} - d_{fi}e_{ri} + d_{ri}e_{fi}}{d_{ri}d_{fi}k_4} \\ \frac{d_{fi}e_{ri} - d_{ri}e_{fi}}{d_{ri}d_{fi}} \end{bmatrix} \tag{A.5}$$

Considering that the sideslip angles are given as in (4.5), then the sideslip angle for a given region in steady state is:

$$\alpha_{eq\,f}^i = -\frac{e_{fi}}{d_{fi}} \tag{A.6}$$

For the tyre forces approximation applied for this problem, as shown in (7.5), the affine terms e_{fi} can be written with respect to the partitioning as:

$$e_{f1} + d_{f1}(-\bar{\alpha}_f) = c_f(-\bar{\alpha}_f) \rightarrow e_{f1} = -\bar{\alpha}_f(c_f - d_{f1}) \tag{A.7}$$

$$e_{f3} + d_{f3}(\bar{\alpha}_f) = c_f(\bar{\alpha}_f) \rightarrow e_{f3} = \bar{\alpha}_f(c_f - d_{f3}) \tag{A.8}$$

Therefore (A.6) can be rewritten as:

$$\begin{aligned} \alpha_{eq\,f}^1 &= -\frac{-\bar{\alpha}_f(c_f - d_{f1})}{d_{f1}} \\ \alpha_{eq\,f}^3 &= -\frac{\bar{\alpha}_f(c_f - d_{f3})}{d_{f3}} \end{aligned} \tag{A.9}$$

The equilibrium point of the whole system is located at the origin, $x_{eq} \in R_2$. In order to ensure global asymptotic stability, it is required that $x_{eq}^1 \notin R_1$ and $x_{eq}^3 \notin R_3$, equivalently $\alpha_{eq}^1 > -\bar{\alpha}_f$ and $\alpha_{eq}^3 < \bar{\alpha}_f$.

Replacing the results of (A.9), the requirements become:

$$-\frac{-\bar{\alpha}_f(c_f - d_{f1})}{d_{f1}} > -\bar{\alpha}_f, \quad -\frac{\bar{\alpha}_f(c_f - d_{f3})}{d_{f3}} < \bar{\alpha}_f \tag{A.10}$$

Dividing them by $-\bar{\alpha}_f$ and $\bar{\alpha}_f$ respectively,

$$\frac{(-c_f + d_{f1})}{d_{f1}} < 1, \quad \frac{-c_f + d_{f3}}{d_{f3}} < 1 \tag{A.11}$$

Since $c_f > 0$, it can be seem that these requirements are not satisfied if $d_{f1,3} < 0$, therefore the tyre force approximation by the piecewise affine functions must have positive slopes.

Appendix B

Steering assistance activation law

Human interactions play an important role in the driving assistance systems, therefore an adequate activation strategy is required. In order to avoid an intrusive assistance that may not be well accepted by drivers, it is important to consider the driver awareness, as well as the risk of lane departure or collision accidents.

In the framework of advanced driving assistance systems (ADAS), many possibilities are shown in the literature concerning the activation strategies of lane keeping systems. The system proposed by [EPG05] perceives the intention of the driver based on the vehicle dynamics and tracks the environment (road geometry, obstacles/vehicles on current and adjacent lanes) to compute the risk of the manoeuvre using the time to lane crossing (TLC) to predict a lane departure. In order to reduce the conflicts between the driver and the system assistance a time-varying parameter is defined by [FA03] so that the control action increases when the driver steering wheel torque decreases; [LSMN02] make use of a weight (between zero and one) which multiplies the proposed LQ steering control in order to reduce the interference with the driver. In the ADAS proposed by [CMR09] and [RG06] an automatic lane keeping is combined with the driver's steering with no need of switching strategies between the driver and the lane keeping control; [RG06] uses the potential field control structure for a vehicle with steer-by-wire. A feedforward and a feedback controller are designed by [IG04] to support the driver in order to reduce his/her workload without reducing the situation awareness and motivation of the driver. The lane keeping system proposed by[MENML09] uses a switching strategy during diminished driving capability or driver inattentiveness to help the controller to fully replace the driver until he/she recovers the attention.

Such activation strategy seems to be the most adequate as according to ergonomic and psychology studies [HYB09] the driver usually does not have time to think and plan in emergency situations. There is only time to react in order to re-establish a safe state, therefore sharing the control with the driver is not really an advantage and in these cases it is better that the controller takes completely the responsibility during the control duration. Therefore the next sections address the activation strategies based on the attentiveness of the driver and the risk of either lane departure during lane keeping or collision avoidance manoeuvres.

B.1 Driver awareness assessment

Assessments of driver's awareness can be found for instance in the works of [TT10] and [TC07]. Other sophisticated strategies could be used to monitor the driver awareness in the design of the driver assistance systems. However, they are beyond the scope of this work, since it focuses

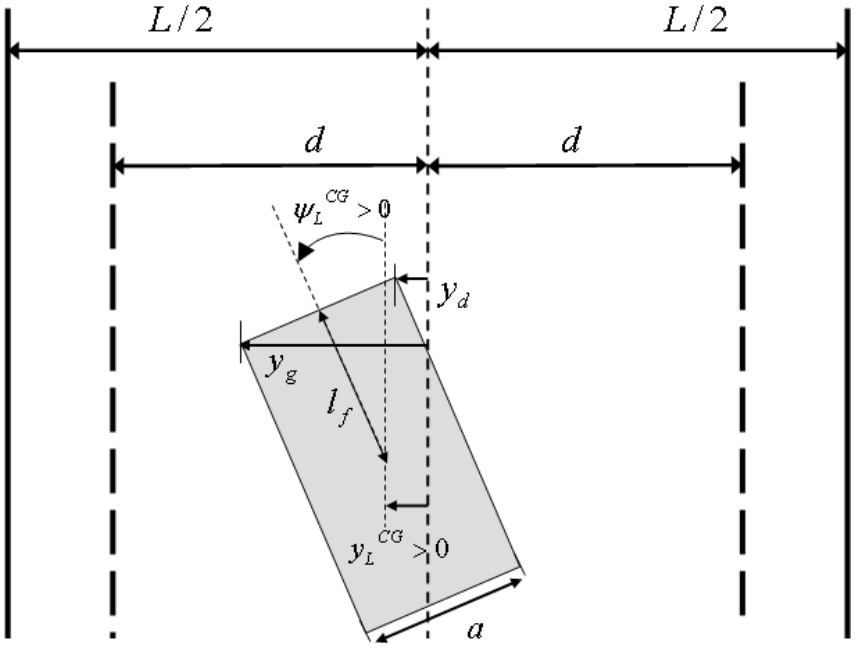

Figure B.1: Relative yaw angle, ψ_L and position of the front wheels with respect to lane.

mainly the control synthesis and its performance.

For this reason, it was chosen to use an already existing strategy at LIVIC to assess the driver's awareness. It is simply based on the driver's input torque on the steering wheel, which is denominated τ_d. If $|\tau_d| < \tau_{on}$ the driver is considered inattentive. The driver has priority and controls the vehicle whenever his awareness is recovered, which corresponds to $|\tau_d| > \tau_{off}$.

B.2 Risk of lane departure

A survey of methods to estimate the risk of lane departure is presented in [MT06]. Due to the simplicity of implementation, the risk of lane departure, based on the position of the front wheels, presented in [MELMN09] has been chosen for this work. It is adequate either for straight road segments as well as for curvy ones.

The risk of lane departure is estimated by the position of the front wheels with respect to a fixed strip of width $2d$ in the centre of the lane, as shown in Fig. B.1.

The positions of the left (right) front wheels, $y_{l,(r)}$, can be described by the following [MELMN09]:

$$\begin{aligned} y_l &= y_L + (l_f - l_s)\psi_L + \tfrac{a}{2}, \\ y_r &= y_L + (l_f - l_s)\psi_L - \tfrac{a}{2}, \end{aligned} \tag{B.1}$$

where a represents the vehicle width. Enforcing the front wheels to remain inside the centred lane strip $\pm d$, yields:

$$-\frac{2d-a}{2} \leq y_L + (l_f - l_s)\psi_L \leq \frac{2d-a}{2} \tag{B.2}$$

This set, corresponding to the region between two parallel hyperplanes, can be written with respect to the variables expressing the positioning of the vehicle, $z = [\psi_L,\ Y_L]^T$, as:

$$\mathcal{T} \triangleq \{z \in R^2 : |Fz| \leq 1\} \tag{B.3}$$

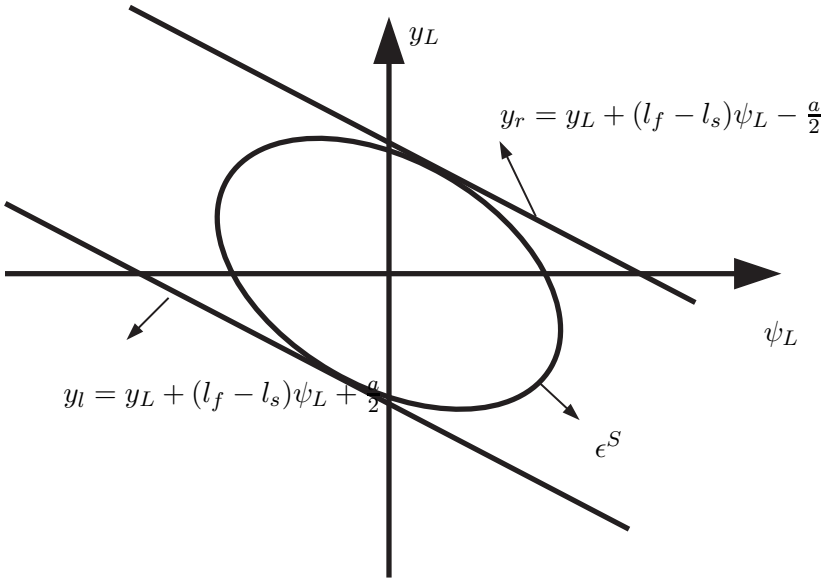

Figure B.2: Safe zone

where $F = \left[\frac{2(l_f - l_s)}{2d-a}, \frac{2}{2d-a}\right]$.

Therefore it can be assumed that there exists risk of lane departure if $|Fz| > 1$.

B.2.1 Normal driving zone

Similarly to the work [MENML09], the driving situation in which the vehicle follows the lane properly (excepting lane change, overtaking, etc) at relatively low lateral acceleration is denoted as "Normal driving".

Such conditions can be mathematically described by sets which are named "Safe Driving Zones". Considering that the control syntheses are based on quadratic or piecewise quadratic Lyapunov functions, ellipsoidal invariant sets can be obtained from the Lyapunov function as:

$$\epsilon^S = \{x | x^T P_{lin} x < c\} \tag{B.4}$$

where P_{lin} represents the piecewise quadratic Lyapunov function corresponding to the operating region of the linear approximation of the tyre forces, and c is a constant such that the ellipsoid ϵ^S is the largest contained in the set $\mathcal{T}$ (B.3), as shown in Fig. B.2

B.3 Activation of lane departure avoidance assistance

In order to take into account the driver awareness and the risk of lane departure, the activation and deactivation, illustrated in Fig. B.3 of the lane departure avoidance assistance system follows:

- *Activate* if $(\tau < \tau_{on})$ & $(|Fz| \geq 1)$
- *Deactivate* if $(\tau \geq \tau_{off})$ & $(x \in \epsilon^S)$,

where & and | are the logical expression *AND* and *OR* respectively.

The numerical values of torque used to assess the driver awareness for the activation of the assistances are shown in Table B.1.

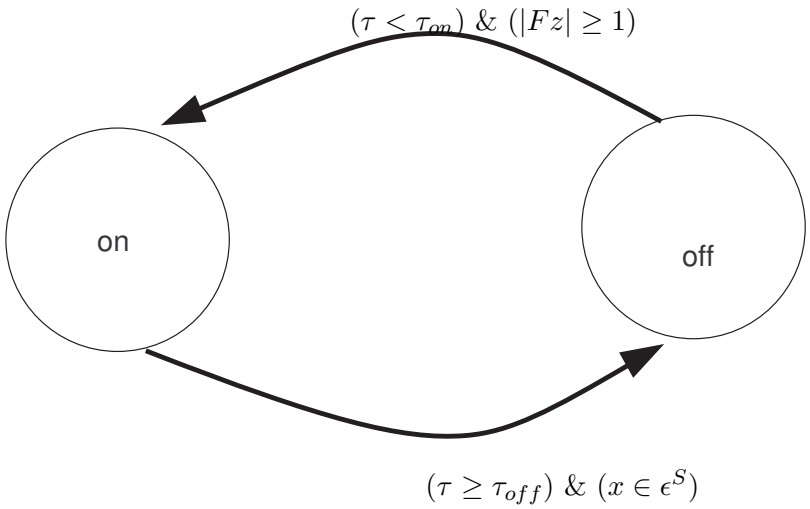

Figure B.3: Schema representing the activation strategy of the lateral assistance.

Table B.1: Assessment of driver awareness

τ_{on}	2 $[Nm]$
τ_{off}	5 $[Nm]$

B.4 Activation for obstacle avoidance assistance or autonomous driving

An important feature that should be added to advanced driver assistance systems is the ability to perceive and avoid obstacles.

Some work has been devoted to this subject, for example, in [VGMG09] obstacle detection and risk analysis based on the surrounding environment is performed to plan an ideal vehicle trajectory.

Such a system can also be incorporated in the activation strategy of the driver assistance system, in which the controller should follow the planned trajectory when the driver is considered inattentive in order to avoid obstacles.

Similarly to the lane keeping case, the driver is not able to retake control of the vehicle until it returns to a safe condition ($x \in \epsilon^S$).

Appendix C

Feasibility of *Controller-5* for multiple partitioning

The LMIs from Theorem 3.5.2 were not feasible for values of $\bar{\alpha}_f \geq 0.08$, therefore these results are not presented in this document.

Table C.1: Feasibility of Quadratic Stabilisation $\bar{\alpha}_f = 0.01$

Row	α_f^{step} $[rad]$	α_f^{end} $[rad]$	d_{lin+1} $[N/m]$	d_{lin+2} $[N/m]$	d_M $[N/m]$	e_M $[N]$	$c_f - d_M$ $[N/m]$	Result
1	0.01	0.02	39988.64	-	39988.64	0.06	6.45	Feasible
2	0.01	0.03	39988.64	39794.39	39794.39	3.95	200.7	Feasible
3	0.01	0.04	39988.64	39794.39	39164.45	22.85	830.64	Feasible
4	0.01	0.05	39988.64	39794.39	37840.22	75.82	2154.88	Feasible
5	0.01	0.06	39988.64	39794.39	35682.59	183.7	4312.5	no
⋮	⋮	⋮	⋮	⋮	⋮	⋮	⋮	no
6	0.02	0.03	39891.52	-	39891.52	1.04	103.58	Feasible
7	0.02	0.05	39891.52	38502.33	38502.33	42.71	1492.76	Feasible
8	0.02	0.07	39891.52	38502.33	34206.52	257.5	5788.57	Feasible
9	0.02	0.09	39891.52	38502.33	27272.14	742.91	12722.95	no
⋮	⋮	⋮	⋮	⋮	⋮	⋮	⋮	no
10	0.03	0.04	39649.16	-	39649.16	3.46	345.93	Feasible
11	0.03	0.07	39649.16	35417.75	35417.75	172.72	4577.34	Feasible
12	0.03	0.1	39649.16	35417.75	25358.52	876.86	14636.57	Feasible
13	0.03	0.13	39649.16	35417.75	14910.48	1921.67	25084.61	no
⋮	⋮	⋮	⋮	⋮	⋮	⋮	⋮	no
14	0.04	0.05	39196.92	-	39196.92	7.98	798.17	Feasible
15	0.04	0.09	39196.92	30739.33	30739.33	430.86	9255.76	Feasible
16	0.04	0.13	39196.92	30739.33	16565.68	1706.49	23429.41	no
⋮	⋮	⋮	⋮	⋮	⋮	⋮	⋮	no

Row	α_f^{step} $[rad]$	α_f^{end} $[rad]$	d_{lin+1} $[N/m]$	d_{lin+2} $[N/m]$	d_M $[N/m]$	e_M $[N]$	$c_f - d_M$ $[N/m]$	Result
17	0.05	0.06	38494.06	-	38494.06	15.01	1501.03	Feasible
18	0.05	0.11	38494.06	25351.5	25351.5	803.56	14643.59	Feasible
19	0.05	0.16	38494.06	25351.5	10132.54	2477.65	29862.56	no
⋮	⋮	⋮	⋮	⋮	⋮	⋮	⋮	no
20	0.06	0.07	37533.46	-	37533.46	24.62	2461.64	Feasible
21	0.06	0.13	37533.46	20134.5	20134.5	1242.54	19860.59	Feasible
22	0.06	0.19	37533.46	20134.5	6064.08	3071.7	33931.01	no
⋮	⋮	⋮	⋮	⋮	⋮	⋮	⋮	no
23	0.07	0.08	36341.35	-	36341.35	36.54	3653.74	Feasible
24	0.07	0.15	36341.35	15598	15598	1696.01	24397.09	no
⋮	⋮	⋮	⋮	⋮	⋮	⋮	⋮	no
25	0.08	0.09	34968.13	-	34968.13	50.27	5026.97	Feasible
26	0.08	0.17	34968.13	11903.95	11903.95	2126.05	28091.14	no
⋮	⋮	⋮	⋮	⋮	⋮	⋮	⋮	no
27	0.09	0.1	33475.14	-	33475.14	65.2	6519.95	Feasible
28	0.09	0.19	33475.14	9012.88	9012.88	2511.43	30982.21	no
⋮	⋮	⋮	⋮	⋮	⋮	⋮	⋮	no
29	0.1	0.11	31922.78	-	31922.78	80.72	8072.31	Feasible
30	0.1	0.21	31922.78	6802.69	6802.69	2843.93	33192.4	no
⋮	⋮	⋮	⋮	⋮	⋮	⋮	⋮	no
31	0.11	0.12	30362.6	-	30362.6	96.32	9632.5	Feasible
32	0.11	0.23	30362.6	5135	5135	3123.64	34860.09	no
⋮	⋮	⋮	⋮	⋮	⋮	⋮	⋮	no
33	0.12	0.13	28833.98	-	28833.98	111.61	11161.11	Feasible
34	0.12	0.25	28833.98	3884.49	3884.49	3355.04	36110.6	no
⋮	⋮	⋮	⋮	⋮	⋮	⋮	⋮	no
35	0.13	0.14	27364.1	-	27364.1	126.31	12630.99	Feasible
36	0.13	0.27	27364.1	2948.34	2948.34	3544.52	37046.75	no
⋮	⋮	⋮	⋮	⋮	⋮	⋮	⋮	no
37	0.14	0.15	25969.68	-	25969.68	140.25	14025.41	Feasible
38	0.14	0.29	25969.68	2246.53	2246.53	3698.73	37748.57	no
⋮	⋮	⋮	⋮	⋮	⋮	⋮	⋮	no
39	0.15	0.16	24659.37	-	24659.37	153.36	15335.73	Feasible
40	0.16	0.17	23436.04	-	23436.04	165.59	16559.05	Feasible
41	0.17	0.18	22298.72	-	22298.72	176.96	17696.37	Feasible
42	0.18	0.19	21244.01	-	21244.01	187.51	18751.08	Feasible
43	0.19	0.2	20267.16	-	20267.16	197.28	19727.93	Feasible
44	0.2	0.21	19362.74	-	19362.74	206.32	20632.36	no
⋮	⋮	⋮	⋮	⋮	⋮	⋮	⋮	no

Table C.2: Feasibility of Quadratic Stabilisation $\bar{\alpha}_f = 0.02$

Row	α_f^{step} $[rad]$	α_f^{end} $[rad]$	d_{lin+1} $[N/m]$	d_{lin+2} $[N/m]$	d_M $[N/m]$	e_M $[N]$	$c_f - d_M$ $[N/m]$	Result
1	0.01	0.03	39787.94	0	39787.94	4.14	207.15	Feasible
2	0.01	0.04	39787.94	39164.45	39164.45	22.85	830.64	Feasible
3	0.01	0.05	39787.94	39164.45	37840.22	75.82	2154.88	Feasible
4	0.01	0.06	39787.94	39164.45	35682.59	183.7	4312.5	no
⋮	⋮	⋮	⋮	⋮	⋮	⋮	⋮	no
5	0.02	0.04	39476.19	0	39476.19	10.38	518.9	Feasible
6	0.02	0.06	39476.19	36761.4	36761.4	118.97	3233.69	Feasible
7	0.02	0.08	39476.19	36761.4	30959.59	467.08	9035.51	Feasible
8	0.02	0.1	39476.19	36761.4	23443.42	1068.37	16551.68	no
⋮	⋮	⋮	⋮	⋮	⋮	⋮	⋮	no
9	0.03	0.05	38930.87	0	38930.87	21.28	1064.22	Feasible
10	0.03	0.08	38930.87	32533.92	32533.92	341.13	7461.17	Feasible
11	0.03	0.11	38930.87	32533.92	21612.78	1214.82	18382.31	Feasible
12	0.03	0.14	38930.87	32533.92	12168.49	2253.69	27826.6	no
⋮	⋮	⋮	⋮	⋮	⋮	⋮	⋮	no
13	0.04	0.06	38118.8	0	38118.8	37.53	1876.29	Feasible
14	0.04	0.1	38118.8	27201.5	27201.5	692.56	12793.59	Feasible
15	0.04	0.14	38118.8	27201.5	13614.25	2051.29	26380.84	no
⋮	⋮	⋮	⋮	⋮	⋮	⋮	⋮	no
16	0.05	0.07	37041.13	0	37041.13	59.08	2953.96	Feasible
17	0.05	0.12	37041.13	21757.57	21757.57	1128.93	18237.53	Feasible
18	0.05	0.17	37041.13	21757.57	8197.62	2756.12	31797.47	no
⋮	⋮	⋮	⋮	⋮	⋮	⋮	⋮	no
19	0.06	0.08	35732.39	0	35732.39	85.25	4262.7	Feasible
20	0.06	0.14	35732.39	16890.64	16890.64	1592.59	23104.46	no
⋮	⋮	⋮	⋮	⋮	⋮	⋮	⋮	no
21	0.07	0.09	34249.99	0	34249.99	114.9	5745.1	Feasible
22	0.07	0.16	34249.99	12877.92	12877.92	2038.39	27117.17	no
⋮	⋮	⋮	⋮	⋮	⋮	⋮	⋮	no
23	0.08	0.1	32660.15	0	32660.15	146.7	7334.94	Feasible
24	0.08	0.18	32660.15	9725.24	9725.24	2440.19	30269.85	no
⋮	⋮	⋮	⋮	⋮	⋮	⋮	⋮	no
25	0.09	0.11	31025.86	0	31025.86	179.38	8969.24	Feasible
26	0.09	0.2	31025.86	7316.47	7316.47	2787.42	32678.63	no
⋮	⋮	⋮	⋮	⋮	⋮	⋮	⋮	no

Row	α_f^{step} $[rad]$	α_f^{end} $[rad]$	d_{lin+1} $[N/m]$	d_{lin+2} $[N/m]$	d_M $[N/m]$	e_M $[N]$	$c_f - d_M$ $[N/m]$	Result
27	0.1	0.12	29399.35	0	29399.35	211.91	10595.75	Feasible
28	0.1	0.22	29399.35	5503.91	5503.91	3079.37	34491.18	no
⋮	⋮	⋮	⋮	⋮	⋮	⋮	⋮	no
29	0.11	0.13	27819.33	0	27819.33	243.52	12175.76	Feasible
30	0.11	0.24	27819.33	4149.75	4149.75	3320.56	35845.35	no
⋮	⋮	⋮	⋮	⋮	⋮	⋮	⋮	no
31	0.12	0.14	26311.52	0	26311.52	273.67	13683.58	Feasible
32	0.12	0.26	26311.52	3140	3140	3517.68	36855.1	no
⋮	⋮	⋮	⋮	⋮	⋮	⋮	⋮	no
33	0.13	0.15	24890.8	0	24890.8	302.09	15104.29	Feasible
34	0.13	0.28	24890.8	2385.94	2385.94	3677.81	37609.15	no
⋮	⋮	⋮	⋮	⋮	⋮	⋮	⋮	no
35	0.14	0.16	23563.96	0	23563.96	328.62	16431.14	Feasible
36	0.15	0.17	22332.1	0	22332.1	353.26	17662.99	Feasible
37	0.16	0.18	21192.7	0	21192.7	376.05	18802.4	Feasible
38	0.17	0.19	20141.01	0	20141.01	397.08	19854.08	Feasible
39	0.18	0.2	19171.16	0	19171.16	416.48	20823.93	no
40	0.19	0.21	18276.82	0	18276.82	434.37	21718.27	no
41	0.2	0.22	17451.63	0	17451.63	450.87	22543.46	no
⋮	⋮	⋮	⋮	⋮	⋮	⋮	⋮	no

Table C.3: Feasibility of Quadratic Stabilisation $\bar{\alpha}_f = 0.03$

Row	α_f^{step} $[rad]$	α_f^{end} $[rad]$	d_{lin+1} $[N/m]$	d_{lin+2} $[N/m]$	d_M $[N/m]$	e_M $[N]$	$c_f - d_M$ $[N/m]$	Result
1	0.01	0.04	38957.29	0	38957.29	31.13	1037.8	Feasible
2	0.01	0.05	38957.29	37840.22	37840.22	75.82	2154.88	Feasible
3	0.01	0.06	38957.29	37840.22	35682.59	183.7	4312.5	no
⋮	⋮	⋮	⋮	⋮	⋮	⋮	⋮	no
4	0.02	0.05	38398.76	0	38398.76	47.89	1596.34	Feasible
5	0.02	0.07	38398.76	34206.52	34206.52	257.5	5788.57	Feasible
6	0.02	0.09	38398.76	34206.52	27272.14	742.91	12722.95	no
⋮	⋮	⋮	⋮	⋮	⋮	⋮	⋮	no
7	0.03	0.06	37493.37	0	37493.37	75.05	2501.72	Feasible
8	0.03	0.09	37493.37	29091.58	29091.58	579.16	10903.52	Feasible
9	0.03	0.12	37493.37	29091.58	18081.18	1570.09	21913.91	no
⋮	⋮	⋮	⋮	⋮	⋮	⋮	⋮	no
10	0.04	0.07	36302.64	0	36302.64	110.77	3692.46	Feasible
11	0.04	0.11	36302.64	23506.77	23506.77	1006.48	16488.32	Feasible
12	0.04	0.15	36302.64	23506.77	11086.92	2372.67	28908.17	no
⋮	⋮	⋮	⋮	⋮	⋮	⋮	⋮	no
13	0.05	0.08	34879.86	0	34879.86	153.46	5115.24	Feasible
14	0.05	0.13	34879.86	18323.66	18323.66	1477.95	21671.44	no
⋮	⋮	⋮	⋮	⋮	⋮	⋮	⋮	no
15	0.06	0.09	33292.47	0	33292.47	201.08	6702.62	Feasible
16	0.06	0.15	33292.47	13971.75	13971.75	1939.94	26023.35	no
⋮	⋮	⋮	⋮	⋮	⋮	⋮	⋮	no
17	0.07	0.1	31612.3	0	31612.3	251.48	8382.79	Feasible
18	0.07	0.17	31612.3	10528.62	10528.62	2359.85	29466.47	no
⋮	⋮	⋮	⋮	⋮	⋮	⋮	⋮	no
19	0.08	0.11	29904.7	0	29904.7	302.71	10090.39	Feasible
20	0.08	0.19	29904.7	7895.55	7895.55	2723.72	32099.54	no
⋮	⋮	⋮	⋮	⋮	⋮	⋮	⋮	no
21	0.09	0.12	28222.04	0	28222.04	353.19	11773.05	Feasible
22	0.09	0.21	28222.04	5918.46	5918.46	3029.62	34076.63	no
⋮	⋮	⋮	⋮	⋮	⋮	⋮	⋮	no
23	0.1	0.13	26601.76	0	26601.76	401.8	13393.34	Feasible
24	0.1	0.23	26601.76	4446.58	4446.58	3281.97	35548.51	no
⋮	⋮	⋮	⋮	⋮	⋮	⋮	⋮	no

Row	α_f^{step} $[rad]$	α_f^{end} $[rad]$	d_{lin+1} $[N/m]$	d_{lin+2} $[N/m]$	d_M $[N/m]$	e_M $[N]$	$c_f - d_M$ $[N/m]$	Result
25	0.11	0.14	25067.55	0	25067.55	447.83	14927.54	Feasible
26	0.11	0.25	25067.55	3353.48	3353.48	3487.8	36641.61	no
⋮	⋮	⋮	⋮	⋮	⋮	⋮	⋮	no
27	0.12	0.15	23632.11	0	23632.11	490.89	16362.98	Feasible
28	0.12	0.27	23632.11	2540.52	2540.52	3654.63	37454.57	no
⋮	⋮	⋮	⋮	⋮	⋮	⋮	⋮	no
29	0.13	0.16	22300.02	0	22300.02	530.85	17695.07	Feasible
30	0.13	0.29	22300.02	1933.57	1933.57	3789.48	38061.52	no
⋮	⋮	⋮	⋮	⋮	⋮	⋮	⋮	no
31	0.14	0.17	21070.46	0	21070.46	567.74	18924.63	Feasible
32	0.15	0.18	19939.2	0	19939.2	601.68	20055.89	no
⋮	⋮	⋮	⋮	⋮	⋮	⋮	⋮	no
33	0.16	0.19	18900.13	0	18900.13	632.85	21094.97	no
⋮	⋮	⋮	⋮	⋮	⋮	⋮	⋮	no
34	0.17	0.2	17946.22	0	17946.22	661.47	22048.87	no
⋮	⋮	⋮	⋮	⋮	⋮	⋮	⋮	no
35	0.18	0.21	17070.25	0	17070.25	687.75	22924.84	no
⋮	⋮	⋮	⋮	⋮	⋮	⋮	⋮	no
36	0.19	0.22	16265.13	0	16265.13	711.9	23729.96	no
⋮	⋮	⋮	⋮	⋮	⋮	⋮	⋮	no
37	0.2	0.23	15524.17	0	15524.17	734.13	24470.92	no
⋮	⋮	⋮	⋮	⋮	⋮	⋮	⋮	no

Table C.4: Feasibility of Quadratic Stabilisation $\bar{\alpha}_f = 0.04$

Row	α_f^{step} $[rad]$	α_f^{end} $[rad]$	d_{lin+1} $[N/m]$	d_{lin+2} $[N/m]$	d_M $[N/m]$	e_M $[N]$	$c_f - d_M$ $[N/m]$	Result
1	0.01	0.05	36802.42	0	36802.42	127.71	3192.67	Feasible
2	0.01	0.06	36802.42	35682.59	35682.59	183.7	4312.5	no
⋮	⋮	⋮	⋮	⋮	⋮	⋮	⋮	no
3	0.02	0.06	36242.51	0	36242.51	150.1	3752.59	Feasible
4	0.02	0.08	36242.51	30959.59	30959.59	467.08	9035.51	Feasible
5	0.02	0.1	36242.51	30959.59	23443.42	1068.37	16551.68	no
⋮	⋮	⋮	⋮	⋮	⋮	⋮	⋮	no
6	0.03	0.07	35071.82	0	35071.82	196.93	4923.27	Feasible
7	0.03	0.1	35071.82	25358.52	25358.52	876.86	14636.57	Feasible
8	0.03	0.13	35071.82	25358.52	14910.48	1921.67	25084.61	no
⋮	⋮	⋮	⋮	⋮	⋮	⋮	⋮	no
9	0.04	0.08	33601.05	0	33601.05	255.76	6394.05	Feasible
10	0.04	0.12	33601.05	19899.78	19899.78	1351.86	20095.32	Feasible
11	0.04	0.16	33601.05	19899.78	8975.48	2662.78	31019.61	no
⋮	⋮	⋮	⋮	⋮	⋮	⋮	⋮	no
12	0.05	0.09	31951.95	0	31951.95	321.73	8043.14	Feasible
13	0.05	0.14	31951.95	15197.65	15197.65	1829.61	24797.44	no
⋮	⋮	⋮	⋮	⋮	⋮	⋮	⋮	no
14	0.06	0.1	30215.17	0	30215.17	391.2	9779.92	Feasible
15	0.06	0.16	30215.17	11435.7	11435.7	2269.14	28559.39	no
⋮	⋮	⋮	⋮	⋮	⋮	⋮	⋮	no
16	0.07	0.11	28463.22	0	28463.22	461.27	11531.87	Feasible
17	0.07	0.18	28463.22	8550.06	8550.06	2651.72	31445.03	no
⋮	⋮	⋮	⋮	⋮	⋮	⋮	⋮	no
18	0.08	0.12	26750.41	0	26750.41	529.79	13244.68	Feasible
19	0.08	0.2	26750.41	6385.93	6385.93	2973.52	33609.16	no
⋮	⋮	⋮	⋮	⋮	⋮	⋮	⋮	no
20	0.09	0.13	25113.61	0	25113.61	595.26	14881.48	Feasible
21	0.09	0.22	25113.61	4779.99	4779.99	3238.63	35215.1	no
⋮	⋮	⋮	⋮	⋮	⋮	⋮	⋮	no
22	0.1	0.14	23574.8	0	23574.8	656.81	16420.29	Feasible
23	0.1	0.24	23574.8	3592.17	3592.17	3454.38	36402.92	no
⋮	⋮	⋮	⋮	⋮	⋮	⋮	⋮	no
24	0.11	0.15	22144.56	0	22144.56	714.02	17850.53	Feasible
25	0.11	0.26	22144.56	2712.52	2712.52	3628.83	37282.57	no
⋮	⋮	⋮	⋮	⋮	⋮	⋮	⋮	no

Row	α_f^{step} $[rad]$	α_f^{end} $[rad]$	d_{lin+1} $[N/m]$	d_{lin+2} $[N/m]$	d_M $[N/m]$	e_M $[N]$	$c_f - d_M$ $[N/m]$	Result
26	0.12	0.16	20825.43	0	20825.43	766.79	19169.66	Feasible
27	0.12	0.28	20825.43	2058.52	2058.52	3769.49	37936.57	no
⋮	⋮	⋮	⋮	⋮	⋮	⋮	⋮	no
28	0.13	0.17	19614.72	0	19614.72	815.21	20380.37	no
⋮	⋮	⋮	⋮	⋮	⋮	⋮	⋮	no
30	0.14	0.18	18506.64	0	18506.64	859.54	21488.45	no
⋮	⋮	⋮	⋮	⋮	⋮	⋮	⋮	no
31	0.15	0.19	17493.8	0	17493.8	900.05	22501.3	no
⋮	⋮	⋮	⋮	⋮	⋮	⋮	⋮	no
32	0.16	0.2	16568.17	0	16568.17	937.08	23426.92	no
⋮	⋮	⋮	⋮	⋮	⋮	⋮	⋮	no
33	0.17	0.21	15721.73	0	15721.73	970.93	24273.36	no
⋮	⋮	⋮	⋮	⋮	⋮	⋮	⋮	no
34	0.18	0.22	14946.8	0	14946.8	1001.93	25048.29	no
⋮	⋮	⋮	⋮	⋮	⋮	⋮	⋮	no
35	0.19	0.23	14236.23	0	14236.23	1030.35	25758.87	no
⋮	⋮	⋮	⋮	⋮	⋮	⋮	⋮	no
36	0.2	0.24	13583.48	0	13583.48	1056.46	26411.61	no
⋮	⋮	⋮	⋮	⋮	⋮	⋮	⋮	no

Table C.5: Feasibility of Quadratic Stabilisation $\bar{\alpha}_f = 0.05$

Row	α_f^{step} $[rad]$	α_f^{end} $[rad]$	d_{lin+1} $[N/m]$	d_{lin+2} $[N/m]$	d_M $[N/m]$	e_M $[N]$	$c_f - d_M$ $[N/m]$	Result
1	0.01	0.06	32489.92	0	32489.92	375.26	7505.17	Feasible
2	0.01	0.07	32489.92	32730.44	32730.44	360.83	7505.17	no
⋮	⋮	⋮	⋮	⋮	⋮	⋮	⋮	no
3	0.02	0.07	32610.18	0	32610.18	369.25	7384.91	Feasible
4	0.02	0.09	32610.18	27272.14	27272.14	742.91	12722.95	no
⋮	⋮	⋮	⋮	⋮	⋮	⋮	⋮	no
5	0.03	0.08	31469.7	0	31469.7	426.27	8525.39	Feasible
6	0.03	0.11	31469.7	21612.78	21612.78	1214.82	18382.31	no
⋮	⋮	⋮	⋮	⋮	⋮	⋮	⋮	no
7	0.04	0.09	29941.16	0	29941.16	502.7	10053.93	Feasible
8	0.04	0.13	29941.16	16565.68	16565.68	1706.49	23429.41	no
⋮	⋮	⋮	⋮	⋮	⋮	⋮	⋮	no
9	0.05	0.1	28259.18	0	28259.18	586.8	11735.91	Feasible
10	0.05	0.15	28259.18	12459.84	12459.84	2166.73	27535.25	no
⋮	⋮	⋮	⋮	⋮	⋮	⋮	⋮	no
11	0.06	0.11	26541.24	0	26541.24	672.69	13453.85	Feasible
12	0.06	0.17	26541.24	9291.47	9291.47	2570.17	30703.62	no
⋮	⋮	⋮	⋮	⋮	⋮	⋮	⋮	no
⋮	⋮	⋮	⋮	⋮	⋮	⋮	⋮	no
13	0.07	0.12	24858.31	0	24858.31	756.84	15136.78	Feasible
14	0.07	0.19	24858.31	6914.81	6914.81	2910.06	33080.28	no
⋮	⋮	⋮	⋮	⋮	⋮	⋮	⋮	no
15	0.08	0.13	23253.42	0	23253.42	837.08	16741.67	Feasible
16	0.08	0.21	23253.42	5155.87	5155.87	3189.76	34839.22	no
⋮	⋮	⋮	⋮	⋮	⋮	⋮	⋮	no
17	0.09	0.14	21750.32	0	21750.32	912.24	18244.77	Feasible
18	0.09	0.23	21750.32	3860.03	3860.03	3416.88	36135.06	no
⋮	⋮	⋮	⋮	⋮	⋮	⋮	⋮	no
19	0.1	0.15	20359.51	0	20359.51	981.78	19635.58	Feasible
20	0.1	0.25	20359.51	2904.61	2904.61	3600.01	37090.48	no
⋮	⋮	⋮	⋮	⋮	⋮	⋮	⋮	no
21	0.11	0.16	19082.74	0	19082.74	1045.62	20912.35	no
⋮	⋮	⋮	⋮	⋮	⋮	⋮	⋮	no
22	0.12	0.17	17916.36	0	17916.36	1103.94	22078.74	no
⋮	⋮	⋮	⋮	⋮	⋮	⋮	⋮	no

Row	α_f^{step} $[rad]$	α_f^{end} $[rad]$	d_{lin+1} $[N/m]$	d_{lin+2} $[N/m]$	d_M $[N/m]$	e_M $[N]$	$c_f - d_M$ $[N/m]$	Result
23	0.13	0.18	16853.68	0	16853.68	1157.07	23141.41	no
⋮	⋮	⋮	⋮	⋮	⋮	⋮	⋮	no
24	0.14	0.19	15886.56	0	15886.56	1205.43	24108.53	no
⋮	⋮	⋮	⋮	⋮	⋮	⋮	⋮	no
25	0.15	0.2	15006.38	0	15006.38	1249.44	24988.72	no
⋮	⋮	⋮	⋮	⋮	⋮	⋮	⋮	no
26	0.16	0.21	14204.65	0	14204.65	1289.52	25790.44	no
⋮	⋮	⋮	⋮	⋮	⋮	⋮	⋮	no
27	0.17	0.22	13473.37	0	13473.37	1326.09	26521.72	no
⋮	⋮	⋮	⋮	⋮	⋮	⋮	⋮	no
28	0.18	0.23	12805.18	0	12805.18	1359.5	27189.91	no
⋮	⋮	⋮	⋮	⋮	⋮	⋮	⋮	no
29	0.19	0.24	12193.4	0	12193.4	1390.08	27801.69	no
⋮	⋮	⋮	⋮	⋮	⋮	⋮	⋮	no
30	0.2	0.25	11632.06	0	11632.06	1418.15	28363.03	no
⋮	⋮	⋮	⋮	⋮	⋮	⋮	⋮	no

Table C.6: Feasibility of Quadratic Stabilisation $\bar{\alpha}_f = 0.06$

Row	α_f^{step} $[rad]$	α_f^{end} $[rad]$	d_{lin+1} $[N/m]$	d_{lin+2} $[N/m]$	d_M $[N/m]$	e_M $[N]$	$c_f - d_M$ $[N/m]$	Result
1	0.01	0.07	25225.27	0	25225.27	886.19	14769.82	Feasible
2	0.01	0.08	25225.27	29188.73	29188.73	608.75	14769.82	no
⋮	⋮	⋮	⋮	⋮	⋮	⋮	⋮	no
3	0.02	0.08	27207	0	27207	767.29	12788.09	Feasible
4	0.02	0.1	27207	23443.42	23443.42	1068.37	16551.68	no
⋮	⋮	⋮	⋮	⋮	⋮	⋮	⋮	no
5	0.03	0.09	26589.85	0	26589.85	804.31	13405.24	Feasible
6	0.03	0.12	26589.85	18081.18	18081.18	1570.09	21913.91	no
⋮	⋮	⋮	⋮	⋮	⋮	⋮	⋮	no
7	0.04	0.1	25325.21	0	25325.21	880.19	14669.88	Feasible
8	0.04	0.14	25325.21	13614.25	13614.25	2051.29	26380.84	no
⋮	⋮	⋮	⋮	⋮	⋮	⋮	⋮	no
9	0.05	0.11	23850.47	0	23850.47	968.68	16144.62	Feasible
10	0.05	0.16	23850.47	10132.54	10132.54	2477.65	29862.56	no
⋮	⋮	⋮	⋮	⋮	⋮	⋮	⋮	no
11	0.06	0.12	22335.52	0	22335.52	1059.57	17659.58	Feasible
12	0.06	0.18	22335.52	7514.95	7514.95	2838.04	32480.15	no
⋮	⋮	⋮	⋮	⋮	⋮	⋮	⋮	no
13	0.07	0.13	20861.75	0	20861.75	1148	19133.34	Feasible
14	0.07	0.2	20861.75	5581.18	5581.18	3134.47	34413.91	no
⋮	⋮	⋮	⋮	⋮	⋮	⋮	⋮	no
15	0.08	0.14	19469.73	0	19469.73	1231.52	20525.36	no
⋮	⋮	⋮	⋮	⋮	⋮	⋮	⋮	no
16	0.09	0.15	18177.78	0	18177.78	1309.04	21817.31	no
17	0.1	0.16	16991.5	0	16991.5	1380.22	23003.59	no
⋮	⋮	⋮	⋮	⋮	⋮	⋮	⋮	no
18	0.11	0.17	15909.2	0	15909.2	1445.15	24085.89	no
⋮	⋮	⋮	⋮	⋮	⋮	⋮	⋮	no
19	0.12	0.18	14925.23	0	14925.23	1504.19	25069.86	no
⋮	⋮	⋮	⋮	⋮	⋮	⋮	⋮	no
20	0.13	0.19	14032.06	0	14032.06	1557.78	25963.03	no
⋮	⋮	⋮	⋮	⋮	⋮	⋮	⋮	no
21	0.14	0.2	13221.47	0	13221.47	1606.42	26773.62	no
⋮	⋮	⋮	⋮	⋮	⋮	⋮	⋮	no

Row	α_f^{step} $[rad]$	α_f^{end} $[rad]$	d_{lin+1} $[N/m]$	d_{lin+2} $[N/m]$	d_M $[N/m]$	e_M $[N]$	$c_f - d_M$ $[N/m]$	Result
23	0.16	0.22	11815.76	0	11815.76	1690.76	28179.33	no
⋮	⋮	⋮	⋮	⋮	⋮	⋮	⋮	no
24	0.17	0.23	11205.77	0	11205.77	1727.36	28789.32	no
⋮	⋮	⋮	⋮	⋮	⋮	⋮	⋮	no
25	0.18	0.24	10648.86	0	10648.86	1760.77	29346.23	no
⋮	⋮	⋮	⋮	⋮	⋮	⋮	⋮	no
26	0.19	0.25	10139.27	0	10139.27	1791.35	29855.82	no
⋮	⋮	⋮	⋮	⋮	⋮	⋮	⋮	no
27	0.2	0.26	9671.89	0	9671.89	1819.39	30323.2	no
⋮	⋮	⋮	⋮	⋮	⋮	⋮	⋮	no
22	0.15	0.21	12485.29	0	12485.29	1650.59	27509.81	no
⋮	⋮	⋮	⋮	⋮	⋮	⋮	⋮	no

Table C.7: Feasibility of Quadratic Stabilisation $\bar{\alpha}_f = 0.07$

Row	α_f^{step} $[rad]$	α_f^{end} $[rad]$	d_{lin+1} $[N/m]$	d_{lin+2} $[N/m]$	d_M $[N/m]$	e_M $[N]$	$c_f - d_M$ $[N/m]$	Result
1	0.01	0.08	14418.91	0	14418.91	1790.33	25576.18	no
⋮	⋮	⋮	⋮	⋮	⋮	⋮	⋮	no
2	0.02	0.09	19887.23	0	19887.23	1407.55	20107.86	no
⋮	⋮	⋮	⋮	⋮	⋮	⋮	⋮	no
3	0.03	0.1	20435.25	0	20435.25	1369.19	19559.85	Feasible
4	0.03	0.13	20435.25	14910.48	14910.48	1921.67	25084.61	no
⋮	⋮	⋮	⋮	⋮	⋮	⋮	⋮	no
5	0.04	0.11	19814.31	0	19814.31	1412.65	20180.78	no
⋮	⋮	⋮	⋮	⋮	⋮	⋮	⋮	no
6	0.05	0.12	18803.6	0	18803.6	1483.4	21191.49	no
⋮	⋮	⋮	⋮	⋮	⋮	⋮	⋮	no
7	0.06	0.13	17672.87	0	17672.87	1562.56	22322.23	no
⋮	⋮	⋮	⋮	⋮	⋮	⋮	⋮	no
8	0.06	0.19	17672.87	6064.08	6064.08	3071.7	33931.01	no
⋮	⋮	⋮	⋮	⋮	⋮	⋮	⋮	no
9	0.07	0.14	16537.53	0	16537.53	1642.03	23457.56	no
⋮	⋮	⋮	⋮	⋮	⋮	⋮	⋮	no
10	0.08	0.15	15450.62	0	15450.62	1718.11	24544.48	no
⋮	⋮	⋮	⋮	⋮	⋮	⋮	⋮	no
11	0.09	0.16	14435.55	0	14435.55	1789.17	25559.54	no
⋮	⋮	⋮	⋮	⋮	⋮	⋮	⋮	no
12	0.1	0.17	13500.61	0	13500.61	1854.61	26494.48	no
⋮	⋮	⋮	⋮	⋮	⋮	⋮	⋮	no
13	0.11	0.18	12646.15	0	12646.15	1914.43	27348.94	no
⋮	⋮	⋮	⋮	⋮	⋮	⋮	⋮	no
14	0.12	0.19	11868.47	0	11868.47	1968.86	28126.62	no
⋮	⋮	⋮	⋮	⋮	⋮	⋮	⋮	no
15	0.13	0.2	11161.96	0	11161.96	2018.32	28833.13	no
⋮	⋮	⋮	⋮	⋮	⋮	⋮	⋮	no
16	0.14	0.21	10520.3	0	10520.3	2063.24	29474.79	no
⋮	⋮	⋮	⋮	⋮	⋮	⋮	⋮	no
17	0.15	0.22	9937.14	0	9937.14	2104.06	30057.95	no
⋮	⋮	⋮	⋮	⋮	⋮	⋮	⋮	no

Row	α_f^{step} $[rad]$	α_f^{end} $[rad]$	d_{lin+1} $[N/m]$	d_{lin+2} $[N/m]$	d_M $[N/m]$	e_M $[N]$	$c_f - d_M$ $[N/m]$	Result
18	0.16	0.23	9406.44	0	9406.44	2141.21	30588.65	no
⋮	⋮	⋮	⋮	⋮	⋮	⋮	⋮	no
19	0.17	0.24	8922.61	0	8922.61	2175.07	31072.48	no
⋮	⋮	⋮	⋮	⋮	⋮	⋮	⋮	no
20	0.18	0.25	8480.61	0	8480.61	2206.01	31514.48	no
⋮	⋮	⋮	⋮	⋮	⋮	⋮	⋮	no
21	0.19	0.26	8075.93	0	8075.93	2234.34	31919.16	no
⋮	⋮	⋮	⋮	⋮	⋮	⋮	⋮	no
22	0.2	0.27	7704.56	0	7704.56	2260.34	32290.53	no
⋮	⋮	⋮	⋮	⋮	⋮	⋮	⋮	no

Bibliography

[ABL07] Tom Alkim, Gerben Bootsma, and Pierre Looman. *The Assisted Driver, Systems that support driving*. Ministry of Transport, Public Works and Water Management, Rijkswaterstaat, 2007.

[AC49] A. Andronov and C. Chaikin. *Theory of oscilations*. Princetown University Press, Princitown, NJ, 1949.

[Aca09] Tankut Acarman. Nonlinear optimal integrated vehicle control using individual braking torque and steering angle with on-line control allocation by using state-dependent Riccati equation technique. *Vehicle System Dymanics*, 47(2):155–177, February 2009.

[Ack97] J. Ackermann. Robust control prevents car skidding. *Control Systems, IEEE*, 17(3):23 –31, jun 1997.

[Ack02] Jurgen Ackermann. *Robust Control*. Springer, London, 2002.

[Aud07] Audi AG. The Audi Q7 4.2 TDI. http://www.audiworld.com/news/07/audi-q7-42-tdi/content.shtml, 1 March 2007.

[B+03] G. Baumgarten et al. Motor vehicle steering system having a yaw rate controller, april 2003. #9.

[BB11] Raymond Brach and Matthew Brach. The tire-force ellipse (friction ellipse) and tire characteristics. In *SAE 2011 World Congress & Exhibition*. Copyright Â© 2011 SAE International, 04 2011.

[BBdB+00] A. Balluchi, L. Benvenuti, M.D. di Benedetto, C. Pinello, and A.L. Sangiovanni-Vincentelli. Automotive engine control and hybrid systems: challenges and opportunities. *Proceedings of the IEEE*, 88(7):888 –912, jul 2000.

[BBF+99] A. Broggi, M. Bertozzi, A. Fascioli, C.G.L. Bianco, and A. Piazzi. The argo autonomous vehicle's vision and control systems. *International Journal of Intelligent Control and Systems*, 3(4):409–441, nov 1999.

[BBFC99] A. Broggi, M. Bertozzi, A. Fascioli, and G. Conte. *Automatic vehicle guidance: the experience of the ARGO autonomous vehicle*. World Scientific Pub Co Inc, 1999.

[BBFH01] F. Borrelli, A. Bemporad, M. Fodor, and D. Hrovat. *A Hybrid Approach to Traction Control*. Springer Berlin / Heidelberg pp. 162-174, 2001.

[BBM00] A. Bemporad, F. Borrelli, and M. Morari. Piecewise linear optimal controllers for hybrid systems. In *American Control Conference, 2000. Proceedings of the 2000*, volume 2, pages 1190–1194, 2000.

[BCBT09] D. Bernardini, S. Di Cairano, A. Bemporad, and H.E. Tseng. Drive-by-wire vehicle stabilization and yaw regulation: A hybrid model predictive control design. In *Joint 48th IEEE Conference on Decision and Control and 28th Chinese Control Conference, Shanghai, P.R. China*, pages 7621–7626, December 2009.

[BGFB94] Stephen Boyd, Laurent El Ghaoui, Eric Feron, and Venkataramanan Balakrishnan. *Linear Matrix Inequalties in System and Control Theory*, chapter 7. SIAM, 1994.

[BH98] David Banjerdpongchai and Jonathan P. How. Parametric robust h2 control design with generalized multipliers via lmi synthesis. *International Journal of Control*, 70(3):481–503, 1998.

[BHL10] A. Bemporad, W.P.M.H. Heemels, and M. Lazar. On the synthesis of piecewise affine control laws. In *Circuits and Systems (ISCAS), Proceedings of 2010 IEEE International Symposium on*, pages 3308–3311, jun 2010.

[BIS08a] Martin Buehler, Karl Iagnemma, and Sanjiv Singh. Editorial. *Journal of Field Robotics*, 25(8):423–424, 2008.

[BIS08b] Martin Buehler, Karl Iagnemma, and Sanjiv Singh. Editorial. *Journal of Field Robotics*, 25(9):567–568, 2008.

[BK11] J. Broughton and J. Knowles. Traffic safety basic facts 2010 - single vehicle accident. Technical report, European Road safety Observatory Deliverable D3.2 of the EC FP7 project DaCoTA., 2011.

[BM99] Alberto Bemporad and Manfred Morari. Control of systems integrating logic, dynamics, and constraints. *Automatica*, 35(3):407–427, 1999.

[BM08] F. Blanchini and S. Miani. *Set-theoretic methods in control*. Springer, 2008.

[Bok81] W. G. V. Bokhoven. *Piecewise linear modelling and analysis*. Deventer, The Netherlands, Kluwer Technische Boeken, 1981.

[Bou11] Phillipe Boulleau. Skid concept. http://www.skid-concept.com, 2011. dossier-de-presse-photos-maj-05-09-conduite-extreme-v3.3.pdf.

[BPK07] S.C. Baslamisli, I. Polat, and I.E. Kose. Gain scheduled active steering control based on a parametric bicycle model. In *Intelligent Vehicles Symposium, 2007 IEEE*, pages 1168 –1173, june 2007.

[Bro93] RW Brockett. Hybrid Models for Motion Control Systems. *Essays on Control: Perspectives in the Theory and its Applications*, page 29, 1993.

[BT99] Vincent D. Blondel and John N. Tsitsiklis. Complexity of stability and controllability of elementary hybrid systems. *Automatica*, 35(3):479 – 489, 1999.

[CDS07] D. Corona and B. De Schutter. Comparison of a linear and a hybrid adaptive cruise controller for a smart. In *Decision and Control, 2007 46th IEEE Conference on*, pages 4779 –4784, dec 2007.

[CG96] Mahmoud Chiali and Pascal Gahinet. Hinf design with pole placement constraints: An lmi approach. *IEEE Transactions on Automatic Control*, 41(3):358–367, March 1996.

[Cit] PSA Peugeot Citroën. Develop driver warning / information systems (lane following, bar codes). http://www.sustainability.psa-peugeot-citroen.com/corporate-citizenship/priorities/overview/achievement.htm?id=2708.

[CK77] L.O. Chua and Sung Mo Kang. Section-wise piecewise-linear functions: Canonical representation, properties, and applications. *Proceedings of the IEEE*, 65(6):915 – 929, june 1977.

[CMR09] Vito Cerone, Mario Milanese, and Diego Regruto. Combined automatic lane-keeping and driver's steering through a 2 dof control strategy. *IEEE Transactions on Control Systems Technology*, 17(1):135–142, January 2009.

[Cou08] European Transport Safety Council. Proposal for regulation: Type-approval requirements for the general safety of motor vehicles. http://www.etsc.eu/documents/ETSC_Position_-_Proposal_for_a_Regulation_on_type_approval.pdf, May 2008.

[CR03] Vito Cerone and Diego Regruto. Robust performance controller design for vehicle lane keeping. In *European Control conference (eec'03), cambrigde, uk*, September 2003.

[CSNM04] Salin Chaib, Mariana S. Netto, and Said Mammar. H-infinity, adaptive, pid and fuzzy control: a comparison of controllers for vehicle lane keeping. In *Proceedings of the IEEE Intelligent Vehicles Symposium, Parma, Italy*, pages 139–144, June 2004.

[CT03] C.Y. Chan and H.S. Tan. Evaluation of magnetic markers as a position reference system for ground vehicle guidance and control. *Institute of Transportation Studies, Research Reports, Working Papers, Proceedings*, 2003.

[Dan04] Jennifer N. Dang. Preliminary results analyzing the effectiviness of electronic stability control (esc) systems. http://www.nhtsa.gov/cars/rules/regrev/evaluate/809790_files/809790.pdf, 12 September 2004. National Highway Traffic Safety Administration.

[DAR04] DARPA. Darpa grand challenge 2004. http://archive.darpa.mil/grandchallenge/index.asp, 2004.

[DAR05] DARPA. Darpa grand challenge 2005. http://archive.darpa.mil/grandchallenge05, 2005.

[DAR08] DARPA. Darpa urban challenge 2008. http://archive.darpa.mil/grandchallenge/index.asp, 2008.

[dBBvdM+08] J.J.T.H. de Best, B.H.M. Bukkems, M.J.G. van de Molengraft, W.P.M.H. Heemels, and M. Steinbuch. Robust control of piecewise linear systems: A case study in sheet flow control. *Control Engineering Practice*, 16(8):991 – 1003, 2008. Special Section: IFAC Conference on Analysis and Design of Hybrid Systems (ADHS'06), IFAC Conference on Analysis and Design of Hybrid Systems.

[DBL+08] M. Doumiati, G. Baffet, D. Lechner, A. Victorino, and A. Charara. Embedded estimation of the tire/road forces and validation in a laboratory vehicle. In *AVEC08 Proceedings of 9th International Symposium on Advanced Vehicle Control, Kobe Japan*, pages 533–538, October 2008.

[DRI02] J. Daafouz, P. Riedinger, and C. Iung. Stability analysis and control synthesis for switched systems: a switched lyapunov function approach. *Automatic Control, IEEE Transactions on*, 47(11):1883 – 1887, nov 2002.

[DS01] D. Delorme and B. Song. Human driver model for SmartAHS. Technical report, California PATH research report, 2001.

[Dup07] Francis Dupin. Equipement d´une direction électrique sur peugeot 307 sw : Spécification des interfaces et des modes de fonctionnement. Technical report, LIVC, 2007.

[DY08] Da-Wei Ding and Guang-Hong Yang. State-feedback control design for continuous-time piecewise linear systems: an lmi approach. In *Proceedings of the IEEE American Control Conference, Seattle, Washington, USA*, pages 1104–1108, June 2008.

[EKSS00] S. Engell, S. Kowalewski, C. Schulz, and O. Stursberg. Continuous-discrete interactions in chemical processing plants. *Proceedings of the IEEE*, 88(7):1050 –1068, jul 2000.

[EPG05] A. Eidehall, J. Pohl, and F. Gustafsson. A new approach to lane guidance systems. In *Intelligent Transportation Systems, 2005. Proceedings. 2005 IEEE*, pages 108–112. IEEE, sep 2005.

[Eur10] European Commission. Eur 24500 - Eu at the steering wheel of road safety, Eu-funded research to make Europe's roads safer. Technical report, 2010.

[Eur11] Eureka. Eureka project: 45 prometheus. http://www.eurekanetwork.org/project/-/id/45, 2011.

[FA03] Y. Fujiwara and S. Adachi. Steering assistance system for driver characteristics using gain scheduling control. In *European Control conference (ECC), cambrigde, UK*, September 2003.

[FB01] J. Farrell and M. Barth. Integration of GPS/INS and Magnetic Markers for Advanced Vehicle Control. Technical report, California PATH research report, 2001.

[FBA+07] P. Falcone, F. Borrelli, J. Asgari, H.E. Tseng, and D. Hrovat. Predictive active steering control for autonomous vehicle systems. *Control Systems Technology, IEEE Transactions on*, 15(3):566–580, may 2007.

[FHL92] Fraichard, M. Hassoun, and N. Lefort. an electronic co-pilot: the prolab-ii demosntrator. In *3rd PROMETHEUS collision avoidance Workshop, Proceedings of the*, pages 230 – 237, jun. 1992.

[Fil88] A.F. Filippov. *Differential equations with discontinuous righthand sides.* Springer, 1988.

[FL68] I. Flügge-Lotz. *Discontinuous and optimal control.* McGraw-Hill New York, 1968.

[Fra10] La Documentation Française. La sécurité routiére en france - bilan de l'année 2009. Technical report, Observatoire National Interministériel de Sécurité Routière, 2010.

[FTCMM02] Giancarlo Ferrari-Trecate, Francesco Alessandro Cuzzola, Domenico Mignone, and Manfred Morari. Analysis of discrete-time piecewise affine and hybrid systems. *Automatica*, 38(12):2139 – 2146, 2002.

[FW76] B.A. Francis and W.M. Wonham. The internal model principle of control theory. *Automatica*, 12(5):457–465, 1976.

[GB11] Michael C. Grant and Stephen Boyd. Cvx: Matlab software for disciplined convex programming. http://cvxr.com/cvx/, 2011.

[GF05] W. Riley Garrott and Garrick J. Forkenbrock. Nhtsa's light vehicle esc research program. http://www.nhtsa.gov/DOT/NHTSA/NRD/Multimedia/PDFs/VRTC/ca/esc/NHTSA_ESCresearch06092005.pdf, 09 June 2005.

[GMW81] Philip E. Gill, Walter Murray, and Margaret H. Wright. *Practical optimization.* London: Academic Press, London, UK, 1981.

[GoAE92] T.D. Gillespie and Society of Automotive Engineers. *Fundamentals of vehicle dynamics.* Society of Automotive Engineers, 1992.

[GR01] J.C. Gerdes and E.J. Rossetter. A unified approach to driver assistance systems based on artificial potential fields. *Journal of Dynamic Systems, Measurement, and Control*, 123:431, 2001.

[GRB+06] N. Giorgetti, G. Ripaccioli, A. Bemporad, I.V. Kolmanovsky, and D. Hrovat. Hybrid model predictive control of direct injection stratified charge engines. *Mechatronics, IEEE/ASME Transactions on*, 11(5):499 –506, oct 2006.

[GSP94] K.-C. Goh, M.G. Safonov, and G.P. Papavassilopoulos. A global optimization approach for the bmi problem. In *Decision and Control, 1994., Proceedings of the 33rd IEEE Conference on*, volume 3, pages 2009 –2014 vol.3, dec 1994.

[GST09] R. Goebel, R. Sanfelice, and A. Teel. Hybrid dynamical systems. *Control Systems Magazine, IEEE*, 29(2):28 –93, april 2009.

[GTP97] J. Guldner, H.S. Tan, and S. Patwardhan. On fundamental issues of vehicle steering control for highway automation. Technical report, California PATH research report, 1997.

[GTS+94] KC Goh, L. Turan, MG Safonov, GP Papavassilopoulos, and JH Ly. Biaffine matrix inequality properties and computational methods. In *American Control Conference, 1994*, volume 1, pages 850–855. IEEE, 1994.

[HAV11] HAVEit. Highly automated vehicles for intelligent transport. http://www.haveit-eu.org/displayITM1.asp?ITMID=6&LANG=EN, 2011.

[HB98] A. Hassibi and S. Boyd. Quadratic stabilization and control of piecewise-linear systems. In *Proceedings of the IEEE American Control Conference, Philadelphia, PA*, pages 3659–3664, 1998.

[Hig07] National Highway Traffic Safety Administration. Federal motor vehicle safety standards; electronic stability control systems; controls and displays. http://www.nhtsa.gov/Laws+&+Regulations/Electronic+Stability+Control+(ESC), Mar 2007.

[HJ99] Sven Hedlund and Mikael Johansson. Pwltlool: A matlab toolbox for analysis of piecewise linear systems, 1999.

[HL95] M. Hassoun and C. Laugier. An architecture for motion planning and motion control of a car-like vehicle. *Mathematical and Computer Modelling*, 22(4-7):329 – 341, 1995.

[HON99] Shinichiro Horiuchi, Kazuyuki Okada, and Shinya Nohtomi. Improvement of vehicle handling by nonlinear integrated control of four wheel steering and four wheel torque. *JSAE*, 20:459–464, 1999.

[HR03] S.J. Hallowell and L.R. Ray. All-wheel driving using independent torque control of each wheel. In *American Control Conference, 2003. Proceedings of the 2003*, volume 3, pages 2590 – 2595 vol.3, jun 2003.

[HSB01] W. P. M. H. Heemels, B. De Schutter, and A. Bemporad. Equivalence of hybrid dynamical models. *Automatica*, 37(7):1085 – 1091, 2001.

[HT91] T. Hessburg and M. Tomizuka. A fuzzy rule-based controller for automotive vehicle guidance. Technical report, California Partners for Advanced Transit and Highways, PATH research report UCB-ITS-PRR-91-18, 1991.

[HV00] R. Horowitz and P. Varaiya. Control design of an automated highway system. *Proceedings of the IEEE*, 88(7):913 –925, July 2000.

[HvS01] Luc Habets and Jan van Schuppen. Control of piecewise-linear hybrid systems on simplices and rectangles. In Maria Di Benedetto and Alberto Sangiovanni-Vincentelli, editors, *Hybrid Systems: Computation and Control*, volume 2034 of *Lecture Notes in Computer Science*, pages 261–274. Springer Berlin / Heidelberg, 2001.

[HWBK06] T.E. Hodrus, F. Wolff, M. Buchholz, and V. Krebs. A local control strategy for the control of discrete-time piecewise affine systems on full-dimensional polytopes. In *IEEE Industrial Electronics, IECON 2006 - 32nd Annual Conference on*, pages 4737 –4742, nov 2006.

[HWGB05] MJ Hancock, RA Williams, TJ Gordon, and M.C. Best. A comparison of braking and differential control of road vehicle yaw-sideslip dynamics. *Proceedings of the Institution of Mechanical Engineers, Part D: Journal of Automobile Engineering*, 219(3):309–327, 2005.

[HYB09] J.M. Hoc, M.S. Young, and J.M. Blosseville. Cooperation between drivers and automation: implications for safety. *Theoretical Issues in Ergonomics Science*, 10(2):135–160, mar 2009.

[IB06] Karl Iagnemma and Martin Buehler. Editorial for journal of field robotic, special issue on the darpa grand challenge. *Journal of Field Robotics*, 23(8):461–462, 2006.

[IG04] Shinnosuke Ishida and Jens E. Gayko. Development evaluation and introduction of a lane keeping assistance system. In *Proceedings of the IEEE Intelligent Vehicles Symposium, Parma, Italy*, pages 139–144, June 2004.

[Iih04] Akira Iihoshi. Driver assistance system (lane keep assist system). Presentation to WP-29 ITS Round Table, Geneva, 08 February 2004.

[IVs01] IVsource. Nissan demos new lane keeping products. www.ivsource.net, 12 February 2001.

[Joh99] Mikael Johansson. *Piecewise Linear Control systems*. PhD thesis, Lund Institute of Technology, 1999.

[Joh02a] T.A. Johansen. On multi-parametric nonlinear programming and explicit nonlinear model predictive control. In *Decision and Control, 2002, Proceedings of the 41st IEEE Conference on*, volume 3, pages 2768 – 2773, dec. 2002.

[Joh02b] Mikael Johansson. *Piecewise Linear Control Systems*. Springer, 2002.

[JR98] M. Johansson and A. Rantzer. Computation of piecewise quadratic lyapunov functions for hybrid systems. *IEEE Transactions on Automatic Control*, 43(4):555–559, 1998.

[JYJ+08] J.-S. JO, S.-H. YOU, J. Y. JOENG, K. I. LEE, and K. YI. Vehicle stability control system for enhancing steerability, lateral stability and roll stability. *International Journal of Automotive Technology*, 9(5):571–576, 2008.

[Kal54] R. Kalman. Phase-plane analysis of automatic control systems with nonlinear gain elements. *AIEE Transactions Part-II: Applications and Industry*, 73:383–390, 1954.

[Kan97] M. Kantner. Robust stability of piecewise linear discrete time systems. In *American Control Conference, 1997. Proceedings of the 1997*, volume 2, pages 1241 –1245, jun 1997.

[KC06] S.D. Keen and D.J. Cole. Steering control using model predictive control and multiple internal models. In *Proceedings of the 8th International Symposium on Advanced Vehicle Control, Taipei, Taiwan*, 2006.

[KH08] I. Kotini and G. Hassapis. A hybrid automaton model of the cement mill control. *Control Systems Technology, IEEE Transactions on*, 16(4):676 –690, july 2008.

[KS03] Michal Kocvara and Michael Stingl. Pennon: A code for convex nonlinear and semidefinite programming. *Optimization Methods and Software*, 18(3):317–333, 2003.

[Kuh05] Dietrich Kuhlgatz. Bosch Automotive, A product history. *Journal of Bosch History*, 2, 2005.

[LDLC06] R. Labayrade, J. Douret, J. Laneurit, and R. Chapuis. A reliable and robust lane detection system based on the parallel use of three algorithms for driving safety assistance. *IEICE Transactions on Information and Systems*, E89-D(7):2092–2100, 2006.

[Löf04] J. Löfberg. Yalmip : A toolbox for modeling and optimization in MATLAB. In *Proceedings of the CACSD Conference*, Taipei, Taiwan, 2004.

[LHT09] M. Lazar, W.P.M.H. Heemels, and A.R. Teel. Lyapunov functions, stability and input-to-state stability subtleties for discrete-time discontinuous systems. *Automatic Control, IEEE Transactions on*, 54(10):2421 –2425, oct 2009.

[Lib03] D. Liberzon. *Switching in systems and control*. Springer, 2003.

[LJ09] Mircea Lazar and Andrej Jokic. *Hybrid Systems: Computation and Control*, volume 5469/2009, chapter Synthesis of Trajectory-Dependent Control Lyapunov Functions by a Single Linear Program, pages 237–251. Springer Berlin / Heidelberg, 2009.

[LMSN04] E. K. Liebemann, K. Meder, J. Schuh, and G. Nenninger. Safety and perfomance enhacement: The bosch electronic stability control. 2004.

[LSMN02] P. Leelavansuk, K. Shitamitsu, H. Mouri, and M. Nagai. Study on cooperative control of driver and lane-keeping assistance system. In *Proceedings of Symposium on Advanced Vehicle Control (AVEC), Hiroshima*, pages 219–224, 2002.

[LTEP96] B. Lennartson, M. Tittus, B. Egardt, and S. Pettersson. Hybrid systems in process control. *Control Systems Magazine, IEEE*, 16(5):45 –56, oct 1996.

[Lu95] P. Lu. Optimal predictive control of continuous nonlinear systems. *International Journal of Control*, 62(3):633–649, 1995.

[Mac81] C. MacAdam. Application of an optimal preview control for simulation of closed-loop automobile driving. *IEEE Trans. on Systems, Man, and Cybernetics*, 11:393–399, June 1981.

[Mam04] Said Mammar. Combining active steering and independent wheels braking for civic lateral assistance. In *Proceedings of the IEEE American Control Conference, Boston Massachusetts*, pages 1469–1474, June 2004.

[Mat94] N. D. Matthews. *Vision Collision Avoidance*. PhD thesis, Southampton University, england, 1994.

[Mat11] Mathworks. http://www.mathworks.fr/help/toolbox/robust/gs/f3-6327.html, 2011.

[MBNGO11] Said Mammar, Andre Benine-Neto, Sebastien Glaser, and Naima Ait Oufroukh. Vehicle handling improvement by fuzzy explicit nonlinear tire forces parametrization. In *Control and Decision Conference (CCDC), 2011 Chinese*, pages 1560 –1565, may 2011.

[ME08] Nicoleta Minoiu-Enache. *Assistance Préventive à la Sortie de Voie*. PhD thesis, Université d'Évry-Val-D'Essonne, 2008.

[MELMN09] N. Minoiu-Enache, B. Lusetti, S. Mammar, and M. Netto. Assistance active de prévention des sorties de voie. prise en compte des virages. *Journal Européen des Systèmes Automatisés*, 43(6):615–646, 2009.

[MEMGL10] N. Minoiu-Enache, S. Mammar, S. Glaser, and B. Lusetti. Vehicle assistance for lane keeping, lane departure avoidance and yaw stability: Approach by simultaneous steering and differential braking. *Journal Européen des Systèmes Automatisés*, 44(7):811–852, September-October 2010.

[MEMNL10] N. Minoiu-Enache, S. Mammar, M. Netto, and B. Lusetti. Driver steering assistance for lane-departure avoidance based on hybrid automata and composite lyapunov function. *Intelligent Transportation Systems, IEEE Transactions on*, 11(1):28 –39, march 2010.

[MENML09] N. Minoiu-Enache, M. Netto, S. Mammar, and B. Lusetti. Driver steering assistance for lane departure avoidance. *Control Engineering Practice*, 17(6):642 – 651, 2009.

[MFTM00] D. Mignone, G. Ferrari-Trecate, and M. Morari. Stability and stabilization of piecewise affine and hybrid systems: an lmi approach. In *Decision and Control, 2000. Proceedings of the 39th IEEE Conference on*, volume 1, pages 504 –509, dec 2000.

[MH04] E. Morinaga and K. Hirata. An l/sub 2/-gain analysis of piecewise affine systems by piecewise quadratic storage functions. In *American Control Conference, 2004. Proceedings of the 2004*, volume 6, pages 5176 –5181 vol.6, jul 2004.

[MK02] S. Mammar and D. Koenig. Vehicle handling improvement by active steering. *Vehicle System Dynamics*, 38(3):211–242, 2002.

[MM95] W.F. Milliken and D.L. Milliken. *Race car vehicle dynamics*. Sae International, 1995.

[MMEG+10] Said Mammar, Nicoleta Minoiu-Enache, Sebastien Glaser, Benoit Lusetti, and Andre Benine-Neto. Lane keeping automation at tire saturation. In *Proceedings of the IEEE American Control Conference, Baltimore*, pages 6466–6471, June 2010.

[Mob] Mobileye. Lane departure warning. http://www.mobileye.com/manufacturer-products/applications/forward/lane-departure.

[MSC07] R Marino, S. Scalzi, and F. Cinili. Nonlinear pi front and rear steering control in four wheel steering vehicles. *Vehicle System Dynamics*, 45(12):1140–1168, October 2007.

[MSC09] Mechanical-Simulation-Corporation. Carsim® 8 math models, june 2009. http://www.carsim.com/downloads/pdf/Math_Models_C80.pdf.

[MSON09] R. Marino, S. Scalzi, G. Orlando, and M. Netto. A nested pid steering control for lane keeping in vision based autonomous vehicles. In *American Control Conference, 2009. ACC '09.*, pages 2885 –2890, june 2009.

[MT06] J. McCall and M. M. Trivedi. Video-based lane estimation and tracking for driver assistance: Survey, system, and evaluation. *IEEE Transactions on Intelligent Transportation System*, 7(1):20–37, March 2006.

[NN94] Y. Nesterov and A. Nemirovskii. *Interior-Point Polynomial Methods in Convex Programming*. Society for Industrial and Applied Mathematics, 1994.

[OBNY+11] N.A. Oufroukh, A. Benine-Neto, Z. Yacine, S. Mammar, and S. Glaser. Invariant set based vehicle handling improvement at tire saturation using fuzzy output feedback. In *Intelligent Vehicles Symposium (IV), 2011 IEEE*, pages 1104 –1109, june 2011.

[OHA+99] E. Ono, S. Hosoe, K. Asano, M. Sugai, and S. Doi. Robust stabilization of the vehicle dynamics by gain-scheduled $h\infty$ control. In *Control Applications, 1999. Proceedings of the 1999 IEEE International Conference on*, volume 2, pages 1679 –1685 vol. 2, 1999.

[OHMK06] E. Ono, Y. Hattori, Y. Muragishi, and K. Koibuchi. Vehicle dynamics integrated control for four-wheel-distributed steering and four-wheel-distributed traction/braking systems. *vehicle system dynamics*, 44(2):139–151, 2006.

[OHTD98] E. Ono, S. Hosoe, H. D. Tuan, and S. Doi. Bifurcation in vehicle dynamics and robust front wheel steering control. *IEEE Trans. on Control System Technology*, 6(3):9–14, May 1998.

[OS06] R. Osborn and T. Shim. Independent control of all-wheel-drive torque distribution. *Vehicle System Dynamics*, 44(7):529–546, 2006.

[Pac04] H.B. Pacejka. *Tire and Vehicle Dynamics*. Elsevier Butterworth-Heinemann, 2004.

[PAT11] PATH. Partners for advanced transportation technology. http://www.path.berkeley.edu/Default.htm, 2011.

[PB02] A. Pauly and G. Baumgarten. Overlay steering system and method for motor vehicles, mar 2002. #27.

[PC00] D.L. Pepyne and C.G. Cassandras. Optimal control of hybrid systems in manufacturing. *Proceedings of the IEEE*, 88(7):1108 –1123, jul 2000.

[PD91] Philippos Peleties and Raymond DeCarlo. Asymptotic stability of m-switched systems using lyapunov-like functions. In *American Control Conference, 1991*, pages 1679 –1684, june 1991.

[PD98] R. Prohaska and P. Devlin. Combined brake and steering actuator for automatic vehicle control. Technical report, California PATH working paper, 1998.

[Pet97] N. Pettit. *The analysis of piecewise linear dynamical systems*, volume 222 of *Lecture Notes in Control and Information Sciences*. Springer Berlin / Heidelberg, 1997. 10.1007/BFb0036083.

[PHB01] Kihong Park, Seung-Jin Heo, and Inho Baek. Controller design for improving lateral vehicle dynamic stability. *JSAE Review*, 22(4):481 – 486, 2001.

[PKL+94] L. Priese, J. Klieber, R. Lakmann, V. Rehrmann, and R. Schian. New results on traffic sign recognition. In *Intelligent Vehicles '94 Symposium, Proceedings of the*, pages 249 – 254, oct. 1994.

[PL06] William Pessilas-Lepine. Hybrid modelling and limit cycle analysis for a class of five-phase anti-lock brake algorithms. *Vehicle System Dynamics*, 44(2):173–188, February 2006.

[PMB10] G. Palmieri, M.Baric, and F. Borrelli. Constrained robust design of lateral vehicle dynamics control systems. In *Proceeding of AVEC*, aug 2010.

[Pol] Imre Polik. http://sedumi.ie.lehigh.edu/.

[Pop61] V. Popov. Absolute stability of nonlinear systems of automatic control. *Automation and Remote Control*, 22:857–875, 1961.

[Pro01] G. Prokop. Modeling human vehicle driving by model predictive online optimization. *Vehicle System Dynamics*, 35(1):19–53, 2001.

[PS82] Y.S. Pyatnitskiy and VI Skorodinskiy. Numerical methods of Lyapunov function construction and their application to the absolute stability problem. *Systems & Control Letters*, 2(2):130–135, 1982.

[PT90] H. Peng and M. Tomizuka. Lateral control of front-wheel-steering rubber-tire vehicles. Technical report, California PATH research report, 1990.

[PTH97] H. Pham, M. Tomizuka, and J.K. Hedrick. Integrated maneuvering control for automated highway systems based on a magnetic reference/sensing system. Technical report, California PATH research report, 1997.

[PUH95] T. Pilutti, G. Ulsoy, and D. Hrovat. Vehicle steering intervention through differential braking. In *American Control Conference, 1995. Proceedings of the*, volume 3, pages 1667 –1671 vol.3, June 1995.

[Raj06a] Rajesh Rajamani. *Vehicle Dynamics and Control*, chapter 8 - Electronic Stability Control, pages 221–256. Springer, 2006.

[Raj06b] Rajesh Rajamani. *Vehicle Dynamics and Control*, chapter 13 - Lateral and longitudinal tire forces, pages 387–432. Springer, 2006.

[Raj06c] Rajesh Rajamani. *Vehicle Dynamics and Control*, chapter 2 - Lateral Vehicle Dynamics, pages 43–46. Springer, 2006.

[Raj06d] Rajesh Rajamani. *Vehicle Dynamics and Control*. Springer, 2006.

[RB05] Luis Rodrigues and Stephen Boyd. Piecewise-affine state feedback for piecewise-affine slab systems using convex optimization. *Systems and Control Letters*, 54:835–853, 2005.

[RG06] Eric J. Rosseter and J. Christian Gerdes. Lyapunov based performance guarantees for potencial field lane keeping assistance system. *Journal of Dynamic Systems, Measurement and Control - Transactions of the ASME*, 128:510–522, September 2006.

[RH03] Luis Rodrigues and Jonathan P. How. Observer based control of piecewise-affine systems. *Int. J. Control*, 76(5):459–477, 2003.

[RHH00] Luis Rodrigues, Arash Hassibi, and Jonathan P. How. Output feedback controller synthesis for piecewise-affine systems with multiple equilibria. In *Proceedings of the IEEE American Control Conference*, pages 1784–1789, 2000.

[RJ00] A. Rantzer and M. Johansson. Piecewise linear quadratic optimal control. *IEEE Transactions on Automatic Control*, 45(4):629–637, 2000.

[Rod02] L. Rodrigues. *Dynamic output feedback controller synthesis for piecewise-affine systems*. PhD thesis, Stanford University., 2002.

[Sch53] J. W. Schwartz. Piecewise linear servomechanisms. *AIEE Transactions*, 72:401–405, 1953.

[Sch10a] Walter E. Scholl. Abschlusspräsentation auf der Teststrecke Mendig: BMWI-Forschungsinitiative AKTIV stellt Ergebnisse für sicheren und möglichst störungsfreien Strassenverkehr vor AKTIV - gemeinsam die Zukunft erfahren. http://www.aktiv-online.org/deutsch/Downloads/PI_AKTIV2010-06-23.pdf, 2010.

[Sch10b] Walter E. Scholl. Active Safety, Activating safety technologies. http://www.aktiv-online.org/deutsch/Downloads/Broschueren/AktivAS-e.pdf, 2010.

[SCM07] J. Stéphant, A. Charara, and D. Meizel. Evaluation of a sliding mode observer for vehicle sideslip angle. *Control Engineering Practice*, 15(7):803 – 812, 2007. Special Issue on Award Winning Applications, 2005 IFAC World Congress.

[SGL94] M.G. Safonov, K.C. Goh, and J.H. Ly. Control system synthesis via bilinear matrix inequalities. In *American Control Conference, 1994*, volume 1, pages 45 – 49 vol.1, jun 1994.

[Shl07] Steven. E. Shladover. Path at 20 - history and major milestones. *IEEE Transactions on Intelligent Transportation Systems*, 8(4):584–592, December 2007.

[SL+91] J.J.E. Slotine, W. Li, et al. *Applied nonlinear control*, volume 461. Prentice hall Englewood Cliffs, New Jersey, 1991.

[SMI+08] Matthias Schulze, Tapani Mäkinen, Joachim Irion, Maxime Flament, and Tanja Kessel. PReVENT final report. Technical report, Sixth Framework Programme, 2008.

[SN99] R.N. Shorten and K.S. Narendra. Necessary and sufficient conditions for the existence of a common quadratic lyapunov function for two stable second order linear time-invariant systems. In *American Control Conference, Proceedings of the 1999*, volume 2, pages 1410–1414, jun 1999.

[SNM03] R. Shorten, K.S. Narendra, and O. Mason. A result on common quadratic lyapunov functions. *Automatic Control, IEEE Transactions on*, 48(1):110 – 113, jan 2003.

[Son81] Eduardo D. Sontag. Nonlinear regulation: The piecewise linear approach. *IEEE Transactions on Automatic Control*, AC-26(2):346–358, April 1981.

[SS99] K. Sawase and Y. Sano. Application of active yaw control to vehicle dynamics by utilizing driving/braking force. *JSAE Review*, 20(2):289–295, 1999.

[SY99] D. Swaroop and S.M. Yoon. The design of a controller for a following vehicle in an emergency lane change maneuver. Technical report, California PATH research report, 1999.

[TC07] M. M. Trivedi and S. Y. Cheng. Holistic sensing and active displays for intelligent driver support systems. *IEEE Computer Magazine*, 40(5):60–68, May 2007.

[TJ05] P. Tøndel and T. A. Johansen. Control allocation for yaw stabilization in automotive vehicles using multiparametric nonlinear programming. In *Proceedings of the IEEE American Control Conference, Portland, OR, USA*, pages 453–458, June 2005.

[TMD+06] Sebastian Thrun, Mike Montemerlo, Hendrik Dahlkamp, David Stavens, Andrei Aron, James Diebel, Philip Fong, John Gale, Morgan Halpenny, Gabriel Hoffmann, Kenny Lau, Celia Oakley, Mark Palatucci, Vaughan Pratt, Pascal Stang, Sven Strohband, Cedric Dupont, Lars-Erik Jendrossek, Christian Koelen, Charles Markey, Carlo Rummel, Joe van Niekerk, Eric Jensen, Philippe Alessandrini, Gary Bradski, Bob Davies, Scott Ettinger, Adrian Kaehler, Ara Nefian, and Pamela Mahoney. Stanley: The robot that won the darpa grand challenge. *Journal of Field Robotics*, 23(9):661–692, sep 2006.

[TPS98] C. Tomlin, G.J. Pappas, and S. Sastry. Conflict resolution for air traffic management: a study in multiagent hybrid systems. *Automatic Control, IEEE Transactions on*, 43(4):509 –521, apr 1998.

[TPT04] Craig Matthew Talbot, Iakovos Papadimitriou, and Masayoshi Tomizuka. Fault Tolerant Autonomous Lateral Control for Heavy Vehicles. Technical report, California PATH research report, 2004.

[TPZS97] H.-S. J. Tsao, T. A. Plocher, W.-B. Zhang, and S. E. Shladover. Major Failure Events of Automated Highway Systems: Three Scenarios from the Driver's Perspective. Technical report, California PATH working paper, 1997.

[TT10] C. Tran and M. M. Trivedi. Towards a vision-based system exploring 3d driver posture dynamics for driver assistance: Issues and possibilities. In *Proceedings of the IEEE Intelligent Vehicles Symposium, San Diego, USA*, pages 179–184, June 2010.

[TWWT01] M. Tai, J.Y. Wang, R. White, and M. Tomizuka. Robust Lateral Control of Heavy Duty Vehicles. Technical report, California PATH research report, 2001.

[Uni68] United Nations. Convention on road traffic (vienna). http://www.unece.org/trans/conventn/crt1968e.pdf, 1968.

[Val04] Valeo. Valeo´s revolutionary lane departure warning system makes debut on nissan infiniti vehicles. http://www.valeo.com/fileadmin/dotcom/uploads/archives/en/ldws_uk.pdf, 31 March 2004.

[VGMG09] Benoit Vanholme, Sebastien Glaser, Said Mammar, and Dominique Gruyer. Manoeuvre based trajectory planning for highly autonomous vehicles on real road with traffic. In *Proceedings of European Control Conference 2009, Budapest, Hungary*, pages 3281–3286, August 2009.

[Visa] Vislab. The artificial vision and intelligent systems laboratory. http://vislab.it/.

[Visb] Vislab. Vislab intercontinental autonomous challenge. http://viac.vislab.it/.

[VZEP95] A.T. Van Zanten, R. Erhardt, and G. Pfaff. VDC, the vehicle dynamics control system of Bosch. *PROGRESS IN TECHNOLOGY*, 57:497–516, 1995.

[WCP+08] Shinq-Jen Wu, Hsin-Han Chiang, Jau-Woei Perng, Chao-Jung Chen, Bing-Fei Wu, and Tsu-Tian Lee. The heterogeneous systems integration design and implementation for lane keeping on a vehicle. *Intelligent Transportation Systems, IEEE Transactions on*, 9(2):246–263, jun 2008.

[Weg11] Fred Wegman. Irtad annual report 2010. Technical report, International Traffic Safety Data and Analysis Group, 2011.

[WWJS11] J. Wang, Q. Wang, L. Jin, and C. Song. Independent wheel torque control of 4wd electric vehicle for differential drive assisted steering. *Mechatronics*, 21(1):63 – 76, 2011.

[YdB99] J.L. Ygnace and E. de Banville. *Les systèmes de transport intelligent: un enjeu stratégique mondial*. Documentation française, 1999.

[YESG08] P. Ye, E. Entcheva, S.A. Smolka, and R. Grosu. Modelling excitable cells using cycle-linear hybrid automata. *Systems Biology, IET*, 2(1):24 –32, january 2008.

[ZTHZ06] Shuibo Zheng, Houjun Tang, Zhengzhi Han, and Yong Zhang. Controller design for vehicle stability enhancement. *Control Engineering Practice*, 14(12):1413 – 1421, 2006.